Design and fabrication of advanced materials obtained from hemp fibers and sustainable polymers

Gianluca Viscusi

UNIVERSITY OF SALERNO

DEPARTMENT OF INDUSTRIAL ENGINEERING

Ph.D. Course in Industrial Engineering
Curriculum in Chemical Engineering - XXXIV Cycle

DESIGN AND FABRICATION OF ADVANCED MATERIALS OBTAINED FROM HEMP FIBERS AND SUSTAINABLE POLYMERS

Supervisor
Prof. Giuliana Gorrasi

Ph.D. student
Gianluca Viscusi

Scientific Referees
Prof. Massimo Viscardi
Prof. Sergio Torres Giner

Ph.D. Course Coordinator
Prof. Francesco Donsì

I List of publications

Viscusi G, Barra G, Verdolotti L, Galzerano B, Viscardi M, Gorrasi G. Natural fiber reinforced inorganic foam composites from short hemp bast fibers obtained by mechanical decortation of unretted stems from the wastes of hemp cultivations. Mater Today Proc 2020. https://doi.org/10.1016/j.matpr.2020.02.672.

Viscusi G, Barra G, Gorrasi G. Modification of hemp fibers through alkaline attack assisted by mechanical milling: effect of processing time on the morphology of the system. Cellulose 2020;27:8653–65. https://doi.org/10.1007/s10570-020-03406-0.

Viscusi G, Pantani R, Gorrasi G. Transport properties of water vapor through hemp fibers modified with a sustainable process: Effect of surface morphology on the thermodynamic and kinetic phenomena. Appl Surf Sci 2021;541:148433. https://doi.org/10.1016/j.apsusc.2020.148433.

Viscusi G, Gorrasi G. A novel approach to design sustainable fiber reinforced materials from renewable sources: mathematical modeling for the evaluation of the effect of fiber content on biocomposite properties. J Mater Res Technol 2021;12:717–26. https://doi.org/10.1016/j.jmrt.2021.03.017.

Viscusi G, Gorrasi G. Gelatin Beads/Hemp Hurd as pH Sensitive Devices for Delivery of Eugenol as Green Pesticide. J Polym Environ 2021 2911 2021;29:3756–69. https://doi.org/10.1007/S10924-021-02148-9.

Viscusi G, Liparoti S, Pantani R, Gorrasi G. Natural resources derived biocomposites as potential carriers of green pesticides in agricultural field: Designing and fabrication of a pot-like device. J Appl Polym Sci 2021:51240. https://doi.org/10.1002/APP.51240.

Viscusi G, Adami R, Gorrasi G. Fabrication of rice flour films reinforced with hemp hurd and loaded with grapefruit seed oil: A simple way to valorize agro-waste resources toward low cost materials with added value. Ind Crops Prod 2021;170:113785. https://doi.org/10.1016/J.INDCROP.2021.113785.

Viscusi G, Lamberti E, Gorrasi G. Hemp fibers modified with graphite oxide as green and efficient solution for water remediation: Application to methylene blue. Chemosphere 2021:132614. https://doi.org/10.1016/J.CHEMOSPHERE.2021.132614.

Viscusi G, Lamberti E, Gorrasi G. Design of sodium alginate/soybean extract beads loaded with hemp hurd and halloysite as novel and sustainable systems

for methylene blue adsorption. Polym Eng Sci 2021. https://doi.org/10.1002/PEN.25839.

Viscusi G, Lamberti E, Gorrasi G. Design of a hybrid bio-adsorbent based on Sodium Alginate/Halloysite/Hemp hurd for methylene blue dye removal: kinetic studies and mathematical modeling, Colloids Surfaces A Physicochem. Eng. Asp. 2022;633:127925. https://doi.org/10.1016/J.COLSURFA.2021.127925

Viscusi G, Liparoti S, Pantani R, Barra G, Gorrasi G. A layer-by-layer approach based on APTES/Cloisite to produce novel and sustainable high performances materials based on hemp fiberboards. Polym Degrad Stab 2022;198. https://doi.org/10.1016/J.POLYMDEGRADSTAB.2022.109892

II Table of content

III Index of figures

IV Index of tables

V Abstract

Nowadays, in the frame of sustainability and circular economy, scientific community is focusing on eco-friendly novel materials as valuable alternative of petroleum-based ones. Since the urge of investigating the fabrication of more sustainable materials as well as of addressing their wide demand in different applications, some natural materials such as hemp fibers are taking a center stage since they are biodegradable, no toxic, non-carcinogenic, recyclable. Compared to synthetic fibers (i.e. glass fibers), natural fibers, such as hemp ones, possess some interesting properties such as low density, eco-friendliness and biodegradability. Moreover, due to their intrinsic drawbacks (i.e. low biological resistance, high flammability, low adhesion properties and high moisture sensitivity), several procedures for modifying hemp fibers have been proposed in the scientific literature. Most of them appeared to be no completely sustainable since the use of toxic solvents or harsh processing conditions. By stating that, this thesis will offer a wide analysis of potential applications of hemp fibers in many industrial fields. The novelty is placed in the design of sustainable modification methodologies aiming to efficiently modify the surface properties of hemp fibers making them a valuable material for the fabrication of eco-friendly materials. So, different modification methodologies will be presented and discussed while the properties of modified hemp fibers will be investigated through spectroscopic, morphological, thermal, mechanical, optical, barrier and magnetic properties analysis.

VI Introduction

In the last decades, many efforts have been making to reduce the use of synthetic materials since they pose serious issues from environmental point of view. The expansive use of fossil resources and the severe environment legislations are leading to the development of environment-friendly green alternatives (Obi Reddy *et al.*, 2012) and to the intensification of the research on natural polymer-based materials derived from bio-renewable resources (Thakur, Rana and Thakur, 2015). In the last few years, the design and preparation of environmentally friendly materials from natural resources is representing one of the greatest challenges. Besides, the rising of environmental issues and society demands is pulling toward the development of bio-based resources derived materials, for example from cellulose based resources (Sobhanadhas et al., 2019). Among them, cellulosic fibers represent a good alternative to synthetic materials due to their intrinsic properties such as great natural abundance, low density, biodegradability, high stiffness and strength to weight ratio, lightweight, lack of irritation, non-carcinogenicity, biodegradability, easy processing and low cost (Pietak *et al.*, 2007; Zhou, Cheng and Jiang, 2014). Moreover, it is worthwhile stating that vegetable fibers, due to their calorific value, could be incinerated for energy recovery (Joseph, Thomas and Pavithran, 1995). Natural fibers from plants are even receiving great attention from the academic research, as well as from the industrial world, for the possibility to be used as fillers in polymer composites for their environmentally friendly nature and sustainability. (Schettini *et al.*, 2013; Sanjay *et al.*, 2019). The interest in using natural fibers, such as bast fibers, leaf fibers, grass fibers, wood, seed, etc., as a potential substitute of synthetic fibers for reinforcing composite materials, has been increasing (Obi Reddy *et al.*, 2012; Moonart and Utara, 2019). Their use is highly beneficial due to the improved strength and toughness of resulting composites.

Among all the natural fibers, hemp fibers (HF), known as *Cannabis sativa L.*, are attracting considerable interest due to their peculiar properties such as thermal insulation, acoustic, antiseptic, and mechanical properties making them a valuable crop for the bio-based economy (Agate *et al.*, 2020). They allow the diversification of crop rotations in arable farmings, requires a low amount of fertilizer and herbicides (Amaducci and Gusovius, 2010). In this regard, hemp is getting a central role in the international landscape (Joshi *et al.*, 2004; Fuqua, Huo and Ulven, 2012; Kabir *et al.*, 2013; Liu *et al.*, 2016). However, the presence of hydrophilic groups on lignocellulosic materials could limit their applications due to the adsorption of water molecules that could make the aging, caused by swelling effect, more pronounced. In addition, some limits related to the use of these kinds of fibers are related to the anisotropic properties and to the variability of the raw materials

(Verdolotti *et al.*, 2012). Moreover, the lack of good adhesion with hydrophobic materials could cause degradation and loss of strength. So, the key feature for a successful use of natural fibers in composite materials is the optimal interfacial contact between the fibers and the matrix. In order to overcome these drawbacks, many chemical and physical treatments have already been proposed with the aim of improving the interfacial adhesion and resistance to moisture absorption of composites. They must also be targeted to optimize the fiber surface properties, by removing the non-cellulosic components. By stating that, this thesis will focus, firstly, on the properties, composition and applications of hemp fibers. Then, the major chemical and physical treatments will be discussed. Finally, designed novel and sustainable methodologies of fibers modification will be presented and discussed focusing on the improved properties of modified and functionalized hemp fibers which, as the least valuable part of hemp plant, gain an added value in different industrial applications. In the perspective of circular economy policy, green and sustainable bio-composite are produced and their potential applications in a wide range of industrial sectors were deeply investigated.

1.Natural fibers: overview

Hemp fibers: structure and composition

Figure (1) presents the structural organization of fiber.

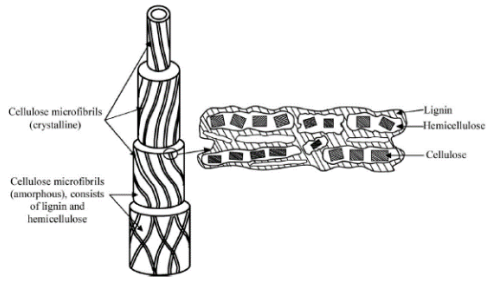

Figure 1 *Structural organization of hemp fibers*

Hemp bast fibers are defined as the continuum of primary and secondary cell walls of the cells that form the cortex sclerenchyma layer of the hemp stem. These bast fibers are particularly long and contain highly crystalline cellulose fibrils. Cellulose micro fibrils are cross-linked by glycans (xyloglucan, glucuronoarabinoxylan, etc) and this network is embedded in a matrix of non-cellulosic material made of pectin and structural aromatic substances (lignin and hydrocinnamates) (Carpita and Gibeaut, 1993). These constituents provide strength, stiffness and structural stability of the fiber (Wang and Lau, 2016). In particular, hemp fibers are generally composed of 53–91% cellulose, 4–18% hemicellulose, 1–17% pectin, and 1–21% lignin (Garcia-Jaldon, Dupeyre and Vignon, 1998; Borsa *et al.*, 2016). In general, the fiber cell can itself be considered a composite material composed of cellulose micro fibrils as reinforcement and non-cellulosic materials (pectin and lignin) as matrix (Pea, Vergara and Carpita, 2008).

Hemp fibers: limits and drawbacks

In natural fibers, pectin substances and hemicellulose, along with other cell wall components, are the primary components contributing to surface hydrophilicity (George *et al.*, 2016), which leads to moisture absorption. These hydroxyl groups are inaccessible and so other chemicals have difficulty penetrating the crystalline region (Figure (2)) (Nykter et al., 2008).

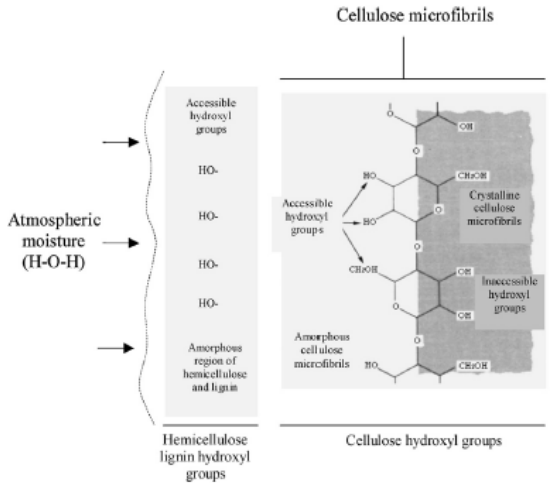

Figure 2 *Schematic presentation of the orientation of fiber constituents*

However, in the amorphous region, the hydroxyl groups are loosely linked with the fiber structure and are relatively free to react with other chemicals. The hydroxyl groups present in the amorphous hemicellulose and lignin initially give access of water molecules to penetrate the fiber surface. Water molecules then combine with the hydroxyl groups that are present in cellulose (in the amorphous region) staying in the fiber structure. This makes the fiber hydrophilic and polar in character. The hydrophilic nature of cellulosic fibers not only makes them less compatible with commonly used polymers, which are usually hydrophobic but also makes them vulnerable to moisture and biological contamination. When natural fibers are exposed to moisture, water uptake in the cell walls occurs along with formation of hydrogen bonds between the hydroxyl groups of carbohydrates (e.g. cellulose, hemicellulose and pectin) and water molecules until an equilibrium is reached, where the hydrogen bonds formed are counterbalanced by the cohesive forces of the plant cell walls (Wang and Lau, 2016). When natural fibers are completely sealed in polymers, polymers form a strong barrier against moisture and biological activities and generally protect fibers from swelling and microbial degradation. However, the matrix polymers can only slow the moisture

diffusion process. Sooner or later (e.g. up to several months), moisture will penetrate through the polymer matrix and contact fibers and cause fiber swelling, leading to a decrease in mechanical properties of the composites (Dhakal, Zhang and Richardson, 2007). A major restriction in the successful use of natural fibers in durable polymer composite applications is that the moisture absorption causes property changes, especially fiber dimensions change. In addition, moisture absorption may introduce delamination and defects at interfaces, which make natural fibers less favourable than synthetic fibers for long-term performance and durability applications
Moreover, hydrophilic fibers worsen the ability to develop adhesive characteristics with most hydrophobic binder materials during composite processing. As a result, strong bondings between fiber and the binder materials are compromised which reduce the mechanical properties of composites (Kabir *et al.*, 2013). So targeted treatments are required for tuning the properties of natural fibers. Treatments can decrease the hydroxyl groups that are present in the amorphous region, remove the lignin and hemicellulose coverings from the fiber surface and expose the cellulose structure to react with binder materials. Therefore, the removal of the components that are more inclined to absorb moisture can improve the moisture resistance of natural fibers. This could lead to increase hydrophobicity, moisture resistance and microbiological decay resistance (Bessadok *et al.*, 2007).

Potential applications of hemp fibers

Although hemp has been traditionally used in textiles, materials for construction, insulation and in pulp and paper industries, nowadays the plant is related to a wide range of products and markets, including agriculture, textile, bio composites, paper-making, automotive, construction, biofuels, functional food, oil, cosmetics, personal care and pharmaceutical industry (Salentijn et al., 2015). Among the potential applications for hemp plant, it is worth considering the use of hemp biomass as a renewable feedstock for energy production or second-generation biofuels as well as the use of natural fibers as reinforcement for bio composite materials and concrete. All the solid materials composed of more than one component in separated phases are known as composite materials. In this class of materials are included fiber-reinforced composites, which as its name suggests, are composed of reinforcement fibers (discontinuous phase) dispersed in a polymer matrix (continuous phase) (Horne, 2012). Currently, the use of fiber-reinforced composites is extended to automotive, building, packaging, wind power, aerospace, construction, consumer goods, marine and infrastructure markets. While the reinforcement acts as load-carrying member, the matrix keeps the fibers in a desired location and orientation, protects them against environmental damage and transfers load to the reinforcement, through the

fiber-matrix interface. In fact, the efficacy of reinforcing fibers is determined by interface, aspect ratio, distribution and orientation (Horne, 2012). Natural Fiber Composites (NFCs) or bio composites are composite materials, in which at least the reinforcing fibers are derived from renewable and carbon dioxide neutral resources, such as wood or plants (Horne, 2012). The possibility of using biopolymers, for instance, epoxidized plant oils, to replace petroleum-based matrixes, has also been considered, but it is still an expensive solution, and thus prohibitive to an industrialization process. Without excluding all the advantages inherent to natural fibers, one of its major drawbacks is related to the variability in their mechanical and physical properties, which in the end will introduce variability in the properties and dimensions of the final composites, and to some extent, can limit their potential applications. The main potentialities and drawbacks of hemp fibers as reinforcement in composites in comparison with other natural or synthetic fibers are reported in the table 1.

Table 1 *Properties and drawbacks of hemp fibers in comparison with other fibers* (Célino *et al.*, 2014; Shahria, 2019)

Property	Hemp	Cotton	Flax	Carbon	Glass
Density (g/cm^3)	1.47	1.55	1.54	2.5	1.4
Tensile strength (MPa)	368-800	287-597	350-2000	4000	2000-3500
Young's Modulus (MPa)	17-70	5.5-12.6	27.5-85	230-240	70
Moisture absorption	10	8-25	8	-	-
Elongation at break (%)	1.6	7-8	1-4	1.4-1.8	2.5

Hemp fibers/matrix composites

As stated before, hemp fibers could potentially substitute synthetic fibres to make a good ecologic and economic composite material. The use of natural fibres in different matrices is highly beneficial since the strength and toughness of the resulting composites are greater than those of the

unreinforced materials. So, in the last decades, natural fibres, such as hemp, have been used as a potential reinforcement of low-cost composite materials The properties of hemp fibers at low weight in combination with their environmentally friendly character lead to the possibility of producing high performant composites to be used in some engineering markets such as automobile, shipbuilding and building industries (Bessadok *et al.*, 2007). The main advantages of using hemp fibers in matrix composites are related to the low environmental impact, high specific stiffness, low density, low hazard manufacturing process, low emission of fumes when the composites are subjected to incineration and composting at end of life. Besides, some disadvantages are linked to the lower durability of natural fibers compared to synthetic ones, high moisture capacity, high variability of natural fibers, low thermal stability, low stability when subjected to microorganisms and reduced fiber matrix adhesion properties.

Hemp fibers based composites: the effect of adhesion and wettability

Concerning the design and fabrication of hemp based composites, one difficulty that has limited the use of natural fibres is the lack of good adhesion to polymeric matrices where high reliability and stability of fibre properties are required. The key feature for successful use of natural fibres in composite materials is the optimal interfacial contact between the fibres and the hydrophobic composite matrix material. The presence of pectin and waxy materials hinders the hydroxyl groups from reacting with polymer matrices. So, the high moisture sorption capacity of natural fibres negatively affect adhesion with a hydrophobic matrix and, as result, it may induce an ineffective interface between the fibres and matrices, with consequent problems such as debonding and voids in resulting composites, decrease stability and durability and provide conditions for microorganisms to thrive. As a result, strong bonding between fibre and the binder materials are compromised which reduced the composites mechanical properties. In order to limit that, surface fibre have been subjected to different modifications. Infact, interfacial adhesion and resistance to moisture absorption of natural-fibre composites can be improved by treating these fibres with suitable methodologies. Treatments can decrease the OH groups in the amorphous region, remove the lignin and hemicellulose coverings from the fibre surface and expose the cellulose structure to react with binder materials. Chemical treatments allow to provide effective means to remove non-cellulosic components in cellulose fibres and add functional groups to enable better bonding in polymer composites (Sawpan, Pickering and Fernyhough, 2011a). In general, targeted fibre treatments aim for overcoming some disadvantages to obtain improved bonding between natural fibres and matrix polymers, reduced moisture uptake/increased moisture resistance, improved mechanical properties of

natural fibres or avoidance of severe decrease in mechanical properties of natural fibres, improved robustness of natural fibres (e.g. thermal stability; resistance to microbial degradation etc.) facing the potential disadvantages of natural fibres for their application as reinforcement in composites (Liu et al., 2017).

Processing and modification of hemp fibers

After harvesting, in order to get high-quality fibers for high-grade composites and textile industries, hemp stems must undergo a pre-treatment to ease the separation of fiber bundles from the woody part of the stem. The ultimate goal is to degrade pectins and other cementing compounds (mainly lignin) in the middle lamella region, which bind individual fibers together and keep them attached to non-fibril materials, and thereby obtain individual fibers and/or fiber bundles (Idler *et al.*, 2011). On the other hand, it is important to reduce the hydrophilicity of the fibers by removing its hydrophilic non-cellulosic components. As stated previously, the hydrophilic nature of natural fibers can compromise the successful use of natural fibers in composite due to the reduced interfacial bonding with the polymeric matrix as well as the water uptake that could lead to a decrease of the stability and durability of composite and the possibility for microorganism to thrive. The most traditional retting methods to achieve defibrillation of hemp fibers are the natural processes field retting and water retting. However, due to some disadvantages of these approaches, in the past few years, researchers have been focused on getting more efficient, controlled and reliable methods in order to improve fiber quality for further applications. Among those methods are chemical, mechanical and enzymatic pre-treatments.

Many fiber treatments have been attempted to increase water resistance ability of natural fibers and NFCs. Some treatments have been shown to be efficient in minimizing natural fiber moisture uptake, such as enzymatic treatment and chemical modification of fiber surface (Alix *et al.*, 2009). Therefore, the most efficient technique to enhance moisture resistance for natural fiber-reinforced composites might be to properly seal the natural fibers within a polymer matrix to avoid that they are directly exposed to moisture (Rouison *et al.*, 2005). Targeted fibre extraction techniques are crucially important to obtain: (1) fibres with highest mechanical performance; (2) fibres with desired morphology and/or structure for composite use; (3) fibres with desired chemical composition for following fibre treatments; and (4) least impact on environment. Besides, improved antimicrobial activity and high moisture resistance of modified cellulosic fibers can be achieved when selective chemical agents or polymers are used for fiber surface modification or treatment. Recently, it has been attempted to modify the traditional composite manufacturing processes as well as to introduce novel composite manufacturing strategies to improve different properties e.g. tensile properties, water resistance and thermal conductivity of NFCs (Xia *et al.*,

2016) or extend the application of NFCs. Therefore, not only fiber pre-treatment techniques need to be assessed, but also the composite manufacturing process should be considered in order to successfully use NFCs in different areas. Although many techniques are available for decreasing moisture absorption of natural fibers, it is currently most efficient to enhance moisture resistance for natural fiber-reinforced composites by ensuring the fibers are sealed within the polymer matrix to avoid that the fibers are exposed to moisture directly. Synthesis of novel polymers with better heat resistance and durability for composite manufacturing is thus an effective way of increasing the durability of NFCs. Chemical and physical treatments are required and they should be designed to overcome the limits abovementioned. The use of fibers as reinforcement is related to the possibility to separate the cellulose fibers, embedded in an internal layer, which are responsible for the improvement of mechanical and thermal properties. To fulfil that, it is always required a defibration process applied to remove non-cellulosic material which allows producing small fiber bundles. Due to that, an increase of surface area is obtained so a higher number of functional groups is free to react with polymeric matrices. In addition, the removal of non-cellulosic components could reduce the presence of voids belonged to non-fiber cells such as epidermal cells and this may, in turn, decrease the porosity of the obtained composite. As a result, mechanical properties increase (Liu *et al.*, 2016). Several methods have already been proposed and all are briefly discussed in the sections below. In the last years, various fiber treatment techniques have been considered for potential upscalability. Steam explosion, controlled microbiological retting and physical treatment have a lower upscalability due to their specific equipment and controlled conditions requirements (i.e. temperature and sterilized environment). Except for those three fiber treatment techniques, the other techniques including chemical and enzymatic fiber treatments have relatively better scalabilities and in turn, the potential to become implemented at industrial scale. At present, the use of enzymes for fiber treatments is more expensive than chemical treatments. However, in terms of environmental impact, enzymatic treatment and enzyme-catalysed fiber treatments (e.g. enzyme treatment and controlled microbiological retting) have a much lower environmental impact than chemical and chemically catalyzed fiber treatments (e.g. esterification and alkali treatment).

Physical modification processes

Traditional retting

Retting is a typical process based on the action of microorganisms to remove non-cellulosic components from natural fibers obtaining cellulose-rich fibers. Nowadays two different traditional retting methods are used: field retting and

water retting (Tahir *et al.*, 2011). Both are based on the proliferation of pectinolytic microbial communities. The water can in this way penetrate in the stem structure increasing the moisture absorption and boosting the proliferation of microorganisms (Musio, Müssig and Amaducci, 2018). In accordance with the presence of glucanase activity, a decrease in mechanical properties of fibers is verified; it is usually attributed to loss and damage of the cellulose in the fibers (Liu *et al.*, 2015). Undoubtedly, traditional water retting consumes a large amount of water and causes eutrophication (van der Werf and Turunen, 2008).

Mechanical treatment

It is often required to separate hemp bast and shives. The products are mainly long fibers which are highly valuable and short fibers that could be used for thermal insulation. The treatment can even decrease some defects such as kink bands. The main drawback is related to the reduction of sever damages generated by mechanical treatment whilst maintaining high efficiency of the process (Keller *et al.*, 2001).

Steam explosion

This is a thermo-mechanical chemical defibration method that allows for breakdown of the lignocellulosic structural components via a sharp pressure change. In order to defibrillate fiber bundles into single fibers and small fibers bundle, the process can degrade and disrupt the middle lamella between the individual fibers (Kukle *et al.*, 2011). It was also shown to be more effective in degrading pectin from middle lamella regions allowing the production of elementary bast fibers.

Microwave and ultrasound treatment

Microwave and ultrasonic treatment have been widely used for treating biomass as well as for degumming process (Nie *et al.*, 2020). These methodologies are supposed to possess high efficiency in modification of biomasses (Klein *et al.*, 2018). The ultrasound treatment is an eco-friendly method which does not require any chemical reagents, even if its effect is very low. The process is able to destroy the surface structure removing the surface wax layer and silica of lignocellulose as well as reducing the particle size (Luo, Fang and Smith, 2014). However, it is quite hard to realize the entire delignification process only by ultrasound. Besides, microwave treatment can complete the delignification process requiring, though, a lot of energy (Yan et al., 2021). The microwave heating could be efficiently applied to biomass structure since it can easily cause molecular friction leading to a uniform heating.

Solid-state mixing: ball milling technology

In recent years, there has been a growing awareness of the importance of the environmentally friendly design of chemical products and processes. The concept of sustainability is strongly impacting the chemical community, which is more and more focusing on minimizing the use of hazardous substances and adopting green strategies (Anastas and Kirchhoff, 2002). Ball milling is a mechanical technique widely used to grind powders into fine particles and blend materials (Moosakazemi et al., 2017). Being an environmentally-friendly, cost-effective technique, it has found wide application in industry all over the world. It generally consists of a hollow cylindrical shell rotating around its axis, which is partially filled with balls made of e.g. steel, stainless steel, ceramic or rubber. It relies on the energy released from impact and friction between the balls (grinding or milling medium) and the powder. The advantages of this technique include cost-effectiveness, reliability, ease of operation, reproducible results due to energy and speed control, applicability in wet and dry conditions on a wide range of materials (e.g. cellulose, chemicals, fibers, polymers, hydroxyapatite, metal oxides, pigments, catalysts). Moreover, ball milling has a high influence on the microscopic and macroscopic properties of the resulting material such as structure, morphology, crystallinity and thermal stability (Piras, Fernández-Prieto and De Borggraeve, 2019). In contrast, potential disadvantages include the possibility of contamination, the formation of nanomaterials with irregular shape, noise, long milling and cleaning times.

Innovative physical treatments

Physical treatment of natural fibers using corona, UV, plasma or gamma radiation can change structural properties and surface properties of the fibers and thereby influence the mechanical bonding between fibers and matrix polymers. Corona treatment is a physical surface modification technique that uses low-temperature corona discharge plasma to oxidize fiber surfaces and impart changes in the surface properties. Corona treatment could result in a surface oxidation and etching effect, leading to an improvement of the interfacial compatibility between fibers and matrix polymers (Faruk *et al.*, 2012).

Ultraviolet (UV) light is known for its shorter wavelength and higher energy than visible light. Exposing natural fibers to UV radiation has been widely used in fiber surface modification. UV light (preferably at wavelength of 185 and 254 nm) in the presence of oxygen generates atomic oxygen and ozone that results in the fiber surface being more hydrophilic. In principle, the increased polarity of fibers after UV treatment is disadvantageous for

composite use especially when other hydrophobic polymers are used, while increased polarity of fibers results in higher grafting and esterification efficiency. Plasma treatment, especially cold plasma treatment, is another physical treatment to modify fiber surface without affecting the bulk properties of fibers. Plasma treatment can be performed under vacuum and under atmospheric conditions (Dorris and Gray, 1979a). The hydrophilic nature of hemp fibers was reduced by the etching effect of plasma, presumably due to the migration of hydrophobic compounds from the fiber bulk to the surface (Dorris and Gray, 1979b). Increased hydrophobicity of the fiber surface is favorable for the mechanical performance of hemp fiber-reinforced composites.

Chemical modification processes

The hydrophilic nature of cellulose-rich fibers is a restriction for successful use of natural fibers in composite applications. The hydrophilicity of natural fibers is mainly contributed by hydroxyl groups of cellulose and other hydrophilic non-cellulosic components. Surface modification aims to reduce the hydrophilic nature of cellulose-rich fibers mainly by replacing hydroxyl groups of cellulose with less hydrophilic (e.g. $O{-}Na^{+}$) or hydrophobic chemical groups (e.g. acetyl groups (CH_3CO)). Reduction of the hydrophilic nature of cellulose-rich fibers is thought to increase bonding between fibers and hydrophobic polymers. Different chemical treatments can be applied to enhance the effectiveness of interfacial bonding between the fibers and the matrix (Ali *et al.*, 2018a). Following some important treatments performed on natural fibers are listed.

Alkali treatment

This process leads to fibrillation of fibers and causes the breakdown of bundles of fibers into smaller fibers. Besides the removal of a certain portion of hemicellulose and lignin through NaOH, known as mercerization, can reduce the amorphous hydroxyl group content by the reaction between alkali and hydroxyl groups, as shown below (Kabir *et al.*, 2013). The removal of hemicellulose and lignin covering materials can expose more hydroxyl groups of cellulose to alkali. As a result, the hydrophilic nature of natural fibers is reduced and the surface of natural fibers becomes very clean and smooth (Sawpan, Pickering and Fernyhough, 2011a), which can improve adhesion between fibers and matrix binders (Das, Prasad and Chakrabarty, 2009).

$$\text{Fibre} - \text{OH} + \text{NaOH} \rightarrow \text{Fibre} - \text{O}{-}\text{Na}^{+} + \text{H}_2\text{O}$$

Due to this, hydrophilic nature of the fiber is reduced. Finally, even the chemical composition of fiber, the degree of polymerization and molecular

orientation of cellulose crystallites are affected by mercerization process since it is able to convert the crystalline form of cellulose I to cellulose II (Bledzki, Fink and Specht, 2004).

Esterification

Esterification treatment is commonly used to reduce the hydrophilic character of natural fibers by forming ester bonds between hydroxyl groups of cellulose-rich fibers and carboxylic acid groups of other chemical reagents such as acetic anhydride, maleic anhydride and vinyl acetate. The esterification reaction may be conducted at room temperature or at elevated temperature with or without catalysts (e.g. acids, pyridine or potassium carbonate) (Özmen, 2012). Acetylation is one of the most commonly used esterification reactions to replace hydroxyl groups (OH) with acetyl groups (CH_3CO) by using acetic anhydride (i.e. glacial acetic acid) or vinyl acetate as reagents. As a result, the hydrophilic nature of the fiber decreases. Treatment also breaks down the hemicellulose–lignin covering from the fiber surface exposing the cellulose surface for matrix adhesion.

Silanization

Alkoxy silane is a multifunctional molecule, which is commonly used as a coupling agent to modify natural fiber surfaces. Alkoxy silanes can form chemical bonds with hydroxyl groups on fiber surfaces (Alix *et al.*, 2009). The vinyltrimethoxysilane and aminopropyl triethoxy silane are the commonly used silane in order to obtain reliable modification of natural fibers (Sanjay *et al.*, 2019). During silane treatment, silanes undergo hydrolysis, condensation and bond formation stage. In the first step, silanols are formed after alkoxysilanes are hydrolyzed in the presence of moisture (Sreekala *et al.*, 2000). The silanols then react with the hydroxyl groups on fiber surface in the condensation stage and eventually form chemical bonds (i.e. fiber-O-Si).

Peroxide treatment

The use of peroxide treatments has gained the interest for treatment of cellulosic fibers, since the ease of the process. Organic peroxides, decomposed to free radicals, can react with cellulose and also hydrogen groups of matrix (Sreekala *et al.*, 2000). The schematization of peroxide treatment is shown below:

$$RO + \text{Cellulose-H} \rightarrow \text{R-OH} + \text{Cellulose}$$

Benzoylation

Benzoylation exploits the use of benzoyl chloride for the fibers treatment. Benzoyl chloride includes benzoyl groups ($C_6H_5C{=}O$) which contributes to

decrease the hydrophilic nature of the treated fiber improving the interaction with the hydrophobic matrix.

Maleic anhydride treatment

This treatment modifies both the fiber surface and polymeric matrix thus improving the interfacial bonding between them (Koohestani *et al.*, 2019). Maleic anhydride is known to remove the hydroxyl groups of the cellulose to make it compatible with polymeric matrix as well as forms carbon–carbon covalent bond. This covalent bonding between OH groups of the fiber and anhydride groups of the maleic anhydride makes a bridge interface for the efficient interlocking (Zhou, Fan and Chen, 2016).

Graft co-polymerization

Besides silanes, other functional molecules have been used in fiber surface modification for improving the wettability of hemp fibers. Wettability can be increased by graft copolymerizing short-chain molecules and polymers onto the fibre surface using silane coupling agents or other copolymers or functional molecules such as isocyanatoethyl methacrylate (IEM) (Chen, Tsai and Yang, 2011), glycidyl methacrylate (GMA) (Singha and Rana, 2010; Moawia *et al.*, 2016), methyl methacrylate (MMA) (Ni *et al.*, 2015) or alkyl gallates (Sreekala *et al.*, 2000). In previous studies, a combination of 1, 6-diisocyanatohexane (DIH) and 2-hydroxyethyl acrylate (HEA) was used to modify hemp fiber surfaces resulting in significantly increased tensile strength, flexural modulus of rupture (MOR), and flexural modulus of elasticity (MOE) in fiber/unsaturated polyester composites (Alix *et al.*, 2009). Other coupling agents such as isocyanatoethyl methacrylate (IEM) have also been tested in hemp fiber surface modification. IEM is a heterofunctional monomer with a reactive isocyanate group and a vinyl polymerizable double bond, and the two functional groups can react independently with other amorphous hydroxyl groups or vinyl monomers on the fiber surface respectively (Sreekala *et al.*, 2000). The treatment effect also changes the contents of cellulose, hemicellulose and lignin.

Microbiological treatment

Enzymes, as biocatalysts, can catalyze selective removal of no cellulosic components from hemp fibers. Compared to chemical treatment, bio catalyzed reactions can be performed under mild conditions, i.e. low temperature and near-neutral pH. Enzyme treatment involves mainly pectinolytic enzymes thus offering an environmentally friendly and efficient method for separating fibers and removing non-cellulosic components from natural plant fibers. In practice, the treatment of natural plant bast fibers with pectinolytic enzymes (e.g. endo-polygalacturonase) induces the release of pectic polymers from the

middle lamella and fiber cell walls as the enzymes catalyze random hydrolysis of the glycosidic bonds of the homogalacturonan backbone to liberate monomeric, dimeric or oligomeric fragments. After removal of pectin, the bonding between fibers becomes weaker and individual fibers and small fibers bundles can be separated from the larger fiber bundles. The fiber surfaces became cleaner after the treatment and an improvement of mechanical properties of fiber-reinforced composites is obtained compared to the composites produced with traditional field retted fibers. Li and Pickering (2008) (Li and Pickering, 2008) reported a decrease in pectin content from 6.2 %wt in untreated fibers to 5.7 %wt after hemp fibers were treated with pectinase. However, the enzymes cannot directly penetrate the hemp fibers to degrade pectin efficiently. The accessibility of the substrate surface to enzymes is therefore important in enzyme treatment of natural fibers, and pre-treatment of natural fibers is thus necessary to achieve well-separated fibers with pectinase treatment.

Environmental and economic consideration

The techniques such as esterification and grafting chemical compounds or polymers onto the fiber surface are usually performed under harsh conditions, which can weaken the fibers and cause environmental problems. Enzyme-catalysed grafting of phenols and other hydrophobic polymers can be accomplished under mild conditions in which no or little damage are introduced to fibers, thus applications of enzymes can overcome the drawbacks of chemically-catalysed/assisted reactions. Those enzymes include oxidase enzymes such as laccase and peroxidases. Those enzymatic fiber pre-treatment methods are environmentally friendly. However, the mechanisms behind enzymatic reactions involving solid substrates (i.e. plant fibers) during fiber treatments are not fully understood. Since the increasing environmental concern is a major driving for intensive studies on renewable and biodegradable materials to replace those petrochemical-based materials, in pre-treatment and production of new materials the environmental effects of fiber treatment techniques should be seriously considered. The use of chemicals especially EDTA, acids, alkalis, metallic salts and other oxidizing agents (e.g. sodium hypochlorite), may not only weaken fibers but also potentially cause environmental problems like soil contamination and soil acidification. The application of enzymes can overcome those drawbacks, and enzymatic treatments are more controlled and more targeted compared to chemical treatments. However, the cost of enzymes is currently higher than chemicals. Therefore, the high cost of enzymes and low impact on environment need to come to a compromise, when enzymes are applied in large-scale fiber treatment (Liu *et al.*, 2017)

2.Aim of the research

The design and the preparation of composite materials made of renewable and sustainable resources has become one of the greatest challenges of materials science and technology. In the framework of sustainability and circular economy, natural cellulosic fibers, such as hemp fibers, are becoming attractive as potential substitutes of synthetic fibers or raw material for the production of novel bio-composites. However, the lack of fundamental knowledge in the processing of the raw materials to produce composites from renewable sources is still a major challenge for their production and applications. The key factor to obtain bio composites with improved physical properties for specific end-use applications concerns a good fiber-matrix adhesion, to tackle the bio fiber drawbacks and to improve compatibility with the matrix. So, it comes up the necessity of performing physical and chemical treatments since it is compulsory to improve the fiber-matrix compatibilization or to confer specific properties to natural fibers. By stating that, this PhD thesis concerns the design of different approaches to improve physical or chemical properties of natural fibers. The novel proposed methods allowed to design novel and sustainable material derived from hemp fibers and sustainable polymers with high performances which emerge to be potentially applicable in different industrial fields such as building sector, magnetic novel materials, water remediation, food packaging and agricultural applications.

3.Materials&Methods

Materials

Hemp fibers (*Cannabis sativa L.*), obtained from the decortication of hemp basts, were supplied by NAFCO Company srl (Naples).

Methods

Scanning electron microscopy (SEM) was adopted to investigate the morphology of the samples. Before the analysis, sample were covered with a thin film of gold by sputtering. Images were acquired by a Phenom ProX microscope integrated energy-dispersive X-ray diffraction (EDS) working in high vacuum mode.

X-Ray diffraction patterns were taken, in reflection, with a Philips X'PERT PRO MPD diffractometer (PANalytical, Royston, UK) operating at 40 kV and 40 mA, with a step size 0.0330 of 2θ degree, and step scan 60 s, using Cu Kα radiation and an X'Celerator detector.

Fourier transform infrared (FT-IR) analysis was performed using a Bruker spectrometer (Bruker Italia, Milano, Italy), model Vertex 70. Attenuated total reflection (ATR) infrared spectra were recorded with an incidence angle of the radiation on the ATR crystals equal to 45°. Analyses were performed by acquiring the background in air and accumulating 32 spectra for each measurement at a resolution of 4 cm^{-1}.

Raman spectra were obtained with a Raman spectrometer Renishaw inVia with a 785 nm excitation wavelength (laser power 30 mW) in the range 100 - 3200 cm^{-1} performed at room temperature.

Thermogravimetric analysis (TGA) were carried out in air or nitrogen atmosphere with a Mettler TC-10 thermobalance at a heating rate of 10 °C/min.

Differential scanning calorimetry (DSC) were carried out with a thermal analyzer Mettler DSC 822/400 under N_2 atmosphere at a heating rate of 10 °C/min.

Sorption-desorption isotherms of water vapor were evaluated using a DVS Automated multi-vapor gravimetric sorption analyzer, using dry nitrogen as a carrier gas. The temperature was fixed to 30°C. Samples were exposed to increasing water vapor pressures obtaining different water activities $a_w=P/P_0$ where P is the partial pressure and P_0 is the saturation water pressure at the temperature of the experiment. The adsorbed and desorbed water mass was measured by a microbalance and recorded as a function of time and expressed as C_{eq} ($g_{solvent}/g_{dry\ basis}$). The sorption parameters (S) were obtained from the equilibrium concentration (C_{eq}) of the permeant vapor as a function of the partial pressure (eq. (1)).

$$S=\frac{dc_{eq}}{dp} \tag{1}$$

The diffusion coefficient for films can be evaluated from sorption kinetics, using Fick's second law solution. From the mass transfer balance, without considering the convection contribution and the diffusion along the edges, the Fick's second law can be expressed by eq. (2):

$$\frac{\partial c}{\partial t}=D\frac{\partial^2 c}{\partial x^2} \tag{2}$$

Where x is the spatial coordinate considering the process isotropic one-dimensional. To be solved, the equation requires two spacial boundary conditions and one boundary condition on time. Considering the permeation through a thin membrane, the equation admits the following solution eq. (3) [46]:

$$\frac{c-c_i}{c_{eq}-c_i}=1-\frac{4}{\pi}\sum_{j=0}^{\infty}\frac{1}{(2j+1)}\frac{\sin(2j+1)\pi x}{d}\exp\left[-\frac{(2j+1)^2\pi^2 Dt}{d^2}\right] \tag{3}$$

where C_i is the initial concentration inside the sample, C_{eq} is the maximum saturation concentration, d is the characteristic length of the sample, and D (cm^2/s) the diffusion coefficient. In order to evaluate the penetrant concentration at the time t, the above equation can be integrated over length x (eq. (4)):

$$\frac{m-m_i}{m_{eq}-m_i} = 1 - \frac{8}{\pi^2}\sum_{j=1}^{\infty}\frac{1}{(2j+1)^2}\exp\left[-\frac{(2j+1)^2\pi^2 Dt}{d^2}\right] \quad (4)$$

with m_i=initial mass of moisture and m_{eq}=mass of moisture when saturation is reached. For cylindrical systems, such as hemp fibers, the evaluation of the diffusion coefficient came from the mathematical analysis of experimental data. Considering the fiber as a cylinder with uniform radius r in which the diffusion is only radial, the second Fick's law can model the behavior of moisture absorption with respect to the time according to eq. (5) (Crank, 1979):

$$\frac{dc}{dt} = \frac{1}{r}\frac{d}{dr}rD\frac{dc}{dr} \quad (5)$$

Assuming that the diffusant is initially uniform in the film, the solution of Fick's second law, for monodimensional transport, is expressed by the following eq. (6) (Crank, 1979):

$$\frac{M_t}{M_\infty} = 1 - \sum_{n=1}^{\infty}\frac{4}{\alpha_n^2}\exp\left(\frac{-\alpha_n^2 * D * t}{r^2}\right) \quad (6)$$

Where t is the experimental time, D is the diffusion coefficient (cm^2/s) and M_∞ is the mass of permeant water absorbed evaluated at equilibrium steady state. The parameter α_n represents the positive roots of the first species of Bessel's function of zero order (Crank, 1979) while r is calculated through the geometric mean of 50 radius values. The permeability is then evaluated by using the eq. (7):

$$P = S * D_0 \quad (7)$$

Mechanical properties of the samples were evaluated, in tensile mode, at room temperature using a dynamometric apparatus INSTRON 4301. Experiments were conducted at room temperature. Elastic modulus was evaluated in the deformation range of 0.1%. Data were averaged on five samples.

The release and adsorption kinetics were performed through an ultraviolet spectrometric measurement using a Spectrometer UV-2401 PC Shimadzu (Japan). Adsorption capacity (q_t) and removal efficiency ($R_{\%}$) were evaluated through eqs (8) and (9):

$$q_t = \frac{(c_0 - c_{eq}) * V}{m} \quad (8)$$

$$R_{\%} = \frac{(c_0 - c_{eq}) * 100}{c_0} \quad (9)$$

Where c_0 (mg/L) is the initial dye concentration, c_{eq} (mg/L) is the equilibrium dye concentration, V(L) is the volume of the dye solution and m (g) is the mass of the beads (Mohammad and Atassi, 2020).

Atomic force microscope coupled with HarmoniX tool (Multimode Dimension V coupled with Nanoscope V, Veeco, Santa Barbara, CA, USA) was adopted for the simultaneous characterization of morphology and elastic modulus distribution of the samples. The HMX probe silicon cantilevers, with 10 nm nominal radii (Bruker, Billerica, MA, USA), was selected for the characterization. The vertical frequency and the torsional frequency were, respectively, 31 kHz and 1114 kHz. The cantilever vibration-free amplitude was of 750 mV, in air 60% of the vibration-free amplitude was adopted for the feedback control and the modulation of the force level. All the acquired maps were obtained with 0.5 Hz scan rates and 21 harmonics. Two movement were applied to the cantilever with the aforementioned configuration of the atomic force microscope, the vertical movement, which allows the characterization of the surface sample topography and the torsional movement, which allows the acquisition of the force generated during the tip-sample approach/withdraw, and allows the characterization of the mechanical properties through the Derjaguin-Muller-Toporov model (Derjaguin, Muller and Toporov, 1975), already implemented in the Bruker NanoScope software, version 7.30. The root mean square, evaluated adopting the plugin implemented in the Nanoscope software, was adopted to characterize the surface roughness (Stoica *et al.*, 2015).

Contact angle measurements were performed using a high-resolution camera. Droplets of solvents (100 μL) were dispensed on a 1x1 cm^2 test sample at room temperature. The contact angle was determined using Drop Analysis software. The estimation of contact angle allowed to evaluate the total surface energy of a solid as the sum of the dispersive and polar surface-energy components, using the two probe liquids method.(Hejda, Solař and Kousal, 2010; Gutierrez-Villarreal, Rodríguez-Gonzalez and Perera-Mercado, 2017) The method, based on a geometric-mean approach developed by Fowkes and later by Owens and Wendt (Tran et al., 2011), consists of a two equations system (eqs (10) and (11)):

$$\gamma_s=\gamma_s^d+\gamma_s^p \tag{10}$$

$$(1+\cos\theta_i)*\gamma_{L,i}=2\sqrt{\gamma_s^d\gamma_{L,i}^d}+2\sqrt{\gamma_s^P\gamma_{L,i}^P} \tag{11}$$

Where γ_s is the surface free energy ($mJ\cdot m^{-2}$); $\gamma_{L,i}$ is the surface free energy of the liquid used ($mJ\cdot m^{-2}$); $\gamma^d_{L,i}$ is the dispersion component of the liquid surface free energy ($mJ\cdot m^{-2}$); $\gamma^p_{L,i}$ is the polar component of the liquid surface free energy ($mJ\cdot m^{-2}$); γ^d_S and γ^p_S are the dispersion and polar components of the fiber surface free energy ($mJ\cdot m^{-2}$); θ is the contact angle of the liquid i

dropped onto the film surface. The polar and disperse components surface energy were determined using the method of Owens–Wendt–Rabel–Kaelble (OWRK) which allows for a linearization of the contact angles using eq. (12) (Pietak et al., 2007) :

$$\frac{(1+\cos\theta)*\gamma_{L,i}}{2\sqrt{\gamma_{L,i}^{d}}}=\sqrt{\gamma_{s}^{p}}\sqrt{\frac{\gamma_{L,i}^{p}}{\gamma_{L,i}^{d}}}+\sqrt{\gamma_{s}^{d}} \quad (12)$$

The unknown parameters γ^{d}_{S} and γ^{p}_{S} were evaluated by linear fitting.

Thermodynamic work of adhesion W_a is the energy required to separate a unit area of interface and can be described with Young-Dupré equation (eq. (13)) (Ebnesajjad and Landrock, 2015):

$$W_A = \gamma_L(1 + \cos\theta) \quad (13)$$

Density was evaluated according to ASTM D792 (*ASTM D792 - 20 Standard Test Methods for Density and Specific Gravity (Relative Density) of Plastics by Displacement*, no date).

Bending properties were evaluated by carrying out the three-point bending test conducted using a SANS Series dynamometer (by MTS, China), according to ASTM D790-03 (D790-07 and 2007, no date). The specimen dimensions for flexural properties were 70 × 13 × thickness; the span-to-depth ratio was 16, coupled with a crosshead speed (R) evaluated by using eq. (14):

$$R=\frac{ZL^2}{6d} \quad (14)$$

The flexural strength (σ_f) was evaluated according to eq. (15):

$$\sigma_f=\frac{3F_{max}S}{2bh^2} \quad (15)$$

Where F_{max} is the maximum load, S is the span in mm, b is the specimen width in mm and h is the specimen height in mm. The flexural modulus E_f was calculated using the initial slope ($\Delta F/\Delta x$) of the load–displacement curve according the eq. (16):

$$E_f=\frac{S^3}{4bh^3}\frac{\Delta F}{\Delta x} \quad (16)$$

Point of zero charge (pH_{PZC}) was evaluated as reported hereinafter. The point of zero charge (PZC) is the pH of the solution at which the net surface charge is zero. An initial solution of $NaNO_3$ (0.1 M) was prepared. An aliquot of 40 mL of $NaNO_3$ solution was collected in ten flasks. The pH was set from 3 to 12 by using HCl (1M) and NaOH (1M) solutions. Then, a fixed amount of sample was placed inside the flasks, shaked for 24 h, at room T and 350 rpm. After that, the solid adsorbent was removed and the final pH (pH_f) was

evaluated by using a pH-meter (Crison-pH-Burette 24 1S). The change in pH was calculated as follows (eq. (17))

$$\Delta pH = pH_i - pH_f \quad (17)$$

A plot of ΔpH versus pH_i was obtained from the experimental data. The pH_{PZC} was easily estimated by the intercept on x-axis of the curve.

Solubility (SOL) was evaluated according to the method described in the literature (Romero-Bastida et al., 2005; Prakash Maran et al., 2013). Samples were weighed and immersed into a beaker with 50 mL of distilled water. The beaker was sealed to avoid water evaporation and stored at 25°C for 24h under mechanical agitation (100 rpm). After 24h, the samples were removed from the beaker and dried in vacuum oven at 40°C. SOL (%) was evaluated through eq. (18):

$$SOL(\%) = \frac{M_0 - M_1}{M_1} * 100 \quad (18)$$

Where M_0 and M_1 were the dry sample weights before and after the test, respectively.

Gas chromatography analysis was performed using a TraceGOLD™ TG-WaxMS GC capillary column (0.25 µm × 0.25 mm × 30 m) from 50 to 250 °C, 6 °C/min. Injector and detector temperatures were set at 200 and 250 °C, respectively. Parameters: Carrier gas helium, column flow 1 mL/min, split flow 50 mL/min, split ratio 50:1; injection volume 1 µL; FID: temperature 250 °C.

Transparency was determined through an ultraviolet–visible (UV–Vis) spectrophotometer UV-2401 PC Shimadzu (Japan) by evaluating the light transmission in UV-Vis range (200nm–800nm) A film sample (4cm×1.5cm) was placed into the cell of the spectrophotometer and the transmission value at a wavelength of 600 nm was recorded. The transparency of the films was then evaluated by using eq. (19) (Han and Floros, 1997; Pérez-Mateos, Montero and Gómez-Guillén, 2009; Pattarasiriroj, Kaewprachu and Rawdkuen, 2020):

$$\text{Transparency (Tr)} = -\frac{\log(T_{600})}{x} \quad (19)$$

Where T_{600} is the transmittance taken at 600 nm, and x is the film thickness (mm). The lower the transparency index value is, the higher is the transparency.

The acid-base potentiometric titration curves in salt concentration (NaCl 0.1M) were used to measure the proton adsorption or proton charge. All

experiments for charge determination were carried out at 25°C. An aliquot of aqueous suspension (40 mL) containing 0.2 g of sample was equilibrated for 30 minutes until equilibrium pH was reached. The titration started with the addition of NaOH; the pH rapidly reached a constant value and remained invariable with time. The titration was carried out using HCl solution (1M) and stopped when the pH was roughly 2.5. The proton adsorption or proton surface charge density σ_H (mol/m^2) determined from potentiometric titration was calculated as the difference between total amounts of H^+ added to the dispersion and that were required to bring a blank solution of the same NaCl concentration to the same pH (A.Kriaa, N.Hamdi and E.Srasra, 2008) (eq. (20))

$$\sigma_H = \frac{V}{m*S} * \left\{ ([H^+]_b - [H^+]_s) - \left(\frac{K_w}{[H^+]_b} - \frac{K_w}{[H^+]_s} \right) \right\} \quad (20)$$

Where V is the volume of electrolyte solution (0.04 L), m is the sample mass, S is the specific surface area, $[H^+]$ is the solution proton concentration (mol/L), subscripts b and s refer to blank and sample solutions while K_w is the dissociation product of water ($1*10^{-14}$).

DC magnetic measurements have been performed by means of a 9 Tesla Quantum Design PPMS (Physical Properties Measurement System), equipped with an AC Measurement System (ACMS) insert, by using DC Extraction Method. Before each measurement, the residual trapped field inside the superconducting magnet was reduced below 1 Oe (Galluzzi *et al.*, 2018) to prevent its effect on the sample response (Galluzzi, Buchkov, *et al.*, 2019; Galluzzi, Nigro, *et al.*, 2019).

Statistical analysis

Statistical analyses were conducted using Origin Lab. Results were expressed as the mean value ± standard deviation (SD). ANOVA and Tukey's tests were performed to compare the obtained results at a significance level of $\alpha < 5\%$. The curve fittings were evaluated by non-linear regression. The coefficient of determination (R^2) was evaluated to assess the goodness of the fitting.

4.Novel mechanochemistry based technique for functionalizing hemp fibers

Preface

In the perspective of obtaining an improved fiber-matrix adhesion, it is necessary to remove non-cellulosic materials of hemp fibers and to expose the crystalline part of the inner cellulosic matrix. Cellulose content is known to influence physical, thermal, mechanical, and chemical properties (Agarwal, Reiner and Ralph, 2010). To achieve this target, physical and chemical transformation is needed to modify the fibers surfaces. Among all, the treatment with alkaline agents are the most used to remove non-cellulosic materials and to debond the amorphous region of hemicellulose and cellulose as well. Moreover, the treatment often requires high temperatures (up to 120 °C) (Zhang, Zhang and Zhang, 2014) or long treatment times (up to 48 h) (Aziz and Ansell, 2004; Le Troëdec *et al.*, 2009; Sullins *et al.*, 2017). To operate at as low as possible temperatures and times, avoiding harsh experimental conditions, an alkaline treatment has been performed by means a solid-state treatment using the mechanical milling (MM) technology. The simultaneous possibility to avoid high temperature, the advantage linked to the promotion of mechano-chemical reactions improving the chemical treatment and, as a consequence, the reduction of the amount of reagent needed as well as the experimental time required to fulfill the process,

represent an added value to the preparation and functionalization of natural fibers with improved functional properties.

Materials

Sodium hydroxide, pectin from apples (molecular weight=30,000–100,000: degree of esterification about 70–75%, on a dry basis) and glycerol were used as reagents.

Hemp fiber treatment

Dried hemp fibers (HF) were soaked in liquid nitrogen for 3 hours. Then, frozen fibers were cut using a grinder (Duronic-CG250). The ground fibers were then treated with a 5% w/w alkaline solution (HF/NaOH=1:1 w/w) fixing a liquor ratio equal to 1:20 through a mechano-chemical functionalization employing a high energy ball milling (HEBM-Retsch-PM 100) using a stainless-steel jar (V= 125 mL) and five zirconium oxide spheres as grinding medium. The rotation speed was set at 350 rpm. The experimental time was varied from 30 minutes to 7 hours. The treated fibers were then washed with distilled water until pH=7 was reached and placed in a vacuum oven at 40 °C for 8 hours. The classical alkalization was carried out by treating raw hemp fibers in 5% NaOH/water solution, fixing the ratio HF/NaOH=1:1 w/w. The rotation of the stirring plate was set at 350 rpm while the experiment was performed at room temperature.

Hemp fibers/Pectin composites preparation method

Bio-composites were prepared by dissolving 1 g pectin in 30 mL of water. The solution was stirred on a stirring plate at 90°C for 1.5h. After completely solubilizing the pectin powder, mechanochemically modified hemp fibers at different percentages (3 %w/w; 7.5 %w/w; 10 %w/w; 20 %w/w by weight), were added and the solution was submitted to ball milling at room temperature for 1 h in a Retsch (Germany) planetary ball mill (model PM 100), using a cylindrical steel jar of 50 cm^3 with 5 zirconium dioxide balls of 10 mm of diameter. The rotation speed used was 450 rpm. The mixtures obtained were poured in Petri dishes and slowly evaporated. Films of pure pectin and pectin filled with raw HF were also prepared in the same described experimental conditions.

Characterization of hemp fibers

The initial exposure of hemp fibers to cryogenic temperature leads to development of residual thermal stress, which induces the forces that

contribute to the destruction of the fiber-gum interface. With the interface weakened, the applied external load generates a crack that extends up to debond the interface between the brittle gum and the ductile fibers (Liu, Guan and Li, 2018). The following alkaline treatment induces chemical and structural modification by breaking hydrogen bonds in the lignocellulosic structure according to the following reaction (Mwaikambo and Ansell, 2002; Obi Reddy *et al.*, 2012):

Fiber-OH + NaOH → Fiber–O-Na + H_2O + Surface impurities

The alkaline treatment can remove the non-cellulosic material (natural fats, pectin and waxes) as well as lignin (Kabir *et al.*, 2013), allowing the splitting of fiber bundles in micro fibrils meanwhile the ball milling technique is supposed to have a significant influence on structure, morphology, crystallinity and thermal stability of the treated material (Piras, Fernández-Prieto and De Borggraeve, 2019). Figure (3) shows the SEM micrographs of untreated hemp fibers at two different magnifications.

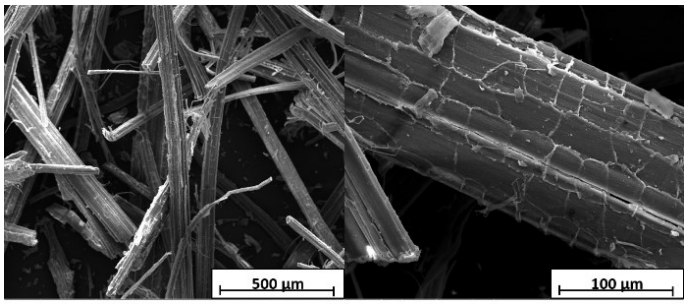

Figure 3 *SEM images of raw hemp fibers*

They show a mean diameter ranging from 25 to 160 µm and a roughened surface due to the presence of non-cellulosic materials. The mechano-chemical treatment induced a conversion in a more irregular state, indicating that the orientation of micro fibrils was disrupted by the treatment. This is evidenced in figure (4), which shows that the surface of hemp fibers after the treatment became smoother as non-cellulosic material and impurities were removed. As a consequence, it was observed a decrease in the fiber diameter (Obi Reddy et al., 2012).

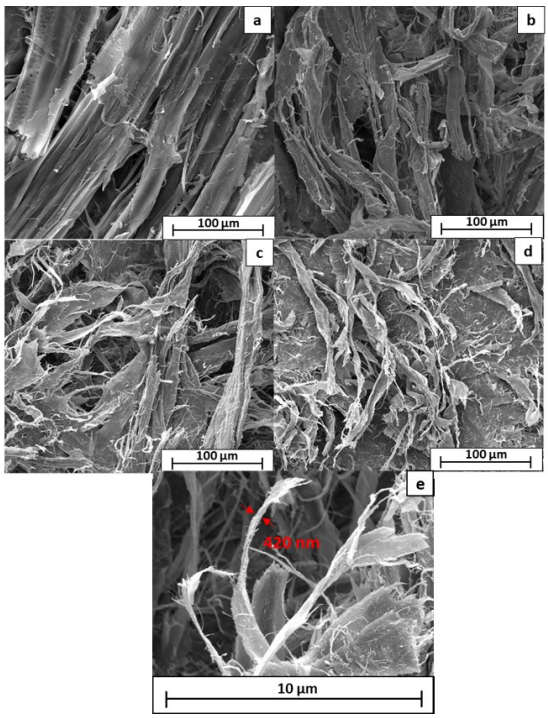

Figure 4 *SEM images of hemp fibers milled for 30 minutes (a), 1 hour (b), 4 hours (c), 7 hours (d) and 7 hours at higher magnification (e)*

As the treatment keeps going, the mechanical action reduces the mean dimension of the fiber bundle, disintegrating it in smaller fibrils with a width of 300-500 nm. The mechanical milling provided shear stresses and turbulence, which combination promoted a high degree of defibrillation. The micro fibrillated cellulose, as aggregates of cellulose nanofibers with amorphous and crystalline regions, was generated. However, since the alkaline ion can induce undesirable reactions leading to cutting down of cellulose chains, the interfibrillar morphology was lost. Figure (5) shows the fiber diameters distributions of raw and treated hemp fibers.

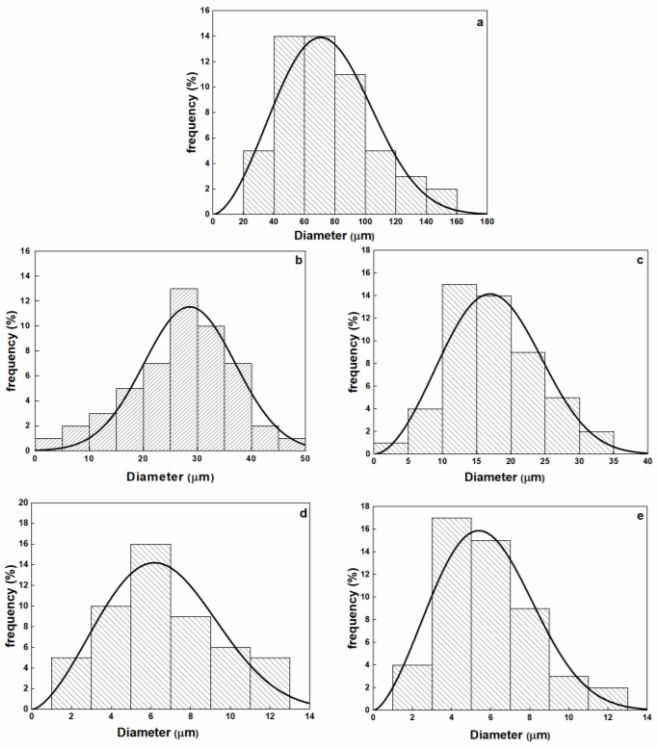

Figure 5 *Diameter distribution for a) raw hemp fibers; b) HF-30min; c) HF-1h; d) HF-4h and e) HF-7h*

The mean diameter ranges from 74.36 ± 29.81 μm (raw hemp fibers) to 17.58 ± 6.79 μm, 6.61 ± 2.79 μm and 5.77 ± 2.42 μm for HF-1h, HF-4h and HF-7h respectively.

AFM provided details about surface topography before and after mechano-chemical treatment. The topographic images obtained by AFM, performed in triplicates, showed considerable changes in fibers topography after the alkali treatment (Figure (6)). The roughness and modulus values (RMS=root mean square, Adhesion and DMT Modulus), evaluated for each sample, were reported in table 2.

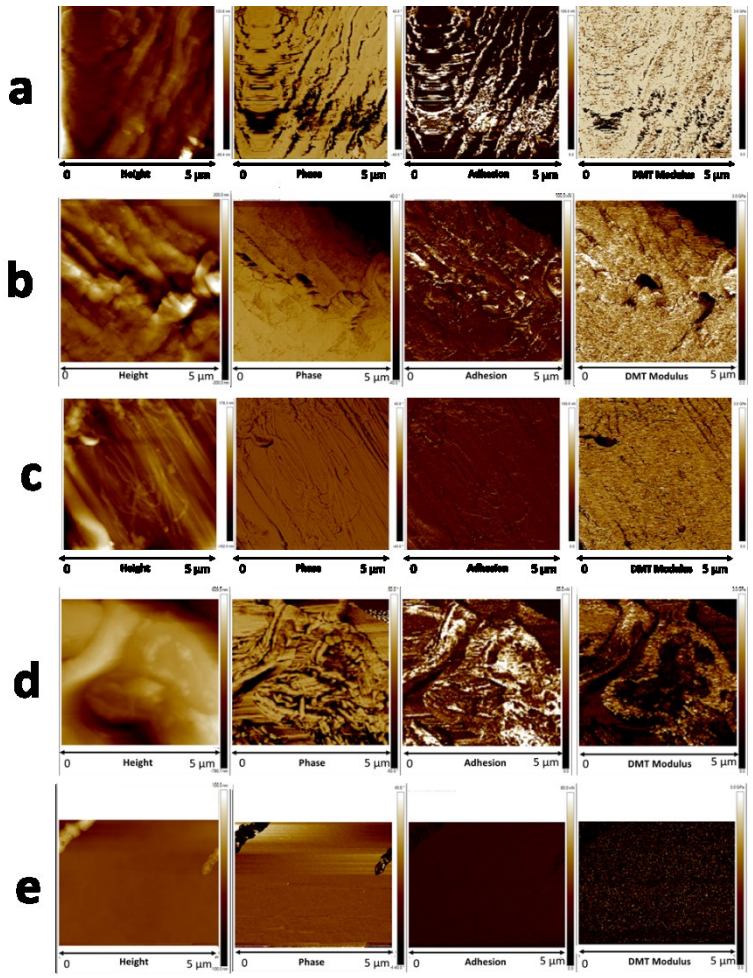

Figure 6 *Topography, phase map, adhesion map and elastic modulus maps of a) HF, b) HF-30min, c) HF-1 h, d) HF-4 h and e) HF-7 h*

Table 2 *RMS, Adhesion and DMT Modulus of raw and mechanochemically treated hemp fibers*

Sample	Rms (nm)	Adhesion (nN)	DMT Modulus (GPa)
Raw hemp fibers	21.34±4.04	44.3±2.27	3.09±0.90
HF-30 min	28.37±2.08	32.3±211	2.01±0.84
HF-1h	33.69±3.35	26.9±3.10	1.67±0.25
HF-4h	39.30±4.20	39.3±11.2	0.82±0.51
HF-7h	1.35±0.02	18.3±2.51	0.40±0.08

The RMS and DMT Modulus were dependent on mechano-chemical treatment time. The removal of non-cellulosic material could affect the macrostructure, leading to a reduction in surface roughness (George *et al.*, 2014). In particular, the AFM analyses revealed that the RMS decreases from 21.34 nm for the raw HF to 1.35 nm for the HF-7h. This effect was due to bundle defibrillation and fiber disruption. Concerning DMT modulus, it decreased as the processing time increases. Such a reduction could be attributed to the removal of external cementing material: the cementing material improved the material rigidity, so its removal led to a modulus reduction (Leite *et al.*, 2006). Concerning the adhesion, the AFM analyses revealed a decrease in such a parameter with the processing time. The values of adhesion depended on the amount of sticky materials, such as waxes. The mechano-chemical treatment induced a significant reduction of waxes amount with the processing time. This finding was consistent with the reduction of the adhesion.

The effect of mechanochemical treatment on crystalline cellulose structure of hemp fibers was firstly studied with X-ray diffraction analysis (figure (7)). The crystallinity index (I_c) was calculated through the Segal equation (eq. (21)) (Segal et al., 1959; Tserki, Panayiotou and Zafeiropoulos, 2005; Le Troëdec et al., 2009; Oudiani et al., 2011; Ling et al., 2019; French, 2020):

$$I_c = \left(\frac{I_{200} - I_{am}}{I_{200}}\right) * 100 \qquad (21)$$

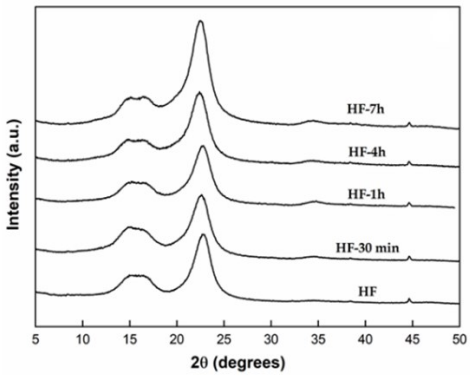

Figure 7 *a) XRD diffractograms of raw and treated hemp fibers*

As far as the raw hemp fibers diffractograms concerns, the two peak at 2θ=14° and 2θ=16°, characteristic of cellulose I, appeared as one band since the presence of amorphous material such as lignin, pectin and hemicellulose (Perel, 1990). As the experimental time increased, the two peaks appeared more pronounced, indicating the removal of the amorphous material. The raw and treated hemp fibres showed the following order of crystallinity index: HF-

30min (I_c=83.87%) > HF-1h (I_c=81.73%) > HF-4h (I_c=80.26%) > HF-7h (I_c=78.57%) ≈ HF (I_c=77.94%). The improved crystallinity index of mechanochemically treated hemp fibers suggests the effective removal of non-crystalline components from the raw hemp fibers. It follows the better packing of cellulose chains (Ouajai and Shanks, 2005) located in the inner part of hemp fibers. The removal of non-cellulosic material promotes the stress relaxation of cellulose chains. Probably, after 30 minutes, the fibrillar region is dense in such a way that the rearrangement is still possible. After that, the effect of either the sodium ion or the mechanical treatment could alter the morphology of the fibers and the length of the polymeric chain. FTIR spectra (figure (8)) were analyzed to investigate the shift of the main functional groups as well as their disappearing/decreasing that confirm the chemical changes due to the mechano-chemical treatment.

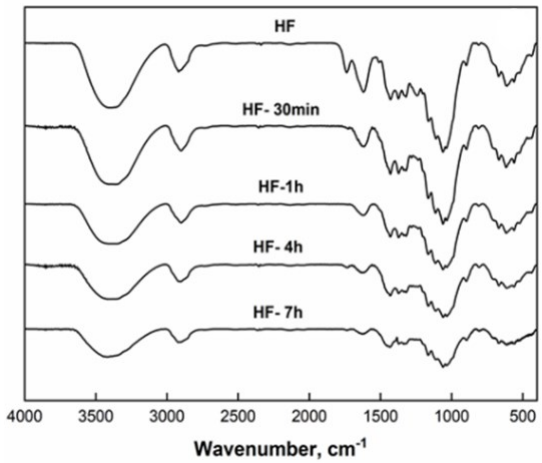

Figure 8 *FTIR Spectra of raw and treated hemp fibers*

The peak area at 3000-3600 cm^{-1}, typical stretching vibration region of OH bonded groups in polysaccharides, underwent a substantial change during the treatment, indicating the modification of the number of OH groups arising due to mechanical-chemical treatment. The cellulose I is stabilized by intermolecular hydrogen linkages involving the C_2 and C_6 positions (Nishimura, Okano and Sarko, 1991). The characteristic bands related to intermolecular hydrogen bonding are located at 3438, 3334, and 3293 cm^{-1}. They belong, respectively, to OH-O bond in C_2-C_6 position, OH-O in C_6-C_6 position, and OH-O bond in C_2-C_2 position. Their characteristic peaks, obtained from the deconvolution process of OH intermolecular band, are shown in figure (9):

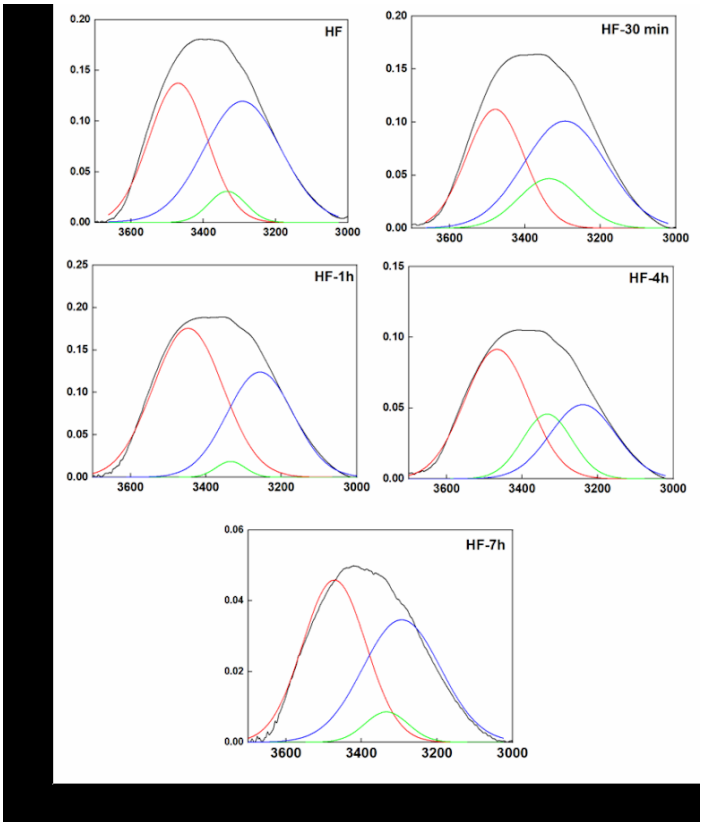

Figure 9 *Characteristic bands of OH bonds in C_2-C_6 position (red curve), C_6-C_6 position (green curve), and C_2-C_2 position (blue curve)*

The intensity of the peak at 3438 cm^{-1} based on the peak absorbance at 1054 cm^{-1} (=C-CO/C-C stretching vibration) could be an estimation of hydrogen bond intensity (Das and Chakraborty, 2006). So, the intensities of C_2-C_6 peak for HF, 30 min, 1h, 4h, and 7h treated hemp fibers at 3438 cm^{-1} are 0.103, 0.171, 0.261, 0.286, and 0.111 respectively. These results are an indication of the effective functionalization through mechano-chemical treatment leading to an intensification of inter and intramolecular hydrogen bonding. The in-plane stretching vibration in the range 2890-3000 cm^{-1} is characteristic of CH groups of hemicellulose and cellulose (Terpáková et al., 2012). The sharp peaks at 2897 cm^{-1} and 2919 cm^{-1} (CH stretching in aromatic methoxyl groups and methylene of cellulose and hemicellulose) seem to be reduced by the treatment and tend to shift toward lower wavenumbers. The removal of hemicellulose could cause the change in these peak positions as reported in other scientific works (Ray and Sarkar, 2001). The effectiveness of mechano-chemical functionalization can be even deduced by the changes in characteristic peak positions such as the disappearing of the peak at 1735 cm^{-}

[1] attributed to C=O stretching vibration of acetyl groups of hemicellulose and methyl ester and carboxylic acid in pectin (Rachini et al., 2009) and the vibration peak at 1373 cm^{-1} belonging to OH groups of carboxylic acids of pectin. This was even confirmed by the reduction of the absorption band at 1555 cm^{-1} representative of ketone and carbonyl groups. The peak at about 1620 cm^{-1} is linked to OH bending of hemicellulose. The reduction of this peak, as ball milling time increases, confirms the effective removal of hemicellulose as the treatment carries on. The effective removal of lignin is demonstrated by the change of C=C aromatic symmetrical stretching vibrations correlated to the changes of vibration peaks at 1510 cm^{-1}, as well as the band at 1454 cm^{-1} belongs to CH_2 bending vibration and the band at 1247 cm^{-1} due to C-O stretching of acetyl (Sawpan, Pickering and Fernyhough, 2011b). The evaluation of the IR crystallinity index could be a useful parameter to evaluate the change in the cellulose structure. The lateral crystallinity index of the fibers was evaluated as the intensity ratio between IR absorptions at 1431 and 897 cm^{-1} assigned to the CH_2 symmetric bending mode and C_1 group frequency, respectively. The peak at 897 cm^{-1} corresponds to β-glycosidic linkages between sugar units in hemicellulose and cellulose (Ray and Sarkar, 2001; Sawpan, Pickering and Fernyhough, 2011b). This small sharp peak underwent a shift to lower wavenumbers (893 cm^{-1}) in the alkali-treated fibers. This could be explained by taking into account the rotation of the glucose residue around the glucosidic bond. The intensity of the 1431 cm^{-1} peak is reduced as the treatment time increases, since it is an indication of the high disorder inside the structure (Krebs, 2012). The evaluated crystallinity indices were 2.05, 1.97, 1.83 and 1.64 for HF-30min, HF-1h, HF-4h and HF-7h respectively. Moreover, a total crystallinity index (TCI) evaluated as the ratio A_{1375}/A_{2900} has also been evaluated (Nelson and O'Connor, 1964). As expected, the total crystallinity index linearly decreased with the milling time, in accordance with XRD analysis. Figure (10) reports the Raman spectra of raw and treated hemp fibers.

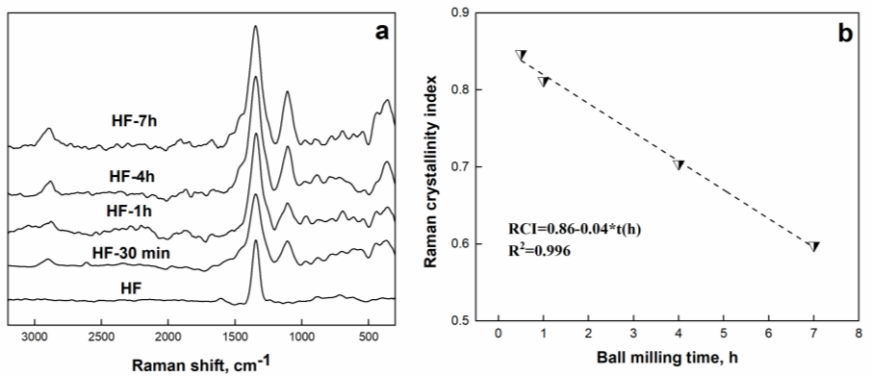

Figure 10 *(a): Raman Spectra of raw HF and treated HF and (b): Raman crystallinity index of treated HF*

The bands at 380 and 1096 cm^{-1}, which were reported to affect the cellulose crystallinity, are sensitive to ball milling (Forziati *et al.*, 1950). The Raman Crystallinity index has been evaluated as the ratio between the peaks at 380 and 1096 cm^{-1}, as reported elsewhere (Agarwal, Reiner and Ralph, 2010). The main peak at 1096 cm^{-1} is characteristic of the C-O stretching mode of cellulose (Eichhorn *et al.*, 2000), while the peak at 380 cm^{-1} is related to only crystalline cellulose I while it is absent for amorphous cellulose.

Sorption and desorption isotherms, obtained by plotting the experimental data of equilibrium moisture content as a function of water activity (a_w from 0.05 to 0.8) are reported in figure (11).

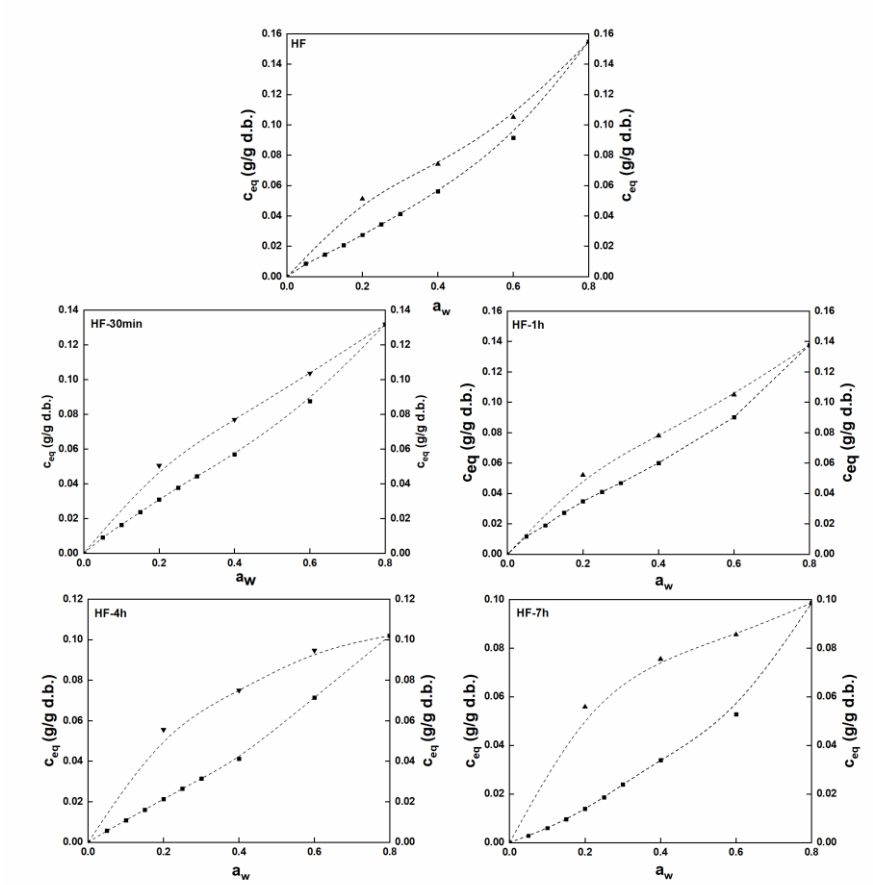

Figure 11 *Sorption (squares) and desorption isotherms (triangles)*

It is evident a different behavior between sorption and desorption cycle of the raw and treated hemp fibers (Okubayashi, Griesser and Bechtold, 2005). The coupled effect due to the fiber size and the alkaline attack could be considered the reason for the noticeable difference in the water absorption (Shinoj, Panigrahi and Visvanathan, 2010). The matrix can be modified by sorbed molecules, which induced swelling phenomena and the expansion of microcapillaries for the thermal motion of water molecules (Tvardovski et al., 1997). After removing water, shrinkage of the cell wall is verified for the relaxation process which is kinetically hindered (Lu and Pignatello, 2002; Hill, Norton and Newman, 2009). Compared to raw HF sample, HF-30 min showed a lower adsorbed water content as a consequence of higher crystalline content (as evidenced from TCI and LOI). As the treatment time increases, the hysteresis loop of treated hemp fibers appeared wider. This is probably due to the bound and freezing water content which increased with the decreasing crystalline content (Hatakeyama and Hatakeyama, 1998). Moreover, the removal of the external layer such as waxy cuticles, which are supposed to possess an open cell structure with capillary network with high tendency to hold water molecules, also reduces the water absorption (Shinoj, Panigrahi and Visvanathan, 2010). All the isotherms follow a typical type II sorption isotherm, according to BET classification (Brunauer et al., 1940), which is a combination of Langmuir behavior and Henry sorption at low activity followed by a power-law behavior typical of Flory Huggins mode. The former induces an increase in polymer chains movement, which leads to a higher sorption rate, so higher diffusion coefficients. The latter generates a larger water molecules size reducing the sorption rate and diffusion coefficient as well. This trend is typical of cellulosic material (Rahman, 2008). The explanation could be attributed to the fact that as the cell wall absorbs moisture, the sorbed water molecules occupy space between the micro fibrils resulting in the expansion of the material. Sorption isotherms show that the adsorbed moisture content dropped as the fiber treatment time increased. The mechano-chemical treatment tends to induce a decrease in sorption, in particular for samples treated for longer times (i.e. 4 and 7 h). The HF-30min possesses a higher crystalline cellulose content, in accordance with FTIR analysis, as a consequence the available OH groups of residual hemicellulose content could explain the initial slight increase in moisture uptake compared to raw fibers. Moreover, as water activity increases, the non-accessible active sites of internal cellulose chains could limit the water molecules affinity and so the sorption properties. For experimental times longer than 30 mins, the hemp fiber bundle structure is converted in a rougher state and the organization and orientation of fibers are totally disrupted. The removal of no-cellulosic material (pectin and amorphous contents) promotes the stress relaxation of cellulose chains which are facilitated to assume a closer packing. As a consequence, the lowering of the interactions water molecules-specific sites, due to the limited accessibility of the active sites, could explain the

reduction in sorption as the milling time increases. In order to analyze the sorption isotherms, the Park multi-sorption model (eq. (22)) was adopted (Stannett et al., 1980):

$$c_{eq} = \frac{A_L * b_L * a_w}{1 + b_L * a_w} + k_H * a_w + k_a * a_w{}^n \quad (22)$$

Where c_{eq} is penetrant concentration at equilibrium, A_L is the Langmuir capacity constant, b_L is the Langmuir affinity constant, k_H is the Henry's solubility coefficient, K_a is the equilibrium constant for cluster formation and n is the mean number of penetrant molecules per cluster. The Park model takes into account the overlapping of three phenomena: 1) Langmuir sorption, 2) Henry sorption, 3) Flory Huggins sorption and water clustering phenomena. The first mode is relative to low activities, the second mode is related to the middle region interstice, while the latter one describes the sorption in the inner region of fibers (Gouanvé et al., 2006). The values of the characteristic parameters of the Park Model are listed in table 3.

Table 3 *Park's model parameters*

	A_L	b_L	k_H	k_a	n	R^2
HF	0.0025	0.050	0.13	0.130	4.21	0.998
HF-30 min	0.0810	0.36	0.12	0.15	8.55	0.997
HF-1h	0.0155	0.093	0.12	0.037	2.19	0.999
HF-4h	0.00088	0.008	0.10	0.099	4.61	0.999
HF-7h	0	0.002	0.076	0.13	5.54	0.998

For the Park model, A_L and b_L are representative of specific hydrophilic groups able to absorb superficial water molecules. The Langmuir capacity A_L is correlated to Langmuir specific charged sites and microvoids as well. For long treatment times (4h and 7h), a better packing of cellulose chains due to the mechanical effect and the decrease in crystalline content (as evidenced by LOI and TCI) can explain the decrease in A_L. The parameter b_L, which represents the Langmuir affinity constant, appeared to slightly increase for HF-30min, probably due to the availability of favorable sites for water adsorption. The decrease in b_L values, for fibers treated at long times, is in compliance with the reduction in surface affinity with solvent molecules and even supports the change of A_L parameter. The disappearing of the rougher surface (due to the presence of pectin and lignin) for the treated hemp fibers limited the retention of water molecules leading to a reduction in the sorption rate. It follows a reduction in the solvent-polymer affinity and a decrease in Henry's sorption parameter (k_H) as well (Bessadok et al., 2007). The k_a and n variation, which could take place in the inner part of the fiber bundle as well as in the macropores of cell-wall (Bessadok et al., 2009), clearly increased for fibers treated at long processing times. In general, the lower are k_a and n values

the smaller is the cluster size. The sorption, diffusion and permeability parameters are reported in table 4.

Table 4 *Sorption, Diffusion and Permeability coefficients*

	Sorption parameter (S) $\frac{g}{g\,d.\,b.} * \frac{1}{atm}$	Diffusion parameter ($\bar{D}$) $cm^2 * s^{-1}$	Permeability (P) $\frac{g}{g\,d.\,b.} * \frac{1}{atm} * cm^2 * s^{-1}$
HF	3.09	$2.91 * 10^{-8}$	$8.99 * 10^{-8}$
HF-30min	2.96	$4.52 * 10^{-9}$	$1.34 * 10^{-8}$
HF-1h	2.82	$1.96 * 10^{-9}$	$5.53 * 10^{-9}$
HF-4h	2.44	$4.91 * 10^{-10}$	$1.20 * 10^{-9}$
HF-7h	1.82	$2.78 * 10^{-11}$	$4.95 * 10^{-11}$

Figure (12) reports the diffusion coefficients, D, as a function of equilibrium moisture content.

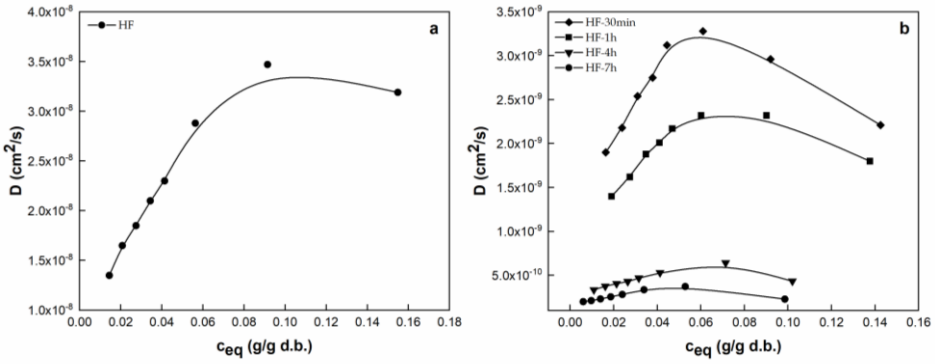

Figure 12 *Diffusion trend as a function of equilibrium moisture content*

Diffusion trend clearly shows an initial increase in water diffusivity inside the fiber, followed by a decrease at high activities (a_w=0.6), which is compliant with the shape of water sorption isotherm. This is indicative of a two-sorption mode mechanism. At low activities, water molecules are adsorbed on specific active sites or dissolved in the matrix due to their high mobility and following a typical Henry mode sorption. The contribution due to the mobility of these molecules led to a further increase in the diffusion coefficient (Henry's process). At higher a_w, water can cause swelling phenomena and leads to water aggregation formation (Gouanvé et al., 2007). The presence of water cluster aggregation could probably induce a decrease in the diffusion coefficients as

the water activity increases, being water a polar molecule that is able to interact with polar polymers and water molecules themselves through hydrogen bonds. The establishment of interactions and the tendency to form aggregates affect sorption phenomena and, in particular, reduce the effect of free volume (J. L. Lundberg, 1972). At high activities, the concentration of water can be so high to induce a relaxation of voids. It follows that the tortuosity brought on a change of the mean pathway of water molecules. Previous studies already examined the sorption and desorption curves associated with a diffusion coefficient which passes through a maximum value at some intermediate concentration (Crank and Henry, 1949). In order to study this behavior, a diffusion coefficient-concentration relationship was proposed (eq. (23)):

$$D=A+\alpha^{*}\,\mathrm{erf}\left(\beta^{*}c_{eq}\right)+\gamma c_{eq} \tag{23}$$

Where A, α, β and γ are constants, which are supposed to have no precise significance (Crank, 1979). It is worthwhile highlighting that as the equilibrium moisture content approaches to zero (c→0), A could be considered the zero-concentration diffusion coefficient (usually termed D_0). The second term ranges from zero (at zero concentration) to α and is meant to describe a diffusivity increase due to plasticization and more available free volume. Under this interpretation, the parameter β describes the mobility of water molecules which allows the dissolution inside the matrix. The rightmost term, which is usually negative, describes the presence of a maximum in the D(c) curve, which is located at a value of concentration c_{max}, so that (eq. (24)):

$$-\gamma=\frac{2\alpha\beta e^{-(\beta c_{max})^{2}}}{\sqrt{\pi}} \tag{24}$$

The decrease of diffusivity for $c > c_{max}$ can be interpreted considering that, at high concentrations, water clustering phenomena is supposed to occur and then the cross section of the penetrant is larger than the cross section of a single water molecule. Therefore, a smaller value of c_{max} describes a larger probability of water cluster formation. To handle the analytical calculation, it could be convenient to approximate the error function with the Burmann's theorem derived expansion. The analytic approximation to the solution is reported as eq. (25) (Schöpf and Supancic, 2014):

$$\mathrm{erf}(z)=\frac{2}{\sqrt{\pi}}\sqrt{1-e^{-z^{2}}}*\left(\frac{\sqrt{\pi}}{2}+\sum_{k=1}^{\infty}c_{k}e^{-kz^{2}}\right) \tag{25}$$

Considering only the first two coefficients ($c_1=\frac{31}{200}$ and $c_2=\frac{-341}{8000}$), the D versus c_{eq} curves can be fitted by using eq. (26):

$$D=A+\frac{2\alpha}{\sqrt{\pi}}*\sqrt{1-e^{-(\beta^{*}c)^{2}}}*\left(\frac{\sqrt{\pi}}{2}+\frac{31}{200}e^{-(\beta^{*}c)^{2}}-\frac{341}{8000}e^{-2(\beta^{*}c)^{2}}\right)+\gamma c \tag{26}$$

If concentration changes are small between the starting values and equilibrium, than diffusion coefficient can be assumed to be constant end equal to its integral mean as described by eq. (27) (Gouanvé et al., 2007):

$$\overline{D}=\frac{1}{c_{i+1}-c_i}\int_{c_i}^{c_{i+1}} D(c)*dc \qquad (27)$$

The $\overline{D}$ parameter can be easily estimated by calculation of the integral area under the curve D=f(c) versus the concentration. Compared to the raw hemp fibers, the barrier properties of treated hemp fibers undergo a reduction. This effect could probably be related to the reduction of solvent-matrix affinity as well as to the change in mean pathway of water molecules. Further, in the case of raw hemp fibers, hemicellulose which is still dispersed in the interfibrillar region allowed to separate cellulose chains. After removing hemicellulose, formation of OH bonds between cellulose chains resulted and the fibrils became more capable of assuming a more compact configuration resulting in a close packing of the fibers (Wang, Koo and Kim, 2003). The decrease in permeability value of treated hemp fibers could be attributed to an increase in packing density due to the removal of cementing materials (hemicellulose and waxes). As experimental time increases, the amorphous content tends to dominate, in agreement with LOI and TCI values. Simultaneously, the mechanical effect induced a decrease in fiber mean diameter, as reported before. This effect leads to a more closing packing of cellulose chains. As a consequence, the less accessible active sites and the change in free water molecules pathway were verified due to the increase in tortuosity which contributed to reduce the possibility, for water molecules, of penetrating the structure. It follows a reduction in barrier properties observed for the sample treated at long experimental times (4 h and 7 h).

The permeation of water vapor is usually determined by the transport of water molecules through the imposition of activity gradient. Since at high activity it is not possible to consider the permeated substance only in an vapor state (Modesti et al., 2004), water clustering phenomena need to be considered (Bessadok et al., 2007). Clustering phenomenon is expected if the number of water molecules adsorbed overcome the bondable water molecules number. It follows that the sorption and diffusion parameters are usually affected by cluster formation. Being water a polar substance, it can interact with polar polymers and water molecules through hydrogen bonds. The establishment of interactions and the tendency to form aggregates affect sorption phenomena and, in particular, reduce the effect of free volume (Sun et al., 1997). At high activity, the concentration of water can be so high to induce a relaxation of voids. This phenomenon causes the swelling of cellulosic material (Bessadok et al., 2007). Zimm-Lundberg theory allowed to evaluate the water clustering degree (Van Der Wel and Adan, 1999). The theory neglects the isothermal compressibility of the polymer-solvent system, so the free energy function is

a function of the first derivative of activity evaluated upon the volume fraction (J L Lundberg, 1972). So, the mean cluster size (MCS) is equal to eq. (28):

$$MCS=1+\frac{\emptyset*G_s}{V_s} \quad (28)$$

The MCS, representing an estimation of cluster size, is evaluated from isotherm sorption curves through the following eq. (29):

$$MCS=(1-\emptyset)*\frac{a_w}{\emptyset}\left(\frac{\partial\emptyset}{\partial a_w}\right)_{p,T} \quad (29)$$

Considering the Park model equation, MCS could be evaluated through the following eq. (30):

$$MCS=\frac{(1-\emptyset)}{\emptyset}*\left\{\frac{\rho_w}{\rho_p}*\frac{k_H a_w+\frac{A_L b_L a_w}{(1+b_L a_w)^2}+k_a n a_w{}^n}{\left(k_H a_w+\frac{A_L b_L a_w}{1+b_L a_w}+k_a a_w{}^n\right)^2*\left(1+\frac{\rho_w}{\rho_p}*\frac{1}{k_H a_w+\frac{A_L b_L a_w}{1+b_L a_w}+k_a a_w{}^n}\right)^2}\right\} \quad (30)$$

The ρ_p is the hemp fiber density approximated with the density of raw hemp fiber (1.4 g/cm^3 (Sanjay et al., 2018)). Figure (13) reports MCS values for raw and treated hemp fibers.

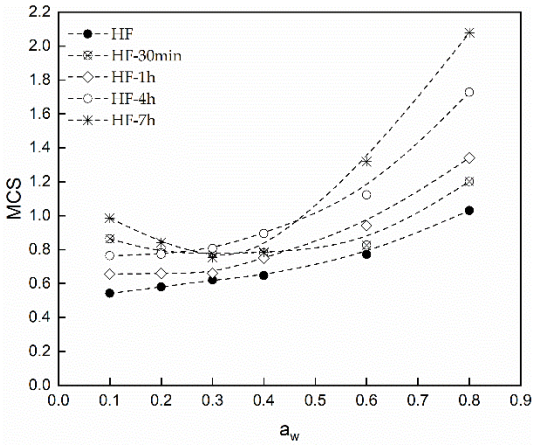

Figure 13 *MCS values for raw and treated hemp fibers*

Generally a MCS>1 indicates the probability of water clustering (Modesti *et al.*, 2004); the water clustering phenomenon is verified for a_w=0.6 (for HF-4h and HF-7h) and for a_w=0.8 for all the treated hemp fibers. In general, at higher activities, the sorbed molecules do not interact with polar sites, since they have been saturated during initial sorption. In this way, water molecules

can resemble bulk water since they are not affected by hydrophilic sites anymore. Considering the treated hemp fibers, the clustering effect for the sample HF-30min was minimized, probably caused by its high LOI and TCI values concerning the crystalline content. The reduced availability of functional groups for hemp fibers treated at higher treatment times could limit the water bondable adsorption. Moreover, the mechanical action of ball milling induced a partial decomposition of cellulose structure which, in turn, reduced the free volume effect. It follows that the tortuosity brought on a change of the mean pathway of water molecules.

Characterization of hemp fibers/pectin composites

The mechanical characterization (figure (14)) was carried out on all samples and pure pectin, taken as reference, to investigate the effect of hemp fiber loading on mechanical properties of biocomposites.

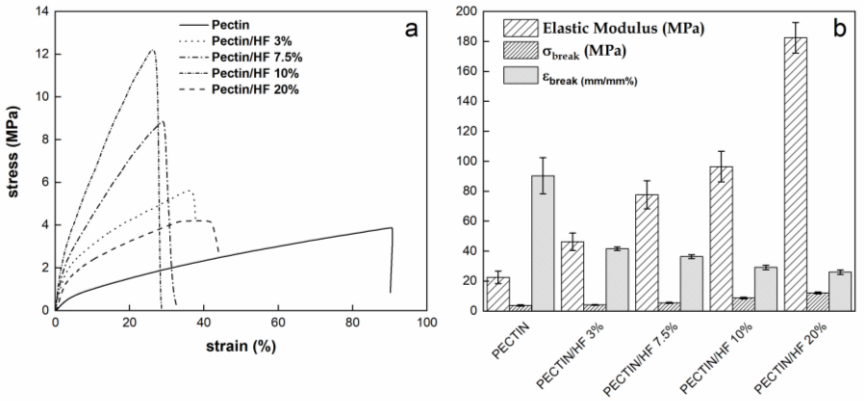

Figure 14 *a) Stress-strain curves and b), c) and d) Mechanical parameters of neat pectin and biocomposites*

Results obtained from the mechanical characterization displayed an increase in either the elastic modulus (up to 800% for a reinforcement loading of 20%wt) or the stress at break point (up to 300% for a reinforcement loading of 20%wt), proving the effect of hemp fibers as reinforcement agent. The effect of mechanochemical treatment could determine an increase in available surface area of hemp fibers and, so, an improvement of mechanical interlocking. It follows an enhanced high load transfer which could justify the increase in mechanical properties. Finally, a decrease in elongation at break point for the composites occurred resulting in a higher brittleness compared to the neat film. As for the mechanical characterization, the change in the barrier properties of pectin composites was investigate and correlated to hemp fiber loading.

In order to demonstrate the main advantages related to the employment of the mechanochemical treatment respect to traditional method, preliminary results of mechanical properties are presented for biobased composites based on pectins filled with 5 % w/w of hemp fibers mechanochemically treated and treated through standard alkalization procedure. The functionalization of surface facilitated mechanical interlocking and bonding reactions improving the interfacial interaction fiber-matrix. As reported before, the HF-30 min, showing the highest CI and a high number of available OH sites as well, led to a strong adhesion with the pectin groups. As a consequence, also the mechanical response was improved. Moreover, the effective removal of hemicellulose for mechanochemically treated HF makes the interfibrillar region less dense, so the fibrils are more capable of rearranging themselves along the direction of deformation. Such rearrangements would imply an improved load distribution among them, resulting in higher stress development in the fiber. The elastic modulus for pectin filled with the classical alkalization is lower (24 MPa compared to 121 MPa for mechanochemicaly treated HF) because of weak interaction between the partially non-cellulosic or amorphous surface of hemp fibers and the functional groups of pectin.

Figure (15) reports the sorption isotherms and the diffusion coefficients of the neat pectin and pectin/HF composites.

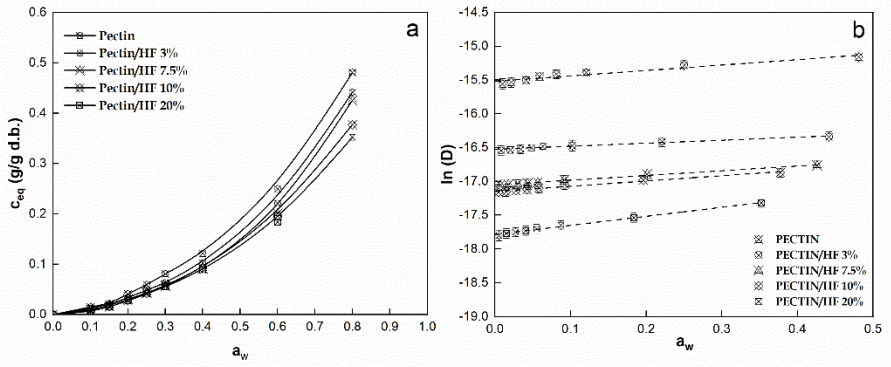

Figure 15 *(a) Equilibrium sorption isotherms and (b) ln(D) vs c_{eq} for neat pectin and biocomposites*

The adsorption isotherms demonstrate an increase in equilibrium moisture content with increasing water activity. This behavior is manifested in the form of Type II isotherm, according to Brunauer's classification (Brunauer *et al.*, 1940). It is evident that the sorption of water decreases with filler loading. This behavior was related to the less hydrophilic character of the fibers in comparison to pectin's highly hydrophilic property. It was demonstrated that

the mechanochemical treatment of hemp fiber, for very short time, led to highly crystalline regions which showed a good resistance to small waters' molecules penetration (Al-Muhtaseb, McMinn and Magee, 2004). The presence of OH sites from hemp fibers contributed to the chemical interactions with polar groups of pectin matrix leading to an improvement of the interfacial adhesion properties. Then, it is clearly evident that the diffusion coefficient of bio composites decreases with filler loading. This could be, firstly, explained by taking into account the interactions fiber-matrix, mainly hydrogen bondings, with hydrophilic groups of pectin matrix. Moreover, from transport phenomena point of view, as the fiber loading increases the mass transfer resistance offered by them increases due to the barrier effect which, likely, led to a reduction of mean cross sectional area available for water diffusion. The correlation between D_0 (diffusion coefficient extrapolated at $c_{eq}=0$) and the fibers volume fraction was investigated through the application of a mathematical model developed by Bruggemann that was used to evaluate the effective thermal conductivity of two-phase systems (Yamada and Ota, 1980). In order to consider the non-spherical shape of dispersed phase, Burgemman equation was corrected by Fricke (Fricke, 1924) through the introduction of an empirical parameter, X, which concerns the aspect ratio (L/d=length/diameter) of the fibers. The modified model is expressed from eq. (31):

$$\left(D^*_{0,c}\right)^{\frac{1}{X+1}}*(1-\phi_f)=\left(D^*_{0,c}-D^*_{0,f}\right)*\left(1-D^*_{0,f}\right)^{-1} \quad (31)$$

The hemp fiber D_0 coefficient was found to be $7.05*10^{-9}$ cm^2/s. Figure (16) shows the fitting process ($R^2=0.989$) of thermodynamic diffusion coefficients (D_0) as function of the fiber volume fraction.

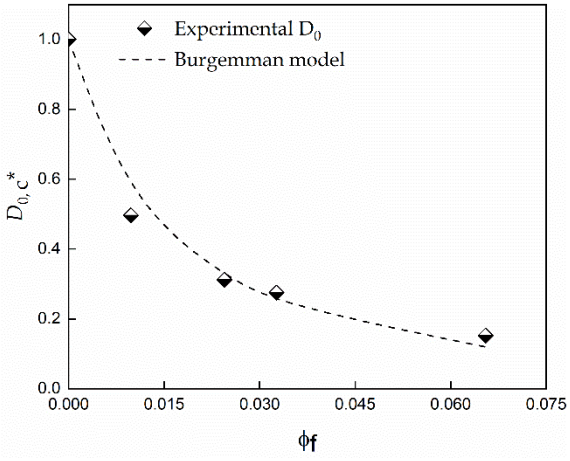

Figure 16 *Fitting process of D_0 experimental data*

The error percent between the experimental data and the predicted values allows to observe that the Burgemman model, accounting for no-sphericity of filler, appeared to well fit the experimental data (R^2=0.989). The parameter X+1 resulted to be equal to 0.898 ±0.012.

Modeling of mechanical properties

Mathematical modeling was applied to describe and to understand the effect of fiber loading on the considered mechanical properties. The effect of fiber loading on elastic modulus of pectin composites was analyzed through the Nielsen model which is considered the most versatile model for short fibers reinforced composites. Such model (eq. (32)) takes into account the filler packing, represented by parameter ψ (Loos, 2015)

$$E_c = E_m * \left(\frac{1+A\eta\phi_f}{1-\eta\psi\phi_f}\right) \quad (32)$$

Where η is a function of the tensile moduli of fibres and matrix (E_f =32 GPa and E_m=22.56 MPa, respectively) (eq. (33)):

$$\eta = \frac{\left(\frac{E_f}{E_m}-1\right)}{\left(\frac{E_f}{E_m}+A\right)} \quad (33)$$

The parameter A=k-1 is related to the Einstein coefficient (k), which is a function of the aspect ratio and orientation of the filler (Loos, 2015). The generalized Einstein coefficient can be defined, as reported by Nielsen et al. (Nielsen, 1970) as eq. (34):

$$k = \frac{d(E_c/E_m - 1)}{d\phi_f} \quad (34)$$

The parameter ψ is introduced to consider the fiber-fiber interaction while the quantity $\psi*\phi_f$ represents a reduced volume fraction of the reinforcement. An empirical form of ψ is proposed (eq. (35)):

$$\psi = \frac{1}{\phi_f}\left[1-\exp\left(\frac{-\phi_f}{1-\frac{\phi_f}{\phi_m}}\right)\right] \quad (35)$$

The parameter ϕ_m is based on filler shape and the maximum packing (Loos, 2015) In a random short fiber system, it is function of the aspect ratio (Milewski and Katz, 1987). For three dimensional random fiber system, ϕ_m can be considered equal to 0.52 (Nielsen, 1974; Keith *et al.*, 2009). By performing some mathematical calculations, the elastic modulus of composites can be evaluated through the eq. (36):

$$E_c = E_m * \left\{ \frac{1 + A\phi_f \frac{\left(\frac{E_f}{E_m} - 1\right)}{\left(\frac{E_f}{E_m} + A\right)}}{1 - \frac{\left(\frac{E_f}{E_m} - 1\right)}{\left(\frac{E_f}{E_m} + A\right)} * \left[1 - \exp\left(\frac{-\phi_f}{1 - \frac{\phi_f}{\phi_m}}\right)\right]} \right\} \quad (36)$$

Figure (17) reports the fitting process of experimental elastic modulus data.

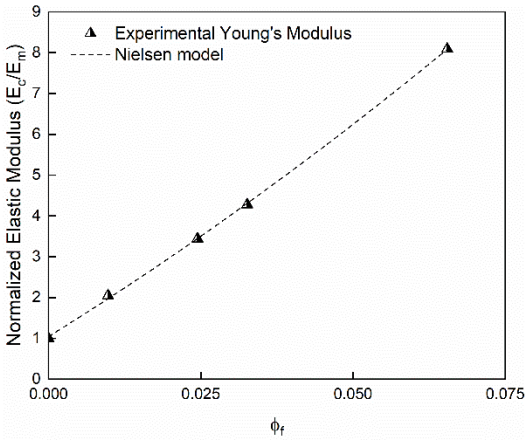

Figure 17 *Fitting of experimental normalized Young's modulus data*

Nielsen's model, widely applied for short fiber reinforced composites, well fitted the experimental data (R^2=0.991). It confirmed that, as the hemp fibers content increases, the elastic modulus increases up to a maximum fiber volume threshold beyond which composite properties deteriorate. This limit for the designed composite is usually roughly 25% w/w. The improvement of elastic modulus as the fiber content increases could be due to the presence of side-chain hydroxyl and polar groups of the hemp fiber responsible of a good adhesion with the hydrophilic matrix. The fibrils tend to rearrange themselves along with the tensile deformation leading to a better load sharing and transfer between fiber-fiber and fiber-matrix. The improved load transfer and the better adhesion, corresponding to continuity of stresses and displacements at the interface, led to an increase in the tensile strength of biocomposites (Hull and Clyne, 1996). The effect of fiber loading on tensile strength of pectin composites was described using the Pukànszky model (Pukánszky *et al.*, 1989) (eq. (37))

$$\frac{\sigma_c}{\sigma_m} = \frac{1 - \phi_f}{1 + A * \phi_f} * \exp(B * \phi_f) \quad (37)$$

Where B represents an interaction parameter related to the macroscopic characteristics of filler-matrix interface (Demir *et al.*, 2006). A is a parameter

which depends on filler shape, size distribution and packing. It is usually known for packed filler with spherical shape but, in our case, the unknown fiber distribution and orientation imposed to consider it in the fitting process. The first term on the right side accounts for the decrease of the effective load-bearing cross-section owing to the introduction of the filler into the polymer matrix (Kiran *et al.*, 2018) while the exponential one accounts for the interfacial properties of the given system. Figure (18) shows the fitting of experimental data of the tensile strength values of fiber composites, normalized respect to tensile strength of neat pectin, with the Pukànszky model that well fits the experimental data.

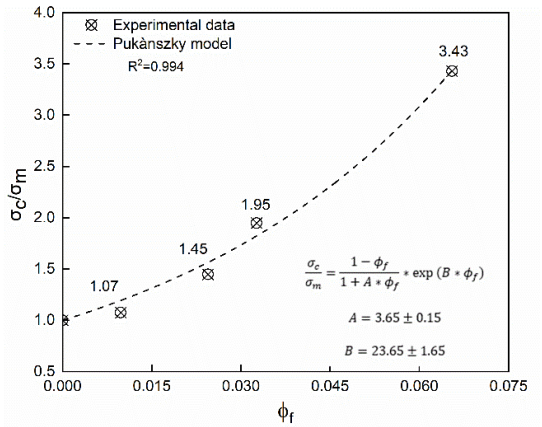

Figure 18 *Fitting of normalized tensile strength vs fiber volume fraction through the application of Pukànszky model*

Since the parameter B in the model represents the strength of interaction between the reinforcement and the polymeric matrix, the higher is B value the better is the interaction (Demir *et al.*, 2006). Low values of B (B<3) are indication of weak interactions between the interfaces of bio composites' components (Sideridis *et al.*, 2009). As expected, the force needed to break the composites was higher than for pure pectin due to the very high strength of the filler, and in good agreement with previously reported works (Dias *et al.*, 2011). The effect of fiber loading on elongation at break point of pectin composites was described considering the Smith model (Smith, 1959). It was proposed in a modified form as expressed by eq. (38):

$$\varepsilon_c = \varepsilon_m * \left(1 - \alpha * \phi_f^{\beta}\right) \quad (38)$$

The α and β parameters concern the geometrical properties of fiber arrays. Both were evaluated through the nonlinear fitting process. Figure (19) reports the experimental data of the normalized elongation at break point of fiber

composites, respect to the elongation at break point of neat pectin, with the modified Smith model.

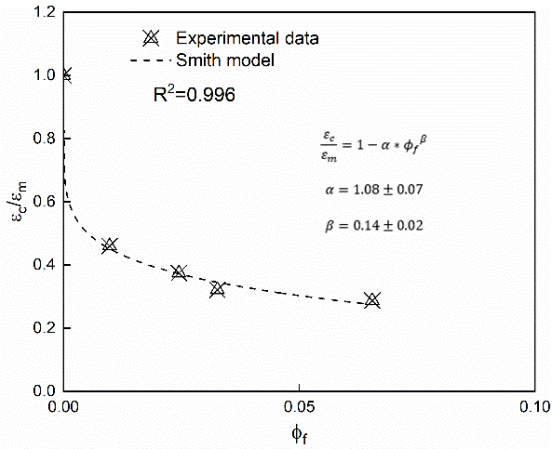

Figure 19 *Fitting of normalized elongation at break point of composites vs fiber volume fraction through the application of Smith model*

As expected, elongation at break point for the composites is lower than the pure pectin. However, due to the formation of a compact structure consequent to high intermolecular hydrogen bond interconnections, the reinforced composites resulted more brittle than the neat film (Bodirlau, Teaca and Spiridon, 2013).

Concluding remarks

A mechanochemical treatment, using NaOH in presence of water, was carried out on hemp fibers (HF) in order to investigate its effect on the chemical structure and properties of such materials. Different processing times have been tested and an extensive characterization was performed to investigate the effect of a hybrid method on hemp fibers properties. The added value given by the mechanochemical treatment was supported and corroborated through a comparison with a classical alkalization by using treated hemp fibers as a reinforcing agent in a polymeric pectin matrix aiming to evaluate the improvement in mechanical properties of the produced bio-composites. The results of this work are in accordance with the importance of developing innovative and environmentally friendly chemical processes or materials.

5.Novel hemp based composites for water remediation

Preface

Nowadays, the presence of synthetic dyes in industrial effluents is leading to environmental concerns due to the impact of such contaminants on ecosystems and human health (Forgacs, Cserháti and Oros, 2004; Yang *et al.*, 2011; Guo and Wilson, 2012; Singh, Sinha and Purkait, 2020; Yun *et al.*, 2020; Renita *et al.*, 2021). These substances can retard photosynthesis process and limit the growth of aquatic biota by limiting the transmission of sunlight in aquatic environments (Forgacs, Cserháti and Oros, 2004; Yang *et al.*, 2020). Among all, methylene blue is a cationic dye with high water solubility. Being exposed to lethal doses of methylene blue might lead to health concerns such as vomiting jaundice, shock, cyanosis and tissue necrosis (Kumar, Ramamurthi and Sivanesan, 2005). Many methods have already been applied to remove synthetic dyes from industrial wastewater such as flocculation, chemical oxidation, solvent extraction, coagulation and adsorption (Tünay *et al.*, 1996; Hao, Kim and Chiang, 2000; Forgacs, Cserháti and Oros, 2004; Zhang, Zeng and Cheng, 2016; Thong *et al.*, 2018; Varghese, Paul and Latha, 2019; Kong and Wilson, 2020). Among all the techniques, adsorption process is the most used one for contaminant removal since its technological simplicity, low cost and wide availability of adsorbents (Sanghi and Bhattacharya, 2002; Bhattacharya and Sharma, 2005; Rafatullah *et al.*, 2010).

Many sorbents have already been tested such as carbon-based inorganic supports (Roy, Wang and Adrian, 1993; Walker and Weatherley, 1997; Shaban *et al.*, 2018), silica (Ahmed and Ram, 1992), alumina (Mahmood *et al.*, 2011), vermiculite (Choi and Cho, 1996), fungus (Mittal and Gupta, 1996), commercial active carbon and natural materials and wastes from agriculture (Kannan and Sundaram, 2001; Rafatullah *et al.*, 2010; Yang *et al.*, 2011; Mahamadi and Mawere, 2014; Crini and Lichtfouse, 2019; Crini *et al.*, 2019; Mashkoor, Nasar and Inamuddin, 2020). Nowadays, there is a prompt to the development of cheap and sustainable alternatives derived from agricultural and other wastes. In an effort to address the need to develop more sustainable biomaterial-based sorbents with improved dye sorption features, two different systems will be presented based on the use of hemp fibers and hemp hurd.

a) modified and engineered hemp fibers based on 3-Aminopropyl triethoxysilane (APTES)/Graphite oxide (GO) modification
b) Sodium Alginate/Hemp Hurd/Halloysite hybrid beads

Hemp fibers/Graphene oxide adsorbent

Materials

(3-Aminopropyl)triethoxysilane (APTES-CAS: 919-30-2-Sigma Aldrich), NaOH (CAS: 1310-73-2) in pellet form, HCl solution 37% v/v (CAS: 7647-01-0-Carlo Erba Reagents), Flake graphite oxide supplied from the laboratory of Professor Hesheng Xia, methylene blue (MB-CAS: 61-73-4-Panreac AppliChem IT Reagents), NaCl and $CaCl_2$ were used as reagents and purchased from Carlo Erba Reagents.

Surface Modification

(3-Aminopropyl)triethoxysilane (APTES) aqueous solution (5% wt) was prepared by prehydrolyzing it at 50°C for 2.5 h. The pH was set at 3 by adding 1 mol/L chloridric acid solution. GO aqueous solution (0.4 mg/mL) was prepared by solubilizing it in 200 mL of water. Ultrasound sonication process was applied for 3 h to form stable graphite oxide (GO) dispersion. HFs were previously washed with distilled water and acetone to remove any trace of impurities. Finally, they were air dried. The obtained HFs were soaked in APTES solution at room temperature for 1.5h, fixing a solid/liquid ratio equal to 0.03 g/mL. After that, silane modified HFs were accurately washed three times with distilled water and dried in vacuum oven at 120°C for 24h. Due to the self-condensation of APTES, silane molecules are able to form siloxane oligomers with Si-OH groups (Raji *et al.*, 2016). These latters are able to form hydrogen bonds with the OH groups of the cellulose (Kale, Potdar and Gorade, 2019). The silane modified HFs were soaked in the GO/water mixture for 48

h at 90°C. Finally, the HF/GO samples were dried in oven at 150°C for 24h. The functionalization of GO with APTES is supposed to involve the OH groups of GO reacting with the silane groups of the APTES through the formation of Si-O-C bonds or involving epoxy groups of GO which react with the amino-groups of the APTES leading to the formation of secondary amines (Li *et al.*, 2016; Serodre *et al.*, 2019).

Characterization of modified hemp fibers

Figure (20) show the SEM micrographs of untreated HF, HF treated with acetone and GO treated HFs. The figure reports even the FTIR spectra of untreated hemp fiberboards and GO treated ones.

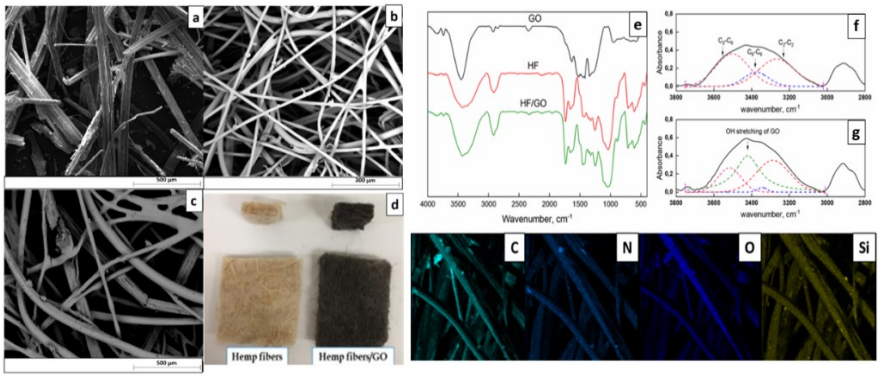

Figure 20 *SEM micrographs of a) HF; b) HF treated with acetone; c) HF-GO; d) pictures of hemp fibers and GO-treated hemp fibers; e) FTIR spectra; f and g) FTIR deconvoluted spectra. On the bottom, EDX maps*

SEM micrographs of raw HFs revealed a roughened surface due to the presence of non-cellulosic materials, mainly pectin and waxes. The removal of non-cellulosic material and impurities was due to the acetone washing which could contribute to even remove external impurities. Besides, after GO treatment, hemp fiber surface still keeps its morphology. Regarding the not modified HF, the IR region 3000 cm^{-1}-3600 cm^{-1} is indicative of hydroxyl groups (OH) in polysaccharides (Terpáková *et al.*, 2012; Khanjanzadeh *et al.*, 2018). Besides, the stretching vibration peaks at about 2910 cm^{-1} and at 1736 cm^{-1} are attributed to asymmetric and symmetric CH stretching of polysaccharides (Agarwal, Reiner and Ralph, 2010; Terpáková *et al.*, 2012) and to C=O stretching vibration of the acetyl groups of hemicellulose and carboxylic acid in pectin (Rachini *et al.*, 2009). The peaks located at 1454, 1373, 1314 and 1254 cm^{-1} are attributed to the CH_2 bending vibrations in lignin, hydroxyl groups bending of carboxylic acids, C-O groups of the rings

in polysaccharides and C-O stretching of acetyl groups (Sawpan, Pickering and Fernyhough, 2011a; Kargarzadeh *et al.*, 2015). Finally, the peaks in the range 1162-1030 cm^{-1} concern the C-O stretching and C-H rocking vibrations of the pyranose ring skeleton (Kargarzadeh *et al.*, 2012). The silanization introduced new characteristic peaks. The band at 1550 cm^{-1} refers to N–H bending vibration of primary amine (Robles *et al.*, 2015; Khanjanzadeh *et al.*, 2018). Besides, the Si-O-Si and Si-O-Cellulose peaks are located at about 1135 and 1150 cm^{-1}, which are not well visible since they are overlapped with the C-O-C vibration band belonging to the same spectral region (Ahmaruzzaman and Gupta, 2011; Allahbakhsh *et al.*, 2017; Khanjanzadeh *et al.*, 2018). The small peaks appearing at 1040 cm^{-1}, 471 cm^{-1} and 780 cm^{-1} could be associated to the Si–O–C, Si-O stretching vibrations and Si-H bond vibrations (Allahbakhsh *et al.*, 2017; Maleki and Karimi-Jashni, 2020). Concerning the GO spectrum, the small peaks at 2927 and 2868 cm^{-1} are associated to OH groups of dimeric COOH groups and intra-molecular bonded O-H groups stretching of alcohols (Szabó, Berkesi and Dékány, 2005; Jeong *et al.*, 2009; Yan *et al.*, 2017). GO showed then the characteristic peak of the stretching of hydroxyl group at 3450 cm^{-1}, which appears after grafting of APTES in the HF/GO spectrum (Bouazizi *et al.*, 2019). Besides, the C=O carbonyl stretching at 1728 cm^{-1} and the C–O epoxide group stretching at 1229 and 1061, 1036 cm^{-1} are even observed (Loryuenyong *et al.*, 2013; Javed and Hussain, 2015; Chong *et al.*, 2018). The results mentioned above indicated the effective deposition of GO onto the surface of hemp fibers. To further prove that, the peaks belonging to OH broad band (3600-3000 cm^{-1}) are analyzed by applying a deconvolution algorithm followed by a curve fitting procedure. Regarding the untreated hemp fibers spectrum , the characteristic bands related to intermolecular hydrogen bonding are located at 3438, 3334, and 3293 cm^{-1}, belonging to OH-O bond in C_2-C_6 position, OH-O in C_6-C_6 position, and OH-O bond in C_2-C_2 position (Viscusi, Barra and Gorrasi, 2020). A further band located at 3450 cm^{-1} is attributed to OH stretching vibration of graphite oxide in the HF/GO spectrum. It puts in evidence that, after the surface treatment, the OH band was broadened (Song *et al.*, 2013a). The silanols could react with OH groups of lignocellulosic hemp fibers resulting in stable covalent bonds which are chemisorbed onto hemp fiber surface (Huda *et al.*, 2008; Song *et al.*, 2013b) and the decay in peak areas intensity for C_2-C_6, C_6-C_6 C_2-C_2 bands justified the reduction in terms of OH groups due to the formation of Si-O-C bonds. The deconvolution process of OH band in FTIR spectra proved the effective modification of hemp fibers with GO. A further proof of the surface composition change after the GO treatment was given by EDX maps. The atomic weight distribution clearly demonstrated the presence of silicon and nitrogen due to the organosilane grafting.

Adsorption studies

Kinetics studies concerning the adsorption of methylene blue were carried out by analyzing the effect of pH level, temperature and MB initial concentration. Before evaluating that, raw HF, silane modified HF and GO modified HF were tested to estimate their adsorption capacity. The dye concentration was fixed at 5 mg/l and the batch studies were conducted at 20°C and pH=7.5. Adsorption curves were reported in figure (21).

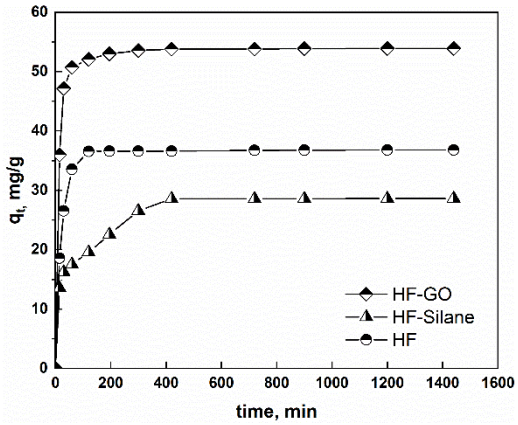

Figure 21 *q_t versus t for adsorption of MB at pH=7.5 and T=20°C for HF, HF-Silane and HF-GO*

It is well clear that GO modification contributed to noticeably increase the MB adsorption capacity changing from 36.7 mg/g for raw HF to 53.86 mg/g with an increase of about 32%. Moreover, the noticeably improvement of adsorption capacity after the modification is even ascribable to the increase in specific surface area due to the intrinsic high surface area of GO. Besides, the HF-Silane appeared to worse the adsorption capacity which could be attribute to the presence of amino groups which hinder the adsorption of MB cations. Finally, BET surface area was evaluated. The BET specific surface areas are 45.4, 40.25 and 82 m^2/g for raw HF, silane modified HF and GO modified HF, respectively. Besides, the porosity (%) increased from 4.5% up to 9.54 % after GO modification, which further demonstrates the improvement of MB adsorption after GO modification. A first set of experiments was performed by evaluating the adsorption capacity of HF-GO membrane at C_0=5 mg/L, varying the experimental temperature and the pH level. Figure (22) shows the profiles of adsorbed dye versus contact time, at pH=7.5 for T=20°C, 50°C and 80°C. By way of example, on the right side the decrease in intensity of MB

peak at different contact times is reported while the insets show the change in color of MB solution during the experiment (pH=7.5).

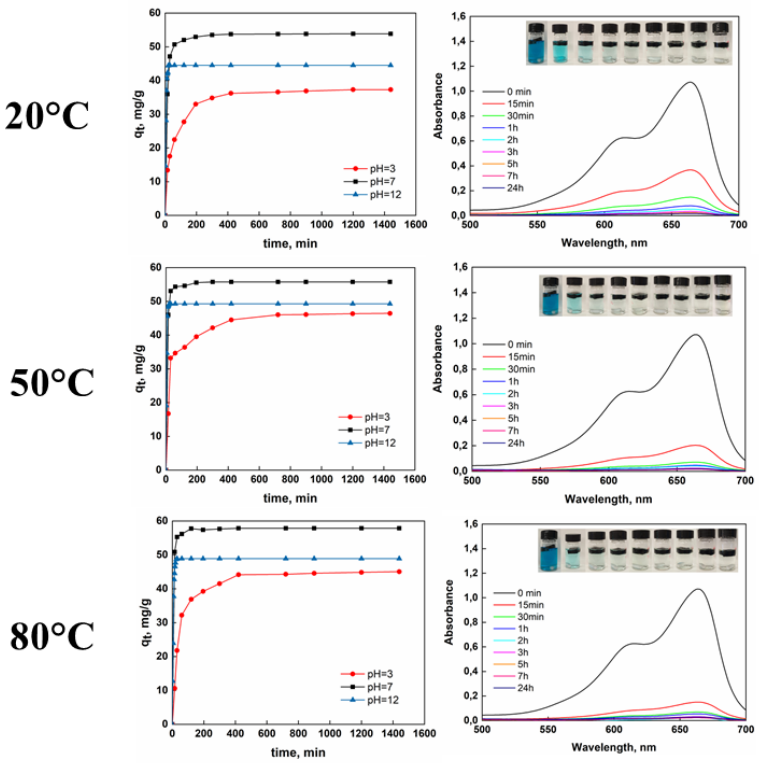

Figure 22 *q_t versus t for adsorption of MB at pH=7.5 at different temperatures. On the right side, UV-Vis spectra variation as function of contact time*

The process was mainly divided into two phases. The first step concerns the fast adsorption rate due to the binding process between MB ions and the adsorption active sites. The second step concerns a slower adsorption process due to the saturation of active sites and, as the time increases, the adsorption rate gradually attains a plateau regime. The above reported figures show that the amount of dye uptake per unit of mass of adsorbent (q_t, mg/g) increased with contact time at all temperatures. It can be claimed that the adsorption rate is quite rapid for short times (<20 min); it proceeds with a slower rate before attaining a plateau regime. The initial rapid adsorption might be attributed to increasing number of vacant sites available initially. It follows that, at low times, it is high the concentration gradient between the liquid and the solid phase, justifying the initial rapid adsorption (Kavitha and Namasivayam, 2007). As we can see, adsorption capacity slightly increases with temperature

changing from 54 mg/g to 58 mg/g at pH=7.5, from 37 mg/g to 45 mg/g at pH=3 and from 44 mg/g to 49 mg/g at pH=12, by increasing the temperature from 20°C to 80°C indicating that the process is slightly endothermic. The aqueous medium pH plays an important role in dye uptake due to the modification of either surface of adsorbent or adsorbate properties. At low pH, the excess of H_3O^+ ions can compete with MB ions. A further increase in pH to 12 slightly reduced the adsorption capacity due to demethylation of MB in alkaline solution (FA and DK, 2007). Moreover, this phenomenon is due to the fact that greater the pH, the lower the competition between the dye molecules and H^+ ions to form electrostatic interaction with the functional groups on the adsorbents (Shaiful Sajab et al., 2011). A pseudo-second order model was used to fit the experimental data by applying the Ho's equation (eq. (39)) (Bulut and Aydin, 2006)**:**

$$\frac{t}{q_t} = \frac{1}{k_{ps} * q_{eq}^2} + \frac{t}{q_{eq}} \quad (39)$$

Where k_{ps} (mg g^{-1} min^{-1}) is the rate constant of second order adsorption and q_{eq} (mg g^{-1}) is the amount adsorbed per gram of adsorbent at equilibrium state. The linearization of pseudo second order equation allowed to easily evaluate the q_{eq} and k_{ps} constants., reported in table 5.

Table 5 *Ho's equation parameters*

		20°C	50°C	80°C
pH=7.5	q_{eq}, (mg g^{-1})	54.2	55.8	57.8
	k_{ps}, (mg g^{-1} min^{-1})	0.0042	0.009	0.014
	R^2	0.999	0.999	0.997
pH=3	q_{eq}, (mg g^{-1})	38.1	45.4	46.3
	k_{ps}, (mg g^{-1} min^{-1})	0.0006	0.0007	0.0009
	R^2	0.999	0.997	0.995
pH=12	q_{eq}, (mg g^{-1})	44.6	49.3	49.5
	k_{ps}, (mg g^{-1} min^{-1})	0.026	0.042	0.053
	R^2	0.993	0.993	0.992

The q_{eq} parameter increases as temperature increases justifying that the adsorption of MB is favored at high temperature. This could be explained by stating that an increase in temperature led to an increase in free volume due to augmented mobility of the solute, solubility and chemical potential of dye molecules (Ho and McKay, 1998; Kuang, Zhang and Zhou, 2020). Besides, the k_{ps} constant rate even was augmented by the increase in temperature. Larger values of k_{ps} indicate faster adsorption (Yang et al., 2010). The

activation energy of adsorption was also calculated from the linearized Arrhenius equation (eq. (40)) (Bulut and Aydin, 2006):

$$\ln K_{ps} = \ln k_0 - {}^{E_A}/_{RT} \quad (40)$$

The activation energy has been evaluated, by way of example, at pH=7.5 from the slope of the linear plot. The obtained result was 17.2 kJ/mol. The wide performed analysis gave also a deep knowledge concerning the enthalpy and entropy changes during the adsorption. The free energy of adsorption of MB (ΔG^0) can be easily evaluated from the eq. (41) (Yao et al., 2010; Rathinam et al., 2017):

$$\Delta G^0 = -RT*\ln(K_L) \quad (41)$$

Where K_L, defined as q_{eq}/c_{eq}, is called adsorption affinity (Bhattacharya and Sharma, 2005). The obtained values ranges from -4.36 to -4.56 changing from 293 K up to 353 K. Enthalpy and entropy were estimated through the following eq. (42) by extrapolating the slope and the intercept (Khan, Riaz-ur-Rehman and Khan, 1995):

$$\ln(K_L) = {}^{\Delta S^0}/_{R} - {}^{\Delta H^0}/_{RT} \quad (42)$$

The negative values of Gibbs energy indicated a spontaneous process while the positive value of enthalpy (3.43 kJ/mol) proved the slight endothermic nature of the process (Li *et al.*, 2020). The increase in temperature contributed to increase the surface activity of the adsorbent a well as the kinetic energy of the adsorbate, leading to an improvement of removal efficiency (Oladipo and Ifebajo, 2018). The positive values of entropy (3.16 J/mol K) proved the randomness at the solid-liquid interface (Guinee *et al.*, 2002; Fan *et al.*, 2017). Such thermodynamic parameters changed in a way that allows to state that a high degree of affinity of dye molecules for HF/GO surface exists. The dye uptake was found to be dependent on pH level; in particular, adsorption capacity increases from 37 mg/g to 44 mg/g from pH=3 to pH=12 (T=20°C), from 46 mg/g to 49 mg/g from pH=3 to pH=12 (T=50°C) and from 45 mg/g to 49 mg/g from pH=3 to pH=12 (T=80°C), as reported for other systems (Karaca *et al.*, 2008; Yagub, Sen and Ang, 2012; Kuang, Zhang and Zhou, 2020). This decrease in adsorption capacity changing from pH=7 to pH=12 might be due to the partial decomposition or damage caused by alkaline environment to certain adsorption sites or functional groups. The explanation can be found in the surface properties of HF/GO membrane. To better understand the effect of pH, the point of zero charge of the adsorbent (pH_{PZC}) was evaluated. The obtained ΔpH vs pH_i curve is reported in figure (23):

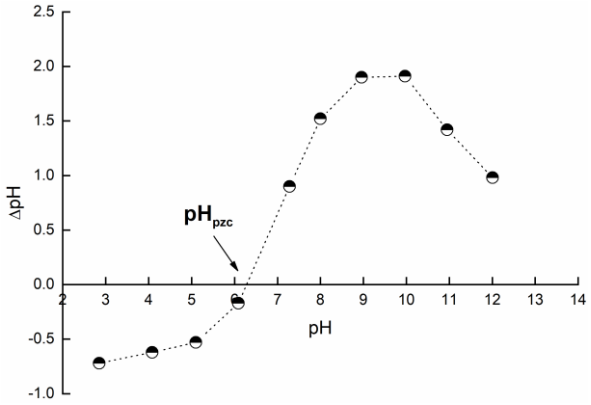

Figure 23 *ΔpH versus pH curve for the evaluation of* pH_{PZC}

The pH_{PZC} value is roughly 6.3. It follow that, as $pH>pH_{PZC}$, there is an excess of negative charge on the HF/GO membrane while as $pH<pH_{PZC}$ there is an excess of positive charge on the surface (Li *et al.*, 2020). It can be deduced that as the $pH> pH_{PZC}$, the excess of negative charge and the presence of OH^- led to an improvement in adsorption capacity since the MB in solution exists as cationic ion. So, the formation of electrostatic interactions between the cationic dye and the electron-rich sites of the membrane surface could justify the increase in q_t as pH increases, creating competition of H^+ with the MB molecules. Even if the low pH favored the positive surface charge of the membrane and, so, didn't improve the adsorption due to the electrostatic repulsion, at low pH there is still a recovery higher than 90%. Finally, the effect of concentration was even evaluated by setting three different initial concentration of MB (5, 20 and 35 mg/L). For each concentration, the adsorption capacity was analyzed as function of pH level and the experimental temperature leading to carry out 27 experiments which allowed to widely understand the effect of the process parameters and the interactions between them. The equilibrium adsorption capacity of the adsorbent for methylene blue increased with increasing initial dye concentration. For example, at pH=7.5 and T=20°C, the adsorbed amount, q_t, changed from 54 mg/g to 372 mg/g, as the adsorbate changed from 5 to 35 mg/L. The removal of dye appears to be concentration-dependent since the higher initial concentration contributed to increase the driving force which overcomes the resistance to the mass transfer of dye between the aqueous and the solid phase (Li *et al.*, 2020).

Design of experiment: modeling of experimental data

After performing the designed 27 experiments, data were statistically modeled. Design of Experiment methodology was applied by inserting, as output variable, the recovery % of MB. A quadratic model was chosen to fit

the experimental data. The ANOVA analysis allowed to estimate the factors which showed a significant effect. The model F-value of 62.35 implies that the model is significant and there is only 0.01% chance that an F-value larger could occur due to noise. It can be deduced from statistical analysis that, according to p-value being significant, the set model is able to describe the experimental data. The Adequate Precision parameter, which measures the signal to noise ratio, is 20.11 and, since it is greater than 4, indicates an adequate signal and the feasibility of navigate the design space by using the chosen model. Moreover, since a factor is statistically significant only if the relative p-value is lower than 0.05, it follows that just some contributions. According to that, the dye uptake was well described by the following eq. (43):

$$(R_{\%}\text{-}44.60)^3 = -2.55*10^5 + 2149.36*T + 92261.16*pH + 2981.27*C - 5054.23*pH^2 + 20.91*T*pH^2 + 44.86*pH^2*C \quad (43)$$

The initial pH of the solution had the greatest effect on $R_{\%}$, followed by concentration (C_0), Temperature (T) and the interaction pH-T and pH-C_0. These results are even justified by Pareto Chart where the reported standardized effects concern the factor statistically significant for the 95% confidence level, setting 26 degrees of freedom and evaluating a t-value equal to 2.056 and the normal probability plot of residuals for $R_{\%}$ which showed how closely the observed values followed the set theoretical distribution. The selected model was adequately able to describe the observed data with a correlation coefficient R^2 equal to 0.99. The surface plots of the response function are useful in understanding both the main and interaction effects of the factors (Bingol, Tekin and Alkan, 2010). The response surface contour plots of interaction effects where one parameter for each graph was set at intermediate value, are reported in figure (24):

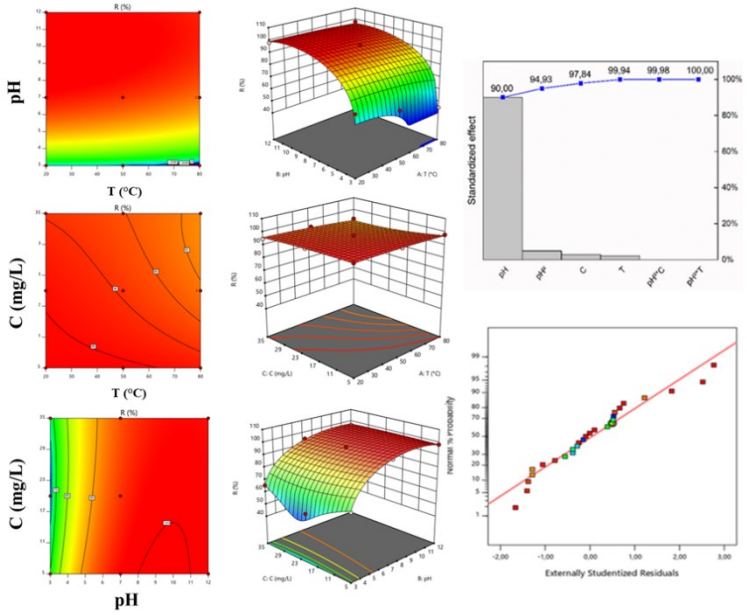

Figure 24 *Countor plots (left side) and 3D surface responses (right side) of T-pH interaction (a and b), T-C interaction (c and d) and C-pH interaction (e and f). On the righ side, Pareto chart of the standardized effects and normal probability plot of standardized residuals*

The contour plots are curved lines which reveal that the effect of pH, as previously reported, was more significant compared to C and T. The parameter T appeared to not consistently affect the recovery % while a slight change raised from the variation of initial concentration.
The Design expert software allowed, finally, to estimate the set of optimal process parameters which can maximize the recovery of MB. The estimated values are: T=53.8°C, pH=9.25 and C_0=13.2 mg/L. Due to the different surface charge of the adsorbent as pH changes, the optimal pH level is above the pH_{PZC}, in agreement with the previously reported results.

Effect of ionic strength

Figure (25) shows the effects of two different electrolytic salt solutions (NaCl and $CaCl_2$) and the ionic strength on the adsorption of MB (previously optimized pH, T and C parameters were set as experimental conditions).

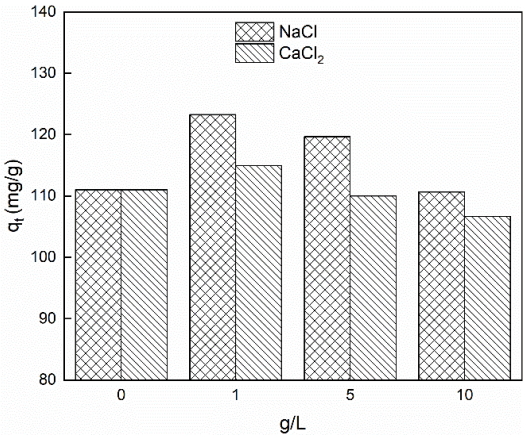

Figure 25 *Effect of ionic strength of Na^+ and Ca^{2+}onto MB adsorption*

It can be seen that the adsorption amount, under the same conditions, is higher for NaCl solution compared to $CaCl_2$ one, indicating that the cations can alter the surface property and thus can influence the adsorption of MB on the surface. The hydrated radius of sodium is 0.358 nm while it is 0.412 nm for calcium (Cheng *et al.*, 2018). It follows that, since Na^+ ion radius is smaller, it tends to less hinder the MB adsorption. On the other hand, the salt contributed to dissociate MB molecules to MB cations by promoting the protonation, leading an enhancement of the electrostatic interactions between the MB cations and adsorbent (Wu *et al.*, 2014). It was seen that the increase in salt concentration resulted in a decrease of MB adsorption, ascribed to the competition between the MB cations and Na^+ or Ca^{2+} ions to occupy the adsorption sites. The negative effect of ionic strength on dye uptake might suggest the possibility of ion exchange mechanism determined by a cations competition in the sorption process (Maurya *et al.*, 2006). Then, the activity of MB is supposed to decrease as ionic strength increases (Han *et al.*, 2006), justifying the reported data.

Desorption studies and reusability

To check the economic feasibility of the adsorption process, desorption and regeneration studies are supposed to be quite crucial. The recovery (%) of MB of the regenerated membrane was reported in figure (26) as function of number of adsorption tests.

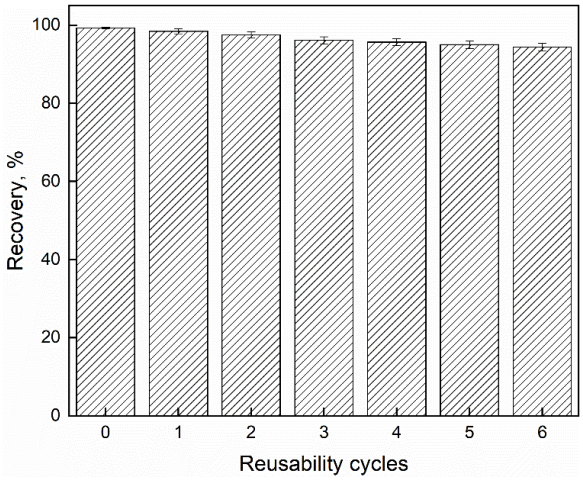

Figure 26 *Recovery (%) of MB as a function of reusability cycles*

Results showed about 1 % drop in the adsorption capacity after first regeneration cycle. The R% slightly decreases for the consecutive cycles (up to six cycles) showing that the adsorbent could be used again and again without losing totally its performance.

Adsorption mechanism

The study of adsorption kinetics in wastewater treatment is important because it gives valuable insights into reaction way and mechanism of adsorption process. A possible adsorption mechanism was proposed by considering the action of electrostatic interaction, hydrogen bond, π–π interactions, and Van der Waals forces (figure (27)). The reported mechanism is just a proposal of a mechanism which can contribute to give more insight into the complexity of adsorption phenomena on natural materials. TGA/DTG, FTIR analysis and SEM micrographs are reported to corroborate the proposed mechanism.

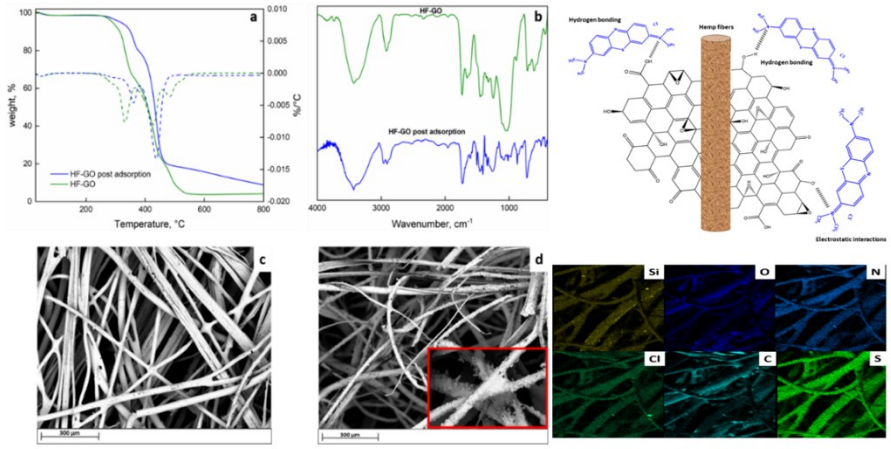

Figure 27 *a) TGA/DTG; b) FTIR curves; c and d) SEM micrographs of HF/GO before and after MB adsorption. On the right side, proposal of adsorption mechanism and EDX maps*

The MB adsorption could be attributed to the generation of electrostatic attractions between positively charged MB ions and negatively charged –OH groups on the surfaces of hemp fiber as well as negatively charged groups (hydroxyl and carbonyl surface groups) on the basal planes and edges of GO sheets. These functional groups play the role of binding sites for the adsorption of MB molecules. The decrease in intensity of either OH band in the range 3200-3600 cm^{-1}or C=O carbonyl stretching at 1728 cm^{-1} or the C-O band at 1110 cm^{-1} is a further proof of the involvement of these groups in MB adsorption. The peaks at 1442 cm^{-1} and 2928 cm^{-1} that appear in HF/GO spectrum after adsorption are characteristic of MB (Xia et al., 2019). These results prove that the adsorption of MB onto GO modified HF occurs by involving the above-named functional groups. Then, π–π conjugation can even be present between C=C double bond of dye and π electron of benzene rings through π–π electron coupling. It follows that the presence of graphene oxide can concur to raise the density of oxygen-containing functional groups (hydroxyl, carboxyl and epoxide group) which led to more electrostatic interactions and π–π electron couplings. The formation of these latter could even contribute to increase the thermal stability of hybrid composite as shown in TGA/DTG profile where it is possible to highlight a shift to higher temperature after MB adsorption over 300°C with a degradation rate changing from 0.00076 up to 0.00046 % $°C^{-1}$. The SEM micrographs show then the presence of some agglomerates in hemp fibers due to dye adsorption which are well visible in the inset image. Finally, the EDX maps clearly demonstrated the presence and the distribution of characteristic elements of MB such as sulphur and chloride. The reported explanations agree well with

our adsorption data. The presence of GO can so contribute to expose a high number of active adsorption sites binding the MB cations according to the formation of the equilibrium:

HF/GO + Methylene blue ↔ [HF/GO-(MB complex)]

Moreover, the possibility of forming electrostatic interactions and π–π electron couplings might be limited in acidic medium (pH=3) since the excess of H^+ ions could partially reduce the availability of anionic functional groups (OH^- and COO^- for example), giving a farther proof of the above reported adsorption kinetic data.

Sodium Alginate/Hemp Hurd/Halloysite hybrid beads

Materials&Methods

Sodium Alginate (SA), Halloysite (HNTs: $H_4Al_2O_9SiO_2(H_2O)_2$, methylene blue ($C_{16}H_{18}ClN_3S$), Calcium chloride ($CaCl_2$), NaOH, HCl solution 37% v/v, $NaNO_3$ were used as reagents.

Beads preparation

Before carrying out the ionotropic gelation process, hemp hurds have been reduced in size using a stainless-steel blade grinder (Duronic-CG250), required to better disperse it inside the polymeric bead. Sodium Alginate (0.6 g), Hemp hurd (0.1 g) and HNTs (5, 20 and 35% wt on total basis) were mixed with 15 mL of water and stirred at 40 °C for 3 hours. The solution was added dropwise to 5% wt $CaCl_2$ solution. The produced beads were kept at 4°C for 24h, before collecting them from the calcium chloride solution and washing several times with distilled water. The obtained beads have been labeled as SHC-y (y =% wt of HNTs clay) composite beads. Finally, the composite beads were air dried for 72 h.

Biocomposite characterization

Figure (28) shows the diameter distributions of composite beads.

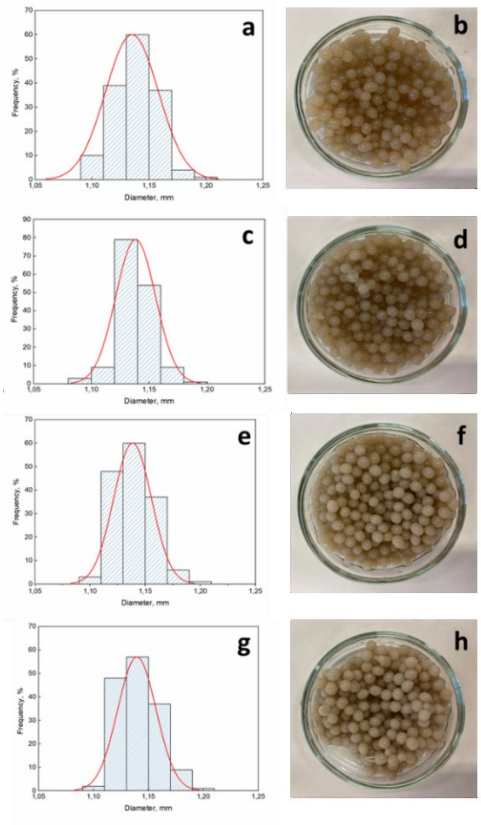

Figure 28 *Diameter distributions and picture of a) and b) SH/HNTs-0; c) and d) SH/HNTs-5; e) and f) SH/HNTs-20; g) and h) SH/HNTs-35*

As evidenced, the diameter of fabricated beads is not pretty affected by introduction of HNTs since they are quite constant for all samples (about 1 mm). So, even after the addiction of inorganic filler, it was possible to preserve the dimensions of the designed composite beads. Then, the pictures on the right side show a regular spherical shape of the produced beads.

Swelling and deswelling behaviour

Due to the presence of sodium alginate, the pH is a crucial factor affecting the release phenomena (Roy, A K Bajpai and Bajpai, 2009). A deep study of the effect of pH on swelling and deswelling behavior has been carried out. Swelling properties of composite beads were determined as function of pH level. Firstly, 50 mg of material were air-dried and then weighed. Then, they were immersed in 25 mL of liquid medium (pH=2, pH=7 and pH=12). The pH values of the tested release media were adjusted at 2 and 12 using 1 M HCl and 1 M NaOH solutions, respectively. Wet samples, after determined contact

times, were wiped with filter paper to remove excess liquid and weighed. Voight-based equation (eq. (44)) has been applied to describe the experimental swelling data (Omidian et al., 1998):

$$S_t = S_{eq}(1-e^{-t/\tau}) \quad (44)$$

where S_t (mg/g) is the swelling at time t, S_{eq} (mg/g) is the equilibrium swelling, τ is a rate constant (min). The deswelling (mg/g) for each pH, due to the dissolution or erosion value, was recorded as a function of the dissolution time and modeled through eq. (45):

$$S_t = S^* + (S_{eq} - S^*) * \exp(-k_{pH} * (t-T)) \quad (45)$$

Where S* represents the mg of water/g of dry mater as time approaches to infinite, k_{pH} represents the constant rate (min^{-1}) and T (min) represents the time corresponding to the stationary phase. Figure (29) reports swelling and deswelling (mg/g) of sodium alginate-hemp hurd beads along the time as a function of pH level. Medium dashed lines represent the fitting curves.

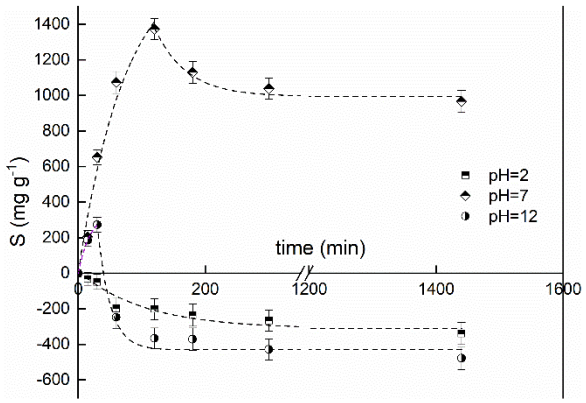

Figure 29 *Swelling and deswelling trends of SHC-0 as function of time at different pHs*

The parameters obtained by fitting the curves are reported in table 6.

Table 6 *Parameters of swelling and deswelling models*

	S_{eq} (mg/g)	S* (mg/g)	τ (min)	k_{pH} (min^{-1})	T (min)
pH=2	0	-334	0	0.006	0
pH=7	1368	1012	55.56	0.016	126
pH=12	351	-443	19.94	0.033	31

It is known that sodium alginate is a pH sensitive polymer due to the presence of D-mannuronic acid (pKa=3.38) and L-guluronic acid units

(pKa=3.65) (Nokhodchi and Tailor, 2004; da Silva Fernandes *et al.*, 2019). In neutral and basic conditions, a rapid water uptake occurred until a S_{eq} of 1368 mg/g and 351 mg/g was reached for pH=7 and 12 respectively leading to a swelling degree of about 137 % after t=126 min for pH=7 and 30% after t =31 min at pH=12. This result is related to the high number of hydroxyl groups and carboxylate ions of alginate molecules [53]. As pH > pKa, the COOH groups are preferably in the form COO^-. The excess of negative charge of deprotonated groups can induce a repulsive interaction and so an expansion of polymeric network. Besides, when pH < pKa, carboxyl groups are preferably in the form COOH. The entry of water can create voids that could aid the adsorption on preferential sites (Lima *et al.*, 2018). After pH=9, the excess of Na^+ ions led to the screening effect shielding the COO^- ions and, therefore, determining a reduction of anion–anion repulsion (Thakur and Arotiba, 2018). In basic conditions (pH=12) the hydrostatic repulsion between charged anionic groups can generate a collapse of the structure. It follows that the alginate bead can retain a lower amount of water compared to neutral conditions and a more rapid deswelling phenomenon occurs. In acidic conditions (pH=2<pKa), no increase in weight was observed probably due to dissolution or surface erosion of alginate structure. Finally, since τ could be related to the resistance to water permeation, lower τ value corresponds to higher water uptake rate, corroborating the previously reported statements. After a certain time, dissolution phenomena occur and deswelling is verified. A decrease in swelling degree (deswelling) can be observed due to the dissolution rate which decreases in acidic and basic conditions compared to neutral condition following an exponential behavior. The k_{pH} constant is related to the dissolution constant rate and it tends to increase as pH increases (from 0.006 min^{-1} at pH=2 to 0.033 min^{-1} at pH=12) justifying the collapse of alginate structure as pH increases.

To better understand the effect of pH on the adsorption phenomena, the point of zero charge of the adsorbent composite (pH_{PZC}) was evaluated. The ΔpH vs pH_i curves were obtained for each specimen and reported in figure (30):

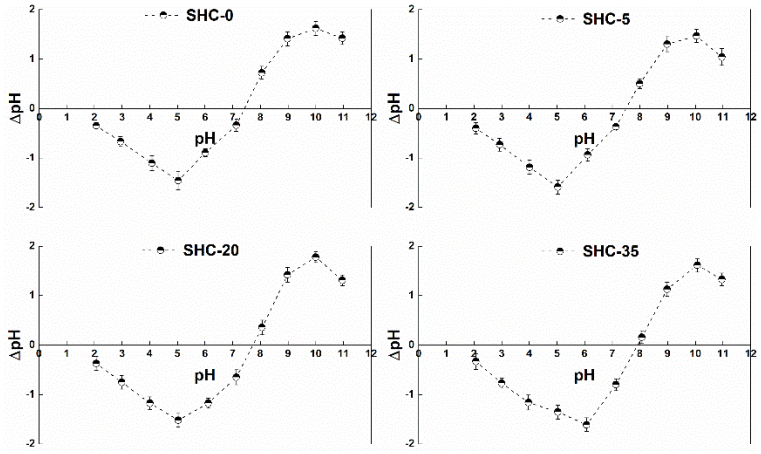

Figure 30 Δ*pH versus pH curves for the composite SHC-y beads*

The pH_{PZC} values of the produced composite beads didn't noticeably change with HNTs content. A slight increase can be observed by adding clay nanotubes from 7.42 to 7.50, 7.75 up to 7.98 for SH/HNTs-0, SH-HNTs-5, SH-HNTs-20 and SH-HNTs-35, respectively. Generally speaking, as $pH>pH_{PZC}$, there is an excess of negative charge which could be attributed to adsorption of OH^- ions and/or the deprotonation of ionizable groups while as $pH<pH_{PZC}$ there is an excess of positive charge on the surface beads (Li *et al.*, 2020). From pH_i 2.0 up to 5.0, a retention of protons occurred which led to an increase in the pH_f value. After pH_i=5, protons retention is gradually reduced up to reaching pH_{pzc}. Above pH_{pzc}, the surface of the materials begins to release protons determining a decrease in pH_f value. This phenomenon occurred until pH_i=10, followed by a further increase in pH_f due to the attraction of the protons onto the surface.

Batch adsorption studies

Adsorption tests, in batch process, were carried out on the dye solution. It was prepared by dissolving MB in distilled water in order to obtain a 20 mg/L solution. Then, a determined amount of the samples was immersed in the MB solution. The pH of the MB solutions was adjusted by adding NaOH (1M) or HCl (1M) solutions. The MB adsorption was followed along the time for 24 h. The concentration of MB in the solution was then calculated through UV–Vis technique by taking the absorbance at 664 nm. Figure (31) shows the profiles of adsorbed dye versus contact time as function of HNTs content and pH regime.

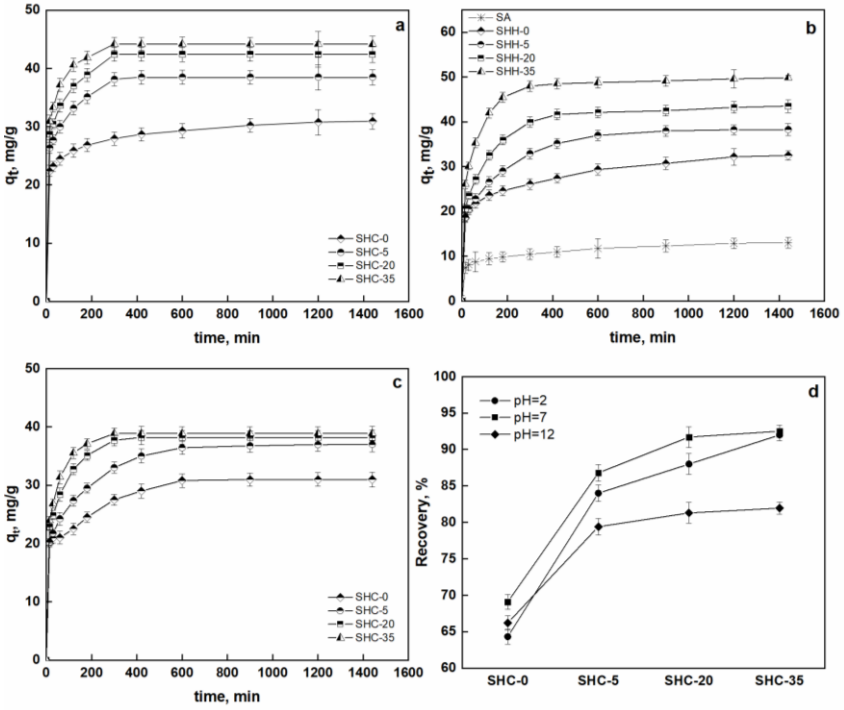

Figure 31 *q_t versus t for MB adsorption of composite beads at a) pH=2; b) pH=7; c) pH=12; d) Recovery efficiency (%) as function of pH level*

Experimental data highlight the direct relationship between the adsorption capacity and the contact time. As expected, the q_t increases sharply for low times. At low contact times (0-1 hour), the dye adsorption concerns the rapid adsorption rate attributed to cationic dye-active sites interactions as well as to the high concentration gradient which represents the initial driving force of adsorption process (Kavitha and Namasivayam, 2007). When the adsorption keeps going, the saturation of active binding sites occurs and other phenomena, such a pore diffusion, determine the slowdown of the adsorption rate which attains an equilibrium after 5 h (pH=2), 36 hours (pH=7) and 10 h (pH=12). It is worthwhile highlighting that, even if the clay is not present (SHC-0 sample), a noticeable adsorption capacity arises probably due to chemisorption on -COOH groups of sodium alginate or functional groups of lignin based materials such as alcohol hydroxyl, phenolic hydroxyl, and carboxymethyl groups (Liu *et al.*, 2012; Jin *et al.*, 2019). For each pH conditions, it can be stated that an increase in clay content determines an improvement in adsorption capacity since they provide a large surface area, a porous structure and a high cation exchange capacity (Zhao *et al.*, 2013). As pH diverges from neutrality, a decrease in adsorption capacity occurs. For

example, the composite coded SHC-35 shows an adsorption capacity of 49.8 mg/g at pH=7 while it decreases to 42.8 mg/g at pH=2 and 40.1 mg/g for pH=12. As pH<7, considering that the PZC of the produced composite is at minimum roughly 7.42, an excess of positive charge on the surface is verified, limiting the adsorption of MB cationic ions since the electrostatic repulsions. Moreover, the slight decrease in the MB removal in acidic conditions might be due to the competition between MB positive ions and H^+ (Rathinam *et al.*, 2017). As pH=12, since it is above the PZC of all the composites, an increase in adsorption capacity is supposed to be verified since the excess of negative charge can interact electrostatically with cationic MB ions. Moreover, a further decrease occurred. Probably, as pH reaches very high values (pH>10), the protonation of functional surface groups can limit the enhancement of MB adsorption by hindering the access to binding sites. Finally, the R% trend follows the adsorption capacity one showing a recovery, for the sample loaded with the 35% wt of clay, of about 88% in acidic conditions, 93% in neutral medium and 86% in basic conditions, proving and corroborating the previously reported statements.

Lagergren's pseudo-first order kinetic model (eq. (46)), Ho's pseudo second order kinetic model (eq. (47)) and intraparticle diffusion model (eq. (48)) were used to fit the experimental adsorption data (Aluigi et al., 2014)**:**

$$\log(q_e\text{-}q_t) = \log(q_e) - \frac{k_1}{2.303} * t \quad (46)$$

$$\frac{t}{q_t} = \frac{1}{k_2 * q_e^2} + \frac{t}{q_e} \quad (47)$$

$$q_t = k_{id} * \sqrt{t} + C \quad (48)$$

Where k_1 (min^{-1}) and k_2 (mg g^{-1} min^{-1}) are the rate constants of first and second order adsorption, q_{eq} (mg g^{-1}) is the amount adsorbed per gram of adsorbent at equilibrium state, C is the intercept of the intraparticle diffusion model while k_{id} is the intraparticle diffusion constant. The parameters, could be easily evaluated by the slope and the intercept of the above reported equations and reported in table 7. Fittings of experimental data are reported in figure (32).

Table 7 *Adsorption kinetic parameters for the MB adsorption at pH=7*

		SH/HNTs 0	SH/HNTs 5	SH/HNTs 20	SH/HNTs 35
Pseudo first order	k_1, (min^{-1})	2.09	1.77	1.60	0.94
	R^2	0.97	0.68	0.73	0.63
Pseudo	q_e,	31	38	43	45

second order	(mg g^{-1})				
	k_2, (mg g^{-1} min^{-1})	0.0014	0.0022	0.025	0.028
	R^2	0.99	0.99	0.99	0.99
Intraparticle diffusion Step 1	k_{id}, (mg g^{-1} $min^{-0.5}$)	0.42	0.89	1.02	0.98
	C (mg g^{-1})	21.0	23.0	25.1	28.3
	R^2	0.98	0.99	0.99	0.94
Intraparticle diffusion Step 2	k_{id}, (mg g^{-1} $min^{-0.5}$)	0.04	0.01	0.01	0.01
	C (mg g^{-1})	25.6	38.5	42.5	44.2
	R^2	0.98	0.98	0.99	0.99

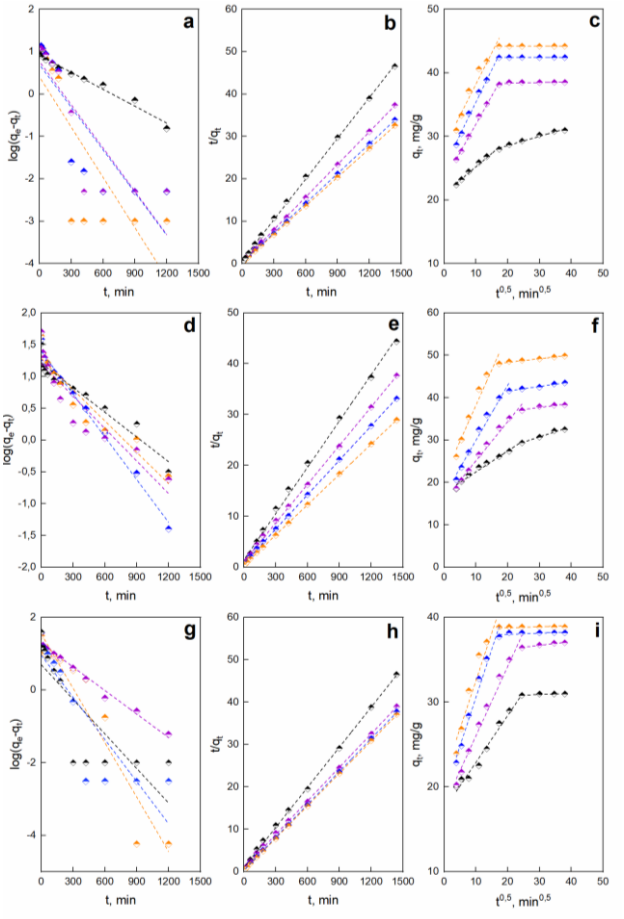

Figure 32 *Kinetic data of pseudo first order, pseudo second order and intraparticle diffusion model at pH=2 (a, b, c); pH=7 (d, e, f); pH=12 (g, h, i). (Black=SHC-0; Purple=SHC-5; Blue=SHC-20; Orange=SHC-35)*

It was also observed that correlation coefficients were quite low for pseudo first order model, proving that the system is not well described by a first order kinetic. Besides, the intraparticle diffusion model is not able to describe the dependence of q_t versus square root of time in the whole range since the plot doesn't pass through the origin. Two linear fitting can be pointed out concerning the boundary layer diffusion (step I-low times) related to the instantaneous adsorption on the external surface or strong electrostatic attraction followed by intraparticle diffusion (step II-long times) (Ahmad, Ahmad Puad and Bello, 2014). The different stages having non-zero intercepts suggests that intraparticle diffusion is not the only rate limiting step in the adsorption process (Nethaji and Sivasamy, 2011). The slope of boundary layer diffusion step (k_{id}) is related to the rate of the adsorption. Lower are the values,

slower is the adsorption process (Lorenc-Grabowska and Gryglewicz, 2007). It can be highlighted that k_{id}, or the initial rate of the adsorption, increases as HNTs content increases since a higher number of functional adsorption sites is available. The value of intercept, C, also increased from first to second stage. due to the boundary layer effect whose increase determines a decrease in the external mass transfer (Bello, Ahmad and Ahmad, 2012).

Finally, the pseudo second order model is fully able to describe the experimental data and calculated values of the adsorption capacities (q_e) were very close to the experimental ones. It can be deduced that the rate-limiting step may be the chemisorption phenomena likely due to weak electrostatic interaction between cationic groups of dye and anionic groups (mainly-COOH of lignocellulosic material) (Vimonses *et al.*, 2009).

Diffusion coefficients evaluation

Finally, the effective diffusion coefficient of cationic dye was evaluated as a parameter affected by pH and HNTs content. For a spherical system, the total amount of dye adsorbed is expressed by eq. (49) (Crank, 1979):

$$\frac{M_{,t}}{M_{,\infty}} = 1 - \frac{6}{\pi^2}\sum_{i=1}^{n}\frac{1}{n^2}\exp\left(-\frac{n^2\pi^2 Dt}{R^2}\right) \quad (49)$$

Where $M_{,t}$ is the amount of dye adsorbed at time t, $M_{,\infty}$ is the amount of dye adsorbed at equilibrium, R is the mean bead radius and D is the dye diffusion coefficient. The corresponding solution for small times is eq. (50):

$$\frac{M_{,t}}{M_{,\infty}} = 6\left(\frac{Dt}{R^2}\right)^{0.5} * \left\{\pi^{-0.5} + 2\sum_{n=1}^{\infty} \text{ierfc}\frac{nR}{\sqrt{Dt}}\right\} - 3\frac{Dt}{R^2} \quad (50)$$

The nonlinear fitting process allowed to extrapolate the diffusion coefficient D (cm^2/s). The extrapolate diffusion coefficients for each pH and as function of HNTs content are reported in table 8.

Table 8 *Dye diffusion coefficients as function of pH and HNTs content*

HNTs (%)	pH	*D* ($10^{-8*}cm^2/s$)
0	2	3.09±0.14
	7	1.96±0.04
	12	2.09±0.12
5	2	3.88±0.11
	7	2.16±0.04
	12	2.55±0.12
20	2	5.43±0.04
	7	2.99±0.09
	12	4.13±0.12

	2	6.73±0.21
35	7	4.59±0.14
	12	6.53±0.12

Empirical models were proposed to correlate the diffusion coefficient to either pH or HNTs content. Figure (33) reports the diffusion coefficient versus HNTs content as function of the pH level.

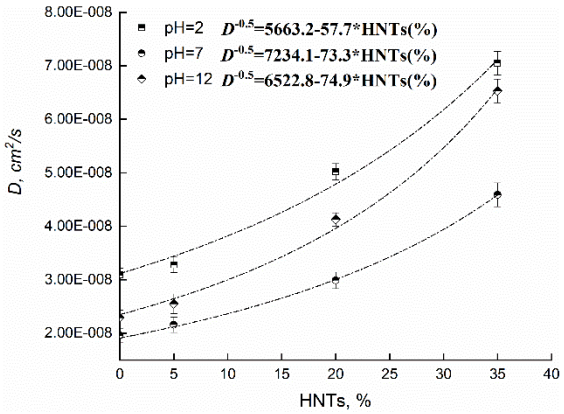

Figure 33 *D versus HNTs (%) for SHC-y beads at different pHs*

Response surface method was applied to correlate the diffusion data to pH and HNTs content. A power model was used with a quadratic type response. The provisional model of diffusivity is expressed by eq. (51):

$$D^{-0.5}=4330.2+703.9*pH-71.4*HNTs-4.2*pH*HNTs-41.3*pH^2 \quad (51)$$

The reported model is able to fit the experimental data with a R^2=0.994 and a F-value of 91.59, proving the adequacy of the chosen model. The equation in terms of actual factors can be used to make predictions about the response for given levels of each factor on the diffusion coefficient.

Modeling of experimental data

After performing the designed 12 experiments, by coupling the HNTs content and the pH level, data were statistically modeled through the design of experiment methodology. The studied output variable was set as the recovery % of MB. A modified 3rd model was chosen to fit the experimental data. The ANOVA test enables to evaluate the significance of the factors or their interactions. The set model is able to describe the experimental data with a R=0.9958. Moreover, since a factor is statistically significant only if the

relative p-value<0.05, it follows that just some contributions (A, B, AB, A^2, B^2 and A^3) were considered. According to that, the dye uptake was well described by the following eq. (52):

$$\sqrt{R_{\%}}=7.81+0.28*HNTs+0.14*pH-7.34*10^{-6}*HNTs*pH-0.016*(HNTs)^2$$
$$-0.01*pH^2+0.00026*(HNTs)^3 \quad (52)$$

The sign before some contributions was used to determine whether each model term affects positively or negatively on the MB adsorption process. As shown, the HNTs amount had the greatest effect on R since the terms of order 1, 2 and 3 concern this variable. Then pH factor and interaction pH-HNTs can even affect the recovery efficiency.

Concluding remarks

The present study concerns the use of an agro-based waste material, such as hemp fibers and hemp hurd as innovative and sustainable adsorbent for the removal of organic dye from aqueous solutions. Batch adsorption studies proved that the designed composite can be used as effective dye adsorbent from aqueous solution. The amount of dye was found to be highly dependent on pH regime, initial concentration of dye, ionic strength and slightly dependent on temperature. The reported data allowed to prove the efficiency of the adsorption of novel, green, inexpensive and sustainable composite materials obtained from agro-waste resources and natural materials.

6.Design of novel bio-packaging

Preface

Over the last decades, the environmental impact caused by fossil fuel derived materials is requiring an intense effort in developing biodegradable and environmentally friendly materials from natural resources (Avérous et al. 2001; Brachi et al. 2014; Bugatti et al. 2019; Al-Tayyar et al. 2020; Priyadarshi et al. 2021). In the perspective of searching alternative solutions, the preparation of green biodegradable materials from natural raw resources is taking a center stage (Tran, Graiver and Narayan, 2006; Yadav, Mehrotra and Dutta, 2021). Recently, agriculture crop flours are gained interest since their high availability, low cost, biodegradability and no-toxicity (Majzoobi *et al.*, 2015; Nouraddini, Esmaiili and Mohtarami, 2018). Among all, rice flour is being considered an interesting natural mixture for preparing biodegradable films (Ahmad *et al.*, 2015; Majzoobi *et al.*, 2015; Soo and Sarbon, 2018; Suriyatem, Auras and Rachtanapun, 2018). Moreover, the heterogeneity of the structure, the poor mechanical and barrier properties represent drawbacks of the obtained composites (Zhou *et al.*, 2002; Vercelheze *et al.*, 2012). To overcome that, natural fibers as reinforcement can be used to improve the abovementioned properties of polymer composites (Sanjay *et al.*, 2019; Viscusi, Pantani and Gorrasi, 2021). Besides, the incorporation of active agents in biodegradable films is of key interest (Gorrasi, Bugatti and Vittoria, 2012; Gorrasi and Bugatti, 2016; Ju *et al.*, 2019). The proposed research focuses on the valorization of rice flour as a low-cost starchy material for the production of sustainable films loaded with grapefruit oil as natural active

substance with potential antifungal, antiparasitic, antibacterial, antioxidant and anticancer properties (Xu *et al.*, 2007; Tan *et al.*, 2015).

Materials

Grapefruit seed oil (100% pure-cold pressed), rice flour, sodium alginate, glycerol and ethanol were used as reagents.

Composite preparation

Hemp hurds were firstly washed with distilled water to remove any trace of impurities. Hemp hurd was grinded using a stainless-steel blade grinder (Duronic-CG250), obtaining powder form solid. Before preparing the bio-composites, hemp hurd powder was mixed with grapefruit oil (7:3 w/w) employing a high energy ball milling for 8 hours at 350 rpm. The final product, labelled as HH-GO, was conditioned under controlled humidity in climatic and temperature chamber. Bio-composites obtained from rice flour were prepared by completely solubilizing 0.9 g of rice flour in 30 mL of distilled water. 0.1 g of sodium alginate was added as film forming material. Glycerol was added as a plasticizer (0.5 g/g of solid mixture). The solution was stirred at 100°C for 2 h. After solubilizing, the desired HH-GO content (2%, 5%, 10% and 20% wt on 1 g of rice flour and alginate basis) was added and the mixture was ball milled for 30 minutes at 350 rpm. The mixture was then poured in Petri dishes and the casting process was carried out at room temperature. Samples of pure rice flour were also prepared by setting the same experimental parameters. The obtained films were, hereinafter, labelled as R-(HH/GO x%) where x= weight content of HH/GO.

Film characterization

The estimated film density values are reported in table 9.

Table 9 *Density values of rice flour composites*

Sample	Density (g/cm^3)
R	1.54±0.21
R-(GO-HH 1%)	1.45±0.11
R-(GO-HH 5%)	1.27±0.12
R-(GO-HH 10%)	1.20±0.09
R-(GO-HH 20%)	1.12±0.10

The incorporation of hemp hurd powder inside the matrix structure led to a reduction in film density. This could be explained taking into account the lower bulk density of lignocellulosic material present into the composites (Dufresne and Vignon, 1998; Nguyen *et al.*, 2009). Figure (34) reports the SEM images of cross sections of rice flour film composites.

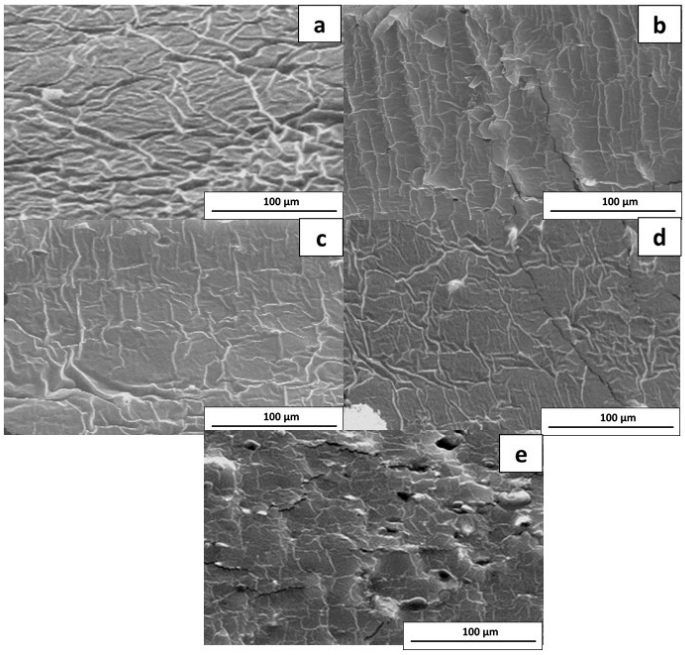

Figure 34 *Micrographs of cross sections a) R; b) R-(HH/GO 2%); c) R-(HH/GO 5%); d) R-(HH/GO 10%) and d) R-(HH/GO 20%)*

The SEM image of a neat rice flour film exhibited a rough surface with a few cracks, pores, and wrinkles which could be attributed to the effects of drying due to water evaporation. The incorporation of hemp hurd and grapeseed oil (up to 10% wt) doesn't contribute to noticeably reduce the compactness and smoothness of the films and an increase in the number of cracks in the film didn't occur. Some aggregations were found at 20% of hemp hurd loadings. An irregular morphology was observed, and aggregation phenomena and appearance of large pores occurred instead of cracks because of the excess of lignocellulosic materials.

The mechanical characterization was performed on all composites and pure rice flour film, taken as reference. The stress-strain deformation curves (figure (35)) allowed to extrapolate the mechanical parameters.

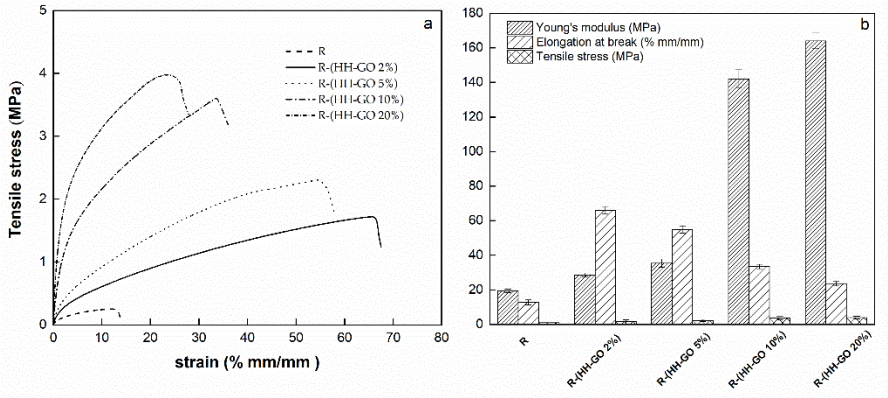

Figure 35 *a) Stress-strain deformation curves of neat rice flour and rice flour composites; b) Mechanical properties*

Results obtained from the mechanical characterization displayed an increase in the analyzed properties, which was proportional to the amount of reinforcement. It is clearly shown an effect of the hemp hurd powder as reinforcing agent in rice flour matrix as evidenced by the increase in the Young's modulus (up to 740% of the pure rice flour film for a reinforcement loading of 20%wt). Probably, due to the mechanical treatment, the available surface area of hemp hurd powder was increased leading to the improvement of mechanical interlocking. It follows an augmented high load transfer which could support the increase in tensile stress of the rice flour composites (up to 300% of the pure rice flour film with a hemp hurd amount of 20%wt) (Guleria, Singha and Rana, 2017; Singh et al., 2019). Then, it is worth noting the improvement of the elongation at break point for the composites compared to the pure rice flour film. The lowest content of reinforcement (2%wt) led to the highest elongation at break point. Moreover, as the reinforcement content increases, the composites are characterized by a higher brittleness which could be attributed to the local disconnection points inside the composite due to the presence of a heterogeneous cellulosic material dispersed inside a polymeric matrix. Figure (36) shows the sorption isotherms of rice flour composites, reporting the equilibrium moisture content (on dry basis) as a function of the water activity.

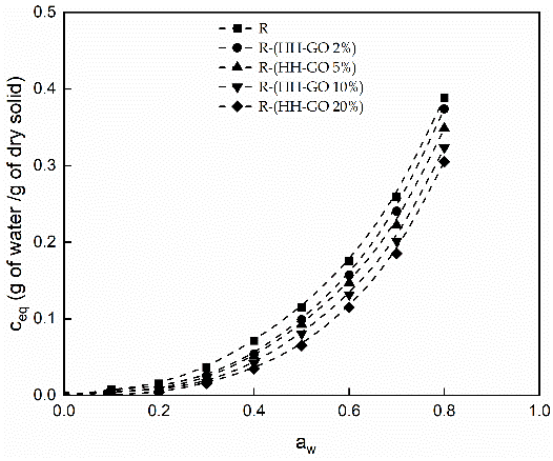

Figure 36 *Sorption isotherms of neat rice flour film and rice flour composites*

The sorption data have been fitted by applying Ferro-Fontan equation (eq. (53)) (Chirife et al., 1983; Saberi et al., 2015):

$$M=\left[\frac{\gamma}{\ln\left(\frac{\alpha}{a_w}\right)}\right]^{\frac{1}{r}} \quad (53)$$

Where M is the equilibrium moisture content (on dry basis), γ is a parameter accounting for the structure of sorbed water while α and r are parameters to be determined. By applying the series expansion of the natural logarithm for $0<\log \text{argument}\leq 2$ and $1<n<10$ and, taking into account that $a_w=P/P_0$, the sorption parameter was evaluated through the eq. (54):

$$S=\frac{10\gamma^{\frac{1}{r}}}{P_0*r}*\left[\ln(\alpha)+\frac{7381}{2520}\right]^{-\frac{(1+r)}{r}} \quad (54)$$

The evaluated parameters are reported in table 10 for each tested sample.

Table 10 *Ferro-Fontan equation's parameters*

Sample	γ	α	r	R^2
R	1.35	4.14	0.21	0.99
R-(GO-HH 2%)	1.47	4.61	0.17	0.99
R-(GO-HH 5%)	2.24	10.33	0.11	0.99
R-(GO-HH 10%)	2.95	31.25	0.098	0.99
R-(GO-HH 20%)	3.71	50.54	0.075	0.99

At lower activity, the adsorption process is supposed to occur on polar sites of rice starch. As activity increases, the plasticizing effect of water and the

increase *in* segmental motion contribute to increase the adsorbed moisture adsorbed. No noticeable difference could be observed for a_w<0.4. As water activity increases, a slight decrease in adsorbed moisture content could be observed. Probably, this effect could be either correlated to the low availability of accessible polar sites which could be involved in weak bonds with hemp hurd functional sites as well as the hydrophobic character of essential oil. Since water absorption largely depends on the water-soluble or hygroscopic components embedded in the matrix, the presence of hemp hurd powder could delay the water vapor molecules transport due to the bondings with rice starch polar groups. Besides, it could constitute a physical barrier for water molecule pathway and, consequently, an increase in tortuosity could explain the noticeable decrease *in* diffusivity. Table 11 reports the D_0, the thermodynamic diffusion coefficients extrapolated at C_{eq}=0, for all the samples as well as the permeability coefficients. These latters appear to follow the same trend of sorption and diffusion coefficients decreasing as HH/GO content increases.

Table 11 *Sorption, diffusion and permeability coefficients*

Sample	S g/100g*mmHg^{-1}	D_0 10^7 cm^2 s^{-1}	P 10^7g/100g*mmHg^{-1}*cm^2 s^{-1}
R	0.112±0.007	2.88±0.21	0.322±0.09
R-(GO-HH 2%)	0.061±0.01	2.51±0.19	0.153±0.05
R-(GO-HH 5%)	0.023±0.010	1.02±0.11	0.024±0.002
R-(GO-HH 10%)	0.019±0.007	0.16±0.03	0.003±0.0004
R-(GO-HH 20%)	0.017±0.006	0.12±0.02	0.002±0.0001

Composites solubility respect to water represents an important factor in determining possible applications for biopolymer films (Pattarasiriroj, Kaewprachu and Rawdkuen, 2020). The film solubility of hemp hurd/Grapefruit oil loaded rice flour films is reported in table 12 and ranges in 41%–58%. Transparency index and water angle contact are even reported.

Table 12 *Solubility (%), transparency and water contact angles of neat rice flour and rice flour composites*

Sample	Solubility %	Transparency	Water contact angle (°)
R	58.05±1.25	1.85±0.24	59.53±0.74
R-(HH-GO 2%)	55.27±1.32	3.44±0.30	73.23±1.65
R-(HH-GO 5%)	51.75±1.03	3.88±0.26	78.52±2.26
R-(HH-GO 10%)	49.35±0.99	4.68±0.31	92.75±2.19
R-(HH-GO 20%)	41.42±1.02	5.09±0.40	98.21±2.40

As expected, the solubility of neat rice flour film is high due to the hydrophilic nature of substances present in rice flour. A reduction in the film solubility was observed, compared with the control film, when hemp hurd powder and grapefruit oil were added. This effect can be attributed to intermolecular OH bonds forming between the hydroxyl groups of hemp hurd and the polar sites of rice flour, leading to reduce the free volume and to enhance the cohesiveness of the polymer matrix. Rice flour film and rice composites containing different amount of hemp hurd and grapeseed oil resulted homogenous and transparent. The neat rice flour film appeared quite clear and transparent. Incorporation of hemp hurd powder mixed with grapeseed oil slightly reduced the transparency of the films. Increasing concentration of reinforcement contributed to reduce the free volume resulting and so the mobility of rice starch chains. It follows a reduction in the transparency. Moreover, oils dispersed in the polymeric matrix are supposed to promote an increase in light scattering and, consequently, in the opacity of the films. This behavior could be attributed to the change in the film refractive index at the polymer interface promoted by essential oil presence (Atarés and Chiralt, 2016; do Evangelho *et al.*, 2019).
The degree of the hydrophilicity was evaluated through the contact angle (CA) measurements. The contact angle of neat rice flour film is about 60°, in accordance with the hydrophilicity degree of starch, the major component of rice flour. Contact angles of (HH/GO)-rice flour composites were higher than neat rice flour film. This could be explained considering either the hydrophobicity of the non-polar constituents of hemp hurd, such as lignin and waxes or the hydrophobicity of grapefruit oil, mainly composed of fatty acids. Meanwhile, the available polar sites of hemp hurd, belonging to hemicellulose and cellulose, could be involved in weak hydrogen interaction with starch matrix of rice flour leading to a reduced wettability. Finally, it is worth considering that the increase in contact angle of rice flour composites could be even attributed to the increase in surface roughness due to the presence of hemp hurd powder. These findings concur with the results obtained from barrier properties evaluation.

Release kinetic studies

Grapefruit seed oil, like all natural essential oils, is a complex mixture of several organic compounds (Shankar and Rhim, 2018). Identification of essential oil compounds was performed by GC analysis (figure (37)).

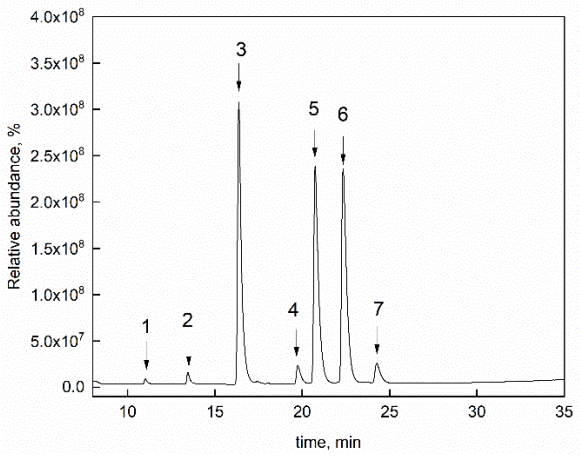

Figure 37 *Gas Chromatograph spectrum of grapefruit seed oil*

Seven main constituents were identified. Among all, palmitic, oleic and linoleic acid. To test the capability of rice flour film to be tested as controlled release system, we followed the release of the major components in the oil mixture which could be detected by UV-Vis spectrophotometer, that is the linoleic acid. The tests were performed using specimens with the same thickness (≅ 200 μm) and an exposed area of about 2 cm^2. Ethanol was used as a solvent. The release medium was withdrawn at fixed time intervals. The considered band was at 210 nm. To analyze the release, a second order model was chosen according to eq. (55) (Ho and Ofomaja, 2006; Hussein-Al-Ali et al., 2014):

$$\frac{t}{q_t} = \frac{1}{kq_e^2} + \frac{t}{q_e} \tag{55}$$

Where q_e (mg/g) and q_t (mg/g) are the equilibrium release amounts and the release amount at any time while k is the second-order rate constant (Dutta, Sarkar and Mukherjee, 2016). Estimation of parameters of pseudo-second order model is done using linear plot of t/q_t versus t. The slope and intercept of the linear regression line were used to calculate the k and q_e. Additionally, initial release rate of linolenic acid (r_{LA}) is given by eq. (56):

$$r_{LA} = kq_e^2 \tag{56}$$

Figure (38) shows released fraction (wt/wt %) as a function of the contact time (hours).

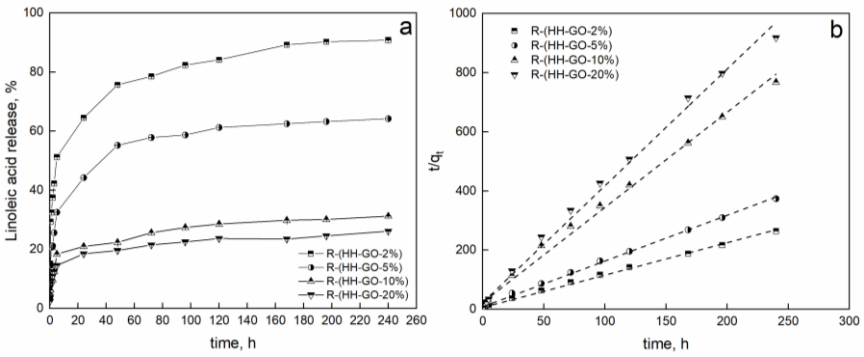

Figure 38 *a) Release of linoleic acid (% wt/wt) and b) t/q_t versus time (h) plots*

The kinetic parameters obtained from the pseudo-second-order model and the values of release rates are listed in table 13.

Table 13 *Pseudo second order parameters and values of release rates*

Sample	k (g mg^{-1} h^{-1})	q_e (mg g^{-1})	r_{LA} (mg g^{-1} h^{-1})	R^2
R-(HH-GO 2%)	0.21±0.02	0.92±0.03	0.17±0.03	0.99
R-(HH-GO 5%)	0.29±0.03	0.64±0.04	0.12±0.01	0.99
R-(HH-GO 10%)	0.45±0.04	0.31±0.08	0.04±0.02	0.99
R-(HH-GO 20%)	0.65±0.01	0.25±0.12	0.04±0.03	0.99

It is clear that the release of linoleic acid from the composites is much slower as the hemp hurd content increases. The r_{LA} values confirm the slowing down of rate release as HH/GO content increases. All the specimens show an initial slow release rate (r_{LA}) due to the movement of free fatty acid molecules, which slightly was reduced as HH/GO content increases. Besides, no noticeable burst effect can be detected. For long times the release profiles noticeably differ each other. The equilibrium release quantity (q_e) showed a significant decrease from 0.92 mg/g to 0.25 mg/g by increasing the HH/GO content from 2% to 20%. Such phenomenon could be attributed to an increase in mass transfer resistance due to the physical hindrance of hemp hurd. Besides, the reduced solubility as the HH/GO increases could lessen the fatty acid diffusion from the bulk of polymeric matrix. The linoleic acid disperse in rice flour matrix is almost fully released in 160 h for R-(HH-GO 2%) sample whereas only 20% is released in the same time from R-(HH-GO 20%). Moreover, it is interesting to observe that a no noticeable differences exists as HH/GO content is higher than 10% wt. It can be supposed that about 10% wt of HH/GO is the optimal concentration which allows for maximize the mass transfer resistance due to either the physical hindrance of hemp hurd which contributes to increase the

tortuosity of molecules pathway, or to the HH-rice flour network formation which could slow down the movement of fatty acid molecules from bulk to the release medium.

Concluding remarks

The use of rice flour and hemp hurd materials can open new perspectives for the development of new low-cost products with targeted performances. Release kinetics of linoleic acid, the main component of grapefruit seed oil, showed that they are dependent on HH/GO loading. The reported results clearly suggest the potential of utilizing a sustainable rice flour composite enriched with an active essential oil as novel bio-composites. Such systems appear very promising in the active packaging field, where a substance with antimicrobial activity drug should not be easily released but a tuned release profile is required.

7.Green modifications of hemp fibers for building applications

Preface

Global interest in the use of plant fibers in natural fiber reinforced composites (NFCs) is growing rapidly. Compared to synthetic materials (e.g. glass fiber), hemp fibers also have other advantages such as low cost and low density together with their high stiffness and strength-to-weight ratios. Hemp fibers, therefore, have potential as replacements for glass fibre as reinforcements for composite materials, (i.e. building sector, environmental sector, etc). A key feature for successful use of natural fibers such as hemp fibers in composite materials is optimal interfacial contact between the fibers and the hydrophilic inorganic material. Targeted modification of natural fibers for NFCs must also be designed to optimize the fiber surface properties and make them suitable for the production of fiber reinforced inorganic foams.

Materials

Hemp fibers were treated with a 10 g/l solution of sodium ascorbate at 25°C for 24h under mechanical stirring. They were then dried in a vacuum oven at 80°C for 8h. Both treated and not treated hemp fibers were used to prepare the fiber-reinforced foams. The fiber-reinforced foams were prepared by adding in the solid mixture (based on diatomite powder (19 wt%), Na_2SiF_6 (8 wt%), Si powder (0.05 wt%), treated and untreated hemp-fibers (3 wt%)) SS (64 wt%). After mixing of aforementioned materials (based on 100 parts of this mixture) 12 part of a “meringue” type foam was added (5.95 wt%) (the foams with treated and untreated fibers were namely FT and FUT

respectively). Pristine foam without fiber addition was also prepared for proper comparison (Pristine foam). The slurry was cast in prismatic open molds (160x40x40mm^3) and cured at 60°C for 24h at room humidity.

Characterization of hemp fibers

Thermogravimetric characterization performed on treated and untreated fibers has demonstrated that the treatment improves thermal stability even at lower temperature. Figure (39) shows the TGA and the DTG curves.

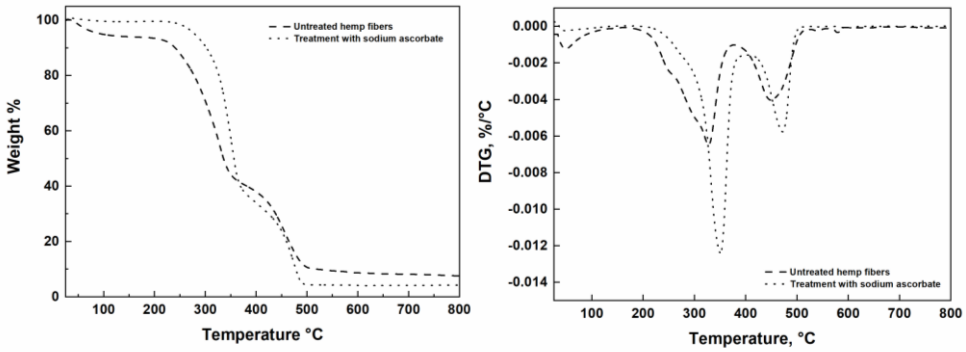

Figure 39 *Thermogravimetric analysis of the untreated and sodium ascorbate treated fibers*

The beginning of the thermal degradation process, defined as 5% mass loss temperature, is at about 95°C for the untreated sample and at about 280°C after the treatment with sodium ascorbate. At temperatures higher than 200°C the TGA profiles of both the samples underline two distinct and well-separated thermal events. For the untreated sample, the first one falls in the temperature range between 200°C and 330°C, and the second one falls in the range between 380 and 500°C. The thermogravimetric analysis for the fibers treated with sodium ascorbate highlights that the same thermal events fall in the range of temperatures between 280 and 380°C and in the range of temperature between 380 and 500°C. From a comparison of the DTG curves of both samples, it is evident that the degradative peaks of the treated sample are shifted at a higher temperature. All these results indicate that the treatment with sodium ascorbate has a not negligible effect on the degradative mechanism of the hemp fibers. Figure (40) shows a comparison of the infrared spectra of the treated and untreated fibers. The peak centered at 3330 cm^{-1} is associated with the intramolecular OH stretching vibrations, and the peak centered at 2916 cm^{-1} is a superimposition of C-H stretching vibrations in all

the polysaccharides. The ratio between the intensity of this peaks, I_{3330}/I_{2916}, change from 1.6 for the untreated sample to 2.1 for the sample treated with sodium ascorbate, indicating that the OH functionality is increased on the surface of the treated fibers.

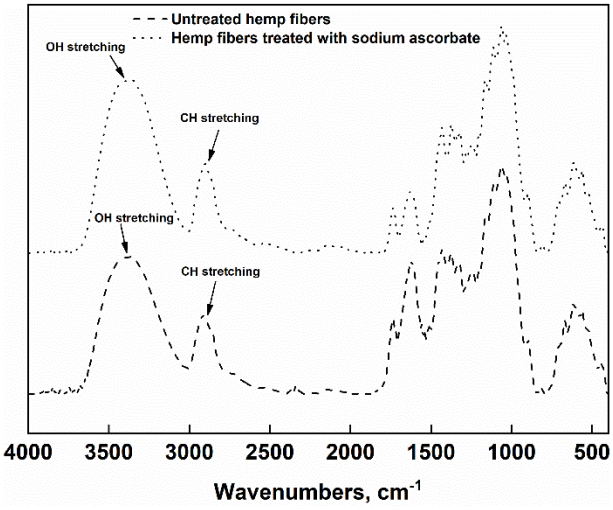

Figure 40 *FTIR spectra of untreated and treated fibers*

The increasing of OH functionalities affected positively the wettability of the hemp fibers making them suitable for the application to produce fiber reinforced foams. The produced fiber reinforced foams were characterized from mechanical point of view through flexural and compressive tests on three samples for each system ($160x40x40mm^3$). In particular, flexural tests were carried out through a quasi-static three-point test, according to ASTM D790 standard on the prismatic specimens. Thermal conductivity of the produced foams was, also, measured by using the Modified Transient Plane Source (MTPS) technique on a C-Therm TCi Thermal Conductivity Analyzer. The effect of fiber (treated and untreated) on mechanical (σ_f: flexural strength and σ_c: compressive strength) and thermal properties (λ: thermal conductivity) of composite foams are reported in Table 14. Mechanical behavior of the pristine foams showed the stress-strain curves with a brittle failure typically correlated to the ceramic materials behaviour (Galzerano *et al.*, 2017). The addition of fiber without chemical treatment induced a decrease in both mechanical and thermal properties of foams, due to a bad distribution of the fibers within the inorganic matrix. Conversely, the FT composite foams, highlighted a ductile behaviour after reaching maximum stress. This is due to the hemp fiber bridging; in fact, part of the stress was carried to the fibers and their progressive resistance to slip from the matrix, as the crack opening of the matrix propagates, until their complete pull-out and failure of the sample. In

this case, the addition of treated fibers in the matrix led to an increase in flexular and compressive strength without influencing the thermal conductivity of the final product with respect to the pristine samples. These outcomes could be correlated to the good chemical interaction between the fibers and the inorganic matrix induced by a higher grip on the fiber surface with respect to the untreated fibers.

Table 14 *Mechanical and thermal properties of produced foams*

Sample	Density (kg/m^3)	σ_f (MPa)	σ_c (MPa)	λ (W/mK)
Pristine foam	350±5.6	0.99±0.01	1.5±0.2	0.06
FUT	360±8.0	0.76±0.03	1.2±0.1	0.07
FT	355±6.3	1.35±0.01	2.8±0.08	0.06

Concluding remarks

The feasibility of using an innovative treatment with sodium ascorbate to improve the wettability of hemp fibers, to be applied in fiber-reinforced foams, was evaluated. Both the treated and untreated fibers were used to prepare diatomite-based fiber-reinforced foams. For these materials, the density and the thermal conductivities were measured. The mechanical characterization by means of mechanical compressive and flexural strength indicated a substantial improvement of the mechanical performances.

8.Novel green carriers for application in agricultural field

Preface

Nowadays, with the emerging intensification of farming systems, higher production and increased efficiency are required. In fact, some agricultural products are sold off season; that is greatly due to the excessive use of synthetic pesticides (Mfarrej and Rara, 2019). Although their benefits, the intensive use of them is leading to serious environmental issues (Silva *et al.*, 2019). However, the misuse of synthetic pesticides over a long period can not only be a source of harmful effect to soil, animals and humans but along with that, it could lead to a series of side effects such as the possibility for some pests to resist to them, the growth of stronger pests, the possibility to attack not targeted organisms, the too high concentration of pesticides in food products. All these unspeakable considerations are requiring, nowadays, a green and innovative alternative to protect crops without generating harmful consequences on ecosystem (Yang *et al.*, 2018; Mfarrej and Rara, 2019). A possible route lies in the use of natural derived substances (in general from plants, seeds, roots, leaves etc.) able to be effective against pests as well as to be safer than synthetic pesticides (Copping and Menn, 2000). These substances could act as insecticides, antifeedants, insects-growth regulators and repellent, representing a valid green alternative to synthetic pesticides. Except from volatilization, the retention on soil particles and degradation biotic and abiotic are the most noteworthy processes that could control the fate of pesticides. To avoid that, the use of new approaches is required aiming at guaranteeing a controlled dispersion of green pesticides in soil (Roy *et al.*, 2014; Bai *et al.*, 2019). Based on the above, this research focuses on the design and the preparation of two innovative green composites made up of hemp

hurds reinforcing gelatin beads as a pH-sensitive delivery system of eugenol and pectin films reinforced with mechanochemically treated hemp fibers as release systems of cinnamic acid.

Gelatin beads/hemp hurd as pH sensitive devices for delivery of eugenol as green pesticide

Materials

Gelatin from bovine skin, eugenol, sunflower oil, NaOH in pellet form, HCl solution 37% v/v were used as reagents.

Beads preparation

Prior to perform droplet gelation process, hemp hurds have been grinded using a stainless-steel blade grinder (Duronic-CG250). Gelatin (Ge; 1.6 g), Eugenol (Eu; 10% wt on gelatin basis) and HH (1%, 3% and 5% on polymer basis) were mixed with 15 mL of water and stirred at 45 °C for 4 hours. The solution was added dropwise to sunflower oil kept at 4°C using ice bath. To complete gelification, the beaker containing the oil and the prepared beads was kept in an ice water mixture for 2h. Then, gelatin beads were collected from the dispersed phase and washed several times with pure ethanol and distilled water to obtain the Ge-Eu-HH-x (x= % wt of hemp hurd powder) composite beads. Finally, the composite beads were air dried for 48 h.

Experimental part and analysis of results

Figure (41) shows the sorption data of gelatin beads composites, reporting the equilibrium moisture content q_e (on dry basis) as a function of the water concentration c_{eq} (g/L). The knowledge of water vapor properties of hydrogel composites is required to better understand the behavior of the produced delivery systems for outdoor exposures such as agricultural ones. The evaluation of barrier properties is crucial since a high moisture content affects dramatically the physical and chemical ageing of the composites and, thus, their lifetime in interactive environments. In order to analyze the sorption isotherms, the Sips model (eq. (57)) was adopted (Sips, 1948; Jeppu and Clement, 2012).

$$q_e = \frac{q_m * a_s c_{eq}^{1/n}}{1 + a_s c_{eq}^{1/n}} \quad (57)$$

Where q_e is the is amount of the adsorbate at equilibrium (mg/g), C_{eq} is equilibrium water concentration of the adsorbate on the adsorbent, q_m is the monolayer adsorption capacity (mg/g), a_s is Sips isotherm model constant and n il related to the heterogeneity of the system.

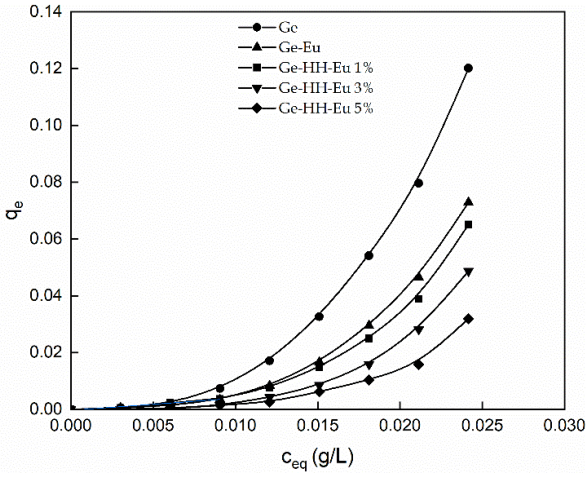

Figure 41 *Sorption isotherms of gelatin beads*

The extrapolated Sips parameters are reported in Table 15:

Table 15 *Sips parameters obtained by fitting experimental data*

Sample	q_m (g/g)	a_s (10^3 g^n*L^{-n})	n
Ge	56±2.52	4.0±0.10	0.36±0.02
Ge-Eu	53±3.66	2.8±0.12	0.32±0.01
Ge-HH-Eu 1%	53±3.21	2.5±0.13	0.31±0.02
Ge-HH-Eu 3%	51±2.54	2.2±0.08	0.26±0.03
Ge-HH-Eu 5%	40±1.95	1.9±0.07	0.24±0.01

Proper interactions are supposed to occur between gelatin matrix and hemp hurd functional groups. The introduction of hemp hurd inside the gelatin matrix led to a decrease in adsorbed moisture content. Then, as hemp hurd concentration increases, sorption parameter underwent a substantial decrease since the hydrophobization offered by the hemp hurd components. Reduced water sorption of gelatin beads as HH amount increases can be a consequence of enhanced interaction of gelatin chain and OH groups that are less available for the interaction with water vapor. Such explanation is supported by decrease in monolayer adsorption capacity (q_m). The 1/n parameters concerns

the heterogeneity of the system and, as the hemp hurd content increases, it underwent an increase since the presence of not-homogeneous phase inside the gelatin matrix (Mohammadi Nafchi et al., 2014). Table 16 reports the D_0, the thermodynamic diffusion coefficients extrapolated at m_{eq}=0 and the water permeability coefficients.

Table 16 *D_0 and Permeability coefficients*

Sample	D_0 (10^{-7} cm^2/s)	P (10^{-7} $g/g*1/atm* cm^2/s$)
Ge	8.91	6.15
Ge-Eu	8.26	4.63
Ge-HH-Eu 1%	3.19	0.97
Ge-HH-Eu 3%	1.55	0.26
Ge-HH-Eu 5%	0.77	0.08

As expected, diffusivity and permeability of the composites decrease with filler loading, in full agreement with the sorption data. This could be, firstly, explained by taking into account the interactions HH-matrix, mainly hydrogen bondings, with hydrophilic groups of gelatin matrix. From transport phenomena point of view, the HH loading increases the mass transfer resistance which, likely, led to a reduction of mean cross sectional area available for water diffusion. The reduction of adsorbed water could be then attributed to the decrease in free volume due to the presence of lignocellulosic reinforcement which constituted a physical hindrance for the diffusion of water molecules, determining a higher heterogeneity of the system (as evidenced by 1/n parameter). It follows that the change in mean water molecules pathway and an increase in the tortuosity of the system occurred, justifying the reduction of D_0 coefficients observed.

In agricultural applications, the pH has to be considered as a crucial factor affecting the release phenomena (Roy, A K Bajpai and Bajpai, 2009). So, a deep study of the effect of pH on swelling and deswelling degree has been accomplished. Swelling properties of gelatin beads were determined since they are supposed to affect the release rate of a delivery system. Firstly, 10 mg of material were air-dried and then weighed. Then, they were immersed in 20 mL of liquid medium (pH=3, pH=7 and pH=12) solution for different periods of time. The pH values of the tested release media were adjusted at 3 and 12 using 0.1 M HCl and 0.1 M NaOH solutions, respectively. Wet samples were wiped with filter paper to remove excess liquid and weighed. The swelling degree (SD) was calculated as (eq. (58)):

$$SD(\%)=\frac{W_w-W_{dry}}{W_{dry}}*100 \quad (58)$$

where W_w and W_{dry} are the weights of the beads measured at a specific time point and the initial weight of air-dried samples. A Voight-based equation (eq. (59)) has been applied to describe the experimental swelling data (Omidian et al., 1998):

$$S_t = S_{eq}(1-e^{-t/\tau}) \quad (59)$$

where S_t is the swelling at time t, S_{eq} is the equilibrium swelling, τ is a rate constant. Dissolution kinetics were determined to better understand the release behavior of composite hydrogels. As first step, gelatin beads were dried for 24 h in a vacuum oven. The dry matter (M_0) was weighed and immersed in 15 mL of liquid medium at different pH values (3, 7 and 12), kept under mechanical stirring. At fixed time intervals, the beads were taken out, dried under vacuum conditions and the weight was recorded. The solubility kinetic, for each pH value, was determined by plotting the gelatin beads weight as a function of the dissolution time. Eq. (60) was proposed to describe the dissolution kinetics of gelatin beads:

$$m(t) = M_{max} * \exp(-k_{pH} * (t-t^*)) \quad (60)$$

Where M_{max} represent the maximum weight of Ge beads reached at stationary phase and t* represent the time corresponding to the stationary phase. Figure (42) reports swelling and deswelling degrees of gelatin beads along the time as a function of pH level.

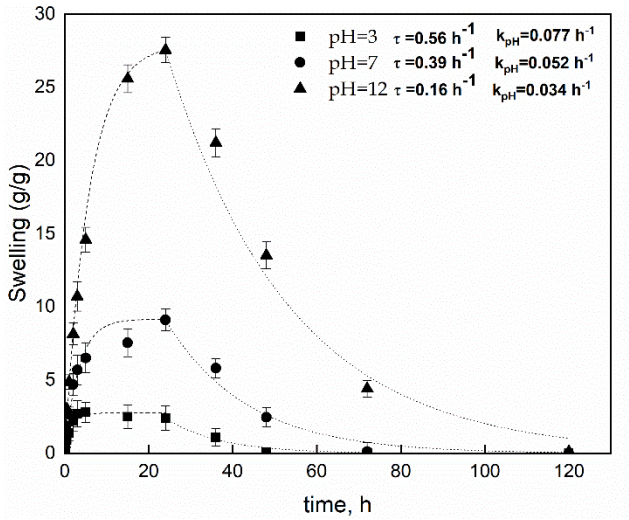

Figure 42 *Swelling and deswelling degrees of Ge beads at different pHs*

For short times, the rate of water uptake sharply increases and then reaches a level off. After a certain time, dissolution phenomena occur and deswelling is

verified. It can be deduced that gelatin swelling and deswelling degrees are clearly affected by pH of the medium due to the presence of ionizable groups (Kalaleh, Tally and Atassi, no date; Gordon et al., 2010). In acidic conditions, NH_3^+ and COOH are present while in basic conditions the species present are NH_2 and COO^-. In neutral conditions, the predominant species are NH_2/COOH (Pourjavadi and Reza MAHDAVINIA, no date). It is reported that gelatin hydrogels swelled less when placed in acidic dissolution medium (pH=3) compared to other media (pH=7 and pH=12) (Oliveira et al., 2010; Wang et al., 2020). Since pKa value of main amino-acids of gelatin (glycine, proline and hydroxyproline) are 9.6, 10.6 and 10.6, as pH of medium is 12, a deprotonation of gelatin and an increase in charge on proteins is supposed to occur. The subsequent charge repulsion of deprotonated groups lead to a higher swelling degree (Yang et al., 1997). It follows that the ionization of all COO^- groups in gelatin increases the swelling degree of the gelatin beads. Ionic repulsion between charged groups incorporated in the gelatin matrix could be assumed to be the main driving force responsible for the swelling behavior. As pH changes, due to the ionizable groups in gelatin chains, there are hydrostatic repulsions between them so, as gelatin beads adsorb water molecules, these latter occupy a certain volume and, as a consequence, an expansion of the structure occurs (Martínez-Ruvalcaba et al., 2009). Besides, the higher swelling at basic pH could be ascribed to the possibility of forming a porous structure due to alkaline hydrolysis (Omidian et al., 1998). Since τ could be considered a measure of the resistance to water permeation, lower τ value corresponds to higher water uptake rate. It is evident that after about 24 hours a decrease in swelling degree can be observed due to the dissolution rate of gelatin. The dissolution of a solid in a liquid regards the transfer of mass from the solid phase to the liquid one. Its rate tends to decrease as pH increases from 3 to 12, following an exponential behaviour. In acidic conditions, gelatin began to break down since the dissociation of the gelatin macromolecular structure. This phenomenon could explain the fast dissolution of gelation. The k_{pH} constant could be considered as an estimation of the dissolution rate constant and noticeably decreases passing from acidic to basic medium as pH level differs from isoelectric point (IP) of gelatin (pH=4.7) (Xiao et al., 2004). The slowdown of gelatin beads dissolution at high pH level could be due to the inherent pH-solubility behavior of gelatin and appears to be a consequence of the physico-chemical properties of gelatin (Zhao et al., 2004). At low pH (pH<IP), the conformation of the gelatin is probably less stable, and its overall net charge is highly positive. It follows that in the gel state, gelatin retains part of its secondary and tertiary structures and the gel rigidity decreases due to the decreased conformation stability. The dissolution of gelatin in water is quite fast and the complete bead erosion occurred in a short time interval.

The effect of pH on the release kinetics and the contribution of hemp hurd on the release phenomena were analyzed. The release of encapsulated compound

is enabled by entry of release fluids through the systems toward the bulk and thereby the counter diffusion movement of molecules to surface of the system followed by the complete release from the polymeric system. The tests were performed using a fixed amount of composite beads (200 mg), placed into 15 mL of ethanol and stirred at 100 rpm in an orbital shaker (VDRL MOD. 711+ Asal S.r.l.). The release medium was withdrawn at fixed time intervals and replenished with fresh medium. The considered band was at 280 nm. The effect of pH and hemp hurd concentration on release kinetics were considered. The experimental data were fitted according to Baker and Lonsdale model (eq. (61)) (Rani et al., 2017).

$$\frac{3}{2}*\left\{1-\left(1-\frac{M_t}{M_\infty}\right)^{2/3}\right\}*\frac{M_t}{M_\infty}=k\frac{t}{r^2} \tag{61}$$

Where M_t is the amount of drug released at time t, M_∞ is the amount of drug release at infinite time, k is the Baker-Lonsdale release constant and r is the radius bead, supposing it to have spherical shape (Chien, 1988). Since the gelatin beads underwent swelling phenomena, which are differently affected by pH level of release medium, the bead radius is supposed to be time-dependent (r=r(t)). Eq. (62), obtained by explicating the definition of Swelling degree (S_t), needs to be considered for the time interval from 0 to 24 hours (maximum time before prevalence of dissolution phenomena):

$$m(t)=M_0*\left[1+S_{eq}(1-e^{-t/\tau})\right] \tag{62}$$

After 24 hours, the dissolution phenomena are supposed to occur and the bead mass underwent a reduction. For a spherical bead, considering the equation of a spherical volume, the time-dependent radius equations were derived. Embedding all the constant parameters in the k' and k'' coefficients. the time-dependent radius equations, reported as eqs. (63) and (64), were obtained:

$$0<t<24h \quad \frac{3}{2}*\left\{1-\left(1-\frac{M_t}{M_\infty}\right)^{2/3}\right\}*\frac{M_t}{M_\infty}=k'\frac{t}{\left[M_{0*}\left(1+S_{eq}(1-e^{-t/\tau})\right)\right]^{\frac{2}{3}}} \tag{63}$$

$$t>24h \quad \frac{3}{2}*\left\{1-\left(1-\frac{M_t}{M_\infty}\right)^{2/3}\right\}*\frac{M_t}{M_\infty}=k''\frac{t}{\left[M_{max}*\exp(-k_{pH}*(t-t^*))\right]^{\frac{2}{3}}} \tag{64}$$

Figures (43) report the release curves of eugenol for pure gelatin and gelatin beads composites varying the pH of the release medium.

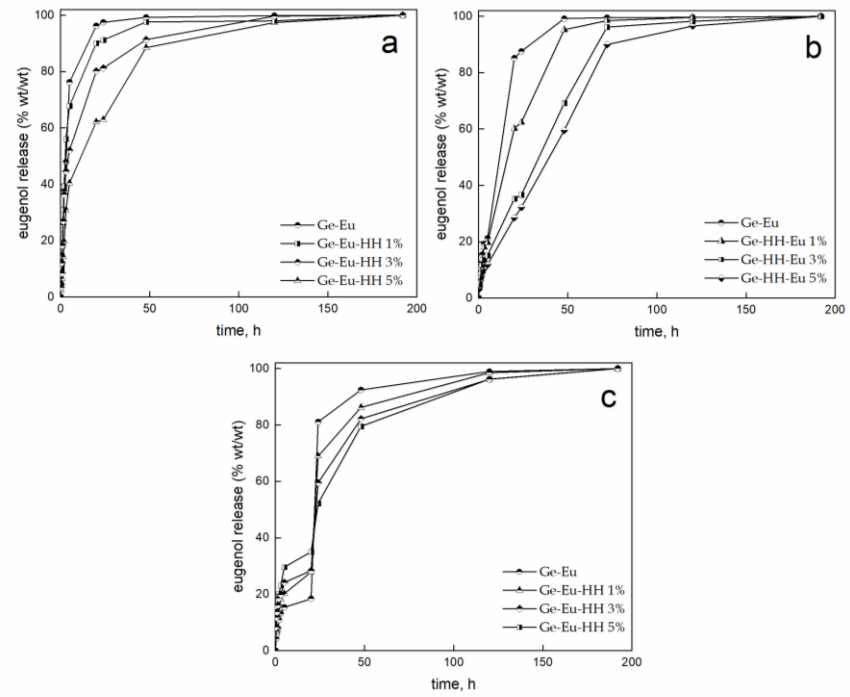

Figure 43 *Eugenol release kinetics of gelatin beads at a) pH=3; b) pH=7 and c) pH=12*

The mechanism and kinetics of drug releases were affected by many parameters such as physical properties of polymers, drug to polymer ratio and geometric shape of release matrix, as well as swelling and dissolution phenomena (Ainurofiq and Choiri, 2015). So, a complex heterogeneous release curves were obtained. The release rate of eugenol is dependent on the pH of the release medium. The initial burst release is supposed to be related to the amount of encapsulated compound not effectively protected by the carrier. It occurred since the initial swelling of the matrix and the osmotic pressure difference between the release medium and the bead (Saber-Samandari *et al.*, 2017). The penetrating water molecules could initially generates phenomena such as relaxation of polymer chains and hydration (Ford *et al.*, 1987). The adsorbed water molecules could then enhance the internal pressure allowing the eugenol to be released and promoting the burst release effect. Moreover, it is worth noting that the burst is reduced as pH increases, as consequence of the higher stability of gelatin network which, probably, is able to better retain the encapsulated eugenol; then a slower and more controlled release follows (Gallagher and Corrigan, 2000). As shown, after 24 hours more than 98% of eugenol is released from gelatin beads at pH=3. Besides, 91%, 81% and 63% of eugenol is released after 24 hours for

gelatin beads with 1%, 3% and 5% of hemp hurd, respectively. As pH level increases, a noticeable change of release kinetic is observed. The released eugenol after 24 hours is 87%, 62%, 37% and 32% wt (pH=7) and 81%, 68%, 60% and 52% wt (pH=12) for Ge-Eu and gelatin beads with 1%, 3% and 5% of hemp hurd, respectively. The low stability of gelatin conformation determined a low gel rigidity, consequently the diffusion of eugenol in the release medium speeded up. As pH>IP, the gelatin structure is more stable. So a slow eugenol release occurred attaining a first plateau probably due to the increase in mass transfer resistance. For longer times, the beads in basic medium tend to increase their volume determining an increase in SD. The adsorption of high amount of water and the increase in gelatin volume could justify the higher amount of eugenol released at pH=12 compared to pH=7 conditions. In any case, the network structure due to hemp hurd located inside gelatin matrix could slow down the release rate of encapsulated eugenol. Probably, hemp hurd acts as a physical barrier which improves the mass transfer resistance by increasing the tortuosity of the system. The fitting process of release kinetic curves allowed to obtain the k' and k'' (expressed in $g^{2/3} * h^{-1}$) parameters which are reported in Table 17:

Table 17 *k' and k'' parameters obtained from fitting of experimental data*

Sample	pH=3		pH=7		pH=12	
	k'	k''	k'	k''	k'	k''
Ge-Eu	0.0342	0.0047	0.0190	0.0039	0.0028	0.0016
Ge-HH-Eu 1%	0.0263	0.0035	0.0062	0.0033	0.0013	0.0015
Ge-HH-Eu 3%	0.0132	0.0028	0.0044	0.0026	0.0011	0.0011
Ge-HH-Eu 5%	0.0091	0.0022	0.0031	0.0014	0.0006	0.0006

The k' diffusion constant underwent a decrease as pH level increases and, for each pH regime, it decreases as hemp hurd concentrations increases. The decrease in k' constant as pH increases could be attributed to different swelling behavior of gelatin beads. Moreover, since k' constant is directly proportional to diffusion coefficient, its reduction as HH concentration increases may be due to increase in mass transfer resistance offered by HH powder which enhances the tortuosity. Besides, the same behavior characterized the k'' constant which refers to dissolution regime. As gelatin bead volume decreases, due to erosion phenomena, the eugenol diffusion is favored. Moreover, a slow deswelling rate, by virtue of a slow erosion kinetic (k_{pH} constant), could partially delay the dissolution of gelatin bead external layer. Moreover, since the rate of dissolution is proportional to surface area, at relatively long experimental times, it slows down the release kinetics allowing to prolong the eugenol diffusion up to 120 h. Results confirmed that

the addition of hemp hurd could lead to a decrease in eugenol released amount. The hydrophobicity of hemp hurd, due to the presence of external non cellulosic material, could enhance the reduction of water uptake rate and, as a consequence, the amount of swelling of the composite beads (Saber-Samandari, Saber-Samandari and Gazi, 2013). Finally, it could be claimed that a novel agricultural compound delivery system, completely based on renewable resources, has been designed to achieve a pH-triggered release. Similar systems have already been reported in literature. Roy et al. developed calcium-alginate microspheres for controlled release of endosulfan (Roy, J. Bajpai and Bajpai, 2009) and alginate-gelatin swellable beads loaded with cypermethrin (Roy, A. K. Bajpai and Bajpai, 2009), reporting similar results and similar trends as pH changes. Moreover, the unique developed release system, made of aqueous gelatin/lignocellulosic material solution, is completely sustainable and no other similar systems have already been reported.

Pectin/hemp fibers biocomposites as carriers of green pesticides in agricultural field: fabrication of a pot-like device

Materials

NaOH, trans-cinnamic acid, Pectins from apple with molecular weight 30,000–100,000 Da and a degree of esterification about 70–75% were used as reagents.

Biocomposite preparation

The functionalization of hemp fibres was conducted through the mechanochemical treatment reported previously by using a high energy ball milling process. Biocomposites obtained from natural pectin from apple were prepared solubilizing 1 g of pectin in 30 mL of distilled water. It was then added glycerol as plasticizer (3 % v/v). The solution was stirred at 80°C for 1.5 h. After completely solubilizing the pectin powder, hemp fibres (3 %w/w), mechanochemically modified at different times, and cinnamic acid (3% w/w) were added and the solution was submitted to ball milling. The rotation speed used was 450 rpm. The mixtures obtained were poured in Petri dishes and slowly evaporated at room temperature. Samples of pure pectin and pectin filled with raw HF were also prepared in the same described experimental conditions.

Experimental results

Barrier properties to water vapor, sorption and diffusion were evaluated on all biocomposites and pure pectin, in order to investigate how the transport phenomena of the pectin matrix are affected by the fibers treatment time. Figure (44) reported the sorption isotherms of the neat pectin and pectin/HF composites, as C_{eq} (g/g on dry basis (d.b.)) versus water activity (a_w).

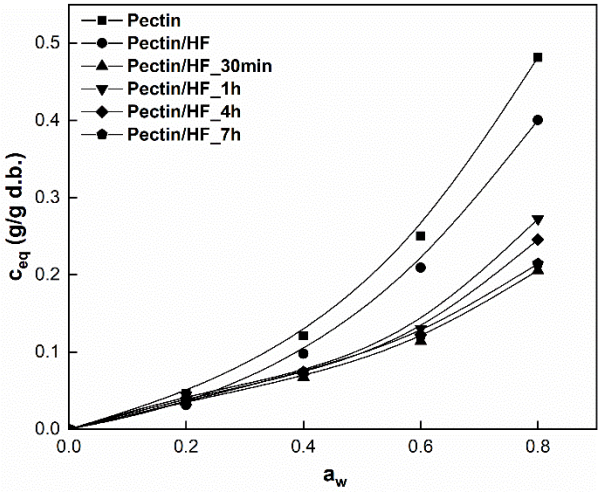

Figure 44 *Equilibrium sorption isotherms for neat pectin and pectin/HF composites.*

For all the composites, a decrease in adsorbed moisture content was evident. The hydrophilic groups of pectin can be involved in weak bonding with external hemp fibres groups reducing the polymer water adsorption. Moreover, this effect could be related either to the chemical interactions fiber-matrix or the mass transfer resistance offered by the hemp fiber. The less availability of polar groups and the increase in tortuosity of the system due to the hindrance effect of the fibres could justify the reduction of water sorption for the pectin/HF composites. Table 18 reports the barrier properties parameters for the neat pectin and pectin/hemp fibres composites.

Table 18 *Sorption coefficients of pectin and pectin/HF composites*

Sample	S ($g/g_{\ d.b.}\ atm^{-1}$)
Pectin	7.25±0.18
Pectin/HF	5.86±0.11
Pectin/HF-0.5h	4.04±0.07
Pectin/HF-1h	4.35±0.07

Pectin/HF-4h	4.27±0.06
Pectin/HF-7h	4.46±0.05

It was evident that the sorption values decrease for the pectin/HF composites respect to the neat pectin. The lowest value for the composite Pectin/HF-30 min is a consequence of the better adhesion filler-pectin matrix and the less availability of polar groups. As milling time increases, the lower crystallinity of hemp fibers as well as the reduction of OH groups could limit the availability of polar groups so the sorption of water was reduced.

Contact angle (CA) measurements were performed on each sample to investigate either the hydrophilicity degree of the composites surface (using water) or the surface energy. Table 19 reports the surface energy and the contact angles of neat pectin and pectin composites.

Table 19 *Contact angle and surface energy of the biocomposites*

Sample	Contact angle (°)		Surface free energy
	water	glycerol	γ_s (mJ/m^2)
Pectin	58.65±1.24	66.54±1.35	52.42±1.22
Pectin/HF	62.23±1.31	68.59±1.37	46.96±1.20
Pectin/HF-0.5h	35.83±1.11	51.95±1.29	81.46±1.65
Pectin/HF-1h	37.51±1.12	53.24±1.24	80.18±1.54
Pectin/HF-4h	38.95±1.05	54.06±1.54	78.42±1.55
Pectin/HF-7h	41.21±1.19	55.95±1.26	76.97±1.42

As reported, CA of biocomposites filled with untreated-HF was higher than neat pectin and treated HF/pectin ones. This could be explained considering the presence of non-polar constituents (lignin, waxes) which make the untreated hemp fibres hydrophobic. The better hydrophobicity came from lower surface energy of the composite film. (Zhao *et al.*, 2017) Moreover, the mechanochemical treatment removed such non-polar materials as confirmed from FTIR, exposing partially OH groups of hemicellulose and cellulose which contributed to make the fiber more hydrophilic. Besides, a decrease of contact angles for treated hemp fiber/pectin composites was observed since the exposition of OH sites of hemp fibres, resulting in an improved wettability. Then, considering the pectin composites reinforced with treated fibres, it was worth noting the slight increase in CA as processing treatment time of hemp fibres increased. This effect could be explained considering other factors such as the increase in fiber roughness, which was supposed to affect the contact angle of biocomposite films. (Ariawan *et al.*, 2017)

Figure (45) reports the release of cinnamic acid (%) loaded in pectin composites reinforced with hemp fibres treated at different times.

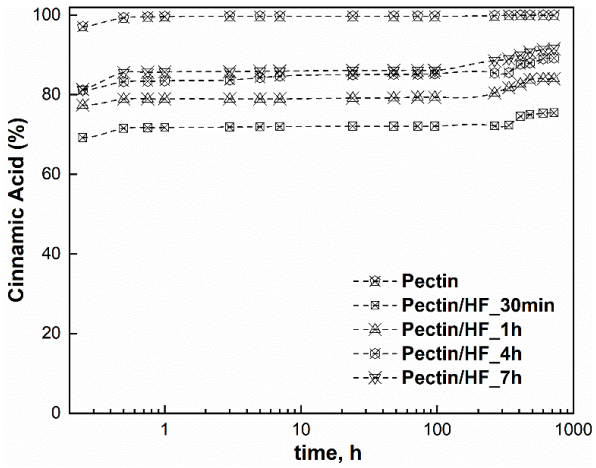

Figure 45 *Release of cinnamic acid as a function of contact time (h)*

By observing data, at first glance it is possible to claim that an improvement and slowing down of release kinetic occurred for fiber reinforced films. Besides, for experimental time longer than 4h, no noticeable differences can be observed. To better understand the phenomena involved, a mathematical modeling was applied. The experimental points were fitted using the Peppas-Sahlin model (eq. (65)). Such a model takes into account the contribution of two mechanisms: diffusion and relaxation (Bruschi, 2015) in terms of the coupled effect of the Fickian diffusion and polymer relaxation mechanisms related to an anomalous release process with two phenomena controlling the drug release: (Peppas and Sahlin, 1989)

$$\frac{M_t}{M_\infty} = K_1 * t^m + K_2 * t^{2m} \quad (65)$$

K_1 is the kinetic constant for Fickian contribution of drug release, K_2 is the kinetic constant for Case-II contribution, and m a diffusional exponent. The term $K_1 * t^m$ represents Fickian contribution, while the term $K_2 * t^{2m}$ is related to the Case-II relaxational contribution. Table 20 reports the kinetic parameters and the correlation coefficient (R^2).

Table 20 *Peppas-Sahlin kinetic parameters*

Sample	K_1 (h^{-m})	K_2 (h^{-2m})	m	R^2
Pectin	1.80	-0.81	0.023	0.999
Pectin/HF-0.5h	0.48	0.23	0.0048	0.996
Pectin/HF-1h	0.52	0.25	0.0059	0.996

Pectin/HF-4h	0.56	0.26	0.0062	0.997
Pectin/HF-7h	0.57	0.27	0.0072	0.999

A higher value of K_1 respect to the K_2 indicates that Fickian diffusion was the predominant mechanism of drug release from the matrix. The negative value of K_2 for the neat pectin indicated the quasi-absent relaxational contribution and, so, a perfectly Fickian behavior. (Baggi and Kilaru, 2016) From the release kinetics, it was possible to observe that for short times an initial burst release step can be visualized. It was due to the burst of the molecules located on the external surface of the materials. Further, a second step could be identified and correlated to the diffusion of the molecules from the bulk. For higher release times, a plateau can be identified. It can be claimed that for all the composites, the presence of the filler slowed down the release rate of cinnamic acid molecules, moving toward a double step release kinetics, respect to the unfilled pectin. This fact could be reasoned in the way that a decrease in porosity or free volume could be verified since the hemp fibres could be involved in weak chemical interaction with polar pectin groups leading to the formation of an interconnected network which in turn slowed down the diffusion of the molecule along its path-length. It is interesting to observe that the release amount of the cinnamic acid decreased with the treatment time of the fibres. Such behavior could be related to the hindrance effect created by the hemp fibres, that delayed the counter-diffusion of the active molecule. As the treatment time of hemp fibres increases, a reduced mean dimension of the fiber was obtained, the crystalline structure is lost, and the adhesion with pectin was reduced. The active molecules can occupy the free volume between the matrix and the reinforcement; as a consequence, a higher amount of filler can be released.

Pot setting up

The biodegradable pot was obtained from the same abovementioned experimental procedure, soaking 20 g of hemp fibers in 30 ml of a 3% (w/v) pectin water solution. In this case, pectin was used as polymeric matrix to confer structure and rigidity to the manufact. The components were mixed for 1h at 80°C. Successively, to shape the pot form, the doughy mixture was poured in an aluminum shaped mold which was previously designed. After pouring the mixture, the two units of the shaped molds were fixed to confer the pot shape. The drying process was carried out in an oven at 70 °C for 36 h, in order to remove the water content. The production of a novel biodegradable pot opens new routes towards the replacement of synthetic plastic pots. The manufacturing process was illustrated in Figure (46)**.**

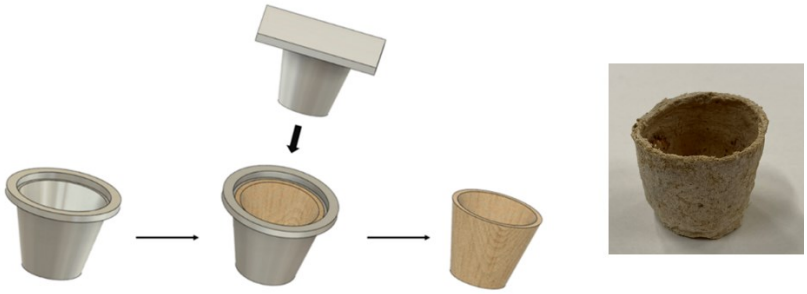

Figure 46 *3D schematization of the manufacturing process and bio based pot manufactured on laboratory scale*

Concluding remarks

In this study two innovative green pesticide release systems were presented. Firstly, pH-responsive composites hemp hurd/gelatin beads were produced through gelation in oil. Eugenol, a green pesticide, was encapsulated. The release kinetics of eugenol were dependent on of hemp hurd and pH. Besides, the inclusion of hemp hurd, at fixed pH level, allowed to tailor the controlled release system due to the physical hindrance of hemp hurd. Secondly, cinnamic acid, a green pesticide active against *phytophthora cinnamomi*, was introduced in the pectin/mechanochemically treated hemp fibers biocomposites. Release kinetics of cinnamic acid showed that they are dependent on the time of mechanochemical treatment of HF that support either the better adhesion of the fibres with the pectin matrix or the hindrance effect by the hemp fibres, that delay the counter-diffusion of the active molecule. A first prototype of pot, made of pectin and hemp fibers, was designed and fabricated. It represents a promising system to be able to substitute the traditional plastic pot for plants, being completely biodegradable and also reservoirs of pesticides. To sum up, the results demonstrated the possibility of tailoring the release of a loaded compound by designing natural polymeric devices through environmentally friendly methodologies.

9.Design of hemp based composites with antiflame properties

Preface

In the last decade the design of environmentally friendly materials in the building industry is becoming a fundamental topic, since the impact of building industry onto the environment is continuously growing, therefore its mitigation and the development of sustainable materials is considered an urgent issue (Franzoni, 2011; Sassoni *et al.*, 2014). A possible route lies either in the reduction of not renewable materials or in the potential substitution of synthetic fibers with natural ones obtained from natural resources (Korjenic *et al.*, 2011; Sassoni *et al.*, 2014). Among the natural materials, natural fibers are taking a central role (Sanjay *et al.*, 2019) since the possibility of substituting synthetic fibers (Fuqua, Huo and Ulven, 2012; Liu *et al.*, 2017; Thomason and Rudeiros-Fernández, 2021). In the framework of the sustainability, hemp fibers (*Cannabis L. Sativa*) are receiving great attention due to their intrinsic properties such as good thermal insulation, low cost, good mechanical properties, rapid growing cycle (Viscusi, Barra and Gorrasi, 2020). Moreover, due to the low mass density, the low thermal conductivity and the cell structure, natural fibers are supposed to be good candidates for applications in thermal insulation (Zach *et al.*, 2013; Keiller *et al.*, 2021). Untreated natural fibers-based materials cannot be employed in green building applications without considering chemical or physical modification. Many chemical treatments have already been proposed to overcome the drawbacks of natural fibers (Li, Xing and Dai, 2008; Sawpan, Pickering and Fernyhough, 2011b; Kabir *et al.*, 2013; Dolez *et al.*, 2017; Liu *et al.*, 2017; Ali *et al.*, 2018b; Sonnier *et al.*, 2018). Actually, physical and chemical methods have already

been proposed, such as esterification, etherification or methods for anchoring low surface energy hydrophobic compounds such as surfactants, silicones, and fluorocarbons on cellulosic fibres, plasma processing techniques and solvent-vaporized controllable crystallization (Jiang, Meng and Qing, 2005; Lee *et al.*, 2005; Balu, Breedveld and Hess, 2008; He, Xu and Zhang, 2013; Sobhana *et al.*, 2017). However, the application of these techniques is restricted due to their high cost and use of harmful compounds. A more sustainable approach is required to improve flame retardancy and water repellency properties of low-density hemp fiberboards (LDHFs). Layer-by-layer assembly is a flexible process based on alternate deposition of a positively charged and negatively charged layer, enables to improve fire retardancy of cellulosic materials through the formation of a coating (Li *et al.*, 2017). The proposed methodology highlights the possibility of designing layered composite materials with improved physical properties exploiting the synergies between a natural clay and an organic compound through the formation of a hybrid system.

Materials

(3-Aminopropyl)triethoxysilane (APTES), HCl solution 37% v/v, Cloisite-Na^+, stearic Acid (SA) and ethanol (EtOH) were used as reagents.

Surface modification

(3-Aminopropyl)triethoxysilane (APTES) aqueous solution (5 %wt) was prepared by firstly prehydrolyzing it at 50 °C for 3 h. The pH value of 3 was regulated by 1M chloridric acid solution. During self-condensation, silane molecules can form siloxane oligomers with reactive Si-OH groups (Raji *et al.*, 2016). Cloisite/water mixture was previously prepared by dispersing cloisite in water (0.05g/mL) through the sonication process for 3 h. LDHFs, which were previously washed with distilled water and air dried, were soaked in APTES solution at room temperature for 1h, fixing a solid/liquid ratio equal to 1g/100mL. After that, silane modified LDHFs were washed several times with distilled water and then dried in oven at 100°C for 1.5h. The silane modified LDHFs were soaked in the cloisite/water mixture for 1 h at room T and then dried in oven at 100 °C for 1.5h. Siloxane oligomers are physically adsorbed to hydroxyl groups of clay minerals by hydrogen bonds on the clay surfaces. A further step of washing and drying is then required to remove the clay excess. Moreover, due to the drying process and dehydration, a robust covalent bond –Si–O–Si– between silanols and hydroxyl groups of clays was formed (Raji *et al.*, 2016). One layer was then obtained after the first treatment cycle. The preparation of subsequent layers followed the same procedure by performing a layer-by layer assembly method; the hemp fiberboards were alternately soaked into APTES and Cloisite solutions until the desired number

of layer (L) was obtained. The obtained sample will be hereinafter labelled as LDHF-xL where x=number of layers. Finally, to achieve the hydrophobicity, the functionalized LDHFs were treated with stearic acid/ethanol solution (0.25 M) for 3h (T=50 °C). The stearic acid functionalized LDHFs (LDHF-xL+SA) were washed with ethanol and dried for 1h at 100°C.

Experimental results

Figure (47) shows the change of LDHF weight as a function of number of layers. The weight gain of hemp fiberboards was determined by measuring the weights before and after the treatment.

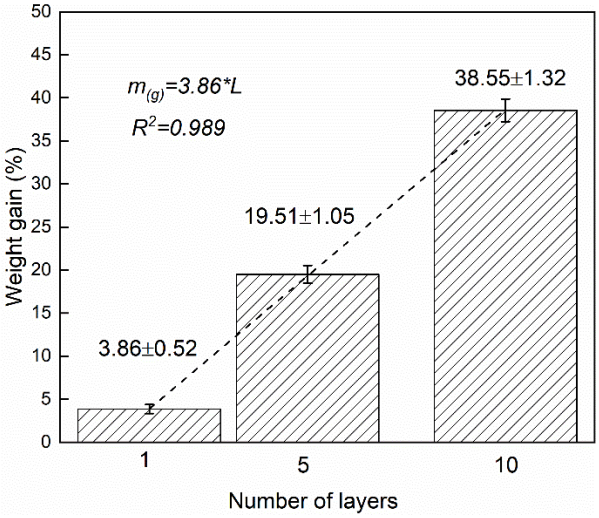

Figure 47 *Increase in composite weight as a function of layers number*

It can be observed that the gain in weight of treated LDHFs is quite linear with the increase in layer number. The increased weight also proved the presence of APTES and cloisite-Na^+. The average density of the samples were evaluated according to ASTM D792 (D792, 2002). The mean values and the standard deviations, obtained after carrying out the analysis in triplicate, are reported in table 21.

Table 21 *Density of LDHFs according to ASTM D792*

Sample	Density (g/cm^3)
LDHF	0.154±0.015

LDHF-1L+SA	0.184±0.023
LDHF-5L+SA	0.231±0.028
LDHF-10L+SA	0.346±0.030

The density of the treated LDHFs gradually increases with the increase in APTES+Cloisite layers, as expected. This could be attributed to the presence of natural clay which density is roughly 2.86 g/cm^3. Statistical analysis indicated that significant differences are evident among the densities obtained from the different LDHFs samples. Figure (48) shows SEM micrographs of untreated and treated LDHFs.

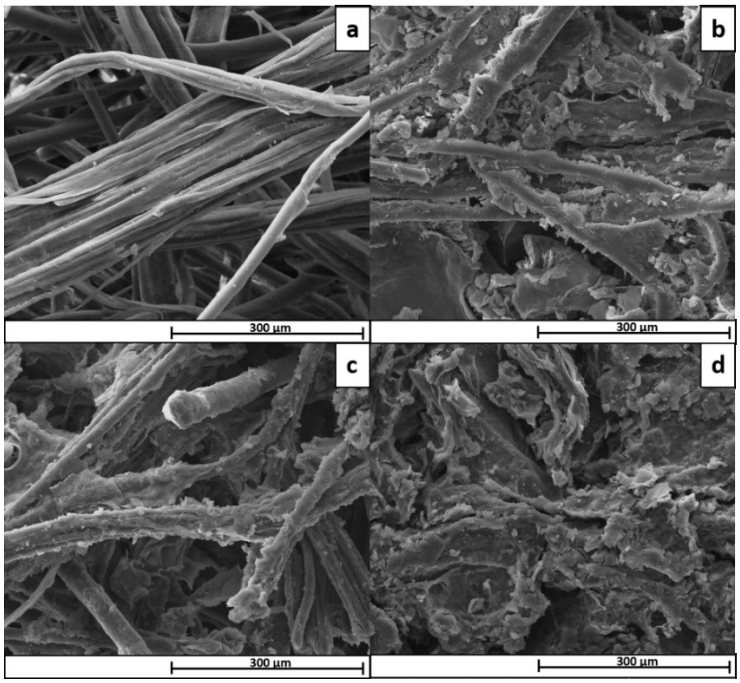

Figure 48 *SEM micrographs of a) LDHF; b) LDHF-1L+SA; c) LDHF-5L+SA and d) LDHF-10L+SA*

As the number of treatment cycles increases, a wider presence of clay platelets is evident leading to a change in fibrillar morphology compared to untreated LDHF and an increase in fibers roughness. The morphological analysis of LDHFs was then further investigated by performing AFM analysis (figure (49)). It was used to provide details about fiber surface characteristics before and after LBL treatment.

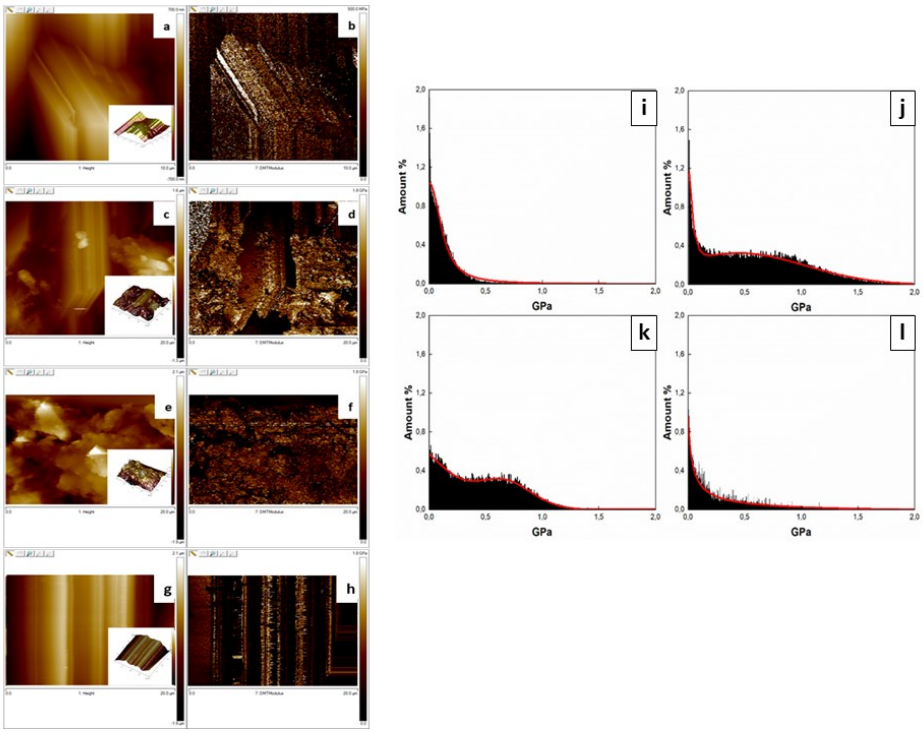

Figure 49 *AFM topographies (height and DMT Modulus) of a and b) LDHF; c and d) LDHF-1L+SA; e and f) LDHF-5L+SA and g and h) LDHF-10L+SA; Modulus distribution over the AFM maps of samples i) LDHF; j) LDHF-1L+SA; k) LDHF-5L+SA and l) LDHF-10L+SA*

The AFM maps revealed morphologies consistent with those observed by SEM. The Average Roughness (Ra, given in nm) and the value of DMT modulus values evaluated from AFM maps are reported in table 22.

Table 22 *Ra and DMT Modulus of untreated and treated LDHFs*

Sample	Average Roughness (Ra), nm	DMT Modulus, MPa
LDHF	67±6	120±90
LDHF-1L+SA	238±10	540±300
LDHF-5L+SA	226±7	440±250
LDHF-10L+SA	216±12	313±253

Ra and DMT Modulus change as a function of the number of treatment layers. The untreated LDHF shows Ra equal to 75±6 nm, and DMT Modulus equal

to 0.12 GPa. Both Ra and DMT Modulus show a maximum value for LDHF-1L+SA and decrease as the number of layers increases. This phenomenon could be related to the formation of highly aggregated clay platelets which led to change in fibrillar morphology, hindering stearic acid molecules to efficiently settle onto the surface. It follows a smoother surface with L>1 as Ra values proved. The modulus distributions obtained from the AFM DMT modulus maps are displayed in the same figure. The LDHF sample is characterized by a high amount of soft material with low modulus values in the range 0.200-0.500 GPa. The samples LDHF-1L+SA and LDHF-5L+SA show a bimodal distribution of the elastic modulus with a soft part with a mean value of 0.05±0.015 GPa and 0.09±0.03 GPa, respectively, and a hard part with a mean value 0.690 GPa for both samples. The sample LDHF-10L+SA shows a modulus distribution similar to the one observed for the untreated sample, LDHF. The LBL treatment induces an increase of the DMT modulus, up to 5 layers. This phenomenon can be ascribed to the cloisite. As the number of treatment increases, the cloisite forms aggregates that limit the stearic acid grafting. Up to 5 layers, the LBL treatment is efficient in producing a strong structure, characterized by high modulus (0.690 GPa), the further increase of the layers makes less efficient the deposition process for the reasons mentioned above. Figure (50) shows the FTIR spectra of untreated hemp fiberboards and SA-cloisite treated ones.

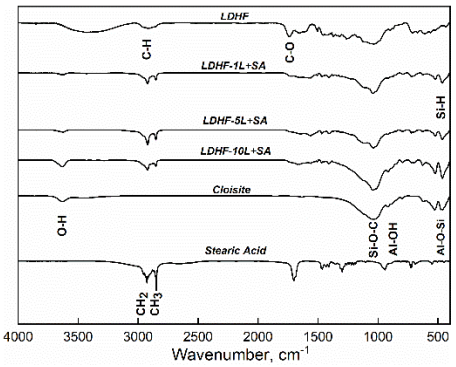

Figure 50 *FTIR spectra of untreated and treated hemp fiberboards*

As far as the untreated LDHF concerns, the region 3000-3600 cm^{-1} is related to hydrogen bonded hydroxyl groups (OH) in polysaccharides (Terpáková et al., 2012). The stretching vibration of CH at about 2910 cm^{-1} is attributed to CH stretching of cellulose and hemicellulose (Agarwal, Reiner and Ralph, 2010; Terpáková et al., 2012). The peak at 1736 cm^{-1} refers to the C=O stretching vibration of the acetyl groups of hemicellulose and carboxylic acid in pectin (Rachini et al., 2009). Besides, the peaks at 1454, 1373 and 1254 cm^{-1} are attributed to the CH_2 bending vibrations in lignin, OH bending of

carboxylic acids of pectin and C-O stretching of acetyl (Sawpan, Pickering and Fernyhough, 2011a). The treated LDHFs samples showed additional characteristic peaks. After the modification, the peak appearing at 471 cm^{-1} and 780 cm^{-1} are considered be due to the vibration of Si-H bond (Allahbakhsh et al., 2017). The shoulder peak at 1110 cm^{-1} is attributed to Si-O-Si bonds (Ahmaruzzaman and Gupta, 2011; Allahbakhsh et al., 2017). The significant enhancement of the absorption peak intensity at 1040 cm^{-1} was attributed to the Si–O–C and Si-O stretching vibrations (Maleki and Karimi-Jashni, 2020). The band centered at 3627 cm^{-1} can be attributed to the stretching vibrations of OH-groups associated with octahedral atoms; the adsorption band centered at 918 cm^{-1} is attributed to Al-OH bending vibration (Maleki and Karimi-Jashni, 2020) while the band at 526 cm^{-1} are related to the vibrations of Al–O–Si (Yang et al., 2009; Ramadan, Esawi and Gawad, 2010). Finally, the LDHF-xL+SA samples evidenced the appearance of new absorption bands at 2915 and 2849 cm^{-1} corresponding to CH stretching and CH_2, CH_3 in-phase stretching groups of stearic acid (Bin Ahmad et al., 2012; Sobhana et al., 2017). The results mentioned above indicated that cloisite mineral and stearic acid have been successfully deposited on the surface of hemp fibers. Figure (51) reports the TGA curves of untreated and treated LDHFs. The thermooxidative degradation of the closite-Na^+ is also reported. Four main thermal events characterize the thermal decomposition process of hemp fibers fiberboards (Yang et al., 2007): i) 50-150 °C correlated to the evaporation of water (Fisher et al., 2002); ii) 220-350 °C degradation of pectin and hemicellulose; iii) 350-450 °C decomposition of cellulose; iv) T>450°C, decomposition of residual lignin and oxidative degradation of charred residue.

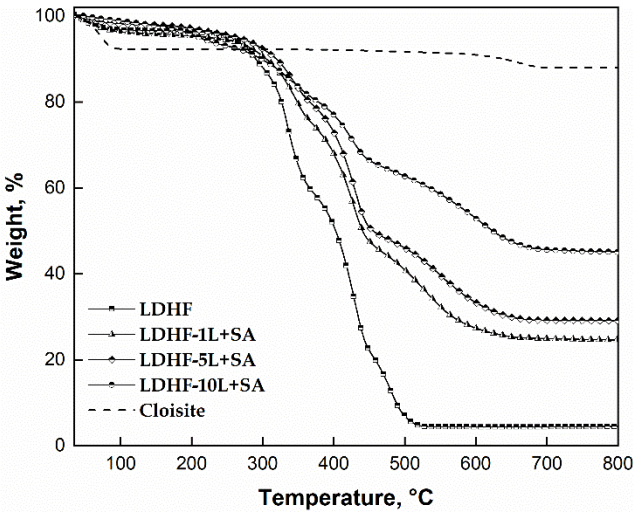

Figure 51 *Thermograms of untreated and treated LDHFs*

Thermograms show significant differences between thermooxidative degradation pathway of untreated LDHFs and SA-clay modified ones. The modified LDHF samples show a reduction of water loss, compared with the untreated one, probably due to the improved hydrophobicity conferred by stearic acid. The treatment with the natural clay led to an improved thermal stability. Due to the lower degradation temperatures of APTES and stearic acid, the modified LDHF samples showed a $T_{5\%}$ lower than untreated one. Meanwhile, the noticeable increase in $T_{50\%}$ values of modified LDHF samples further confirmed that the LBL assembly could effectively impede the thermal oxidative degradation of hemp fibers for the effect of inorganic clay. In fact, the mineral clay forms an effective diffusion barrier and thus hinders the diffusion of low molecular weight compounds during thermal degradation (Benhacine, Yahiaoui and Hadj-Hamou, 2014). Besides, it is necessary to take into account the overlapping of heat and mass transfer phenomena that occurs during the degradation (Sánchez-Jiménez *et al.*, 2009). As the organic material decomposes, the presence of clay on the fiber surface generates a thermally stable phase which can act as a mass transport barrier between the heat source and the material to achieve flame retardant purposes. It is favorable for serving as physical barrier and shielding combustible products from oxygen and heat, efficiently protecting the cellulosic fiberboard during burning (Liu *et al.*, 2020). It follows that the O_2 gas transport at the interface is limited as the kinetic of degradation reactions, contributing to reduce the decomposition rate and slowing down further thermal breakdown by reducing the heat flow and energy exchange (Allen and Edge, 1992). In fact, the maximum decomposition rate decreased from 0.0065 %/°C (LDHF) to 0.0057 %/°C, 0.0051 %/°C and 0.0026 %/°C for LDHF -1L+SA, LDHF 5L+SA and LDHF -10L+SA, respectively. This effect can be verified by the increase in char residue.

Figure (52) shows flexural stress (MPa)-deflection curves from one-point bending test of the specimens. On the right side, maximum load (P) and flexural modulus (E_f) of the tested specimens are reported

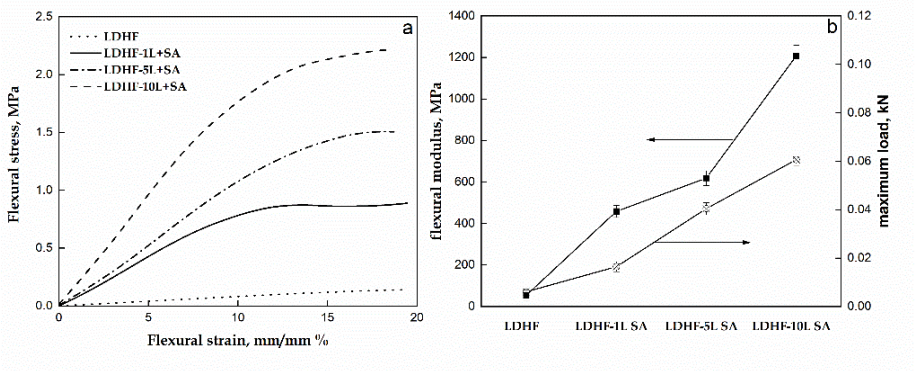

Figure 52 *(a) Flexural stress-strain curves and (b) flexural modulus (MPa) and maximum load (kN)*

The first part of the curves shows a linear behavior from which the elastic moduli were determined. It is evident that the maximum load and flexural modulus values of the specimens increased with the increase in clay amount. In particular, the flexural modulus of treated LDHFs shows an increase of 744%, 1039% and 2125% for LDHF-1L+SA, LDHF-5L+SA and LDHF-10L+SA compared to LDHF one while the maximum load increased of 170%, 560% and 892% for LDHF-1L+SA, LDHF-5L+SA and LDHF-10L+SA respect to LDHF one. It could be supposed that all the composite specimens retain their structure since no crack was observed neither at higher strains. Figure (53) reports the sorption isotherms of the LDHFs.

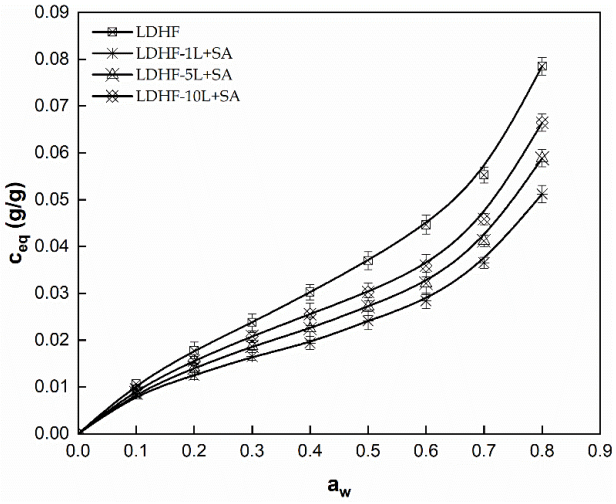

Figure 53 *Sorption isotherms of LDHFs and treated LDHFs*

A generalized form of Guggenheim, Anderson, de Boer equation (GAB) known as Viollaz-GAB model, was used to correlate the sorption data in the whole range of activities (Basu, Shivhare and Mujumdar, 2006). The model allowed to describe the shape of type II isotherm (Timmermann, 2003). The Viollaz GAB model is expressed by eq. (66):

$$c_{eq} = \frac{M_0 C K a_w}{(1-Ka_w)[(1+(C-1)Ka_w]} + \frac{M_0 C K K_2 a_w^2}{(1-Ka_w)(1-a_w)} \quad (66)$$

where M is the equilibrium moisture content ($g/g_{dry\ matter}$), M_0 is the monolayer moisture content ($g/g_{dry\ matter}$) while K and C are dimensionless GAB

parameters (Blahovec and Yanniotis, 2008). Table 23 reports the evaluated GAB parameters.

Table 23 *Viollaz-GAB parameters*

Sample	M_0 ($g/g_{dry\ matter}$)	C	K	K_2	R^2
LDHF	0.036±0.003	8.95±0.81	0.42±0.05	$5.3*10^{-2}$±$2.2*10^{-3}$	0.999
LDHF-1L+SA	0.021±0.001	14.31±0.61	0.39±0.02	$9.9*10^{-4}$±$3*10^{-5}$	0.996
LDHF-5L+SA	0.028±0.002	19.72±0.88	0.22±0.03	$1.9*10^{-3}$±$5*10^{-5}$	0.998
LDHF-10L+SA	0.031±0.004	23.32±1.05	0.18±0.01	$2.3*10^{-3}$±$8*10^{-5}$	0.995

The GAB parameters, C and K, are associated to the geometrical shape of sorption isotherms. K is a dimensionless parameter that refers to the heat of the sorption of the multilayer region, which is associated to the curvature of the sorption curve, while C is related to the heat of the sorption of the monolayer region which concerns the knee of sorption isotherm (Basu, Shivhare and Mujumdar, 2006). The decrease in M_0 value, representative of maximum monolayer water capacity, justifies the reduction of polar accessible sorption sites as a consequence of the hydrophobization. In fact, for all the composites, a decrease in adsorbed moisture content is evident. The low moisture resistance of lignocellulosic fibers is noticeably improved. This phenomenon is attributed to enhanced mass transfer resistance as well as the hydrophobicity conferred by stearic acid covering. The hydrophobization of LDHFs surface and the increase of tortuosity of the system can justify the reduction of water sorption for treated LDHFs (Pinto et al., 2007). Moreover, as the number of clay layers increases, a significant increase in moisture adsorption is evident and associated to the hydrophilicity of natural clay which naturally tend to adsorb moisture. The sorption parameters (S) were obtained from the equilibrium concentration (C_{eq}) of the permeant vapor as a function of the partial pressure. Even though the surface of treated LDHFs has been hydrophobized, the increase in clay justifies the slight increase in sorption value (Wahab et al., 2019). Moreover, the sorption value is supposed to be affected by cluster formation and reduction of free volume (Sun et al., 1997). Zimm-Lundberg theory was applied to evaluate the water clustering degree (Van Der Wel and Adan, 1999). The free energy function is a function of the first derivative of activity evaluated upon the volume fraction (J L Lundberg, 1972). So, the mean cluster size (MCS) is evaluated from eq. (67):

$$MCS=1+\frac{\emptyset*G_s}{V_s} \quad (67)$$

where G_s is the cluster integral V_s is the partial molar volume of penetrant, Ø is the volume fraction of penetrant. The MCS, representing an estimation of cluster size, is evaluated from isotherm sorption curves through the following eq. (68):

$$MCS=(1-\emptyset)*\frac{a_w}{\emptyset}\left(\frac{\partial\emptyset}{\partial a_w}\right)_{p,T} \quad (68)$$

Considering the GAB-Viollaz model equation, MCS could be evaluated through the following relation (eq. (69)):

$$MCS=\frac{(1-\emptyset)}{\emptyset}*\left(\frac{\rho_s}{\rho_s+\rho_w}\right)*a_w M_0 CK*\left\{\frac{1-2K^2a_w^2+a_w(2K-K^2+K^2C)}{(1-Ka_w)^2(1+(C-1)Ka_w)^2}+K_2*a_w\frac{2-a_w(K+1)}{(1-Ka_w)^2(1-a_w)^2}\right\} \quad (69)$$

Where ρ_w is the water vapor density at the experimental temperature while ρ_s is the LDHF density evaluated according to ASTM D792. Figure (54) reports the estimated MCS values.

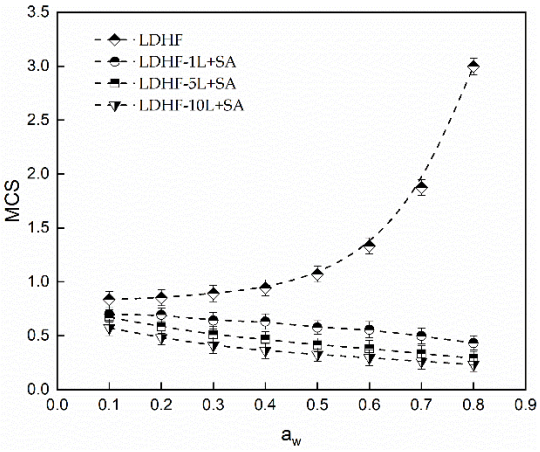

Figure 54 *MCS values for LDHFs as function of water activity*

Generally a MCS>1 indicates the probability of water clustering (Modesti *et al.*, 2004). The water clustering is verified for a_w=0.5 only for untreated LDHF, in compliance with the behavior of sorption isotherms. In general, at higher activities, the sorbed molecules do not interact with polar sites, since they have been saturated during initial sorption. The hydrophobization could limit the absorbable water adsorption minimizing the probability of clustering. The reduction of free volume and the change in mean water molecules pathway could even corroborate the MCS trend and allowed to suppose that the diffusion coefficient decreases after the LBL assembly.

Contact angle (CA) measurements were performed on each sample to investigate the hydrophilicity degree of the composite's surface, the surface energy and the work of adhesion. Figure (55) represents water and glycerol contact angles for all the specimens with the estimated surface energy and work of adhesion.

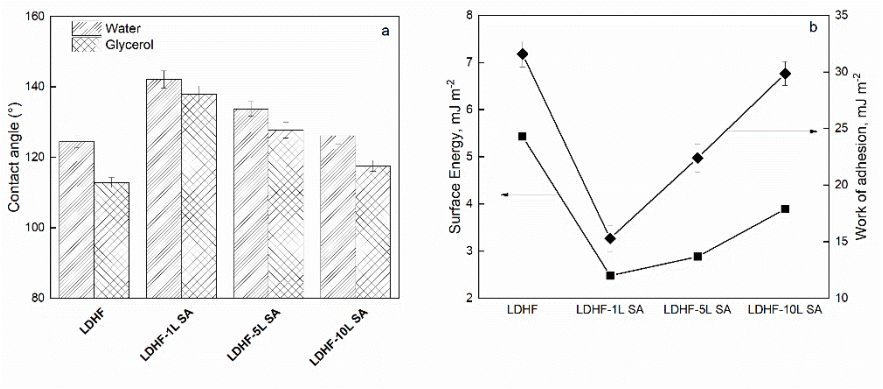

Figure 55 *a) Contact angle (water and glycerol) and b) Surface energy and work of adhesion of LDHF samples*

As depicted, an increase in hydrophobicity after the treatment occurred. The highest contact angle was obtained after the treatment which could be ascribed to the hydrophobization conferred by long chain stearic acid, a non-polar compound. Hybridization of Cloisite grafted LDHF with SA causes micro-roughness which can improve the wettability. Thus, the surface properties of LDHF have been completely changed from slightly hydrophilic to hydrophobic. Moreover, as the clay layers number increases, the hydrophobization seemed to be reduced. This phenomenon could be due to the hydrophilicity of clay particles which could be easily wetted by water as well as to other factors such as the increase in fiber roughness, which is supposed to affect the contact angle (Ariawan et al., 2017). Moreover, the presence of a thicker layer of natural clay on substrate material could be able to reduce the surface roughness and diminish the accumulation of excess SA. Hence, the possibility of SA molecules to cover on cloisite platelets deposited on LDHFs was negated. A further proof was placed in the estimation of surface energy and work of adhesion. The better hydrophobicity comes from lower surface energy of the composite film (Zhao et al., 2017). Besides, a decrease of contact angles for L>1 resulted in an increase in work of adhesion in comparison with LDHF-1L+SA.

Flame retardancy test were then performed using the vertical burning test. Sample were cutted into specimens 70x13mm^2 and conditioned at 21±2°C with a relative humidity of 50±5%. A methane flame 20 mm high was applied for 5 s at the bottom of specimens, repeating the test 3 times for each of them. A Flammability Performance Index (FPI, %/s) was calculated as the ratio of final residue content to the total burning time and used as an evaluation parameter (Alongi, Ciobanu and Malucelli, 2011; Rosace et al., 2018). Besides, residue weight after burning (RWAB, %) and burning rate (BR, mm/s) were also evaluated.

Images of samples after burning are reported in figure (56).

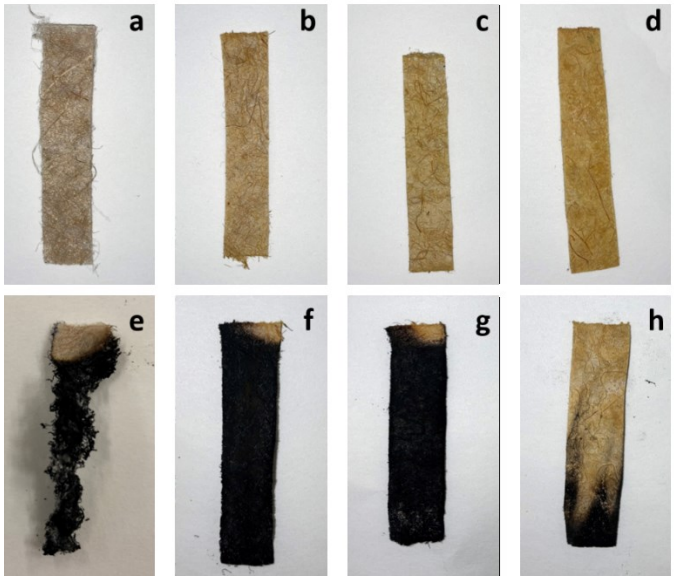

Figure 56 *Sample before and after burning test; LDHF (a and e); LDHF-1L+SA (b and f); LDHF-5L+SA (c and g) and LDHF-10L+SA (d and h)*

Burning rate (mm/s), residue weight after burning (g) and FPI (%/s) are summarized in table 24.

Table 24 *FPI, RWAB and BR of untreated and treated LDHFs*

Sample	FPI (%°s^{-1})	Residue weight after burning (RWAB) (%)	Burning rate (mm s^{-1})
LDHF	1.61±0.11	18.05±0.51	6.24±0.51
LDHF-1L+SA	2.00±0.14	40.22±0.75	3.48±0.40

LDHF-5L+SA	2.17±0.19	51.14±1.02	2.98±0.32
LDHF-10L+SA	2.35±0.18	61.79±0.88	2.66±0.15

The results of the multilayers samples exposed to flame show significant differences compared to untreated one. The untreated LDHF burned fast, intensely, and completely, leaving a very low amount of ash (residue=18%). The flame extinguished in a total of 14 s giving a slightly shrunken charred solid. In contrast, when the LDHFs are treated by natural clay coatings, a remarkable modification in their flammability is observed. The black char formed could be due to stearic acid decomposition. The RWAB of treated LDHFs remarkably increased compared to untreated one leaving, after burning, a thick, compact and dense residue weight equal to about 40%, 51% and 62% for L=1, 5 and 10, respectively. The combustion proceeds without after glowing. In details, by comparing the burning rates, the treated LDHFs decrease their ignitability and slowlier burned after flame contact. In good agreement with TGA data, these results further support the effectiveness of proposed clay-coating. Besides, considering the Flammability Performance Index (FPI), clay coated LDHFs generally showed better performances compared to untreated one. The higher the FPI values, the better is the flame retardancy performance (Alongi, Ciobanu and Malucelli, 2011). The oil absorption data, obtained from adsorption analysis to assess the oleophilicity of treated LDHF surface, are reported in figure (57). Oil adsorption capacity was evaluated using sunflower oil. The sorption experiments were carried out at room temperature as follows: small pieces (2x2 cm^2; thickness≅0.4cm) of the pre-weighed LDHF samples were dipped in the oil (15 mL) for regular time interval and then hung in the air for 15 min to let the surface residual oil drip away before being weighed.

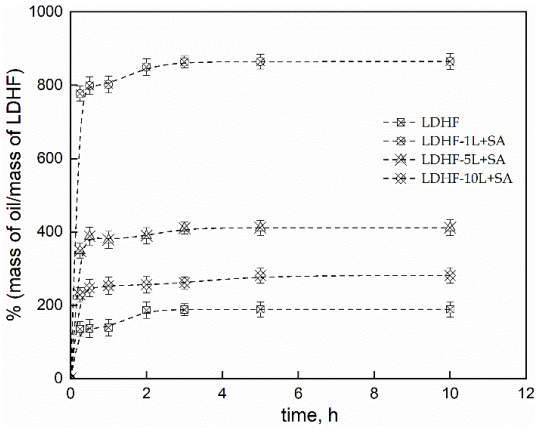

Figure 57 *Oil adsorption, mass oil/mass of LDHF (%), of untreated and treated LDHFs*

The adsorbed oil content is affected by fiber surface modification and it could be correlated to clay layers. Compared to untreated LDHF, LDHF-1L+SA was able to adsorb a noticeable amount of oil (8.64 g/g of sample) while, the adsorbed content seemed to decrease as the number of layers increased (4.11g/g and 2.81g/g for LDHF-5L+SA and LDHF-10L+SA, respectively) caused, probably, by the agglomeration of clay platelets as well as the decrease in specific surface area available for adsorption. The hybrid treatment allowed to retain a higher amount of oil compared to raw LDHF and it confirms the successful oleophilicity of treated low density hemp fiberboards.

A proposal of flame retardancy mechanism

The flame retardancy of LDHFs samples covered with cloisite and stearic acid and their thermal stability increase can be explained as overlapping of complex phenomena. During the combustion process, organic material is supposed to form carbon dioxide and water, while cloisite platelets could quickly form an inorganic protective ceramizing layer on the surface of hemp fibers. Firstly, the role of the stearic acid, being an organic compound, is to produce a char layer on the surface, which separates the flame from the underlying material further slowing the heat transfer to the inner unburned cellulosic fibers. The protective layer made by char amount and silicate oxides can represent a physical barrier which delay the transfer of heat, oxygen, and the diffusion of volatilized products between the combustion zone and the unburned fibers, being able to block the further combustion. The flame retardant could then stop the radical mechanism of combustion process taking place in the gas phase. Moreover, the cloisite platelets can form a silicate skeleton frame which might cover the surface of LDHF sample acting as a physical barrier against heat propagation and fire protecting the underlying polymer from further decomposition. Finally, the role of CO_2 and water as inert gases need to be taken into account since they can dilute the oxygen concentration as well as help the formed char to expand and swell (Zammarano et al., 2005; Rajaei et al., 2019). These gaseous substances, produced by thermal degradation of organic components, contributed to lower the partial pressure of combustible gases and, hence, lowering the combustion rate of cellulosic material. A proposal of flame retardant and thermal degradation mechanisms is reported in the figure (58).

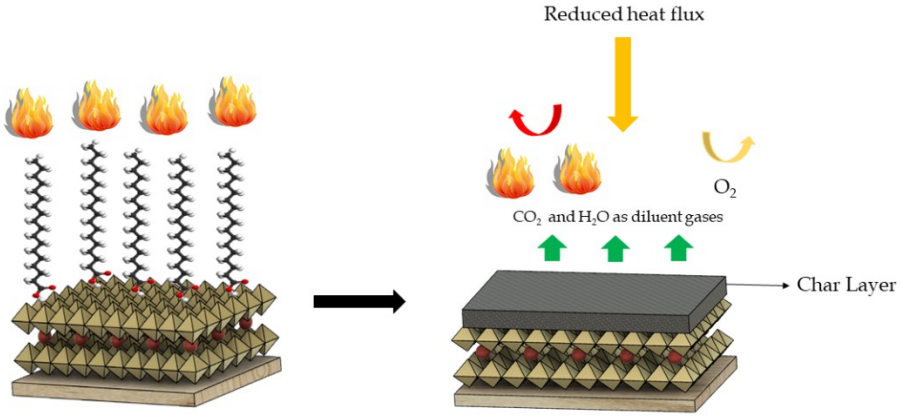

Figure 58 *A proposal of flame retardancy mechanism*

Concluding remarks

A hybrid approach was proposed to design a novel multi-layered composite obtained from low density hemp fiberboards treated with a natural clay and stearic acid through the application of LBL assembly. Morphological and spectroscopic analysis (FTIR) proved the presence and the deposition of clay platelets and stearic acid on hemp fibers surface. Thermogravimetric analysis (TGA) demonstrated the improvement in thermal stability, attributed to the presence of clay. Mechanical properties, evaluated in terms of bending properties, demonstrated the retention of composite structure since cracking phenomena didn't occur. The analysis of barrier properties to water vapor showed a noticeable improvement of hydrophobicity. Finally, an increase in flammability performance index and a decrease in burning rate were observed for the treated LDHFs samples.

10. Design of hybrid ferromagnetic hemp based materials

Preface

Nowadays, the importance of fabricating new fillers for improving the performances of matrices which they are loaded in is taking a center stage (Boccalon *et al.*, 2021). Usually, these fillers are introduced in polymeric, cementitious or resin matrices in order to maximize physical properties or tailor the release kinetic of a particular molecule (Costantino *et al.*, 2008a; Liu *et al.*, 2014; Gorrasi, Bugatti and Sorrentino, 2018). The rising of environmental issues and society demands is pulling toward the development of bio-based resources derived materials, for example from cellulose based resources with tailored properties such as magnetic ones (Sobhanadhas *et al.*, 2019). Two in-situ methodologies were proposed to modify the surface of alkali-treated and bleached hemp fibers to produce hierarchically structured materials with different morphology and magnetic behavior. The first method concerns the precipitation of Fe/Al layered double hydroxides (LDH) onto HF surface in urea solution. LDHs consist of stacks of positively charged metal hydroxide layers which require the presence of interlayer anions to maintain overall charge neutrality (Crepaldi, Pavan and Valim, 2000). They are a class of natural lamellar clay with exchangeable anions between layers whose general composition is: $[M(II)_{1-x}M(III)_x(OH)_2]^{x+}[A_{x/2}{*}mH_2O]$ where M(II) is a divalent cation, M(III) is a trivalent cation and the group A^- is the exchangeable anion (Pavan, De A. Gomes and Valim, 1998; Costantino *et al.*, 2008b; Bugatti, Vertuccio, *et al.*, 2019). A second strategy was proposed to fabricate hemp fibers modified with Fe/Al through a two-step process. A first step goes through the employment of a simple, easy and cost-effective method

using hemp fibers powder as template aiming to producing AlOOH modified hemp fibers. The obtained architecture was then further modified by an *in-situ* methodology to deposit Fe_3O_4 particles onto it. The process exploits the coprecipitation of Fe^{2+}/Fe^{3+} ions in ammonia solution. To the best of our knowledge, no deep studies concerning the production of novel hemp derived hybrid fillers with magnetic properties are present as for yet.

Materials & Methods

Urea, Sodium hydroxide, $Al(NO_3)_3*9H_2O$, NH_4OH, $Fe(SO_4)_2*7H_2O$, HCl solution 37% v/v, $NaNO_3$, NaCl and $FeCl_3$, NaOH and H_2O_2 were used as reagents.

Pre-treatment of hemp fibers

Hemp fibers were firstly washed with water to remove the superficial impurities and dried. The fibers were then treated with a 5% w/w alkaline solution (HF/NaOH=1:1 w/w) fixing a liquor ratio equal to 1:20 for 5 h, at 25°C fixing a stirring speed of 300 rpm. The fibers were washed several times until pH approaches to 7 and then dried at 80°C. The alkali-treated fibers were subjected to bleaching in H_2O_2 fixing a fiber/liquid ratio=1g/100 mL for 24 h, 80°C with a stirring speed of 300 rpm. The resulting fibers were washed with water-ethanol solution and dried at 80°C. The obtained fibers were reduced in size using a grinder (Duronic-CG250) and then milled through a high energy ball milling (HEBM-Retsch-PM 100) using a stainless-steel jar (V= 125 mL) and five zirconium oxide spheres as grinding medium. The rotation speed was set at 350 rpm for 15 minutes. The obtained powder-like hemp fibers was sieved using a 250-micron molecular sieve. Hereafter, the obtained product will be labeled as modified hemp fibers (MHF).

Modification of hemp fibers

MHF interfacing LDH Fe/Al was prepared by coprecipitation method. First, an aqueous solution of NaOH/Urea/H_2O was prepared with the ratio 7:12:81 w/w. The solution was stirred at 300 rpm for 3h and cooled down at -6°C for 12 h. Besides, an aqueous solution (100 mL) of $Fe(SO_4)_2*7H_2O$ (40 mmol) and $Al(NO_3)_3*9H_2O$ (20 mmol) was prepared. This latter solution was added dropwise to the NaOH/Urea solution which was kept at 50°C and stirred at 350 rpm. The pH was kept at 9.5 by adding NaOH (1M) solution. Afterward, the slurry was aged for 24 h at 50 °C. Then, the precipitate was centrifuged and washed continuously with bi-distilled water and ethanol. Finally, it was dried at 100 °C under vacuum for 24 h. The obtained sample will be labeled hereafter as MHF@LDH Fe/Al.

Briefly, 10.0 g of aluminum nitrate nonahydrate was dissolved in 100 mL of deionized water/EtOH (50:50 v/v) under vigorous stirring until all the solid was dissolved. Ammonium Hydroxide (1 M) was then slowly added dropwise to the solution, and the mixture pH was held in the range of 8~9. 2g of HF were dispersed into resulting mixture for 5h and 50°C. The sample (MHF-AlOOH) was washed with water and dried at 100°C. Besides, an aqueous solution (200 mL) of $Fe(SO_4)_2$*$7H_2O$ and $FeCl_3$ (Fe^{2+}/Fe^{3+}=1:2 molar ratio) was prepared. After mixing it for 1h at 300 rpm, 0.5 g of MHF-AlOOH was added to the Fe^{3+}/Fe^{2+} solution. The pH was kept at 9.5 by adding NH_4OH. Afterward, the slurry was aged for 24 h at 80°C. Then, the precipitate was centrifuged and washed continuously with bi-distilled water and ethanol. Finally, it was dried at 100 °C under vacuum for 24 h. The obtained sample will be labeled hereafter as MHF@AlOOH-FePs.

Experimental results

Figure (59) shows SEM micrographs of untreated and Fe/Al treated hemp fibers.

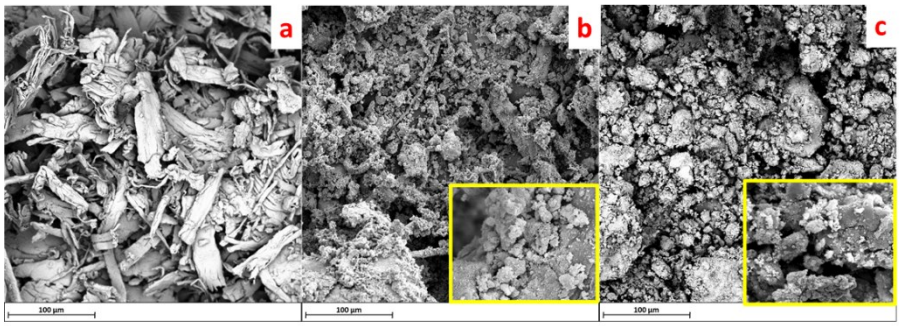

Figure 59 *SEM micrographs of a) MHF; b) MHF@LDH Fe/Al and c) MHF@AlOOH+FePs*

The hemp flakes appear quite irregular with a not well-defined structure. After the Fe/Al treatment, in both cases, hemp fibers were coated with the Fe/Al LDH (59b) and Fe particles (59c). In fact, the sample 59b clearly showed the characteristic structure of LDH with platelets deposited onto the surface with a 3D structured network while the MHF@AOOH+FePs sample showed agglomerates of different sizes covered with randomly distributed quasi-spherical particles associated with iron precipitation. In this latter case, severe aggregation can be observed. Figure (60) reports EDX maps, FTIR and XRD spectra of the two Fe/Al treated samples.

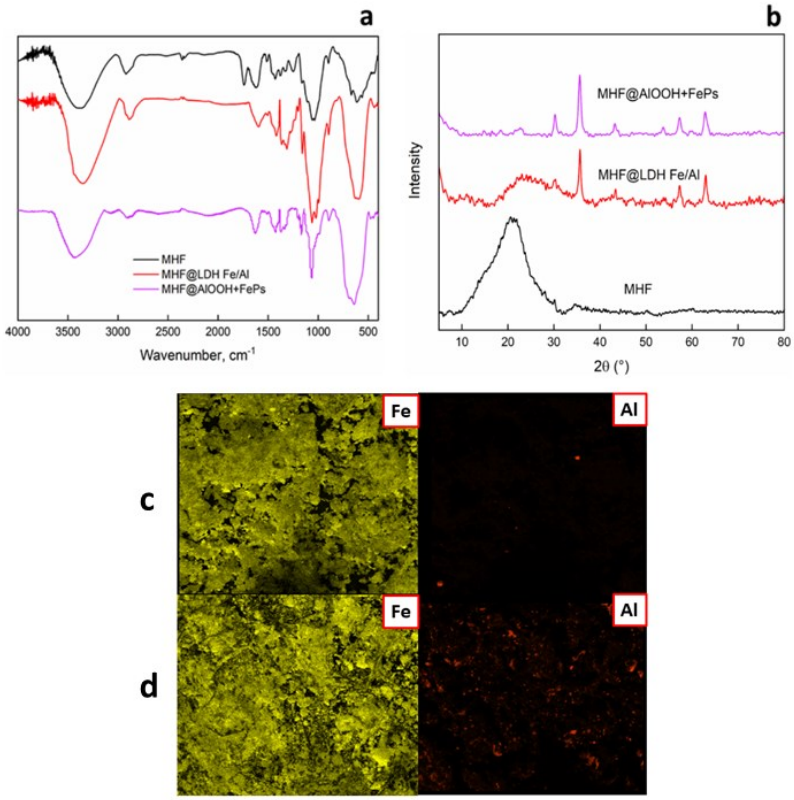

Figure 60 *a) FTIR, b) XRD spectra and EDX maps of c) MHF@LDH Fe/Al and MHF@AlOOH+FePs*

For Fe/Al LDH (a) it can be observed a better and homogeneous deposition of the two metals which are supposed to be structured in LDH conformation. The element distribution is in agreement with SEM analysis which showed a homogeneous distribution of iron particles onto hemp surface which prevails on aluminum distribution. FTIR spectrum of MHF shows the characteristic peaks of hemp fibers. The peak area at 3000-3600 cm^{-1} is the typical stretching vibration region of OH bonded groups in polysaccharides. The stretching vibration in the range 2890-3000 cm^{-1} is characteristic of CH groups of hemicellulose and cellulose (Terpáková *et al.*, 2012). The peak at 1735 cm^{-1} is attributed to C=O stretching vibration of acetyl groups of hemicellulose and methyl ester and carboxylic acid in pectin (Rachini *et al.*, 2009) while the vibration peak at 1373 cm^{-1} belongs to OH groups of carboxylic acids of pectin. The peak at about 1620 cm^{-1} is linked to OH bending of hemicellulose. The lignin C=C aromatic symmetrical stretching vibrations is located at 1510 cm^{-1}, while the band at 1454 cm^{-1} belongs to CH_2 bending vibration and the band at 1247 cm^{-1} to C-O stretching of acetyl (Sawpan, Pickering and

Fernyhough, 2011b). In the FTIR of MHF@LDH Fe/Al the band at 3000-3500 cm^{-1} is related to OH stretching vibrations and the absorption band at 1628 cm^{-1} belonged to the bending vibration of the interlayer water molecules and adsorbed water molecules. The complex and merge band around 3450 cm^{-1} may be due to overlap of bands of hydroxyl group of brucite layers and uncoordinated -OH groups (Parida, Sahoo and Singha, 2010). The sharp peak in the range 500-800 cm^{-1} corresponds to M-OH and O-M-O stretching where M is the metal (Iftekhar, Srivastava and Sillanpää, 2017). The increase in intensity of bands in the region of 700–500 cm^{-1} is associated to the iron oxides presence (Maziarz *et al.*, 2019). Concerning X-ray analysis, as far as the MHF spectrum concerns, the characteristic peaks of cellulose I at 2θ=14° and 2θ=16° didn't appear indicating the removal of the amorphous material since the alkali-H_2O_2 treatment. The intensity of the (200) peak at 2θ = 22.2° represents the cellulose crystallographic plane (Dai and Fan, 2010; Stevulova *et al.*, 2014). The fabricated Fe/Al modified samples showed typically well-crystallized nature with a series of reflections appearing as narrow, symmetric and strong lines. In the Fe/Al LDH spectrum, a small peak at 11.6° concerns the 003 facet of LDH (Xiaoliang Fan *et al.*, 2021) while the broad peak at 23° is related to (006) index. For MHF@AOOH+FePs, characteristic peaks of Fe_3O_4 particles are evident and related to the indices (200) at 30.1°, (311) at 35°, (400) at 43°, (422) at 54° and (440) at 63° (Shagholani, Ghoreishi and Mousazadeh, 2015). The small peaks at 2θ=16° and 23° are related to boehmite presence (Zhao *et al.*, 2010).

Concerning the magnetic properties, M(T) measurements of the magnetization M as a function of the temperature T have been performed on MHF@LDH Fe/Al and on MHF@AlOOH-FePs in presence of a magnetic field H equal to 100 Oe (see Figure (61)). It is possible to observe positive magnetization values for both the samples and the absence of peaks in the ZFC curves. Moreover, the ZFC (zero field cooled) and FC (field cooled) curves are separated in all the temperature range. These features in the M(T) curves suggest a ferromagnetic behavior of the samples with a Curie Temperature T_c > 300 K.

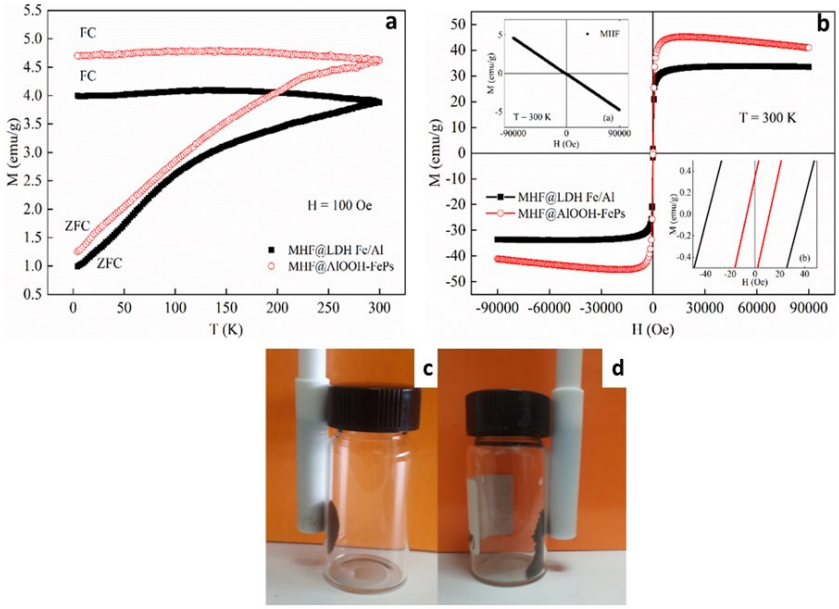

Figure 61 *a) ZFC and FC curves of M(T), b) Magnetization curves, c) MHF@AlOOH-FePs and d) MHF@LDH Fe/Al samples in contact with a magnet*

The above reported figure shows the pictures of both modified samples in contact with a small magnet where it is possible to observe the magnetic properties of functionalized hemp fibers.

In order to confirm the ferromagnetic behavior of the samples, magnetization as a function of the magnetic field M(H) have been performed at T = 300 K Looking at high fields in the main panel, it can be noted a negative slope for both the samples due to the diamagnetic response of the MHF. On the other hand, the inset(b) shows an enlargement of the near zero field region of the samples. It is important to note that the coercive fields are $H_c \approx \pm 10$ Oe for MHF@AlOOH-FePs and ±40 Oe for MHF@LDH Fe/Al indicating a ferromagnetic behavior of the samples in agreement with the behavior found in the M(T) measurements. Another interesting feature of the magnetic response of MHF@LDH Fe/Al and MHF@AlOOH-FePs is the fact that the 90% of the maximum magnetization is already reached at about 4000 Oe and 3000 Oe, respectively. The key magnetic parameters extracted from the measurements are summarized in Table 25.

Table 25 *Magnetic features of the samples*

Sample	T_c (K)	Coercive field (Oe)	H (90% M_{max}) (Oe)
MHF@LDH Fe/Al	> 300	40	4000
MHF@AlOOH-FePs	> 300	10	3000

Conclusions

Hemp fibers, after NaOH and bleaching treatment, were modified through two methodologies concerning the deposition of Fe and Al in order to produce different structured materials potentially applicable as fillers in polymeric composite. A wide characterization of produced fillers has been carried out. SEM micrographs confirm the presence of LDH platelets for MHF@LDH Fe/Al and agglomerates of quasi spherical particles due to iron precipitation for MHF@AOOH+FePs. Besides, the effective deposition was confirmed by EDX maps, FTIR and XRD spectra. Concerning magnetic properties, measurements of the magnetization M as a function of the temperature T were carried out showing positive magnetization values for both the samples and the absence of peaks in the ZFC curves. Since the ZFC and FC curves are separated in all the temperature range, a ferromagnetic behavior of the samples with a Curie Temperature Tc > 300 K is supposed to exist. This feature was then confirmed by magnetization-magnetic field M(H) curves which showed a coercive field of $H_c \approx \pm 10$ Oe for MHF@AlOOH-FePs and ±40 Oe for MHF@LDH Fe/Al corroborating the existence of a ferromagnetic behavior

11. Optical properties of Ni/Al modified hemp fibers reinforced Poly(ethylene-co-vinyl acetate) matrix

Preface

The hybrid organic–inorganic materials are emerging as promising materials belonging to solid state chemistry. The combination of an inorganic and organic structural components contributed to confer to them interesting properties (thermal, barrier, mechanical, optical and magnetic) making them good candidates for high potential technological applications (Saad *et al.*, 2019). Actually, in many areas, a deep knowledge of absorptive/optical properties is important for materials used in displays, light emitting-diodes, and solar-cells and also for bulk materials used in rare-earth lasers, optical components, and photoconductive switches (Look and Leach, no date). For semiconductors, the optical properties (in the ultraviolet, or visible range) are related to the characteristics of the electronic bands of the semiconductors or ultimately to their atomic structure and chemical bonding (Zanatta, 2019). On the other hand, it could be interesting to highlight that the organic compounds which possess aromatic moieties exhibit higher nonlinear optical properties as well as strong donor–acceptor intermolecular interaction. Their special properties are linked to delocalized electrons (Crasta *et al.*, 2004; Prabu *et al.*, 2014). By stating that, it was proposed, for the first time, the design and fabrication of nickel/aluminum modified hemp fibers as novel hybrid material to be used as reinforcement in polymeric films. The methodology concerns

the precipitation of Ni (II)/Al (III) salts onto HF surface in urea based medium. Poly(ethylene-co-vinyl acetate) (PEVA) film reinforced with different amounts of Ni/Al modified HF were prepared by compression molding and characterized on terms of light absorption properties. Besides, the UV–Vis optical characterization technique in combination with the Tauc's method was applied as procedure for bandgap determination (Tauc, Grigorovici and Vancu, 1966).

Materials & Methods

Hemp fibers were supplied by NAFCO (Naples, Italy). Urea, Sodium hydroxide, $Al(NO_3)_3*9H_2O$, Nickel(II) acetate tetrahydrate and Poly(ethylene-co-vinyl acetate) were used as reagents.

Pre-treatment of hemp fibers

Hemp fibers were firstly washed with water to remove the superficial impurities and dried. The fibers were then treated with a 5% w/w alkaline solution (HF/NaOH=1:1 w/w) fixing a liquor ratio equal to 1:20 for 5 h, at 25°C fixing a stirring speed of 300 rpm. The fibers were washed several times until pH approaches to 7 and then dried at 80°C. The alkali-treated fibers were subjected to bleaching in H_2O_2 fixing a fiber/liquid ratio=1g/100 mL for 24 h, 80°C with a stirring speed of 300 rpm. The resulting fibers were washed with water-ethanol solution and dried at 80°C. The obtained fibers were reduced in size using a grinder (Duronic-CG250) and then milled through a high energy ball milling (HEBM-Retsch-PM 100) using a stainless-steel jar (V= 125 mL) and five zirconium oxide spheres as grinding medium. The rotation speed was set at 350 rpm for 15 minutes. The obtained powder-like hemp fibers was sieved using a 250-micron molecular sieve. Hereafter, the obtained product will be labeled as modified hemp fibers (HF).

Modification of hemp fibers

HF interfacing Ni/Al was prepared by coprecipitation method. First, an aqueous solution of NaOH/Urea/H_2O was prepared with the ratio 7:12:81 w/w. The solution was stirred at 300 rpm for 3h and cooled down at -6°C for 12 h. Besides, an aqueous solution (100 mL) of $Ni(OCOCH_3)_2$ $4H_2O$ (40 mmol) and $Al(NO_3)_3*9H_2O$ (20 mmol) was prepared. This latter solution was added dropwise to the NaOH/Urea solution which was kept at 50°C and stirred at 350 rpm. The pH was kept at 9.5 by adding NaOH (1M) solution. Afterward, the slurry was aged for 24 h at 80 °C. Then, the precipitate was centrifuged and washed continuously with bi-distilled water and ethanol.

Finally, it was dried at 100 °C under vacuum for 24 h. The obtained sample will be labeled hereafter as HF@Ni/Al. Composites based on PEVA and HF@Ni/Al (0.5%, 1.25%, 2.50 and 5% w/w) were prepared by compression molding at 120°C, using a Carver Laboratory press, and cooled at room temperature. Films of neat PEVA were produced using the same experimental conditions.

Experimental results

Figure (62)70 shows EDX maps, X-ray, FTIR spectra and TGA curves of HF and HF@Ni/Al.

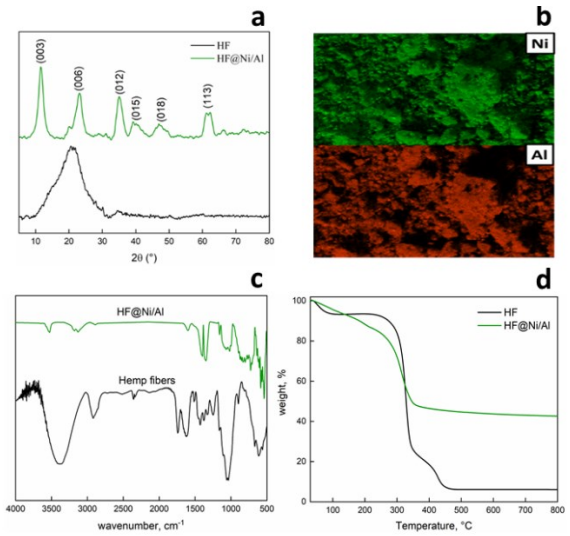

Figure 62 *a) X-ray spectra; b) EDX maps; c) FTIR spectra and d) TGA curves of HF and HF@Ni/Al samples*

It can be observed a good and homogeneous deposition of the two metals which are supposed to be structured in LDH conformation. Concerning the X-ray spectra, a broad peak appears in the interval $10°<2\theta<30°$. The intensity of the (200) peak at $2\theta = 22.2°$ represents the cellulose crystallographic plane (Dai and Fan, 2010; Stevulova *et al.*, 2014). The spectrum of HF@Ni/Al reports some sharp peaks which could be related to crystalline material. The reflections peaks at 11.6°, 23.1°, 35.0°, 39.1°, 46.8°, and 60.9° could be associated to the plane families (003), (006), (012), (015), (018) and (0015), respectively (Abo El-Reesh *et al.*, 2020; Wen, 2020). The small peak at 19.5° could be associated to β-$Ni(OH)_2$ (Guo *et al.*, 2020). FTIR spectrum of HF

shows the characteristic peaks of hemp fibers. The peak area at 3000-3600 cm^{-1} is the typical stretching vibration region of OH bonded groups in polysaccharides. The stretching vibration in the range 2890-3000 cm^{-1} is characteristic of CH groups of hemicellulose and cellulose (Terpáková *et al.*, 2012). The peak at 1735 cm^{-1} is attributed to C=O stretching vibration of acetyl groups of hemicellulose and methyl ester and carboxylic acid in pectin (Rachini *et al.*, 2009) while the vibration peak at 1373 cm^{-1} belongs to OH groups of carboxylic acids of pectin. The peak at about 1620 cm^{-1} is linked to OH bending of hemicellulose. The lignin C=C aromatic symmetrical stretching vibrations is located at 1510 cm^{-1}, while the band at 1454 cm^{-1} belongs to CH_2 bending vibration and the band at 1247 cm^{-1} to C-O stretching of acetyl (Sawpan, Pickering and Fernyhough, 2011b). In the FTIR of HF@Ni/Al the band at 3000-3500 cm^{-1} is related to OH stretching vibrations. The sharp peak in the range 500-800 cm^{-1} corresponds to M-OH and O-M-O stretching (where M is the metal) in the brucite like layers (Iftekhar, Srivastava and Sillanpää, 2017; Musella *et al.*, 2021). The hydrotalcite adsorption bands will appear in the region between 1300 cm^{-1} and 600 cm^{-1}. Finally, the fingerprint peaks of LDHs appear in the region at 400-800 cm^{-1} which is known to be associated to stretching and bending of Ni-O, Al-O, Ni-O-Al, O-Ni-O, O-Al-O (Dwiasi, Mudasir and Roto, 2019). TGA curves display three main thermal events (Yang *et al.*, 2007): i) 50-150°C correlated to the evaporation of water (Fisher *et al.*, 2002); ii) 220-300 °C degradation of pectin and hemicellulose; iii) 300-450°C decomposition of cellulose. The decomposition of lignin starts at about 280°C and ends at roughly 500°C. After the pre-treatment with NaOH and H_2O_2, the removal of the components with the lowest thermal stability such as pectin and hemicellulose, led to the disappearing of the characteristic peak at about 260°C and a higher thermal stability of the fibers, probably due to the formation of new lignin-cellulose complexes compared to raw hemp fibers (Reddy, Bhaduri and Sen, 1990). So, the main decomposition step at about 320°C is mainly related to the decomposition of cellulose and residual hemicellulose. The last peak at about 440-460°C identifies the oxidative degradation of charred residue (Viscusi, Barra and Gorrasi, 2020). The HF@Ni/Al sample showed a shift of the main thermal decomposition step occurred towards lower temperatures. In the same thermal range, dehydroxylation could even happen (Sharif et al., 2021). The residue amount is noticeably higher than treated HF (42% for HF@Ni/Al and 5 % for HF). Such improvement could be attributed to higher stability of Ni/Al as well as to the fact that the transmission of oxygen and other gaseous products is hindered by inorganic coating which could slow down further thermal breakdown, being a barrier between the heat source and the material.

UV protection measurements

The optical measurement was carried out in the range 200–800 nm. Figure (63) shows the transmittance versus wavelength for all the specimens.

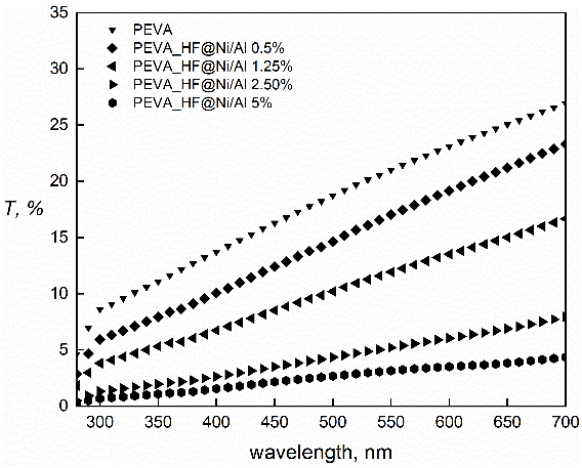

Figure 63 *Transmittance spectra of composite specimens*

The introduction of HF@Ni/Al induced a noticeable reduction of transmission along the entire wavelength range. This phenomenon can be related to the effect of loading concentration which causes light scattering as well as to the formation of intermolecular hydrogen bonding between Ni/Al and the OH groups of polymeric chains. The decrease in transmission for doped PEVA arises due to the change in polymer structure (Abdelaziz, 2011). The obtained values allowed to calculate the ultraviolet protection factor as well as the UV-A and UV-B protection factors. The obtained data are reported in table 26.

Table 26 *UPFs, UV-A and UV-B blocking factors calculations*

Sample	UPF	% blocking UV-A	% blocking UV-B
PEVA	10.8	92.43	88.47
PEVA_HF@Ni/Al 0.5%	15.5	94.85	91.75
PEVA_HF@Ni/Al 1.25%	23.8	96.69	94.51
PEVA_HF@Ni/Al 2.5%	75.3 (50+)	99.01	98.15
PEVA_HF@Ni/Al 5%	128 (50+)	99.43	98.85

Optical Measurements

The optical absorption edge is an important parameter for describing solid-state materials. For disordered materials, it is studied in terms of direct or indirect transition through the estimation of optical band gap. Among all, the absorption coefficient (α) is calculated by using the eq. (70) (Eshaghi and Graeli, 2014; Saad et al., 2019):

$$\alpha = \frac{2.303 * A}{d} \tag{70}$$

where A is the absorbance and d is the thickness (cm). It is defined as the decrement ratio of incident radiation relative to unit length in the direction of wave propagation in the medium. The variation of parameter α of tested samples as a function of wavelength is shown in figure (64):

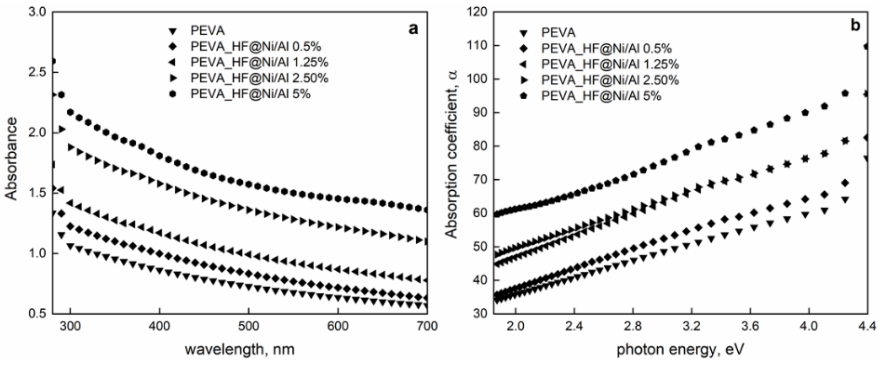

Figure 64 *a) Absorbance spectra and b) absorption coefficient of composite specimens*

The decrease of absorption coefficient as a function of wavelength. All the spectra exhibit a shoulder peak for λ<300 nm which can be assigned to the carbonyl groups associated with ethylene unsaturation. Besides, the absorption coefficient (α) has a minimum at low energy and increases with photon energy simulating the absorption edge of the semiconductors. The UV absorption edge is found to shift to higher wavelengths. As shown, the absorption increases for all samples in the UV region probably due to the excitations of donor level electrons to the conduction band. The high absorbance of loaded PEVA films in UV region are attributed to the energy of photon enough to interact with atoms; the electron excites from a lower to higher energy level by absorbing a photon of known energy. Since the absorbance increases and the transmittance decreases with the increasing of the HF@Ni/Al concentrations, agglomeration of filler particles as well as increase in the number of charge carriers could be considered the main causes.

When increasing the concentration of HF@Ni/Al particles, they can create a sort of paths network inside the polymeric matrix where charge carriers are allowed to pass through the paths.

The optical band gap (E_g) is related to absorption coefficient (α) and photon energy (h) according to the Tauc relation (eq. (71) (Ayeshamariam et al., 2014):

$$(\alpha h\nu)^{1/n}=B^*(h\nu-E_g) \quad (71)$$

where B is the band tailing constant, hν is the photon energy (eV), E_g is an optical band gap and n is the index, which takes different values depending on the mechanism of interband transition. n=2 and n=1/2 corresponding to indirect and direct transitions, respectively (Makuła, Pacia and Macyk, 2018). The optical curves exhibit linear and nonlinear portions which are the characteristics of the allowed transition. The linear portion of the curve located at high energy of the Tauc's plot characterizes the fundamental absorption of the materials, whereas the nonlinear portion concerns the residual absorption involving defect states. The direct bandgap value can be extrapolated by evaluating the intercept on x-axis of the tangent line to the linear part of curves. The estimation of the bandgap of a material is a key optical property in the optoelectronic, electronic and solar industries (Sangiorgi et al., 2017). It refers to the energy difference between the top of the valence band to the bottom of the conduction band (Zanatta, 2019) and represents a pivotal characteristic of the electronic structure of materials which affects the potential applications in devices (Jubu et al., 2020).

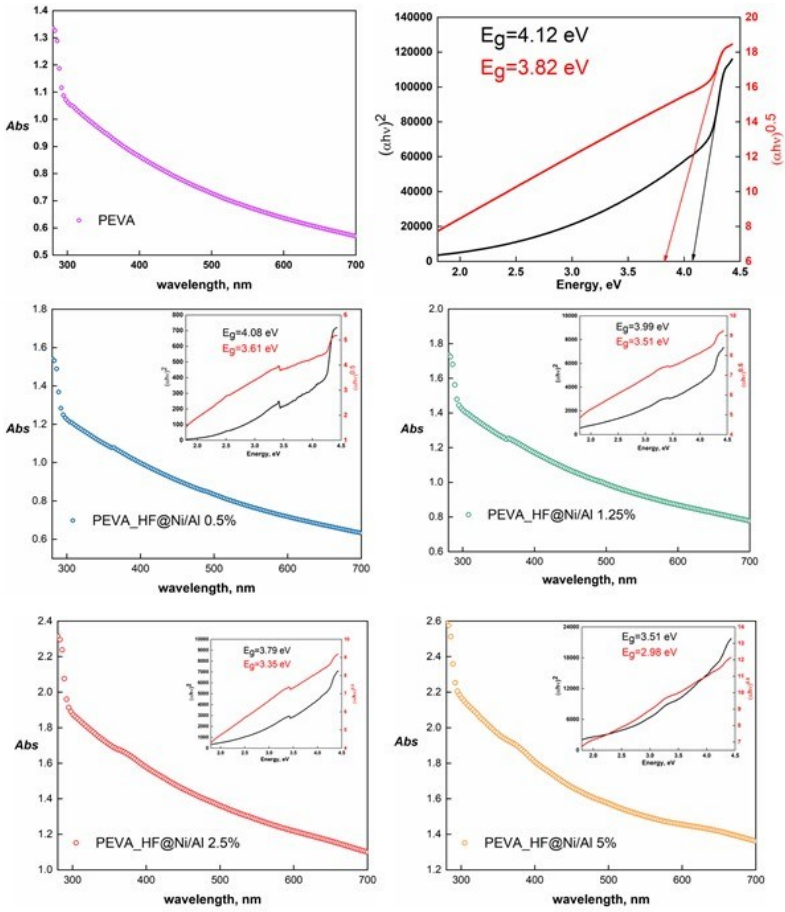

Figure 65 *Tauc's plots for PEVA composites. Insets report the Tauc's plots with band gap energies*

Figure (65) reports the absorbance trends of tested specimens in the wavelength range. Insets report the Tauc's plots for direct and indirect transition (black and red lines). Moreover, they report the band gap energy for the two transition states. The band edge showed a decrease with increasing concentration of hybrid filler in PEVA matrix with a shift towards higher wavelength (lower energy values) and proving the decrease in optical bandgap for PEVA composites. The shift towards lower energy could be associated with changes in the electron hole in conduction and valence bands due to Ni and Al presence. Their presence could be responsible of localized electronic states in HOMO-LUMO gap by defining trapping and recombination centers improving, in this way, the optical bandgap. This phenomenon also reflects the increased packing density inside the polymeric structure (Rozra *et al.*,

2012) and the presence of defects in the films due to the hybrid filler introduction. These defects are responsible of the localized states in the optical band gap. In fact, it is known that the density of the localized states is proportional to the concentration of the defects. Besides, the decrease in the optical band gap reflects the increase in the degree of disorder in the films. Yakuphanoglu (Yakuphanoglu, Barim and Erol, 2007) and Abdelaziz (Abdelaziz, 2011) observed similar results. The energy of incident photon allowed the electron to transit from the valence band to the conduction band. Since it can be stated that new energy levels in the energy gap are present, the transition occurred from the valence band passing through the local levels in energy gap. So, a small amounts of dopant forms charge transfer complexes in the host matrix and the band gap energy decreases. As the HF@Ni/Al concentration is increased, the filler could act as bridging the gap separating the valence and conduction band lowering the potential barrier between them, thereby facilitating the transfer of charge carrier between two localized states and determining the decrease in E_g value (figure (66)) (Sangawar et al., 2007).

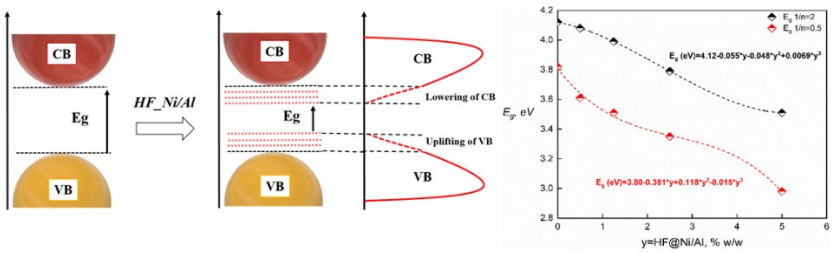

Figure 66 *Effect of filler loading on E_g lowering*

To further understand the interaction of HF@Ni/Al filler with PEVA matrix, optical properties such as dielectric constant (real part: ε_r (eq. (72)) and imaginary part: ε_{imm} (eq. (73)).

$$\varepsilon_r = n^2 - k^2 \quad (72)$$

$$\varepsilon_{imm} = 2nk \quad (73)$$

Where k is the extinction coefficient defined as eq. (74) and n is the refractive index defined as eq. (75):

$$k = \frac{\alpha^* \lambda}{4\pi} \quad (74)$$

$$n = \frac{1}{T,\%} + \sqrt{\frac{1}{T,\%-1}} \quad (75)$$

Besides, figure (67)71 reports the real and imaginary parts of dielectric constants.

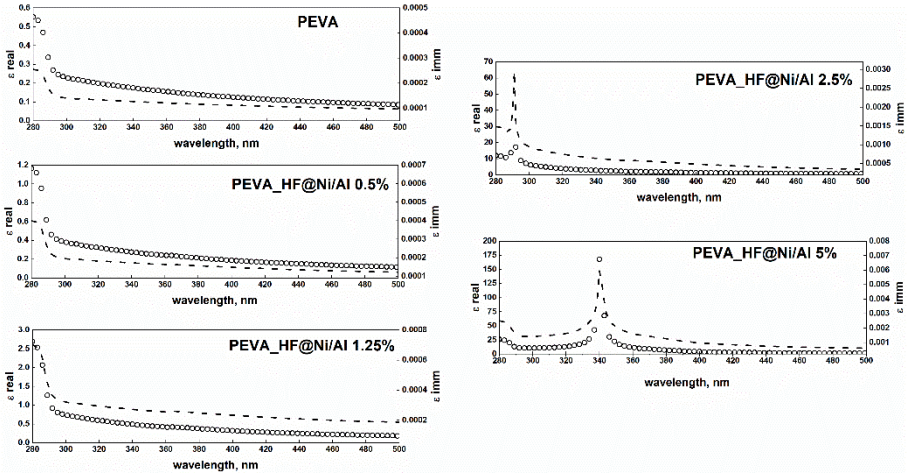

Figure 67 *Real (circles) and Imaginary (short line) parts of dielectric constants*

The dielectric constants depends sensitively on the band structure of the material (Kittel, McEuen and McEuen, 1996). It is obvious that the dielectric constant increases with increasing the HF@Ni/Al concentration. The increase in dielectric constant is related to the probable existence of higher energy density of states and so an increase of polarization. At lower wavelengths the optical dielectric constants show a dispersion region while at higher wavelengths the functions are almost constant. The real parts increase as filler loading decreases while the imaginary part showed an increase with filler loading. The real part of dielectric constant is related to the dispersion due to the actual motion of the electrons in the medium while the imaginary part concerns the dissipative rate of electromagnetic wave propagation in the medium (Ghanipour and Dorranian, 2013). Such behaviour of dielectric constant spectra plays an important role for practical applications in the field of optical communication (Muhammad and Sulaiman, 2011). It is clear that the loss peaks in the ultraviolet region (from 200 to 400 nm) shifts to higher wavelength upon the addition of 2.5 and 5 % of HF@Ni/Al. These shiftings indicate that the optical relaxation time (τ) decreases with increasing the charge carrier concentration (Yakuphanoglu *et al.*, no date).

Figure (68) reports the optical conductivity of PEVA films defined as eq. (76):

$$\sigma_{opt} = \frac{\alpha^* n^* c}{4\pi} \qquad (76)$$

Where c= light velocity.

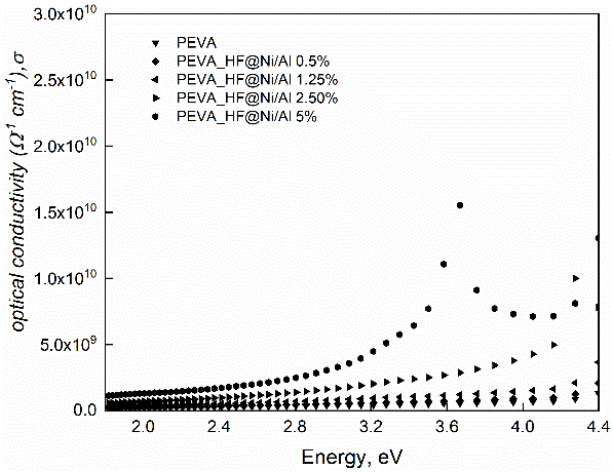

Figure 68 *Optical conductivity of neat PEVA and PEVA composites*

It clearly shows an increase in optical conductivity as filler loading increase probably associated to the increasing of electron mobility or the creation of localized levels in the energy gap; since that, an increase in the density of localized stages in the band structure occurred, hence, increasing the absorption coefficient as well the optical conductivity (Venkatarayappa, Kilarkaje and Prasad, 2011). The reason for this increment may be due to some changes in the structure of the film due to the filler introduction and the charge ordering effect. This increase could be responsible of the formation of new levels in the band gap which facilitate the crossing of electrons from the valence band to the local levels to the conduction band; consequently, the band gap decreases and the conductivity increase.

Concluding remarks

Hemp fibers, after NaOH and bleaching treatment, were modified through coprecipitation of Ni and Al salts in urea based aqueous medium to produce novel hybrid structured materials as reinforcement in PEVA films. A wide characterization of produced fillers has been carried out. SEM and EDX micrographs confirm the presence of Ni/Al platelets. Besides, the effective deposition was confirmed by FTIR and XRD spectra. Then, the metals presence ensured a high thermal stability in both cases as demonstrated by TGA analysis. After fabricating PEVA composites, UV protection factor and optical properties were studied.

Conclusions

The environmental impact caused by fossil fuel derived materials is requiring an intense effort in developing biodegradable and environmentally friendly materials from natural resources. The concept of sustainability paves the way to the production of novel materials fabricated from natural or recycled resources. These approaches are taking a center stage in developing countries, where, usually, there are no well-defined recycling policies and there is a wide availability of large quantities of agricultural and industrial by-products. One of them, hemp fibers derived from decortication processes of hemp plant, represents the focus of this thesis. Potential applications of modified hemp fibers were presented by focusing on alternative and sustainable techniques to physically or chemically modify the hemp fibers surface. The potential of a green, fast, simple, ecological, and cost-effective technology, such as high energy ball milling, was fully exploited highlighting the possibility of performing and improving the functionalization of natural fibers avoiding harsh experimental conditions, and allowing to work at room temperature and quite reduced processing times. Novel and green surface modification methods were presented which are based on the use of organic compounds, natural clay or nanocarbons. Possibility of using hemp by products as filler in hydrogels was then investigated. Finally, the application of coprecipitation technique to fabricated metal structured hemp fibers was fully investigated to produce novel magnetic hybrid materials.

The results of this work are in accordance with the importance of developing innovative and environmentally friendly chemical processes or materials. The use of these novel materials can open new perspectives for the development of new low-cost products with targeted performances. So, it is raising up as an alternative for costlier and less sustainable materials used in different industrial fields.

Bibliography

A.Kriaa, N.Hamdi and E.Srasra (2008) 'Determination Of Point Of Zero Charge Of Tunisian Kaolinites By Potentiometric And Mass Titration Methods', *Analytical Chemistry: An Indian Journal*, 2(1). Available at: https://www.tsijournals.com/abstract/determination-of-point-of-zero-charge-of-tunisian-kaolinites-by-potentiometric-and-mass-titration-methods-19.html (Accessed: 17 August 2021).

Abdelaziz, M. (2011) 'Cerium (III) doping effects on optical and thermal properties of PVA films'. doi: 10.1016/j.physb.2011.01.021.

Abo El-Reesh, G. Y. *et al.* (2020) 'Novel synthesis of Ni/Fe layered double hydroxides using urea and glycerol and their enhanced adsorption behavior for Cr(VI) removal', *Scientific Reports 2020 10:1*, 10(1), pp. 1–20. doi: 10.1038/s41598-020-57519-4.

Agarwal, U. P., Reiner, R. S. and Ralph, S. A. (2010) 'Cellulose I crystallinity determination using FT-Raman spectroscopy: Univariate and multivariate methods', *Cellulose*, 17(4), pp. 721–733. doi: 10.1007/s10570-010-9420-z.

Agate, S. *et al.* (2020) 'Innovating Generation of Nanocellulose from Industrial Hemp by Dual Asymmetric Centrifugation', *ACS Sustainable Chemistry and Engineering*, 8(4), pp. 1850–1858. doi: 10.1021/acssuschemeng.9b05992.

Ahmad, M. *et al.* (2015) 'Optical and thermo-mechanical properties of composite films based on fish gelatin/rice flour fabricated by casting technique', *Progress in Organic Coatings*, 84, pp. 115–127. doi: 10.1016/j.porgcoat.2015.02.016.

Ahmad, M. A., Ahmad Puad, N. A. and Bello, O. S. (2014) 'Kinetic, equilibrium and thermodynamic studies of synthetic dye removal using pomegranate peel activated carbon prepared by microwave-induced KOH activation', *Water Resources and Industry*, 6, pp. 18–35. doi: 10.1016/j.wri.2014.06.002.

Bin Ahmad, M. *et al.* (2012) 'Antibacterial activity of silver bionanocomposites synthesized by chemical reduction route', *Chemistry Central Journal*, 6(1), pp. 1–9. doi: 10.1186/1752-153X-6-101.

Ahmaruzzaman, M. and Gupta, V. K. (2011) 'Rice husk and its ash as low-cost adsorbents in water and wastewater treatment', *Industrial and Engineering Chemistry Research*, 50(24), pp. 13589–13613. doi: 10.1021/ie201477c.

Ahmed, M. N. and Ram, R. N. (1992) 'Removal of basic dye from waste-water using silica as adsorbent', *Environmental Pollution*, 77(1), pp. 79–86. doi: 10.1016/0269-7491(92)90161-3.

Ainurofiq, A. and Choiri, S. (2015) 'Drug Release Model and Kinetics of

Natural Polymers-Based Sustained Release Tablet', *LATIN AMERICAN JOURNAL OF PHARMACY*, 37(7), pp. 1328–1337.
Al-Muhtaseb, A. H., McMinn, W. A. M. and Magee, T. R. A. (2004) 'Water sorption isotherms of starch powders: Part 1: mathematical description of experimental data', *Journal of Food Engineering*, 61(3), pp. 297–307. doi: 10.1016/S0260-8774(03)00133-X.
Al-Tayyar, N. A., Youssef, A. M. and Al-hindi, R. (2020) 'Antimicrobial food packaging based on sustainable Bio-based materials for reducing foodborne Pathogens: A review', *Food Chemistry*. Elsevier Ltd, p. 125915. doi: 10.1016/j.foodchem.2019.125915.
Ali, A. *et al.* (2018a) 'Hydrophobic treatment of natural fibers and their composites-A review', 47(8), pp. 2153–2183. doi: 10.1177/1528083716654468.
Ali, A. *et al.* (2018b) 'Hydrophobic treatment of natural fibers and their composites—A review', *Journal of Industrial Textiles*, 47(8), pp. 2153–2183. doi: 10.1177/1528083716654468.
Alix, S. *et al.* (2009) 'Effect of chemical treatments on water sorption and mechanical properties of flax fibres', *Bioresource Technology*, 100(20), pp. 4742–4749. doi: 10.1016/j.biortech.2009.04.067.
Allahbakhsh, A. *et al.* (2017) '3-Aminopropyl-triethoxysilane-functionalized rice husk and rice husk ash reinforced polyamide 6/graphene oxide sustainable nanocomposites', *European Polymer Journal*, 94, pp. 417–430. doi: 10.1016/j.eurpolymj.2017.07.031.
Allen, N. S. and Edge, M. (1992) *Fundamentals of polymer degradation and stabilisation*.
Alongi, J., Ciobanu, M. and Malucelli, G. (2011) 'Novel flame retardant finishing systems for cotton fabrics based on phosphorus-containing compounds and silica derived from sol-gel processes', *Carbohydrate Polymers*, 85(3), pp. 599–608. doi: 10.1016/j.carbpol.2011.03.024.
Aluigi, A. *et al.* (2014) 'Study of Methylene Blue adsorption on keratin nanofibrous membranes', *Journal of Hazardous Materials*, 268, pp. 156–165. doi: 10.1016/j.jhazmat.2014.01.012.
Amaducci, S. and Gusovius, H.-J. (2010) 'Hemp - Cultivation, Extraction and Processing', in *Industrial Applications of Natural Fibres*. Chichester, UK: John Wiley & Sons, Ltd, pp. 109–134. doi: 10.1002/9780470660324.ch5.
Anastas, P. T. and Kirchhoff, M. M. (2002) 'Origins, current status, and future challenges of green chemistry', *Accounts of Chemical Research*, 35(9), pp. 686–694. doi: 10.1021/ar010065m.
Ariawan, D. *et al.* (2017) 'Wettability and interfacial characterization of alkaline treated kenaf fiber-unsaturated polyester composites fabricated by resin transfer molding', *Polymer Composites*, 38(3), pp. 507–515. doi: 10.1002/pc.23609.
ASTM D792 - 20 Standard Test Methods for Density and Specific Gravity

(Relative Density) of Plastics by Displacement (no date). Available at: https://www.astm.org/Standards/D792 (Accessed: 15 October 2020).
Atarés, L. and Chiralt, A. (2016) 'Essential oils as additives in biodegradable films and coatings for active food packaging', *Trends in Food Science and Technology*. Elsevier Ltd, pp. 51–62. doi: 10.1016/j.tifs.2015.12.001.
Avérous, L., Fringant, C. and Moro, L. (2001) 'Plasticized starch-cellulose interactions in polysaccharide composites', *Polymer*, 42(15), pp. 6565–6572. doi: 10.1016/S0032-3861(01)00125-2.
Ayeshamariam, A. *et al.* (2014) 'Preparation and characterizations of SnO2 nanopowder and spectroscopic (FT-IR, FT-Raman, UV–Visible and NMR) analysis using HF and DFT calculations', *Spectrochimica Acta Part A: Molecular and Biomolecular Spectroscopy*, 118, pp. 1135–1143. doi: 10.1016/J.SAA.2013.09.030.
Aziz, S. H. and Ansell, M. P. (2004) 'The effect of alkalization and fibre alignment on the mechanical and thermal properties of kenaf and hemp bast fibre composites: Part 1 - polyester resin matrix', *Composites Science and Technology*, 64(9), pp. 1219–1230. doi: 10.1016/j.compscitech.2003.10.001.
Baggi, R. B. and Kilaru, N. B. (2016) 'Calculation of predominant drug release mechanism using Peppas-Sahlin model, Part-I (substitution method): A linear regression approach', *Asian Journal of Pharmacy and Technology*, 6(4), p. 223. doi: 10.5958/2231-5713.2016.00033.7.
Bai, B. *et al.* (2019) 'Lauric acid-modified nitraria seed meal composite as green carrier material for pesticide controlled release', *Journal of Chemistry*, 2019. doi: 10.1155/2019/5376452.
Balu, B., Breedveld, V. and Hess, D. W. (2008) 'Fabrication of "roll-off" and "sticky" superhydrophobic cellulose surfaces-via plasma processing', *Langmuir*, 24(9), pp. 4785–4790. doi: 10.1021/la703766c.
Basu, S., Shivhare, U. S. and Mujumdar, A. S. (2006) 'Models for sorption isotherms for foods: A review', *Drying Technology*. Taylor & Francis Group , pp. 917–930. doi: 10.1080/07373930600775979.
Bello, O. S., Ahmad, M. A. and Ahmad, N. (2012) 'Adsorptive features of banana (Musa paradisiaca) stalk-based activated carbon for malachite green dye removal', *Chemistry and Ecology*, 28(2), pp. 153–167. doi: 10.1080/02757540.2011.628318.
Benhacine, F., Yahiaoui, F. and Hadj-Hamou, A. S. (2014) 'Thermal Stability and Kinetic Study of Isotactic Polypropylene/Algerian Bentonite Nanocomposites Prepared via Melt Blending', *Journal of Polymers*, 2014, pp. 1–9. doi: 10.1155/2014/426470.
Bessadok, A. *et al.* (2007) 'Effect of chemical treatments of Alfa (Stipa tenacissima) fibres on water-sorption properties', *Composites Science and Technology*, 67(3–4), pp. 685–697. doi: 10.1016/j.compscitech.2006.04.013.
Bessadok, A. *et al.* (2009) 'Study of water sorption on modified Agave fibres', *Carbohydrate Polymers*, 76(1), pp. 74–85. doi: 10.1016/j.carbpol.2008.09.033.

Bhattacharya, K. G. and Sharma, A. (2005) 'Kinetics and thermodynamics of Methylene Blue adsorption on Neem (Azadirachta indica) leaf powder', *Dyes and Pigments*, 65(1), pp. 51–59. doi: 10.1016/j.dyepig.2004.06.016.
Bingol, D., Tekin, N. and Alkan, M. (2010) 'Brilliant Yellow dye adsorption onto sepiolite using a full factorial design', *Applied Clay Science*, 50(3), pp. 315–321. doi: 10.1016/j.clay.2010.08.015.
Blahovec, J. and Yanniotis, S. (2008) 'Gab generalized equation for sorption phenomena', *Food and Bioprocess Technology*, 1(1), pp. 82–90. doi: 10.1007/s11947-007-0012-3.
Bledzki, A. K., Fink, H. P. and Specht, K. (2004) 'Unidirectional hemp and flax EP- and PP-composites: Influence of defined fiber treatments', *Journal of Applied Polymer Science*, 93(5), pp. 2150–2156. doi: 10.1002/APP.20712.
Boccalon, E. *et al.* (2021) 'Solvent-free synthesis of halloysite-layered double hydroxide composites containing salicylate as novel, active fillers', *Colloids and Surfaces A: Physicochemical and Engineering Aspects*, 627, p. 127135. doi: 10.1016/J.COLSURFA.2021.127135.
Bodirlau, R., Teaca, C. A. and Spiridon, I. (2013) 'Influence of natural fillers on the properties of starch-based biocomposite films', *Composites Part B: Engineering*, 44(1), pp. 575–583. doi: 10.1016/j.compositesb.2012.02.039.
Borsa, J. *et al.* (2016) 'Effect of mild alkali/ultrasound treatment on flax and hemp fibres: the different responses of the two substrates', *Cellulose*, 23(3), pp. 2117–2128. doi: 10.1007/s10570-016-0909-y.
Bouazizi, N. *et al.* (2019) 'Entrapment and stabilization of iron nanoparticles within APTES modified graphene oxide sheets for catalytic activity improvement', *Journal of Alloys and Compounds*, 771, pp. 1090–1102. doi: 10.1016/j.jallcom.2018.08.240.
Brachi, P. *et al.* (2014) 'Fluidized bed co-gasification of biomass and polymeric wastes for a flexible end-use of the syngas: Focus on bio-methanol', *Fuel*, 128, pp. 88–98. doi: 10.1016/j.fuel.2014.02.070.
Brunauer, S. *et al.* (1940) 'On a Theory of the van der Waals Adsorption of Gases', *Journal of the American Chemical Society*, 62(7), pp. 1723–1732. doi: 10.1021/ja01864a025.
Bruschi, M. L. (2015) *Strategies to Modify the Drug Release from Pharmaceutical Systems*, *Strategies to Modify the Drug Release from Pharmaceutical Systems*. Elsevier Inc. doi: 10.1016/C2014-0-02342-8.
Bugatti, V., Vertuccio, L., *et al.* (2019) 'Green pesticides based on cinnamate anion incorporated in layered double hydroxides and dispersed in pectin matrix', *Carbohydrate Polymers*, 209, pp. 356–362. doi: 10.1016/j.carbpol.2019.01.033.
Bugatti, V., Brachi, P., *et al.* (2019) 'Valorization of Tomato Processing Residues Through the Production of Active Bio-Composites for Packaging Applications', *Frontiers in Materials*, 6. doi: 10.3389/fmats.2019.00034.
Bulut, Y. and Aydin, H. (2006) 'A kinetics and thermodynamics study of methylene blue adsorption on wheat shells', *Desalination*, 194(1–3), pp.

259–267. doi: 10.1016/j.desal.2005.10.032.
Carpita, N. C. and Gibeaut, D. M. (1993) ‘Structural models of primary cell walls in flowering plants: Consistency of molecular structure with the physical properties of the walls during growth’, *Plant Journal*, 3(1), pp. 1–30. doi: 10.1111/j.1365-313X.1993.tb00007.x.
Célino, A. *et al.* (2014) ‘The hygroscopic behavior of plant fibers: A review’, *Frontiers in Chemistry*, 1(JAN), p. 43. doi: 10.3389/FCHEM.2013.00043/BIBTEX.
Chen, H. C., Tsai, C. H. and Yang, M. C. (2011) ‘Mechanical properties and biocompatibility of electrospun polylactide/poly(vinylidene fluoride) mats’, *Journal of Polymer Research*, 18(3), pp. 319–327. doi: 10.1007/s10965-010-9421-5.
Cheng, W. *et al.* (2018) ‘Selective removal of divalent cations by polyelectrolyte multilayer nanofiltration membrane: Role of polyelectrolyte charge, ion size, and ionic strength’, *Journal of Membrane Science*, 559, pp. 98–106. doi: 10.1016/J.MEMSCI.2018.04.052.
Chien, Y. W. (1988) ‘Controlled release of biologically active agents’, *Journal of Pharmaceutical Sciences*, 77(4), p. 371. doi: 10.1002/jps.2600770422.
Chirife, J. *et al.* (1983) ‘A New Model for Describing the Water Sorption Isotherm of Foods’, *Journal of Food Science*, 48(4), pp. 1382–1383. doi: 10.1111/j.1365-2621.1983.tb09245.x.
Choi, Y. S. and Cho, J. H. (1996) ‘Color removal from dye wastewater using vermiculite’, *Environmental Technology (United Kingdom)*, 17(11), pp. 1169–1180. doi: 10.1080/09593331708616487.
Chong, K. Y. *et al.* (2018) ‘Simplified production of graphene oxide assisted by high shear exfoliation of graphite with controlled oxidation’, *New Journal of Chemistry*, 42(6), pp. 4507–4512. doi: 10.1039/c7nj04911k.
Copping, L. G. and Menn, J. J. (2000) ‘Biopesticides: A review of their action, applications and efficacy’, in *Pest Management Science*, pp. 651–676. doi: 10.1002/1526-4998(200008)56:8<651::AID-PS201>3.0.CO;2-U.
Costantino, U. *et al.* (2008a) ‘Hydrotalcite-like compounds: Versatile layered hosts of molecular anions with biological activity’, *Microporous and Mesoporous Materials*, 107(1–2), pp. 149–160. doi: 10.1016/J.MICROMESO.2007.02.005.
Costantino, U. *et al.* (2008b) ‘Hydrotalcite-like compounds: Versatile layered hosts of molecular anions with biological activity’, *Microporous and Mesoporous Materials*, 107(1–2), pp. 149–160. doi: 10.1016/j.micromeso.2007.02.005.
Crank, J. (1979) *The mathematics of diffusion. 2nd Edn.* Clarendon Press. doi: 10.1088/0031-9112/26/11/044.
Crank, J. and Henry, M. E. (1949) ‘Diffusion in media with variable properties: Part I. The effect of a variable diffusion coefficient on the rates of absorption and desorption’, *Transactions of the Faraday Society*, 45(0), pp.

636–650. doi: 10.1039/tf9494500636.
Crasta, V. *et al.* (2004) 'Growth and characterization of an organic NLO crystal: 1-(4-methylphenyl)- 3-(4-methoxyphenyl)-2-propen-1-one', *Journal of Crystal Growth*, 267(1–2), pp. 129–133. doi: 10.1016/J.JCRYSGRO.2004.03.037.
Crepaldi, E. L., Pavan, P. C. and Valim, J. B. (2000) 'Comparative study of the coprecipitation methods for the preparation of Layered Double Hydroxides', *Journal of the Brazilian Chemical Society*, 11(1), pp. 64–70. doi: 10.1590/S0103-50532000000100012.
Crini, G. *et al.* (2019) 'Conventional and non-conventional adsorbents for wastewater treatment', *Environmental Chemistry Letters*. Springer Verlag, pp. 195–213. doi: 10.1007/s10311-018-0786-8.
Crini, G. and Lichtfouse, E. (2019) 'Advantages and disadvantages of techniques used for wastewater treatment', *Environmental Chemistry Letters*. Springer Verlag, pp. 145–155. doi: 10.1007/s10311-018-0785-9.
D790-07, I. A.-A. and 2007, undefined (no date) 'Standard test methods for flexural properties of unreinforced and reinforced plastics and electrical insulating materials', *ci.nii.ac.jp*. Available at: https://ci.nii.ac.jp/naid/10030128663/ (Accessed: 19 October 2020).
D792, A. (2002) 'Standard Test Methods for Density and Specific Gravity of Plastics by Displacement'.
Dai, D. and Fan, M. (2010) 'Characteristic and Performance of Elementary Hemp Fibre', *Materials Sciences and Applications*, 01(06), pp. 336–342. doi: 10.4236/MSA.2010.16049.
Das, M. and Chakraborty, D. (2006) 'Influence of alkali treatment on the fine structure and morphology of bamboo fibers', *Journal of Applied Polymer Science*, 102(5), pp. 5050–5056. doi: 10.1002/app.25105.
Das, M., Prasad, V. S. and Chakrabarty, D. (2009) 'Thermogravimetric and weathering study of novolac resin composites reinforced with mercerized bamboo fiber', *Polymer Composites*, 30(10), pp. 1408–1416. doi: 10.1002/pc.20705.
Demir, H. *et al.* (2006) 'The effect of fiber surface treatments on the tensile and water sorption properties of polypropylene-luffa fiber composites', *Composites Part A: Applied Science and Manufacturing*, 37(3), pp. 447–456. doi: 10.1016/j.compositesa.2005.05.036.
Derjaguin, B. . V., Muller, V. . M. and Toporov, Y. . P. (1975) 'Effect of contact deformations on the adhesion of particles', *Journal of Colloid and Interface Science*, 53(2), pp. 314–326. doi: 10.1016/0021-9797(75)90018-1.
Dhakal, H. N., Zhang, Z. Y. and Richardson, M. O. W. (2007) 'Effect of water absorption on the mechanical properties of hemp fibre reinforced unsaturated polyester composites', *Composites Science and Technology*, 67(7–8), pp. 1674–1683. doi: 10.1016/j.compscitech.2006.06.019.
Dias, A. B. *et al.* (2011) 'Mechanical and barrier properties of composite films based on rice flour and cellulose fibers', *LWT - Food Science and*

Technology, 44(2), pp. 535–542. doi: 10.1016/j.lwt.2010.07.006.
Dolez, P. I. *et al.* (2017) 'Hydrophobic treatments for natural fibers based on metal oxide nanoparticles and fatty acids', in *Procedia Engineering*. Elsevier Ltd, pp. 81–88. doi: 10.1016/j.proeng.2017.07.013.
Dorris, G. M. and Gray, D. G. (1979a) 'Adsorption, spreading pressure, and london force interactions of hydrocarbons on cellulose and wood fiber surfaces', *Journal of Colloid And Interface Science*, 71(1), pp. 93–106. doi: 10.1016/0021-9797(79)90224-8.
Dorris, G. M. and Gray, D. G. (1979b) 'Adsorption, spreading pressure, and london force interactions of hydrocarbons on cellulose and wood fiber surfaces', *Journal of Colloid And Interface Science*, 71(1), pp. 93–106. doi: 10.1016/0021-9797(79)90224-8.
Dufresne, A. and Vignon, M. R. (1998) 'Improvement of starch film performances using cellulose microfibrils', *Macromolecules*, 31(8), pp. 2693–2696. doi: 10.1021/ma971532b.
Dutta, R., Sarkar, U. and Mukherjee, A. (2016) 'Pseudo-kinetics of batch extraction of Crotalaria juncea (Sunn hemp) seed oil using 2-propanol', *Industrial Crops and Products*, 87, pp. 9–13. doi: 10.1016/j.indcrop.2016.04.006.
Dwiasi, D. W., Mudasir, M. and Roto, R. (2019) 'Ion Exchange of Benzoate in Ni-Al-Benzoate Layered Double Hydroxide by Amoxicillin', *Open Chemistry*, 17(1), pp. 1043–1049. doi: 10.1515/CHEM-2019-0122/MACHINEREADABLECITATION/RIS.
Ebnesajjad, S. and Landrock, A. H. (2015) 'Surface Tension and Its Measurement', in *Adhesives Technology Handbook*. Elsevier, pp. 19–34. doi: 10.1016/b978-0-323-35595-7.00002-4.
Eichhorn, S. J. *et al.* (2000) 'Stress induced shifts in the Raman spectra of natural cellulose fibers', *Journal of Materials Science Letters*, 19(8), pp. 721–723. doi: 10.1023/A:1006787300815.
Eshaghi, A. and Graeli, A. (2014) 'Optical and electrical properties of indium tin oxide (ITO) nanostructured thin films deposited on polycarbonate substrates "thickness effect"', *Optik*, 125(3), pp. 1478–1481. doi: 10.1016/J.IJLEO.2013.09.011.
do Evangelho, J. A. *et al.* (2019) 'Antibacterial activity, optical, mechanical, and barrier properties of corn starch films containing orange essential oil', *Carbohydrate Polymers*, 222, p. 114981. doi: 10.1016/j.carbpol.2019.114981.
FA, B. and DK, S. (2007) 'Simulation of dye adsorption by beech sawdust as affected by pH', *Journal of hazardous materials*, 141(3), pp. 668–679. doi: 10.1016/J.JHAZMAT.2006.07.033.
Fan, S. *et al.* (2017) 'Removal of methylene blue from aqueous solution by sewage sludge-derived biochar: Adsorption kinetics, equilibrium, thermodynamics and mechanism', *Journal of Environmental Chemical Engineering*, 5(1), pp. 601–611. doi: 10.1016/j.jece.2016.12.019.

Faruk, O. *et al.* (2012) 'Biocomposites reinforced with natural fibers: 2000-2010', *Progress in Polymer Science*. Pergamon, pp. 1552–1596. doi: 10.1016/j.progpolymsci.2012.04.003.
Fisher, T. *et al.* (2002) 'Pyrolysis behavior and kinetics of biomass derived materials', *Journal of Analytical and Applied Pyrolysis*, 62(2), pp. 331–349. doi: 10.1016/S0165-2370(01)00129-2.
Ford, J. L. *et al.* (1987) 'Importance of drug type, tablet shape and added diluents on drug release kinetics from hydroxypropylmethylcellulose matrix tablets', *International Journal of Pharmaceutics*, 40(3), pp. 223–234. doi: 10.1016/0378-5173(87)90172-4.
Forgacs, E., Cserháti, T. and Oros, G. (2004) 'Removal of synthetic dyes from wastewaters: A review', *Environment International*. Elsevier Ltd, pp. 953–971. doi: 10.1016/j.envint.2004.02.001.
Forziati, F. H. *et al.* (1950) *Cotton Powder for Infrared Transmission Measurements 1*, *Journal of Research of the National Bureau of Standards*.
Franzoni, E. (2011) 'Materials selection for green buildings: Which tools for engineers and architects?', in *Procedia Engineering*. Elsevier Ltd, pp. 883–890. doi: 10.1016/j.proeng.2011.11.2090.
French, A. D. (2020) 'Increment in evolution of cellulose crystallinity analysis', *Cellulose*. Springer, pp. 5445–5448. doi: 10.1007/s10570-020-03172-z.
Fricke, H. (1924) 'A mathematical treatment of the electric conductivity and capacity of disperse systems I. The electric conductivity of a suspension of homogeneous spheroids', *Physical Review*, 24(5), pp. 575–587. doi: 10.1103/PhysRev.24.575.
Fuqua, M. A., Huo, S. and Ulven, C. A. (2012) 'Natural fiber reinforced composites', *Polymer Reviews*. Taylor & Francis Group , pp. 259–320. doi: 10.1080/15583724.2012.705409.
Gallagher, K. M. and Corrigan, O. I. (2000) 'Mechanistic aspects of the release of levamisole hydrochloride from biodegradable polymers', *Journal of Controlled Release*, 69(2), pp. 261–272. doi: 10.1016/S0168-3659(00)00305-9.
Galluzzi, A. *et al.* (2018) 'Determination of the Transition Temperature of a Weak Ferromagnetic Thin Film by Means of an Evolution of the Method Based on the Arrott Plots', *Journal of Superconductivity and Novel Magnetism*, 31(4), pp. 1127–1132. doi: 10.1007/S10948-017-4281-4/FIGURES/5.
Galluzzi, A., Nigro, A., *et al.* (2019) 'DC magnetic characterization and pinning analysis on Nd1.85Ce0.15CuO4 cuprate superconductor', *Journal of Magnetism and Magnetic Materials*, 475, pp. 125–129. doi: 10.1016/J.JMMM.2018.11.119.
Galluzzi, A., Buchkov, K., *et al.* (2019) 'Pinning energy and anisotropy properties of a Fe(Se, Te) iron based superconductor', *Nanotechnology*, 30(25). doi: 10.1088/1361-6528/AB0C23.

Galzerano, B. *et al.* (2017) 'Hemp reinforcement in lightweight geopolymers':, *https://doi.org/10.1177/0021998317744036*, 52(17), pp. 2313–2320. doi: 10.1177/0021998317744036.
Garcia-Jaldon, C., Dupeyre, D. and Vignon, M. R. (1998) 'Fibres from semi-retted hemp bundles by steam explosion treatment', *Biomass and Bioenergy*, 14(3), pp. 251–260. doi: 10.1016/S0961-9534(97)10039-3.
George, M. *et al.* (2014) 'Characterization of chemically and enzymatically treated hemp fibres using atomic force microscopy and spectroscopy', *Applied Surface Science*, 314, pp. 1019–1025. doi: 10.1016/j.apsusc.2014.06.080.
George, M. *et al.* (2016) 'Enzymatically treated natural fibres as reinforcing agents for biocomposite material: mechanical, thermal, and moisture absorption characterization', *Journal of Materials Science*, 51(5), pp. 2677–2686. doi: 10.1007/s10853-015-9582-z.
Ghanipour, M. and Dorranian, D. (2013) 'Effect of Ag-Nanoparticles Doped in Polyvinyl Alcohol on the Structural and Optical Properties of PVA Films', *Journal of Nanomaterials*, 2013. doi: 10.1155/2013/897043.
Gordon, P. W. *et al.* (2010) 'Studies into the swelling of gelatine films using a scanning fluid dynamic gauge', *Food and Bioproducts Processing*, 88(4), pp. 357–364. doi: 10.1016/j.fbp.2010.08.012.
Gorrasi, G. and Bugatti, V. (2016) 'Edible bio-nano-hybrid coatings for food protection based on pectins and LDH-salicylate: Preparation and analysis of physical properties', *LWT - Food Science and Technology*, 69, pp. 139–145. doi: 10.1016/j.lwt.2016.01.038.
Gorrasi, G., Bugatti, V. and Sorrentino, A. (2018) 'Nanohybrid Active Fillers in Food Contact Bio-based Materials', *Bionanocomposites for Packaging Applications*, pp. 71–94. doi: 10.1007/978-3-319-67319-6_4.
Gorrasi, G., Bugatti, V. and Vittoria, V. (2012) 'Pectins filled with LDH-antimicrobial molecules: Preparation, characterization and physical properties', *Carbohydrate Polymers*, 89(1), pp. 132–137. doi: 10.1016/j.carbpol.2012.02.061.
Gouanvé, F. *et al.* (2006) 'Study of water sorption in modified flax fibers', *Journal of Applied Polymer Science*, 101(6), pp. 4281–4289. doi: 10.1002/app.23661.
Gouanvé, F. *et al.* (2007) 'Kinetics of water sorption in flax and PET fibers', *European Polymer Journal*, 43(2), pp. 586–598. doi: 10.1016/j.eurpolymj.2006.10.023.
Guinee, T. P. *et al.* (2002) 'Effect of pH and calcium concentration on some textural and functional properties of Mozzarella cheese', *Journal of Dairy Science*, 85(7), pp. 1655–1669. doi: 10.3168/jds.S0022-0302(02)74238-0.
Guleria, A., Singha, A. S. and Rana, R. K. (2017) 'Preparation of starch-based biocomposites reinforced with mercerized lignocellulosic fibers: Evaluation of their thermal, morphological, mechanical, and biodegradable properties', *International Journal of Polymer Analysis and Characterization*,

22(7), pp. 595–609. doi: 10.1080/1023666X.2017.1345558.
Guo, R. and Wilson, L. D. (2012) 'Synthetically engineered chitosan-based materials and their sorption properties with methylene blue in aqueous solution', *Journal of Colloid and Interface Science*, 388(1), pp. 225–234. doi: 10.1016/j.jcis.2012.08.010.
Guo, S. *et al.* (2020) 'A facile and sensitive electrochemical sensor for non-enzymatic glucose detection based on three-dimensional flexible polyurethane sponge decorated with nickel hydroxide', *Analytica Chimica Acta*, 1109, pp. 130–139. doi: 10.1016/J.ACA.2020.02.037.
Gutierrez-Villarreal, M. H., Rodríguez-Gonzalez, F. J. and Perera-Mercado, Y. (2017) 'Estimation of Surface Free Energy of Poly(lactic acid) During UV-Grafting with N-Vinylpyrrolidone', *Macromolecular Symposia*, 374(1). doi: 10.1002/masy.201600130.
Han, J. H. and Floros, J. D. (1997) 'Casting antimicrobial packaging films and measuring their physical properties and antimicrobial activity', *Journal of Plastic Film and Sheeting*, 13(4), pp. 287–298. doi: 10.1177/875608799701300405.
Han, R. *et al.* (2006) 'Removal of methylene blue from aqueous solution by chaff in batch mode', *Journal of Hazardous Materials*, 137(1), pp. 550–557. doi: 10.1016/J.JHAZMAT.2006.02.029.
Hao, O. J., Kim, H. and Chiang, P. C. (2000) 'Decolorization of wastewater', *Critical Reviews in Environmental Science and Technology*. CRC Press LLC, pp. 449–505. doi: 10.1080/10643380091184237.
Hatakeyama, H. and Hatakeyama, T. (1998) 'Interaction between water and hydrophilic polymers', *Thermochimica Acta*, 308(1–2), pp. 3–22. doi: 10.1016/s0040-6031(97)00325-0.
He, M., Xu, M. and Zhang, L. (2013) 'Controllable stearic acid crystal induced high hydrophobicity on cellulose film surface', *ACS Applied Materials and Interfaces*, 5(3), pp. 585–591. doi: 10.1021/am3026536.
Hejda, F., Solař, P. and Kousal, J. (2010) *Surface Free Energy Determination by Contact Angle Measurements-A Comparison of Various Approaches*.
Hill, C. A. S., Norton, A. and Newman, G. (2009) 'The water vapor sorption behavior of natural fibers', *Journal of Applied Polymer Science*, 112(3), pp. 1524–1537. doi: 10.1002/app.29725.
Ho, Y. S. and McKay, G. (1998) 'Sorption of dye from aqueous solution by peat', *Chemical Engineering Journal*, 70(2), pp. 115–124. doi: 10.1016/s0923-0467(98)00076-1.
Ho, Y. S. and Ofomaja, A. E. (2006) 'Pseudo-second-order model for lead ion sorption from aqueous solutions onto palm kernel fiber', *Journal of Hazardous Materials*, 129(1–3), pp. 137–142. doi: 10.1016/j.jhazmat.2005.08.020.
Horne, M. R. L. (2012) 'Bast fibres: hemp cultivation and production', in *Handbook of Natural Fibres*. Elsevier, pp. 114–145. doi:

10.1533/9780857095503.1.114.
Huda, M. S. *et al.* (2008) 'Effect of fiber surface-treatments on the properties of laminated biocomposites from poly(lactic acid) (PLA) and kenaf fibers', *Composites Science and Technology*, 68(2), pp. 424–432. doi: 10.1016/j.compscitech.2007.06.022.
Hull, D. and Clyne, T. W. (1996) *An Introduction to Composite Materials*, *An Introduction to Composite Materials*. Cambridge University Press. doi: 10.1017/cbo9781139170130.
Hussein-Al-Ali, S. H. *et al.* (2014) 'Antimicrobial and controlled release studies of a novel nystatin conjugated iron oxide nanocomposite', *BioMed Research International*, 2014. doi: 10.1155/2014/651831.
Idler, C. *et al.* (2011) 'Wet processing of hemp: An overview', *Journal of Natural Fibers*, 8(2), pp. 59–80. doi: 10.1080/15440478.2011.576089.
Iftekhar, S., Srivastava, V. and Sillanpää, M. (2017) 'Synthesis and application of LDH intercalated cellulose nanocomposite for separation of rare earth elements (REEs)', *Chemical Engineering Journal*, 309, pp. 130–139. doi: 10.1016/J.CEJ.2016.10.028.
Javed, S. I. and Hussain, Z. (2015) *Covalently Functionalized Graphene Oxide-Characterization and Its Electrochemical Performance*, *Int. J. Electrochem. Sci*. Available at: www.electrochemsci.org (Accessed: 28 December 2020).
Jeong, H. K. *et al.* (2009) 'Thermal stability of graphite oxide', *Chemical Physics Letters*, 470(4–6), pp. 255–258. doi: 10.1016/j.cplett.2009.01.050.
Jeppu, G. P. and Clement, T. P. (2012) 'A modified Langmuir-Freundlich isotherm model for simulating pH-dependent adsorption effects', *Journal of Contaminant Hydrology*, 129–130, pp. 46–53. doi: 10.1016/j.jconhyd.2011.12.001.
Jiang, W.-C., Meng, W.-D. and Qing, F.-L. (2005) 'Synthesis of a novel perfluorooctylated polyacrylate and its application on cotton fabrics', *Journal of Applied Polymer Science*, 98(1), pp. 222–226. doi: 10.1002/app.22067.
Jin, Y. *et al.* (2019) 'Efficient adsorption of methylene blue and lead ions in aqueous solutions by 5-sulfosalicylic acid modified lignin', *International Journal of Biological Macromolecules*, 123, pp. 50–58. doi: 10.1016/j.ijbiomac.2018.10.213.
Joseph, K., Thomas, S. and Pavithran, C. (1995) 'Effect of ageing on the physical and mechanical properties of sisal-fiber-reinforced polyethylene composites', *Composites Science and Technology*, 53(1), pp. 99–110. doi: 10.1016/0266-3538(94)00074-3.
Joshi, S. V. *et al.* (2004) 'Are natural fiber composites environmentally superior to glass fiber reinforced composites?', in *Composites Part A: Applied Science and Manufacturing*. Elsevier, pp. 371–376. doi: 10.1016/j.compositesa.2003.09.016.
Ju, J. *et al.* (2019) 'Application of essential oil as a sustained release

preparation in food packaging', *Trends in Food Science and Technology*. Elsevier Ltd, pp. 22–32. doi: 10.1016/j.tifs.2019.08.005.
Jubu, P. R. *et al.* (2020) 'Tauc-plot scale and extrapolation effect on bandgap estimation from UV–vis–NIR data – A case study of β-Ga2O3', *Journal of Solid State Chemistry*, 290, p. 121576. doi: 10.1016/J.JSSC.2020.121576.
Kabir, M. M. *et al.* (2013) 'Effects of chemical treatments on hemp fibre structure', *Applied Surface Science*, 276, pp. 13–23. doi: 10.1016/j.apsusc.2013.02.086.
Kalaleh, H.-A., Tally, M. and Atassi, Y. (no date) *Preparation of poly(sodium acrylate-co-acrylamide) superabsorbent copolymer via alkaline hydrolysis of acrylamide using microwave irradiation*.
Kale, R. D., Potdar, T. and Gorade, V. (2019) 'Treatment of C.I. reactive blue-21 effluent by microcrystalline cellulose grafted with APTES: Kinetics, isotherm and thermodynamic study', *Sustainable Environment Research*, 1(1). doi: 10.1186/s42834-019-0007-6.
Kannan, N. and Sundaram, M. M. (2001) 'Kinetics and mechanism of removal of methylene blue by adsorption on various carbons - A comparative study', *Dyes and Pigments*, 51(1), pp. 25–40. doi: 10.1016/S0143-7208(01)00056-0.
Karaca, S. *et al.* (2008) 'Adsorption of cationic dye from aqueous solutions by activated carbon', *Microporous and Mesoporous Materials*, 115(3), pp. 376–382. doi: 10.1016/j.micromeso.2008.02.008.
Kargarzadeh, H. *et al.* (2012) 'Effects of hydrolysis conditions on the morphology, crystallinity, and thermal stability of cellulose nanocrystals extracted from kenaf bast fibers', *Cellulose*, 19(3), pp. 855–866. doi: 10.1007/s10570-012-9684-6.
Kargarzadeh, H. *et al.* (2015) 'Cellulose nanocrystal: A promising toughening agent for unsaturated polyester nanocomposite', *Polymer*, 56, pp. 346–357. doi: 10.1016/j.polymer.2014.11.054.
Kavitha, D. and Namasivayam, C. (2007) 'Experimental and kinetic studies on methylene blue adsorption by coir pith carbon', *Bioresource Technology*, 98(1), pp. 14–21. doi: 10.1016/j.biortech.2005.12.008.
Keiller, B. G. *et al.* (2021) 'Elucidating the degradation reaction pathways for the hydrothermal carbonisation of hemp via biochemical compositional analysis', *Fuel*, 294, p. 120450. doi: 10.1016/J.FUEL.2021.120450.
Keith, J. M. *et al.* (2009) 'Tensile modulus modeling of carbon-filled liquid crystal polymer composites', *Polymer Composites*, 30(8), pp. 1166–1174. doi: 10.1002/pc.20673.
Keller, A. *et al.* (2001) 'Influence of the growth stage of industrial hemp on chemical and physical properties of the fibres', *Industrial Crops and Products*, 13(1), pp. 35–48. doi: 10.1016/S0926-6690(00)00051-0.
Khan, S. A., Riaz-ur-Rehman and Khan, M. A. (1995) 'Adsorption of chromium (III), chromium (VI) and silver (I) on bentonite', *Waste Management*, 15(4), pp. 271–282. doi: 10.1016/0956-053X(95)00025-U.

Khanjanzadeh, H. *et al.* (2018) 'Surface chemical functionalization of cellulose nanocrystals by 3-aminopropyltriethoxysilane', *International Journal of Biological Macromolecules*, 106, pp. 1288–1296. doi: 10.1016/j.ijbiomac.2017.08.136.
Kiran, M. D. *et al.* (2018) 'Review-Effect of Fillers on Mechanical Properties of Polymer Matrix Composites', in *Materials Today: Proceedings*. Elsevier Ltd, pp. 22421–22424. doi: 10.1016/j.matpr.2018.06.611.
Kittel, C., McEuen, P. and McEuen, P. (1996) 'Introduction to solid state physics'. Available at: https://science.sciencemag.org/content/sci/118/3065/local/back-matter.pdf (Accessed: 1 January 2022).
Klein, J. M. *et al.* (2018) 'Preparation of cashew gum-based flocculants by microwave- and ultrasound-assisted methods', *International Journal of Biological Macromolecules*, 107, pp. 1550–1558. doi: 10.1016/J.IJBIOMAC.2017.09.118.
Kong, D. and Wilson, L. D. (2020) 'Uptake of Methylene Blue from Aqueous Solution by Pectin–Chitosan Binary Composites', *Journal of Composites Science*, 4(3), p. 95. doi: 10.3390/jcs4030095.
Koohestani, B. *et al.* (2019) 'Comparison of different natural fiber treatments: a literature review', *International Journal of Environmental Science and Technology*, 16(3), pp. 629–642. doi: 10.1007/s13762-018-1890-9.
Korjenic, A. *et al.* (2011) 'Development and performance evaluation of natural thermal-insulation materials composed of renewable resources', *Energy and Buildings*, 43(9), pp. 2518–2523. doi: 10.1016/j.enbuild.2011.06.012.
Krebs, F. C. (2012) *Stability and Degradation of Organic and Polymer Solar Cells*, *Stability and Degradation of Organic and Polymer Solar Cells*. John Wiley and Sons. doi: 10.1002/9781119942436.
Kuang, Y., Zhang, X. and Zhou, S. (2020) 'Adsorption of Methylene Blue in Water onto Activated Carbon by Surfactant Modification', *Water*, 12(2), p. 587. doi: 10.3390/w12020587.
Kukle, S. *et al.* (2011) *THE EFFECT OF STEAM EXPLOSION TREATMENT ON TECHNICAL HEMP FIBRES*, *Rēzeknes Augstskola*.
Kumar, K. V., Ramamurthi, V. and Sivanesan, S. (2005) 'Modeling the mechanism involved during the sorption of methylene blue onto fly ash', *Journal of Colloid and Interface Science*, 284(1), pp. 14–21. doi: 10.1016/j.jcis.2004.09.063.
Lee, M. *et al.* (2005) 'Change of Surface Characteristic of Cotton and Polyester Fabrics Treated with Silicone Resin by Washing and Subsequent Heat Treatment', *FIBER*, 61(11), pp. 309–312. doi: 10.2115/fiber.61.309.
Leite, F. L. *et al.* (2006) 'Investigation of sisal fibers by atomic force microscopy: Morphological and adhesive characteristics', *Journal of*

Nanoscience and Nanotechnology, 6(8), pp. 2354–2361. doi: 10.1166/jnn.2006.522.
Li, H. *et al.* (2020) 'High-efficiency adsorption and regeneration of methylene blue and aniline onto activated carbon from waste edible fungus residue and its possible mechanism', *RSC Advances*, 10(24), pp. 14262–14273. doi: 10.1039/d0ra01245a.
Li, J. *et al.* (2016) 'Silanized graphene oxide reinforced organofunctional silane composite coatings for corrosion protection', *Progress in Organic Coatings*, 99, pp. 443–451. doi: 10.1016/j.porgcoat.2016.07.008.
Li, Y. and Pickering, K. L. (2008) 'Hemp fibre reinforced composites using chelator and enzyme treatments', *Composites Science and Technology*, 68(15–16), pp. 3293–3298. doi: 10.1016/j.compscitech.2008.08.022.
Li, Z. F. *et al.* (2017) 'Fire retardant and thermal degradation properties of cotton fabrics based on APTES and sodium phytate through layer-by-layer assembly', *Journal of Analytical and Applied Pyrolysis*, 123, pp. 216–223. doi: 10.1016/j.jaap.2016.11.026.
Li, Z., Xing, Y. and Dai, J. (2008) 'Superhydrophobic surfaces prepared from water glass and non-fluorinated alkylsilane on cotton substrates', *Applied Surface Science*, 254(7), pp. 2131–2135. doi: 10.1016/j.apsusc.2007.08.083.
Lima, D. S. *et al.* (2018) 'pH-responsive alginate-based hydrogels for protein delivery', *Journal of Molecular Liquids*, 262, pp. 29–36. doi: 10.1016/j.molliq.2018.04.002.
Ling, Z. *et al.* (2019) 'Effects of ball milling on the structure of cotton cellulose', *Cellulose*, 26(1), pp. 305–328. doi: 10.1007/s10570-018-02230-x.
Liu, J., Guan, Z. and Li, Z. (2018) 'Application of cryogenic and mechanical treatment in degumming of hemp stems', *Biosystems Engineering*, 174, pp. 144–152. doi: 10.1016/j.biosystemseng.2018.07.007.
Liu, L. *et al.* (2012) 'The removal of dye from aqueous solution using alginate-halloysite nanotube beads', *Chemical Engineering Journal*, 187, pp. 210–216. doi: 10.1016/j.cej.2012.01.136.
Liu, M. *et al.* (2015) 'Effect of harvest time and field retting duration on the chemical composition, morphology and mechanical properties of hemp fibers', *Industrial Crops and Products*, 69, pp. 29–39. doi: 10.1016/j.indcrop.2015.02.010.
Liu, M. *et al.* (2016) 'Effect of pectin and hemicellulose removal from hemp fibres on the mechanical properties of unidirectional hemp/epoxy composites', *Composites Part A: Applied Science and Manufacturing*, 90, pp. 724–735. doi: 10.1016/j.compositesa.2016.08.037.
Liu, M. *et al.* (2017) 'Targeted pre-treatment of hemp bast fibres for optimal performance in biocomposite materials: A review', *Industrial Crops and Products*. Elsevier B.V., pp. 660–683. doi: 10.1016/j.indcrop.2017.07.027.
Liu, X. *et al.* (2014) 'Effects of inorganic fillers on the thermal and mechanical properties of poly(lactic acid)', *International Journal of Polymer*

Science, 2014. doi: 10.1155/2014/827028.
Liu, X. *et al.* (2020) 'Flame retardant cellulosic fabrics via layer-by-layer self-assembly double coating with egg white protein and phytic acid', *Journal of Cleaner Production*, 243, p. 118641. doi: 10.1016/j.jclepro.2019.118641.
Look, D. C. and Leach, J. H. (no date) 'On the accurate determination of absorption coefficient from reflectance and transmittance measurements: application to Fe-doped GaN'.
Loos, M. (2015) 'Fundamentals of Polymer Matrix Composites Containing CNTs', in *Carbon Nanotube Reinforced Composites: CNR Polymer Science and Technology*. Elsevier Inc., pp. 125–170. doi: 10.1016/B978-1-4557-3195-4.00005-9.
Lorenc-Grabowska, E. and Gryglewicz, G. (2007) 'Adsorption characteristics of Congo Red on coal-based mesoporous activated carbon', *Dyes and Pigments*, 74(1), pp. 34–40. doi: 10.1016/j.dyepig.2006.01.027.
Loryuenyong, V. *et al.* (2013) 'Preparation and characterization of reduced graphene oxide sheets via water-based exfoliation and reduction methods', *Advances in Materials Science and Engineering*, 2013. doi: 10.1155/2013/923403.
Lu, Y. and Pignatello, J. J. (2002) 'Demonstration of the "conditioning effect" in soil organic matter in support of a pore deformation mechanism for sorption hysteresis', *Environmental Science and Technology*, 36(21), pp. 4553–4561. doi: 10.1021/es020554x.
Lundberg, J. L. (1972) 'Molecular Clustering And Segregation In Sorption Systems', *Pure and Applied Chemistry*, 31(1–2), pp. 261–282. doi: 10.1351/pac197231010261.
Lundberg, J L (1972) *MOLECULAR CLUSTERING AND SEGREGATION IN SORPTION SYSTEMS*.
Luo, J., Fang, Z. and Smith, R. L. (2014) 'Ultrasound-enhanced conversion of biomass to biofuels', *Progress in Energy and Combustion Science*, 41(1), pp. 56–93. doi: 10.1016/J.PECS.2013.11.001.
Mahamadi, C. and Mawere, E. (2014) 'High adsorption of dyes by water hyacinth fixed on alginate', *Environmental Chemistry Letters*, 12(2), pp. 313–320. doi: 10.1007/s10311-013-0445-z.
Mahmood, F. *et al.* (2011) 'Thermodynamics of adsorption of Rhodamine-B and nile blue sulfate on alumina from aqueous-solutions', *Journal of The Chemical Society of Pakistan*, 16(4), p. 83. Available at: https://jcsp.org.pk/home.aspx (Accessed: 6 January 2021).
Majzoobi, M. *et al.* (2015) 'Physical properties of biodegradable films from heat-moisture-treated rice flour and rice starch', *Starch/Staerke*, 67(11–12), pp. 1053–1060. doi: 10.1002/star.201500102.
Makuła, P., Pacia, M. and Macyk, W. (2018) 'How To Correctly Determine the Band Gap Energy of Modified Semiconductor Photocatalysts Based on UV-Vis Spectra', *Journal of Physical Chemistry Letters*, 9(23), pp. 6814–

6817. doi: 10.1021/ACS.JPCLETT.8B02892/SUPPL_FILE/JZ8B02892_LIVESLIDES.MP4.
Maleki, S. and Karimi-Jashni, A. (2020) 'Optimization of Ni(II) adsorption onto Cloisite Na+ clay using response surface methodology', *Chemosphere*, 246, p. 125710. doi: 10.1016/j.chemosphere.2019.125710.
Martínez-Ruvalcaba, A. *et al.* (2009) 'Polyacrylamide-gelatin polymeric networks: Effect of pH and gelatin concentration on the swelling kinetics and mechanical properties', *Polymer Bulletin*, 62(4), pp. 539–548. doi: 10.1007/s00289-008-0037-4.
Mashkoor, F., Nasar, A. and Inamuddin (2020) 'Carbon nanotube-based adsorbents for the removal of dyes from waters: A review', *Environmental Chemistry Letters*. Springer, pp. 605–629. doi: 10.1007/s10311-020-00970-6.
Maurya, N. S. *et al.* (2006) 'Biosorption of dyes using dead macro fungi: Effect of dye structure, ionic strength and pH', *Bioresource Technology*, 97(3), pp. 512–521. doi: 10.1016/J.BIORTECH.2005.02.045.
Maziarz, P. *et al.* (2019) 'Highly effective magnet-responsive LDH-Fe oxide composite adsorbents for As(V) removal', *Chemical Engineering Journal*, 362, pp. 207–216. doi: 10.1016/J.CEJ.2019.01.017.
Mfarrej, M. F. B. and Rara, F. M. (2019) 'Competitive, Sustainable Natural Pesticides', *Acta Ecologica Sinica*, 39(2), pp. 145–151. doi: 10.1016/j.chnaes.2018.08.005.
Milewski, J. V. and Katz, H. S. (1987) *Handbook of reinforcements for plastics*. Van Nostrand Reinhold Co.
Mittal, A. K. and Gupta, S. K. (1996) 'Biosorption of cationic dyes by dead macro fungus Fomitopsis carnea: Batch studies', in *Water Science and Technology*. Elsevier Science Inc., pp. 81–87. doi: 10.1016/S0273-1223(96)00700-7.
Moawia, R. M. *et al.* (2016) 'Modification of flax fibres by radiation induced emulsion graft copolymerization of glycidyl methacrylate', *Radiation Physics and Chemistry*, 122, pp. 35–42. doi: 10.1016/j.radphyschem.2016.01.008.
Modesti, M. *et al.* (2004) 'Mathematical model and experimental validation of water cluster influence upon vapour permeation through hydrophilic dense membrane', *Journal of Membrane Science*, 229(1–2), pp. 211–223. doi: 10.1016/j.memsci.2003.10.030.
Mohammad, N. and Atassi, Y. (2020) 'Adsorption of methylene blue onto electrospun nanofibrous membranes of polylactic acid and polyacrylonitrile coated with chloride doped polyaniline', *Scientific Reports*, 10(1). doi: 10.1038/s41598-020-69825-y.
Mohammadi Nafchi, A. *et al.* (2014) 'Effects of nanorod-rich ZnO on rheological, sorption isotherm, and physicochemical properties of bovine gelatin films', *LWT - Food Science and Technology*, 58(1), pp. 142–149.

doi: 10.1016/j.lwt.2014.03.007.
Moonart, U. and Utara, S. (2019) ‘Effect of surface treatments and filler loading on the properties of hemp fiber/natural rubber composites’, *Cellulose*, 26(12), pp. 7271–7295. doi: 10.1007/s10570-019-02611-w.
Moosakazemi, F. *et al.* (2017) ‘Effect of design and operational parameters on particle morphology in ball mills’, *International Journal of Mineral Processing*, 165, pp. 41–49. doi: 10.1016/j.minpro.2017.06.001.
Muhammad, F. F. and Sulaiman, K. (2011) ‘Utilizing a simple and reliable method to investigate the optical functions of small molecular organic films – Alq3 and Gaq3 as examples’, *Measurement*, 44(8), pp. 1468–1474. doi: 10.1016/J.MEASUREMENT.2011.05.017.
Musella, E. *et al.* (2021) ‘Electrosynthesis of Ni/Al layered double hydroxide and reduced graphene oxide composites for the development of hybrid capacitors’, *Electrochimica Acta*, 365, p. 137294. doi: 10.1016/J.ELECTACTA.2020.137294.
Musio, S., Müssig, J. and Amaducci, S. (2018) ‘Optimizing hemp fiber production for high performance composite applications’, *Frontiers in Plant Science*, 871. doi: 10.3389/fpls.2018.01702.
Mwaikambo, L. Y. and Ansell, M. P. (2002) ‘Chemical modification of hemp, sisal, jute, and kapok fibers by alkalization’, *Journal of Applied Polymer Science*, 84(12), pp. 2222–2234. doi: 10.1002/app.10460.
Nelson, M. L. and O’Connor, R. T. (1964) ‘Relation of certain infrared bands to cellulose crystallinity and crystal lattice type. Part II. A new infrared ratio for estimation of crystallinity in celluloses I and II’, *Journal of Applied Polymer Science*, 8(3), pp. 1325–1341. doi: 10.1002/app.1964.070080323.
Nethaji, S. and Sivasamy, A. (2011) ‘Adsorptive removal of an acid dye by lignocellulosic waste biomass activated carbon: Equilibrium and kinetic studies’, *Chemosphere*, 82(10), pp. 1367–1372. doi: 10.1016/j.chemosphere.2010.11.080.
Nguyen, T. T. *et al.* (2009) ‘Influence of compactness and hemp hurd characteristics on the mechanical properties of lime and hemp concrete’, *European Journal of Environmental and Civil Engineering*, 13(9), pp. 1039–1050. doi: 10.1080/19648189.2009.9693171.
Ni, X. *et al.* (2015) ‘Jute/polypropylene composites: Effect of enzymatic modification on thermo-mechanical and dynamic mechanical properties’, *Fibers and Polymers*, 16(10), pp. 2276–2283. doi: 10.1007/s12221-015-5475-7.
Nie, K. *et al.* (2020) ‘A Facile Degumming Method of Kenaf Fibers Using Deep Eutectic Solution’, *Journal of Natural Fibers*. doi: 10.1080/15440478.2020.1795778.
Nielsen, L. E. (1970) ‘Generalized equation for the elastic moduli of composite materials’, *Journal of Applied Physics*, 41(11), pp. 4626–4627. doi: 10.1063/1.1658506.

Nielsen, L. E. (1974) 'The Thermal and Electrical Conductivity of Two-Phase Systems', *Industrial and Engineering Chemistry Fundamentals*, 13(1), pp. 17–20. doi: 10.1021/i160049a004.
Nishimura, H., Okano, T. and Sarko, A. (1991) 'Mercerization of cellulose. 5. Crystal and molecular structure of Na-cellulose I', *Macromolecules*, 24(3), pp. 759–770. doi: 10.1021/ma00003a020.
Nokhodchi, A. and Tailor, A. (2004) 'In situ cross-linking of sodium alginate with calcium and aluminum ions to sustain the release of theophylline from polymeric matrices', *Farmaco*, 59(12), pp. 999–1004. doi: 10.1016/j.farmac.2004.08.006.
Nouraddini, M., Esmaiili, M. and Mohtarami, F. (2018) 'Development and characterization of edible films based on eggplant flour and corn starch', *International Journal of Biological Macromolecules*, 120, pp. 1639–1645. doi: 10.1016/j.ijbiomac.2018.09.126.
Nykter, M. *et al.* (2008) 'Effects of thermal and enzymatic treatments and harvesting time on the microbial quality and chemical composition of fibre hemp (Cannabis sativa L.)', *Biomass and Bioenergy*, 32(5), pp. 392–399. doi: 10.1016/j.biombioe.2007.10.015.
Obi Reddy, K. *et al.* (2012) 'Mechanical and physical characterization of sodium hydroxide treated Borassus fruit fibers', *Journal of Forestry Research*, 23(4), pp. 667–674. doi: 10.1007/s11676-012-0308-7.
Okubayashi, S., Griesser, U. J. and Bechtold, T. (2005) 'Water accessibilities of man-made cellulosic fibers-effects of fiber characteristics'. doi: 10.1007/s10570-005-2179-y.
Oladipo, A. A. and Ifebajo, A. O. (2018) 'Highly efficient magnetic chicken bone biochar for removal of tetracycline and fluorescent dye from wastewater: Two-stage adsorber analysis', *Journal of Environmental Management*, 209, pp. 9–16. doi: 10.1016/j.jenvman.2017.12.030.
Oliveira, G. F. *et al.* (2010) 'Chitosan-pectin multiparticulate systems associated with enteric polymers for colonic drug delivery', *Carbohydrate Polymers*, 82(3), pp. 1004–1009. doi: 10.1016/j.carbpol.2010.06.041.
Omidian, H. *et al.* (1998) 'A model for the swelling of superabsorbent polymers', *Polymer*, 39(26), pp. 6697–6704. doi: 10.1016/S0032-3861(98)00095-0.
Ouajai, S. and Shanks, R. A. (2005) 'Composition, structure and thermal degradation of hemp cellulose after chemical treatments', *Polymer Degradation and Stability*, 89(2), pp. 327–335. doi: 10.1016/j.polymdegradstab.2005.01.016.
Oudiani, A. El *et al.* (2011) 'Crystal transition from cellulose I to cellulose II in NaOH treated Agave americana L. fibre', *Carbohydrate Polymers*, 86(3), pp. 1221–1229. doi: 10.1016/j.carbpol.2011.06.037.
Özmen, N. (2012) *Vinyl acetylation of hemp fibers*, *BioResources*.
Parida, K. M., Sahoo, M. and Singha, S. (2010) 'Synthesis and characterization of a Fe(III)-Schiff base complex in a Zn-Al LDH host for

cyclohexane oxidation', *Journal of Molecular Catalysis A: Chemical*, 329(1–2), pp. 7–12. doi: 10.1016/J.MOLCATA.2010.06.010.
Pattarasiriroj, K., Kaewprachu, P. and Rawdkuen, S. (2020) 'Properties of rice flour-gelatine-nanoclay film with catechin-lysozyme and its use for pork belly wrapping', *Food Hydrocolloids*, 107, pp. 105951–105960. doi: 10.1016/j.foodhyd.2020.105951.
Pavan, P. C., De A. Gomes, G. and Valim, J. B. (1998) 'Adsorption of sodium dodecyl sulfate on layered double hydroxides', *Microporous and Mesoporous Materials*, 21(4–6), pp. 659–665. doi: 10.1016/S1387-1811(98)00054-7.
Pea, M. J., Vergara, C. E. and Carpita, N. C. (2008) 'The Structures and Architectures of Plant Cell Walls Define Dietary Fibre Composition and the Textures of Foods', in *Advanced Dietary Fibre Technology*. Blackwell Science Ltd, pp. 42–60. doi: 10.1002/9780470999615.ch5.
Peppas, N. A. and Sahlin, J. J. (1989) 'A simple equation for the description of solute release. III. Coupling of diffusion and relaxation', *International Journal of Pharmaceutics*, 57(2), pp. 169–172. doi: 10.1016/0378-5173(89)90306-2.
Perel, J. (1990) 'An X-ray study of regain-dependent deformations in cotton crystallites', *Journal of the Textile Institute*, 81(3), pp. 241–244. doi: 10.1080/00405009008658707.
Pérez-Mateos, M., Montero, P. and Gómez-Guillén, M. C. (2009) 'Formulation and stability of biodegradable films made from cod gelatin and sunflower oil blends', *Food Hydrocolloids*, 23(1), pp. 53–61. doi: 10.1016/j.foodhyd.2007.11.011.
Pietak, A. *et al.* (2007) 'Atomic force microscopy characterization of the surface wettability of natural fibres', *Applied Surface Science*, 253(7), pp. 3627–3635. doi: 10.1016/j.apsusc.2006.07.082.
Pinto, M. R. O. *et al.* (2007) 'International Journal of Polymeric Materials Water Sorption of a Polyurethane/Bentonite Composite: Effects of Bentonite Content and Drying Conditions'. doi: 10.1080/00914030601123351.
Piras, C. C., Fernández-Prieto, S. and De Borggraeve, W. M. (2019) 'Ball milling: A green technology for the preparation and functionalisation of nanocellulose derivatives', *Nanoscale Advances*. Royal Society of Chemistry, pp. 937–947. doi: 10.1039/c8na00238j.
Pourjavadi, A. and Reza MAHDAVINIA, G. (no date) *Superabsorbency, pH-Sensitivity and Swelling Kinetics of Partially Hydrolyzed Chitosan-g-poly(Acrylamide) Hydrogels*.
Prabu, S. *et al.* (2014) 'Synthesis, crystal growth, studies on vibrational spectroscopy and nonlinear optical properties of 4-methoxy-4′-chlorochalcone', *Materials Research Bulletin*, 50, pp. 446–453. doi: 10.1016/J.MATERRESBULL.2013.11.003.
Prakash Maran, J. *et al.* (2013) 'Response surface modeling and analysis of barrier and optical properties of maize starch edible films', *International*

Journal of Biological Macromolecules, 60, pp. 412–421. doi: 10.1016/j.ijbiomac.2013.06.029.
Priyadarshi, R., Kim, S. M. and Rhim, J. W. (2021) 'Pectin/pullulan blend films for food packaging: Effect of blending ratio', *Food Chemistry*, 347, p. 129022. doi: 10.1016/j.foodchem.2021.129022.
Pukánszky, B. *et al.* (1989) 'The possible mechanisms of polymer-filler interaction in polypropylene-CaCO3 composites', *Journal of Materials Science Letters*, 8(9), pp. 1040–1042. doi: 10.1007/BF01730480.
Rachini, A. *et al.* (2009) 'Comparison of the thermal degradation of natural, alkali-treated and silane-treated hemp fibers under air and an inert atmosphere', *Journal of Applied Polymer Science*, 112(1), pp. 226–234. doi: 10.1002/app.29412.
Rafatullah, M. *et al.* (2010) 'Adsorption of methylene blue on low-cost adsorbents: A review', *Journal of Hazardous Materials*. Elsevier, pp. 70–80. doi: 10.1016/j.jhazmat.2009.12.047.
Rahman, S. (2008) 'Food properties handbook', *Agricultural and Food Engineering Technologies Service*, pp. 1–34. doi: 10.1201/9781420003093.
Rajaei, M. *et al.* (2019) 'A comparative study on effects of natural and synthesised nano-clays on the fire and mechanical properties of epoxy composites', *Composites Part B: Engineering*, 165, pp. 65–74. doi: 10.1016/j.compositesb.2018.11.089.
Raji, M. *et al.* (2016) 'Nanoclay Modification and Functionalization for Nanocomposites Development: Effect on the Structural, Morphological, Mechanical and Rheological Properties', in. Springer, Singapore, pp. 1–34. doi: 10.1007/978-981-10-1953-1_1.
Ramadan, A. R., Esawi, A. M. K. and Gawad, A. A. (2010) 'Effect of ball milling on the structure of Na+-montmorillonite and organo-montmorillonite (Cloisite 30B)', *Applied Clay Science*, 47(3–4), pp. 196–202. doi: 10.1016/j.clay.2009.10.002.
Rani, S. *et al.* (2017) 'Polymeric Nanoparticles in Targeting and Delivery of Drugs', in *Nanotechnology-Based Approaches for Targeting and Delivery of Drugs and Genes*. Elsevier Inc., pp. 223–255. doi: 10.1016/B978-0-12-809717-5.00008-7.
Rathinam, K. *et al.* (2017) 'Polyimide derived laser-induced graphene as adsorbent for cationic and anionic dyes', *Carbon*, 124, pp. 515–524. doi: 10.1016/j.carbon.2017.08.079.
Ray, D. and Sarkar, B. K. (2001) 'Characterization of alkali-treated jute fibers for physical and mechanical properties', *Journal of Applied Polymer Science*, 80(7), pp. 1013–1020. doi: 10.1002/app.1184.
Reddy, S. S., Bhaduri, S. K. and Sen, S. K. (1990) 'Infrared spectra of alkali treated jute stick', *Journal of Applied Polymer Science*, 41(12), pp. 329–336. doi: 10.1002/app.1990.070410125.
Renita, A. A. *et al.* (2021) 'Effective removal of malachite green dye from aqueous solution in hybrid system utilizing agricultural waste as particle

electrodes', *Chemosphere*, 273, p. 129634. doi: 10.1016/j.chemosphere.2021.129634.
Robles, E. *et al.* (2015) 'Surface-modified nano-cellulose as reinforcement in poly(lactic acid) to conform new composites', *Industrial Crops and Products*, 71, pp. 44–53. doi: 10.1016/j.indcrop.2015.03.075.
Romero-Bastida, C. A. *et al.* (2005) 'Physicochemical and microstructural characterization of films prepared by thermal and cold gelatinization from non-conventional sources of starches', *Carbohydrate Polymers*, 60(2), pp. 235–244. doi: 10.1016/j.carbpol.2005.01.004.
Rosace, G. *et al.* (2018) 'Thermal and flame retardant behaviour of cotton fabrics treated with a novel nitrogen-containing carboxyl-functionalized organophosphorus system', *Carbohydrate Polymers*, 196, pp. 348–358. doi: 10.1016/j.carbpol.2018.05.012.
Rouison, D. *et al.* (2005) 'Water absorption of hemp fiber/unsaturated polyester composites', *Polymer Composites*, 26(4), pp. 509–525. doi: 10.1002/pc.20114.
Roy, A. *et al.* (2014) 'Controlled pesticide release from biodegradable polymers', *Central European Journal of Chemistry*. De Gruyter, pp. 453–469. doi: 10.2478/s11532-013-0405-2.
Roy, A., Bajpai, A. K. and Bajpai, J. (2009) 'Designing Swellable Beads of Alginate and Gelatin for Controlled Release of Pesticide (Cypermethrin)', *Journal of Macromolecular Science, Part A*, 46(9), pp. 847–859. doi: 10.1080/10601320903077976.
Roy, A., Bajpai, A K and Bajpai, J. (2009) 'Journal of Macromolecular Science®, Part A: Pure and Applied Chemistry Designing Swellable Beads of Alginate and Gelatin for Controlled Release of Pesticide (Cypermethrin) Designing Swellable Beads of Alginate and Gelatin for Controlled Release of Pesticide (Cypermethrin)'. doi: 10.1080/10601320903077976.
Roy, A., Bajpai, J. and Bajpai, A. K. (2009) *Development of calcium alginate-gelatin based microspheres for controlled release of endosulfan as a model pesticide*, *Indian Journal of Chemical Technology*.
Roy, D., Wang, G. te and Adrian, D. D. (1993) 'A simplified solution technique for carbon adsorption model', *Water Research*, 27(6), pp. 1033–1040. doi: 10.1016/0043-1354(93)90067-R.
Rozra, J. *et al.* (2012) 'Cu nanoparticles induced structural, optical and electrical modification in PVA', *Materials Chemistry and Physics*, 134(2–3), pp. 1121–1126. doi: 10.1016/J.MATCHEMPHYS.2012.04.004.
Saad, I. Ben *et al.* (2019) 'Optical, UV-Vis spectroscopy studies, electrical and dielectric properties of transition metal-based of the novel organic-inorganic hybrid (C 6 H 10 N 2)(Hg 2 Cl 5) 2 .3H 2 O'. doi: 10.1142/S2010135X19500401.
Saber-Samandari, Samaneh *et al.* (2017) 'Adsorption of anionic and cationic dyes from aqueous solution using gelatin-based magnetic nanocomposite beads comprising carboxylic acid functionalized carbon nanotube',

Chemical Engineering Journal, 308, pp. 1133–1144. doi: 10.1016/j.cej.2016.10.017.
Saber-Samandari, Samaneh, Saber-Samandari, Saeed and Gazi, M. (2013) 'Cellulose-graft-polyacrylamide/hydroxyapatite composite hydrogel with possible application in removal of Cu (II) ions', *Reactive and Functional Polymers*, 73(11), pp. 1523–1530. doi: 10.1016/j.reactfunctpolym.2013.07.007.
Saberi, B. *et al.* (2015) 'Water Sorption Isotherm of Pea Starch Edible Films and Prediction Models', *Foods*, 5(4), p. 1. doi: 10.3390/foods5010001.
Salentijn, E. M. J. *et al.* (2015) 'New developments in fiber hemp (Cannabis sativa L.) breeding', *Industrial Crops and Products*, 68, pp. 32–41. doi: 10.1016/j.indcrop.2014.08.011.
Sánchez-Jiménez, P. E. *et al.* (2009) 'Combined kinetic analysis of thermal degradation of polymeric materials under any thermal pathway', *Polymer Degradation and Stability*, 94(11), pp. 2079–2085. doi: 10.1016/j.polymdegradstab.2009.07.006.
Sangawar, V. S. *et al.* (2007) 'Structural characterization and thermally stimulated discharge conductivity (TSDC) study in polymer thin films', *Bulletin of Materials Science*, 30(2), pp. 163–166. doi: 10.1007/S12034-007-0029-2.
Sanghi, R. and Bhattacharya, B. (2002) 'Review on decolorisation of aqueous dye solutions by low cost adsorbents', *Coloration Technology*, 118(5), pp. 256–269. doi: 10.1111/j.1478-4408.2002.tb00109.x.
Sangiorgi, N. *et al.* (2017) 'Spectrophotometric method for optical band gap and electronic transitions determination of semiconductor materials', *Optical Materials*, 64, pp. 18–25. doi: 10.1016/J.OPTMAT.2016.11.014.
Sanjay, M. R. *et al.* (2018) 'Characterization and properties of natural fiber polymer composites: A comprehensive review', *Journal of Cleaner Production*. Elsevier Ltd, pp. 566–581. doi: 10.1016/j.jclepro.2017.10.101.
Sanjay, M. R. *et al.* (2019) 'A comprehensive review of techniques for natural fibers as reinforcement in composites: Preparation, processing and characterization', *Carbohydrate Polymers*. Elsevier Ltd, pp. 108–121. doi: 10.1016/j.carbpol.2018.11.083.
Sassoni, E. *et al.* (2014) 'Novel sustainable hemp-based composites for application in the building industry: Physical, thermal and mechanical characterization', *Energy and Buildings*, 77, pp. 219–226. doi: 10.1016/j.enbuild.2014.03.033.
Sawpan, M. A., Pickering, K. L. and Fernyhough, A. (2011a) 'Effect of various chemical treatments on the fibre structure and tensile properties of industrial hemp fibres', *Composites Part A: Applied Science and Manufacturing*, 42(8), pp. 888–895. doi: 10.1016/j.compositesa.2011.03.008.
Sawpan, M. A., Pickering, K. L. and Fernyhough, A. (2011b) 'Effect of various chemical treatments on the fibre structure and tensile properties of

industrial hemp fibres', *Composites Part A: Applied Science and Manufacturing*, 42(8), pp. 888–895. doi: 10.1016/j.compositesa.2011.03.008.
Schettini, E. *et al.* (2013) 'Recycled wastes of tomato and hemp fibres for biodegradable pots: Physico-chemical characterization and field performance', *Resources, Conservation and Recycling*, 70, pp. 9–19. doi: 10.1016/j.resconrec.2012.11.002.
Schöpf, H. and Supancic, P. (2014) 'On Bürmann's Theorem and Its Application to Problems of Linear and Nonlinear Heat Transfer and Diffusion', *The Mathematica Journal*, 16. doi: 10.3888/tmj.16-11.
Segal, L. *et al.* (1959) 'An Empirical Method for Estimating the Degree of Crystallinity of Native Cellulose Using the X-Ray Diffractometer', *Textile Research Journal*, 29(10), pp. 786–794. doi: 10.1177/004051755902901003.
Serodre, T. *et al.* (2019) 'Surface silanization of graphene oxide under mild reaction conditions', *Journal of the Brazilian Chemical Society*, 30(11), pp. 2488–2499. doi: 10.21577/0103-5053.20190167.
Shaban, M. *et al.* (2018) 'Novel bentonite/zeolite-NaP composite efficiently removes methylene blue and Congo red dyes', *Environmental Chemistry Letters*, 16(1), pp. 275–280. doi: 10.1007/s10311-017-0658-7.
Shagholani, H., Ghoreishi, S. M. and Mousazadeh, M. (2015) 'Improvement of interaction between PVA and chitosan via magnetite nanoparticles for drug delivery application', *International Journal of Biological Macromolecules*, 78, pp. 130–136. doi: 10.1016/J.IJBIOMAC.2015.02.042.
Shahria, S. (2019) 'Fabrication and Property Evaluation of Hemp–flax Fiber Reinforced Hybrid Composite', *Chemical and Materials Engineering*, 7(2), pp. 17–23. doi: 10.13189/CME.2019.070202.
Shaiful Sajab, M. *et al.* (2011) 'Citric acid modified kenaf core fibres for removal of methylene blue from aqueous solution'. doi: 10.1016/j.biortech.2011.05.011.
Shankar, S. and Rhim, J. W. (2018) 'Antimicrobial wrapping paper coated with a ternary blend of carbohydrates (alginate, carboxymethyl cellulose, carrageenan) and grapefruit seed extract', *Carbohydrate Polymers*, 196, pp. 92–101. doi: 10.1016/j.carbpol.2018.04.128.
Shinoj, S., Panigrahi, S. and Visvanathan, R. (2010) 'Water absorption pattern and dimensional stability of oil palm fiber-linear low density polyethylene composites', *Journal of Applied Polymer Science*, 117(2), pp. 1064–1075. doi: 10.1002/app.31765.
Sideridis, E. *et al.* (2009) 'The effect of low-filler volume fraction on the elastic modulus and thermal expansion coefficient of particulate composites simulated by a multiphase model', *Journal of Applied Polymer Science*, 111(1), pp. 203–216. doi: 10.1002/app.28886.
da Silva Fernandes, R. *et al.* (2019) 'Development of alginate/starch-based hydrogels crosslinked with different ions: Hydrophilic, kinetic and spectroscopic properties', *Materials Today Communications*, 21, p. 100636.

doi: 10.1016/j.mtcomm.2019.100636.
Silva, V. *et al.* (2019) 'Pesticide residues in European agricultural soils – A hidden reality unfolded', *Science of the Total Environment*, 653, pp. 1532–1545. doi: 10.1016/j.scitotenv.2018.10.441.
Singh, R., Sinha, M. K. and Purkait, M. K. (2020) 'Stimuli responsive mixed matrix polysulfone ultrafiltration membrane for humic acid and photocatalytic dye removal applications', *Separation and Purification Technology*, 250, p. 117247. doi: 10.1016/j.seppur.2020.117247.
Singh, T. *et al.* (2019) 'Agriculture waste reinforced corn starch-based biocomposites: Effect of rice husk/walnut shell on physicomechanical, biodegradable and thermal properties', *Materials Research Express*, 6(4), p. 045702. doi: 10.1088/2053-1591/aafe45.
Singha, A. S. and Rana, R. K. (2010) 'Graft copolymerization of methyl methacrylate (MMA) onto agave americana fibers and evaluation of their physicochemical properties', *International Journal of Polymer Analysis and Characterization*, 15(1), pp. 27–42. doi: 10.1080/10236660903299283.
Sips, R. (1948) 'On the Structure of a Catalyst Surface', *Physical Adsorption on Non-Uniform Surfaces The Journal of Chemical Physics*, 16(5), p. 931. doi: 10.1063/1.1746922.
Smith, T. L. (1959) 'Volume Changes and Dewetting in Glass Bead-Polyvinyl Chloride Elastomeric Composites Under Large Deformations', *Transactions of the Society of Rheology*, 3(1), pp. 113–136. doi: 10.1122/1.548847.
Sobhana, S. S. L. *et al.* (2017) 'Layered double hydroxide interfaced stearic acid – Cellulose fibres: A new class of super-hydrophobic hybrid materials', *Colloids and Surfaces A: Physicochemical and Engineering Aspects*, 522, pp. 416–424. doi: 10.1016/j.colsurfa.2017.03.025.
Sobhanadhas, L. S. *et al.* (2019) 'Layered Double Hydroxide-Cellulose Hybrid Beads: ANovel Catalyst for Topochemical Grafting of Pulp Fibers', *ACS Omega*, 4(1), p. 320. doi: 10.1021/ACSOMEGA.8B03061.
Song, Y. *et al.* (2013a) 'Mechanical Properties of Poly (Lactic Acid)/Hemp Fiber Composites Prepared with a Novel Method', *Journal of Polymers and the Environment*, 21(4), pp. 1117–1127. doi: 10.1007/s10924-013-0569-z.
Song, Y. *et al.* (2013b) 'Mechanical Properties of Poly (Lactic Acid)/Hemp Fiber Composites Prepared with a Novel Method', *Journal of Polymers and the Environment*, 21(4), pp. 1117–1127. doi: 10.1007/s10924-013-0569-z.
Sonnier, R. *et al.* (2018) 'Flame Retardancy of Natural Fibers Reinforced Composites', in. Springer, Cham, pp. 73–98. doi: 10.1007/978-3-319-67083-6_3.
Soo, P. Y. and Sarbon, N. M. (2018) 'Preparation and characterization of edible chicken skin gelatin film incorporated with rice flour', *Food Packaging and Shelf Life*, 15, pp. 1–8. doi: 10.1016/j.fpsl.2017.12.009.
Sreekala, M. S. *et al.* (2000) 'Oil palm fibre reinforced phenol formaldehyde composites: influence of fibre surface modifications on the mechanical

performance', *Applied Composite Materials*, 7(5–6), pp. 295–329. doi: 10.1023/A:1026534006291.
Stannett, V. *et al.* (1980) 'Sorption and transport of water vapor in glassy poly(acrylonitrile)', *Polymer Engineering and Science*, 20(4), pp. 300–304. doi: 10.1002/pen.760200414.
Stevulova, N. *et al.* (2014) 'Properties Characterization of Chemically Modified Hemp Hurds', *Materials 2014, Vol. 7, Pages 8131-8150*, 7(12), pp. 8131–8150. doi: 10.3390/MA7128131.
Stoica, I. *et al.* (2015) 'Establishing proper scanning conditions in atomic force microscopy on polyimide and polyurethane samples and their effect on 3D surface texture parameters', *Scanning*, 37(5), pp. 335–349. doi: 10.1002/sca.21216.
Sullins, T. *et al.* (2017) 'Hemp fiber reinforced polypropylene composites: The effects of material treatments', *Composites Part B: Engineering*, 114, pp. 15–22. doi: 10.1016/j.compositesb.2017.02.001.
Sun, Y. M. *et al.* (1997) 'Sorption and diffusion of organic vapors in poly[bis(trifluoroethoxy)phosphazene] and poly [bis(phenoxy)phosphazene] membranes', *Journal of Membrane Science*, 134(1), pp. 117–126. doi: 10.1016/S0376-7388(97)00126-9.
Suriyatem, R., Auras, R. A. and Rachtanapun, P. (2018) 'Improvement of mechanical properties and thermal stability of biodegradable rice starch–based films blended with carboxymethyl chitosan', *Industrial Crops and Products*, 122, pp. 37–48. doi: 10.1016/j.indcrop.2018.05.047.
Szabó, T., Berkesi, O. and Dékány, I. (2005) 'DRIFT study of deuterium-exchanged graphite oxide', *Carbon*, 43(15), pp. 3186–3189. doi: 10.1016/j.carbon.2005.07.013.
Tahir, P. M. *et al.* (2011) *Review of bast fiber retting*, *BioResources*.
Tan, Y. M. *et al.* (2015) 'Functional chitosan-based grapefruit seed extract composite films for applications in food packaging technology', *Materials Research Bulletin*, 69, pp. 142–146. doi: 10.1016/j.materresbull.2014.11.041.
Tauc, J., Grigorovici, R. and Vancu, A. (1966) 'Optical Properties and Electronic Structure of Amorphous Germanium', *physica status solidi (b)*, 15(2), pp. 627–637. doi: 10.1002/PSSB.19660150224.
Terpáková, E. *et al.* (2012) 'Chemical modification of hemp shives and their characterization', in *Procedia Engineering*. Elsevier Ltd, pp. 931–941. doi: 10.1016/j.proeng.2012.07.486.
Thakur, M. K., Rana, A. and Thakur, V. K. (2015) 'Chemical functionalization of cellulosic fibers for green polymer composites applications', in *Biomass and Bioenergy: Applications*. Springer International Publishing, pp. 233–250. doi: 10.1007/978-3-319-07578-5_12.
Thakur, S. and Arotiba, O. A. (2018) 'Synthesis, swelling and adsorption studies of a pH-responsive sodium alginate–poly(acrylic acid) superabsorbent hydrogel', *Polymer Bulletin*, 75(10), pp. 4587–4606. doi:

10.1007/s00289-018-2287-0.
Thomason, J. L. and Rudeiros-Fernández, J. L. (2021) 'Thermal degradation behaviour of natural fibres at thermoplastic composite processing temperatures', *Polymer Degradation and Stability*, p. 109594. doi: 10.1016/j.polymdegradstab.2021.109594.
Thong, Z. *et al.* (2018) 'Fabrication of loose outer-selective nanofiltration (NF) polyethersulfone (PES) hollow fibers via single-step spinning process for dye removal', *Separation and Purification Technology*, 192, pp. 483–490. doi: 10.1016/j.seppur.2017.10.031.
Timmermann, E. O. (2003) 'Multilayer sorption parameters: BET or GAB values?', *Colloids and Surfaces A: Physicochemical and Engineering Aspects*, 220(1–3), pp. 235–260. doi: 10.1016/S0927-7757(03)00059-1.
Tran, L. Q. N. *et al.* (2011) 'Wetting analysis and surface characterisation of coir fibres used as reinforcement for composites', *Colloids and Surfaces A: Physicochemical and Engineering Aspects*, 377(1–3), pp. 251–260. doi: 10.1016/j.colsurfa.2011.01.023.
Tran, P., Graiver, D. and Narayan, R. (2006) 'Biocomposites synthesized from chemically modified soy oil and biofibers', *Journal of Applied Polymer Science*, 102(1), pp. 69–75. doi: 10.1002/app.22265.
Le Troëdec, M. *et al.* (2009) 'Influence of various chemical treatments on the interactions between hemp fibres and a lime matrix', *Journal of the European Ceramic Society*, 29(10), pp. 1861–1868. doi: 10.1016/j.jeurceramsoc.2008.11.016.
Tserki, V., Panayiotou, C. and Zafeiropoulos, N. E. (2005) 'A study of the effect of acetylation and propionylation on the interface of natural fibre biodegradable composites', *Advanced Composites Letters*, 14(2), pp. 65–71. doi: 10.1177/096369350501400202.
Tünay, O. *et al.* (1996) 'Color removal from textile wastewaters', in *Water Science and Technology*. Elsevier Science Ltd, pp. 9–16. doi: 10.1016/S0273-1223(96)00815-3.
Tvardovski, A. V. *et al.* (1997) 'Hysteresis phenomena in the study of sorptive deformation of sorbents', *Journal of Colloid and Interface Science*, 191(1), pp. 117–119. doi: 10.1006/jcis.1997.4890.
Varghese, A. G., Paul, S. A. and Latha, M. S. (2019) 'Remediation of heavy metals and dyes from wastewater using cellulose-based adsorbents', *Environmental Chemistry Letters*. Springer, pp. 867–877. doi: 10.1007/s10311-018-00843-z.
Venkatarayappa, M., Kilarkaje, S. and Prasad, A. (2011) 'Refractive Index and Dispersive Energy of NiSO4 Doped Poly (Ethylene Oxide) Films', *Materials Science*.
Vercelheze, A. E. S. *et al.* (2012) 'Properties of baked foams based on cassava starch, sugarcane bagasse fibers and montmorillonite', *Carbohydrate Polymers*, 87(2), pp. 1302–1310. doi: 10.1016/j.carbpol.2011.09.016.

Verdolotti, L. *et al.* (2012) 'A novel hybrid PU-alumina flexible foam with superior hydrophilicity and adsorption of carcinogenic compounds from tobacco smoke', *Microporous and Mesoporous Materials*, 151, pp. 79–87. doi: 10.1016/j.micromeso.2011.11.010.
Vimonses, V. *et al.* (2009) 'Kinetic study and equilibrium isotherm analysis of Congo Red adsorption by clay materials', *Chemical Engineering Journal*, 148(2–3), pp. 354–364. doi: 10.1016/j.cej.2008.09.009.
Viscusi, G., Barra, G. and Gorrasi, G. (2020) 'Modification of hemp fibers through alkaline attack assisted by mechanical milling: effect of processing time on the morphology of the system', *Cellulose*, 27(15), pp. 8653–8665. doi: 10.1007/s10570-020-03406-0.
Viscusi, G., Pantani, R. and Gorrasi, G. (2021) 'Transport properties of water vapor through hemp fibers modified with a sustainable process: Effect of surface morphology on the thermodynamic and kinetic phenomena', *Applied Surface Science*, 541, p. 148433. doi: 10.1016/j.apsusc.2020.148433.
Wahab, N. *et al.* (2019) 'Synthesis, Characterization, and Applications of Silk/Bentonite Clay Composite for Heavy Metal Removal From Aqueous Solution', *Frontiers in Chemistry*, 7, p. 654. doi: 10.3389/fchem.2019.00654.
Walker, G. M. and Weatherley, L. R. (1997) 'Adsorption of acid dyes on to granular activated carbon in fixed beds', *Water Research*, 31(8), pp. 2093–2101. doi: 10.1016/S0043-1354(97)00039-0.
Wang, H. and Lau, K.-T. (2016) *WOVEN HEMP FABRIC REINFORCED VINYL ESTER COMPOSITE: EFFECT OF WATER ABSORPTION ON THE MECHANICAL PROPERTIES DEGRADATION 1 MOHD IQBAL MISNON, 2 MD MAINUL ISLAM, 3 JAYANTHA ANANDA EPAARACHCHI*, *International Journal of Advances in Science Engineering and Technology*.
Wang, S. *et al.* (2020) 'The production of gel beads of soybean hull polysaccharides loaded with soy isoflavone and their pH-dependent release', *Food Chemistry*, 313, p. 126095. doi: 10.1016/j.foodchem.2019.126095.
Wang, Y. S., Koo, W. M. and Kim, H. Do (2003) 'Preparation and properties of new regenerated cellulose fibers', *Textile Research Journal*, 73(11), pp. 998–1004. doi: 10.1177/004051750307301110.
Van Der Wel, G. K. and Adan, O. C. G. (1999) 'Moisture in organic coatings - a review', *Progress in Organic Coatings*. Elsevier Sequoia SA, pp. 1–14. doi: 10.1016/S0300-9440(99)00058-2.
Wen, X. (2020) 'NiFe-LDH/MWCNTs/NF nanohybrids as a high-performance bifunctional electrocatalyst for overall urea electrolysis', *International Journal of Hydrogen Energy*, 45(29), pp. 14660–14668. doi: 10.1016/J.IJHYDENE.2020.03.192.
van der Werf, H. M. G. and Turunen, L. (2008) 'The environmental impacts of the production of hemp and flax textile yarn', *Industrial Crops and*

Products, 27(1), pp. 1–10. doi: 10.1016/j.indcrop.2007.05.003.
Wu, Z. *et al.* (2014) 'Adsorptive removal of methylene blue by rhamnolipid-functionalized graphene oxide from wastewater', *Water Research*, 67, pp. 330–344. doi: 10.1016/J.WATRES.2014.09.026.
Xia, C. *et al.* (2016) 'Property enhancement of kenaf fiber reinforced composites by in situ aluminum hydroxide impregnation', *Industrial Crops and Products*, 79, pp. 131–136. doi: 10.1016/j.indcrop.2015.11.037.
Xia, Y. *et al.* (2019) 'Comparative adsorption of methylene blue by magnetic baker's yeast and EDTAD-modified magnetic baker's yeast: Equilibrium and kinetic study', *Arabian Journal of Chemistry*, 12(8), pp. 2448–2456. doi: 10.1016/J.ARABJC.2015.03.010.
Xiao, L. *et al.* (2004) 'Swelling studies of chitosan-gelatin films cross-linked by sulfate', *Wuhan University Journal of Natural Sciences*, 9(2), pp. 247–251. doi: 10.1007/bf02830611.
Xiaoliang Fan *et al.* (2021) 'A Fenton-like system of biochar loading Fe–Al layered double hydroxides (FeAl-LDH@BC) / H2O2 for phenol removal', *Chemosphere*, 266, p. 128992. doi: 10.1016/J.CHEMOSPHERE.2020.128992.
Xu, W. T. *et al.* (2007) 'Postharvest grapefruit seed extract and chitosan treatments of table grapes to control Botrytis cinerea', *Postharvest Biology and Technology*, 46(1), pp. 86–94. doi: 10.1016/j.postharvbio.2007.03.019.
Yadav, S., Mehrotra, G. K. and Dutta, P. K. (2021) 'Chitosan based ZnO nanoparticles loaded gallic-acid films for active food packaging', *Food Chemistry*, 334, p. 127605. doi: 10.1016/j.foodchem.2020.127605.
Yagub, M. T., Sen, T. K. and Ang, H. M. (2012) 'Equilibrium, kinetics, and thermodynamics of methylene blue adsorption by pine tree leaves', *Water, Air, and Soil Pollution*, 223(8), pp. 5267–5282. doi: 10.1007/s11270-012-1277-3.
Yakuphanoglu, F. *et al.* (no date) 'The determination of the optical constants of Cu (II) compound having 1-chloro-2, 3-o-cyclohexylidinepropane thin film', *Elsevier*. Available at: https://www.sciencedirect.com/science/article/pii/S0030401804005358?casa_token=5PfCJ_XHmuAAAAAA:y5f4MauqIhRrqEbHMIgFfC2u_CyWuqneT4angbtVaqtwT0h4HxlfQ1m2ecH4Y8lbiNRKO4WLf1Q (Accessed: 1 January 2022).
Yakuphanoglu, F., Barim, G. and Erol, I. (2007) 'The effect of FeCl3 on the optical constants and optical band gap of MBZMA-co-MMA polymer thin films', *Physica B: Physics of Condensed Matter*, 1(391), pp. 136–140. doi: 10.1016/J.PHYSB.2006.09.009.
Yamada, E. and Ota, T. (1980) 'Effective thermal conductivity of dispersed materials', *Wärme- und Stoffübertragung*, 13(1–2), pp. 27–37. doi: 10.1007/BF00997630.
Yan, D. *et al.* (2021) 'Multimode-ultrasound and microwave assisted natural ternary deep eutectic solvent sequential pretreatments for corn straw biomass

deconstruction under mild conditions', *Ultrasonics Sonochemistry*, 72, p. 105414. doi: 10.1016/J.ULTSONCH.2020.105414.
Yan, S. *et al.* (2017) 'Influence of 3-aminopropyltriethoxysilane- graphite oxide composite on thermal stability and mechanical property of polyethersulfone', *High Performance Polymers*, 29(8), pp. 960–975. doi: 10.1177/0954008316665679.
Yang, C. *et al.* (2020) 'Novel negatively charged nanofiltration membrane based on 4,4′-diaminodiphenylmethane for dye removal', *Separation and Purification Technology*, 248, p. 117089. doi: 10.1016/j.seppur.2020.117089.
Yang, H. *et al.* (2007) 'Characteristics of hemicellulose, cellulose and lignin pyrolysis', *Fuel*, 86(12–13), pp. 1781–1788. doi: 10.1016/j.fuel.2006.12.013.
Yang, J. S. *et al.* (2010) 'Removal of metal ions from aqueous solutions using sawdust modified with citric acid or tartaric acid', *Separation Science and Technology*, 45(12), pp. 1963–1974. doi: 10.1080/01496395.2010.493782.
Yang, R. *et al.* (2018) 'Natural products-based pesticides: Design, synthesis and pesticidal activities of novel fraxinellone derivatives containing N-phenylpyrazole moiety', *Industrial Crops and Products*, 117, pp. 50–57. doi: 10.1016/j.indcrop.2018.02.088.
Yang, S. *et al.* (2009) 'Sorption of Ni(II) on GMZ bentonite: Effects of pH, ionic strength, foreign ions, humic acid and temperature', *Applied Radiation and Isotopes*, 67(9), pp. 1600–1608. doi: 10.1016/j.apradiso.2009.03.118.
Yang, S. T. *et al.* (2011) 'Removal of methylene blue from aqueous solution by graphene oxide', *Journal of Colloid and Interface Science*, 359(1), pp. 24–29. doi: 10.1016/j.jcis.2011.02.064.
Yang, X. J. *et al.* (1997) 'Swelling behaviour and elastic properties of gelatin gels', *Polymer International*, 44(4), pp. 448–452. doi: 10.1002/(SICI)1097-0126(199712)44:4<448::AID-PI845>3.0.CO;2-M.
Yao, Y. *et al.* (2010) 'Adsorption behavior of methylene blue on carbon nanotubes', *Bioresource Technology*, 101(9), pp. 3040–3046. doi: 10.1016/j.biortech.2009.12.042.
Yun, J. *et al.* (2020) 'High efficient dye removal with hydrolyzed ethanolamine-Polyacrylonitrile UF membrane: Rejection of anionic dye and selective adsorption of cationic dye', *Chemosphere*, 259, p. 127390. doi: 10.1016/j.chemosphere.2020.127390.
Zach, J. *et al.* (2013) 'Development of thermal insulating materials on natural base for thermal insulation systems', in *Procedia Engineering*. Elsevier Ltd, pp. 1288–1294. doi: 10.1016/j.proeng.2013.04.162.
Zammarano, M. *et al.* (2005) 'Preparation and flame resistance properties of revolutionary self-extinguishing epoxy nanocomposites based on layered double hydroxides', *Polymer*, 46(22), pp. 9314–9328. doi: 10.1016/j.polymer.2005.07.050.
Zanatta, A. R. (2019) 'Revisiting the optical bandgap of semiconductors and

the proposal of a unified methodology to its determination', *Scientific Reports 2019 9:1*, 9(1), pp. 1–12. doi: 10.1038/s41598-019-47670-y.
Zhang, Jie, Zhang, H. and Zhang, Jianchun (2014) 'Effect of Alkali Treatment on the Quality of Hemp Fiber', *Journal of Engineered Fibers and Fabrics*, 9(2), p. 155892501400900. doi: 10.1177/155892501400900202.
Zhang, L., Zeng, Y. and Cheng, Z. (2016) 'Removal of heavy metal ions using chitosan and modified chitosan: A review', *Journal of Molecular Liquids*. Elsevier, pp. 175–191. doi: 10.1016/j.molliq.2015.12.013.
Zhao, C. *et al.* (2017) 'Fabrication of hydrophobic biocomposite by combining cellulosic fibers with polyhydroxyalkanoate', *Cellulose*, 24(5), pp. 2265–2274. doi: 10.1007/s10570-017-1235-8.
Zhao, F. *et al.* (2004) 'Effect of Sodium Lauryl Sulfate in Dissolution Media on Dissolution of Hard Gelatin Capsule Shells', *Pharmaceutical Research*, 21(1), pp. 144–148. doi: 10.1023/B:PHAM.0000012162.52419.b3.
Zhao, Y. *et al.* (2010) 'Hierarchical films of layered double hydroxides by using a sol–gel process and their high adaptability in water treatment', *Chemical Communications*, 46(17), pp. 3031–3033. doi: 10.1039/B926906A.
Zhao, Y. *et al.* (2013) 'Halloysite nanotubule clay for efficient water purification', *Journal of Colloid and Interface Science*, 406, pp. 121–129. doi: 10.1016/j.jcis.2013.05.072.
Zhou, F., Cheng, G. and Jiang, B. (2014) 'Effect of silane treatment on microstructure of sisal fibers', *Applied Surface Science*, 292, pp. 806–812. doi: 10.1016/j.apsusc.2013.12.054.
Zhou, Y., Fan, M. and Chen, L. (2016) 'Interface and bonding mechanisms of plant fibre composites: An overview', *Composites Part B: Engineering*, 101, pp. 31–45. doi: 10.1016/J.COMPOSITESB.2016.06.055.
Zhou, Z. *et al.* (2002) 'Composition and functional properties of rice', *International Journal of Food Science and Technology*, pp. 849–868. doi: 10.1046/j.1365-2621.2002.00625.x.

List of symbols

A= absorbance
A_L= Langmuir capacity constant
A_s= specific surface area of the water molecules
a_s= Sips constant
a_w= water activity
b= width
b_L= Langmuir affinity constant
B= band tailing constant
c_0= initial dye concentration
C= dimensionless GAB parameter
C_{eq}= equilibrium moisture content
d= thickness
D= diffusion coefficient (cm^2/s)
$D_{0,c}$*= Diffusivities of composite normalized respect to the D_0 coefficient
$D_{0,f}$*= D_0 diffusivities normalized respect to the D_0 coefficient
D_0= zero concentration diffusion coefficient
E_f= flexural modulus
E_g= band gap energy
G_s= cluster integral
G_s= cluster integral
h= Planck constant
H_c= coercive field
k= Baker-Lonsdale release constant
k= extinction coefficient
K= dimensionless GAB parameter
k_0= independent temperature factor
K_1= kinetic constant for Fickian contribution (Peppas-Sahlin model)
K_1= rate constant of first order adsorption
K_2= rate constant of second order adsorption
K_2= kinetic constant for Case-II contribution (Peppas-Sahlin model)
K_a= equilibrium constant for cluster formation
k_{id}= intraparticle diffusion constant
K_L= adsorption affinity
k_{pH}= constant rate pH dependent
k_{ps}= rate constant of second order adsorption
M(T)= magnetization function of temperature
$M_{,\infty}$= equilibrium amount of dye adsorbed
$M_{,t}$= amount of dye adsorbed at time t
M= diffusional exponent (Peppas-Sahlin model)
m= mass

M_0= monolayer moisture content
M_∞= amount of drug release at infinite time
MCS= mean cluster size
M_{max}= maximum weight after swelling at stationary phase
M_t= amount of drug released at time t
M_w= molar mass
n(P)= capacity of adsorbed molecules per unit of adsorbent mass
n= mean number of penetrant molecules per cluster
n= refractive index
Ø= volume fraction
p= partial pressure
q_{eq} or q_e= equilibrium adsorption capacity
q_{eq}= amount adsorbed per gram of adsorbent at equilibrium state
q_m= monolayer adsorption capacity
q_t= adsorption capacity
R= cross head speed
R= universal gas constant
R_a= average roughness
S= span
S= sorption coefficient
S_{eq} = equilibrium
S_t = swelling at time t
t*= time corresponding to the stationary phase
T= temperature
T= time of stationary phase in deswelling
T_c= Curie Temperature
T, %=transmittance (%)
V= volume
V_s= partial molar volume
V_s= partial molar volume of penetrant
W_a= work of adhesion
α= absorption coefficient
λ= wavelength
$\gamma^d_{L,i}$= dispersion component of the liquid surface free energy
γ^d_S= dispersion component of the fiber surface free energy
$\gamma_{L,i}$= surface free energy of the liquid
$\gamma^p_{L,i}$= polar component of the liquid surface free energy
γ^p_S= polar component of the fiber surface free energy
γ_s = surface free energy
ΔG^0= free energy of adsorption
θ= the contact angle
π= spreading pressure
ρ_p = hemp fibers density
ρ_s= hemp fiberboard density

ρ_w= water vapor density
ρ_w= water vapor density
σ_c= tensile strength of composites
σ_f= flexural strength
σ_m= tensile strength of matrix
τ= rate constant
ϕ_f= fiber volume fraction
ϕ_m= maximum packing fraction
ψ= fiber-fiber interaction
ν= frequency